Norwegian University of Life Sciences
Faculty of Environmental Sciences
and Natural Resource Management

Philosophiae Doctor (PhD)
Thesis 2019:72

Mobility of naturally occurring radionuclides and stable elements in alum shale: A case study of Gran, Highway 4, Norway

Mobiliteten til naturlig forekommende radionuklider og stabile grunnstoffer i alunskifer: En kasusstudie av Gran, riksvei 4, Norge

Frøydis Meen Wærsted

Mobility of naturally occurring radionuclides and stable elements in alum shale: A case study of Gran, Highway 4, Norway

Mobiliteten til naturlig forekommende radionuklider og stabile grunnstoffer i alunskifer:
En kasusstudie av Gran, riksvei 4, Norge

Philosophiae Doctor (PhD) Thesis

Frøydis Meen Wærsted

Norwegian University of Life Sciences
Faculty of Environmental Sciences and Natural Resource Management

Ås (2019)

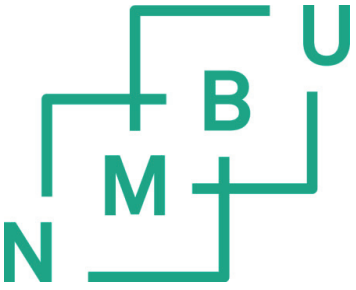

Thesis number 2019:72
ISSN 1894-6402
ISBN 978-82-575-1632-1

PhD supervisors

Professor Lindis Skipperud
Faculty of Environmental Sciences and Natural Resource Management
Norwegian University of Life Sciences
P.O. Box 5003, 1432 Ås, Norway
E-mail: lindis.skipperud@nmbu.no

Professor Brit Salbu
Faculty of Environmental Sciences and Natural Resource Management
Norwegian University of Life Sciences
P.O. Box 5003, 1432 Ås, Norway
E-mail: brit.salbu@nmbu.no

Dr. Justin Brown
Norwegian Radiation and Nuclear Safety Authority
Grini næringspark 13, 1361 Østerås, Norway
E-mail: justin.brown@dsa.no

Juan Carlos Mora Cañadas
Centro de Investigaciones Energéticas, Medioambientales y Tecnológicas (CIEMAT)
Avenida Complutense, 40, 28040 Madrid, Spain
E-mail: jc.mora@ciemat.es

Evaluation Committee

Dr. Per Roos
Center for Nuclear Technologies, Technical University of Denmark,
Frederiksborgvej 399, DK-4000 Roskilde, Denmark
E-mail: roos@dtu.dk

Dr. Nathalie Impens
Biosphere Impact Studies in the institute Environment Health and Safety (EHS) at the Belgian Nuclear Research Institute (SCK•CEN)
Research Centre Mol, Boeretang 200, 2400 Mol, Belgium
E-mail: nathalie.impens@sckcen.be

Associate professor Mona Henriksen
Faculty of Environmental Sciences and Natural Resource Management
Norwegian University of Life Sciences
P.O. Box 5003, 1432 Ås, Norway
E-mail: mona.henriksen@nmbu.no

Acknowledgements

This PhD has been funded by the Department of Environmental Sciences at NMBU, by the Norwegian Public Road Administration (NPRA) through the NORWAT (Nordic Road Water) programme and by the Norwegian Research Council through its Centre of Excellence (CoE) funding scheme (Project 223268/F50).

First, I would like to thank my supervisors, Lindis Skipperud, Brit Salbu, Juan Carlos Mora Cañadas and Justin Brown. To my main supervisor Lindis, thank you for giving me the opportunity to do this PhD, for all the freedom I've had in choosing my own ways, and for your support along the road. Brit, thank you for your critical and very useful feedback, especially in the last phase of the thesis writing. Juan Carlos, thank you for helping me see things from a wider perspective and helping me delimit my work. Justin, it is always nice to have a native speaker to approve the language!

I've had the pleasure of being co-supervisor for master students Christian Schöpke and Peter Kariuki Maina in these years, and also being involved in the master projects of Martine Digerud Melgård and Maren Hjulstad. Thank you for letting me help and learn. I would also like to thank everyone, at NMBU and elsewhere, who has taken the time to answer my questions and provide help.

This journey would have been much less pleasant without all the amazing people in the lab. For good collaboration and discussions, thanks to Karl Andreas, Estela and Hans-Christian. To everyone else, thanks for enjoyable lunch discussions, for answering my questions and making a nice atmosphere: Marit, Mirian, Shane, Ian, Pablo, Keke, Yet, Solfrid, Anicke, Signe, Lene, Merethe, Emil, Mina, Susanne, Cato and everyone else. Erica, Yevgeniya, Lisa and Estela: I would not have survived without the coffee breaks!

Big thanks to my family, for always being understanding, loving and supporting. And to all my friends out there that I've barely seen the last years – I plan to have more spare time now!

To Patrick, I'm so grateful for all your help and feedback every time I was stuck, for your support and love and for always believing in me 

Frøydis Meen Wærsted, Ås, July 2019

Contents

Summary

Alum shale is an acid-producing type of rock that can be encountered in mining and construction work in Northern Europe. Such shales can have high levels of naturally occurring radioactive material (NORM) and stable trace elements ("heavy metals"). Acid rock drainage (ARD) with high levels of these elements can develop under the right conditions.

At Gran, Hadeland, Norway, a new tunnel was constructed, and large amounts of alum shale containing NORM were excavated. These masses were used to fill an excavated bog under the planned road. In the present work, leaching experiments with alum shale from Gran were performed to investigate the potential mobility of NORM and stable trace elements under different storage conditions. Of special interest was the assessment of mobility of NORM at the site, of which ^{238}U and daughters like ^{226}Ra are most important.

In order to obtain detailed results on the behaviour of ^{226}Ra in the leaching experiments, a method for direct determination of ^{226}Ra in water and digested geological material was developed utilizing triple quadrupole inductively coupled plasma mass spectrometry (ICP-QQQ). The method utilizes N_2O as a reaction gas to ensure interference-free measurements. The detection limit for water samples was 0.42 pg L^{-1} ^{226}Ra (15 mBq L^{-1}), which is compliant with the specifications for methods used for routine analysis of drinking water quality according to European and U.S. regulations. The method was also applied to water samples with high total dissolved solids (TDS) after dilution, and to digested geological samples including alum shale. The developed method is substantially time and resource saving compared to existing methods for measurement of ^{226}Ra.

Alum shale debris was collected from the tunnel during the construction work, and used for the leaching experiments. The alum shale was geochemically classified to be from horizon 3a of the alum shale formation, and had high levels of ^{238}U (and daughters) and stable trace elements. The ratio of the neutralization potential (NP) to the acidification potential (AP) was about 0.2, and the debris was clearly expected to be acid producing.

The effect of oxygen access on the leaching potential of the alum shale debris was investigated with one-year batch experiments performed in atmospheric oxygen conditions (AOC) and low oxygen conditions (LOC). High sulphate concentrations, especially in the leachate from the AOC treatment, indicated sulphide oxidation, but the

buffer capacity of the rock was not depleted after one year, and pH in leachates of both treatments was 7.7. Leaching of several elements was nevertheless high, and indicated that especially Mo, Ni, Zn, Cd and U are of environmental concern. While the results varied for different elements, the LOC storage conditions seemed to give an overall slower release of contaminants to the environment.

An additional batch experiment was set up to investigate effects of variations of natural wet – dry climatic conditions on the leaching from the debris. The effect of a) cyclic exchange of the leachant in contact with the debris, and b) periods of drying and wetting the rock debris were investigated over a 28 week period. In the WET treatment, the water was exchanged every 5 weeks, and in the DRY treatment the debris was exposed to cycles of 3 weeks in water followed by 2 weeks drying in air. Again, sulphate concentrations indicated sulphide oxidation, and drying of the debris seemed to increase the oxidation. However, the buffer capacity of the debris was not exceeded, and at the end of the experiment, the pH was about 7.6 in the leachates of both treatments. The content of calcite and carbonates in the debris (representing the NP) was, however, reduced to less than half in both treatments at the end of the experiment. The experiment demonstrated that exchange of water increased the leaching of elements that had limited solubility, such as As, V, Ba and ^{226}Ra. Periods of drying the alum shale in air increased leaching of Li, V, Mo and ^{226}Ra, and would thereby increase their mobility in the environment. Exchange of water resulted in depletion of inherent buffer capacity of the alum shale, which will increase the risk of ARD as well as likely reduce the time before onset of ARD.

Results from the AOC-LOC experiment were compared to concentrations in water samples from the disposal site at Gran. The water samples from the disposal site, had similar pH, Ca and SO_4^{2-} concentrations, but much lower concentrations of Mo, Mn, Co, Ni, Zn, Cd and U, and much higher concentrations of NO_3^-, Cl^-, Na, As and Sb.

Results from this work shows that when alum shale or other acid-producing rocks are stored in water, it is crucial to avoid intrusion of air and exchange of water. Water exchange will lead to oxygenated water coming in, which increases the sulphide oxidation and thereby acid production. Furthermore, contaminated water could leak out, and dissolved carbonates could be washed out, depleting the NP. Thus, proper storage of excavated alum shale and other acid-producing rocks is of crucial importance to avoid adverse environmental effects.

Sammendrag

Alunskifer er en syreproduserende bergart man ofte støter på i Nord-Europa i forbindelse med gruvedrift og anleggsarbeid. Denne skiferen har ofte høye nivåer av naturlig forekommende radioaktive materialer (Naturally Occurring Radioactive Materials, NORM) og stabile sporstoffer («tungmetaller»). Sur avrenning (Acid Rock Drainage, ARD) med høye nivåer av disse grunnstoffene kan derfor utvikle seg under gitte betingelser.

Under utbyggingen av den nye tunnelen på Gran (Hadeland, Norge) ble store mengder alunskifer med høye nivåer av NORM gravd ut. Steinmassene ble brukt til å fylle en utgravd myr som lå under den planlagte veitraséen. I det foreliggende arbeidet ble utlekkingsforsøk med alunskifer fra Gran gjennomført for å undersøke potensiell mobilitet av NORM og stabile sporstoffer ved ulike lagringsforhold. Fokus ble spesielt rettet mot å vurdere mobiliteten til NORM i deponiet, hvorav ^{238}U og urandøtre som ^{226}Ra er viktigst.

For å kunne samle detaljert informasjon om oppførselen til ^{226}Ra i utlekkingsforsøkene ble det utviklet en metode for direkte bestemmelse av ^{226}Ra i vann og oppsluttet geologisk materiale, ved bruk av trippel kvadrupol induktivt koblet plasma massespektrometri (ICP-QQQ). Metoden benytter N_2O som reaksjonsgass for å unngå interferenser ved måling. Deteksjonsgrensen for vannprøver var 0,42 pg L^{-1} ^{226}Ra (15 mBq L^{-1}), og metoden oppfyller dermed kravene for rutineanalyser av drikkevann i henhold til regelverkene i EU og USA. Analysemetoden ble også brukt for vann med høyt totalt oppløst faststoff etter fortynning, samt for oppsluttet geologisk materiale, inkludert alunskifer. Sammenlignet med eksisterende metoder for måling av ^{226}Ra er den utviklede metoden særdeles tids- og ressursbesparende.

Alunskifer til utlekkingsforsøkene ble hentet fra tunnelen på Gran i konstruksjonsperioden. Etter geokjemisk klassifisering ble alunskiferprøven bestemt til å være fra lag 3a i alunskiferformasjonen. Prøven hadde høye nivåer av ^{238}U (med døtre) samt stabile sporstoffer. Forholdet mellom nøytraliseringspotensiale (NP) og syredanningspotensiale (AP) var ca. 0,2, og materialet var følgelig antatt å være netto syreproduserende.

Effekten av oksygentilgang på utlekkingspotensialet til alunskifermaterialet ble undersøkt med et ettårig batchforsøk utført ved atmosfæriske oksygenbetingelser

(Atmospheric Oxygen Conditions, AOC) og ved lite oksygen tilgjengelig (Low Oxygen Conditions, LOC). Høye konsentrasjoner av sulfat, spesielt i vannfasen i AOC-behandlingen, indikerte sulfidoksidasjon, men bufferkapasiteten til skiferen var ikke overskredet etter et år, og i begge behandlingene var pH i vannfasen ca. 7,7. En rekke grunnstoffer ble allikevel frigjort i høye konsentrasjoner, og spesielt Mo, Ni, Zn, Cd og U skaper miljømessig bekymring. Generelt så det ut til at lagring ved LOC betingelser var gunstig for å redusere spredning av potensielt skadelige stoffer til miljøet, men resultatene varierte noe for de ulike grunnstoffene.

Et annet batchforsøk ble satt opp for å undersøke effekter av væting og tørking av alunskiferen med tanke på naturlige klimatiske variasjoner. Effekten av a) syklisk utskifting av vannfasen i kontakt med alunskifermaterialet, og b) perioder med tørking og væting av alunskifermaterialet ble undersøkt i en periode på 28 uker. I WET-behandlingen ble vannfasen skiftet ut hver femte uke, mens i DRY-behandlingen ble alunskifermaterialet eksponert for sykluser bestående av 3 uker i vann etterfulgt av 2 uker tørking i luft. Også i dette forsøket indikerte sulfatkonsentrasjonene at det foregikk oksidasjon av sulfider, samt at tørking av alunskifermaterialet så ut til å øke denne oksidasjonen. Bufferkapasiteten til alunskiferen ble allikevel ikke overskredet, og på slutten av forsøket var pH i vannfasen omtrent 7,6 for begge behandlingene. Dog var innholdet av kalsitt og karbonater i materialet (dvs. NP) mer enn halvert i begge behandlingene etter forsøket. Utskifting av vannfasen økte utlekkingen av grunnstoffer med lav løselighet, for eksempel As, V, Ba og ^{226}Ra. Perioder med tørking av alunskiferen i luft økte utlekkingen av Li, V, Mo og ^{226}Ra, og forventes å øke mobiliteten av disse i miljøet. Utskifting av vannfasen resulterte i utarming av alunskiferens iboende bufferkapasitet, noe som vil øke risikoen for sur avrenning (ARD) og sannsynligvis redusere tiden før det inntreffer.

Resultater fra AOC-LOC eksperimentet ble sammenlignet med konsentrasjoner i vannprøver fra alunskiferdeponiet på Gran. Vannprøvene fra deponiet hadde lignende pH og konsentrasjoner av Ca og SO_4^{2-}, men mye lavere konsentrasjoner av Mo, Mn, Co, Ni, Zn, Cd og U, samt mye høyere konsentrasjoner av NO_3^-, Cl^-, Na, As og Sb.

Resultater fra dette arbeidet viser at dersom alunskifer eller andre syreproduserende steinmasser lagres i vann er det av avgjørende betydning å unngå luftinfiltrasjon og utskifting av vannet. Utskifting av vannet vil føre til at oksygenrikt vann kommer inn, noe

som øker sulfidoksidasjonen og dermed syreproduksjonen. Videre fører utskifting av vannet til at forurenset vann lekker ut samt at karbonater i løsning fjernes, hvilket fører til en utarming av nøytraliseringspotensialet. Følgelig er riktig lagring av alunskifermasser og andre syredannende bergarter avgjørende for å unngå negative effekter på miljøet.

List of papers

Paper I: Wærsted, F. M., Jensen, K. A., Reinoso-Maset, E., & Skipperud, L. (2018). *High Throughput, Direct Determination of ^{226}Ra in Water and Digested Geological Samples.* Analytical Chemistry, 90(20), 12246-12252. doi:10.1021/acs.analchem.8b03494

Paper II: Wærsted, F. M., Reinoso-Maset, E., Salbu, B., & Skipperud, L. (manuscript). *Rainwater leaching of alum shale debris under atmospheric and low oxygen conditions.*

Paper III: Wærsted, F. M., Riss, P. J., & Skipperud, L. (manuscript). *The effect of water exchange on the leaching of alum shale.*

Other work

Peer-reviewed publications

Schöpke, C., Wærsted, F. M., Jensen, L. K. & Skipperud, L. (manuscript) *Uranium and toxic metal uptake by the earthworm* Eisenia hortensis *in contaminated soils*.

Skipperud, L., Teien, H.-C., Tollefsen, K. E., &. Wærsted, F. M (manuscript) *Dispersion, Transfer and Risk of NOR and Metals due to Construction in U-bearing Minerals.*

Thørring, H., Wærsted, F. M., Raaness, A., Skipperud, L. & Jensen, L. K. (manuscript) *Natural radioactivity in forest and mountain areas of arctic Norway – local geology, soil characteristics, and transfer to biota.*

Teien, H.-C., Wærsted, F. M., Hjulstad, M. Hertel-Aas, T. & Skipperud, L. (manuscript) *Leaching, uptake and effects in brown trout (*Salmo trutta*) of radionuclides and metals from black shales and sulphur bearing gneiss*.

Other publications

Jensen, L. K., Finne, I., Thørring, H., Kolstad, T., Aas-Hansen, Ø., Raaness, A., Watson, R. J., Baranwal, V. C., Rønning, J. S., Wærsted, F. M., Skipperud, L., & Normann, A. K. (2018) *One uranium mountain – different trails to the summit.* Fram Forum. Retrieved from https://issuu.com/framcentre/docs/framforum-2018-issuu

Skipperud, L., Alvarenga, E., Lind, O. C., Teien, H.-C., Tollefsen, K. E., Salbu, B., & Wærsted, F. M. (2016). *Effekter og miljørisiko knyttet til inngrep i områder med sulfidrike mineraler. Case: Deponi i forbindelse med tunnelbygging i alunskiferområder* (651). Retrieved from https://www.vegvesen.no/fag/publikasjoner/publikasjoner/Statens+vegvesens+rapporter

Abbreviations

AOC	atmospheric oxygen conditions
AMD	acid mine drainage
AP	acidification potential
ARD	acid rock drainage
CR	concentration ratio
CRM	certified reference material
DL	detection limit
DOC	dissolved organic carbon
ICP-MS	inductively coupled plasma mass spectrometry
ICP-QQQ	triple quadrupole ICP-MS
kDa	kilo dalton
K_{SP}	solubility product
LMM	low molecular mass (<10 kDa)
LOC	low oxygen conditions
LOI	loss on ignition
ORP	oxidation-reduction potential
ppm	parts per million
NORM	naturally occurring radioactive material(s)
NP	neutralization potential
NPRA	Norwegian Public Roads Administration (Statens Vegvesen)
NRD	neutral rock drainage
QL	quantification limit
P_{CO2}	partial pressure of CO_2
REE	rare earth elements
RSD	relative standard deviation
SI	supporting information
Stot	total sulphur
TDS	total dissolved solids
TIC	total inorganic carbon
TOC	total organic carbon
XRD	X-ray diffraction
µ-XRF	micro X-ray fluorescence

Element symbols

Al	aluminium
Ag	silver
As	arsenic
Au	gold
B	boron
Ba	barium
Bi	bismuth
C	carbon
Ca	calcium
Cd	cadmium
Cl	chlorine
Co	cobalt

Cr	chromium
Cs	caesium
Cu	copper
F	fluorine
Fe	iron
Ge	germanium
H	hydrogen
Hg	mercury
In	indium
Ir	iridium
K	potassium
Li	lithium
Mg	magnesium
Mn	manganese
Mo	molybdenum
N	nitrogen
Na	sodium
Ni	nickel
O	oxygen
Pb	lead
Pd	palladium
Ra	radium
Rb	rubidium
Rh	rhodium
Ru	ruthenium
S	sulphur
Sb	antimony
Se	selenium
Si	silicon
Sn	tin
Sr	strontium
Te	tellurium
Tl	thallium
Th	thorium
U	uranium
V	vanadium
Zn	zinc

1 Introduction

Crushed rock masses produced in mining and construction work represent an important source of naturally occurring radioactive materials (NORM) and stable elements that potentially can be released to the environment. Processing and storage of rock masses under conditions different from the natural deposit may expose the rock surfaces to weathering, and can subsequently cause release of harmful elements to the environment. Certain types of rock can produce acid when exposed to air and water, causing *acid rock drainage* (ARD), which greatly enhances the leaching of several elements from the rocks, and thereby increases the risk of adverse effects on downstream organisms. This is a widespread problem in mining areas (*acid mine drainage*, AMD) and in other places where acid-producing rocks are weathered (Appelo & Postma, 2010; vanLoon & Duffy, 2011).

Alum shale is an acid-producing type of rock commonly encountered in construction work in the Oslo Region of Norway (Figure 1). In 2013-2015, a tunnel was constructed to take national road no. 4 (Riksvei 4) around Gran centre, Hadeland, and about 66 500 m^3 of alum shale were excavated in the process. The alum shale debris from the tunnel construction was used to fill a bog situated at the southern entrance of the tunnel, partly underlying the new road.

Alum shale is often enriched in several potentially problematic trace elements as well as NORM, specifically the uranium-series (Falk et al., 2006; Owen et al., 1990; Pabst et al., 2016). As uranium-238 (^{238}U) decays, highly radiotoxic daughter nuclides like radium-226 (^{226}Ra) are produced. During weathering of the rock, these stable and radioactive elements can be released in potentially harmful amounts into the surroundings. Terrestrial and aquatic biota downstream of weathering rock masses can therefore experience a *multiple stressor scenario* with exposure to harmful levels of both stable and radioactive elements possibly associated with acidic water. From alum shale, production of acid is expected when the rock surface is exposed to air and water. As a result, increased leaching of a number of elements is likely when debris is stored with free access to air. Acid production is not expected in alum shale kept under anoxic conditions. However, there can still be leaching of several elements that are soluble by circumneutral pH, giving *neutral rock drainage* (NRD), but the release rate is expected to be slower

compared to by low pH values. Thus, for the storage site at Gran, measures were taken to reduce water exchange and hinder oxygen intrusion into the stored alum shale masses.

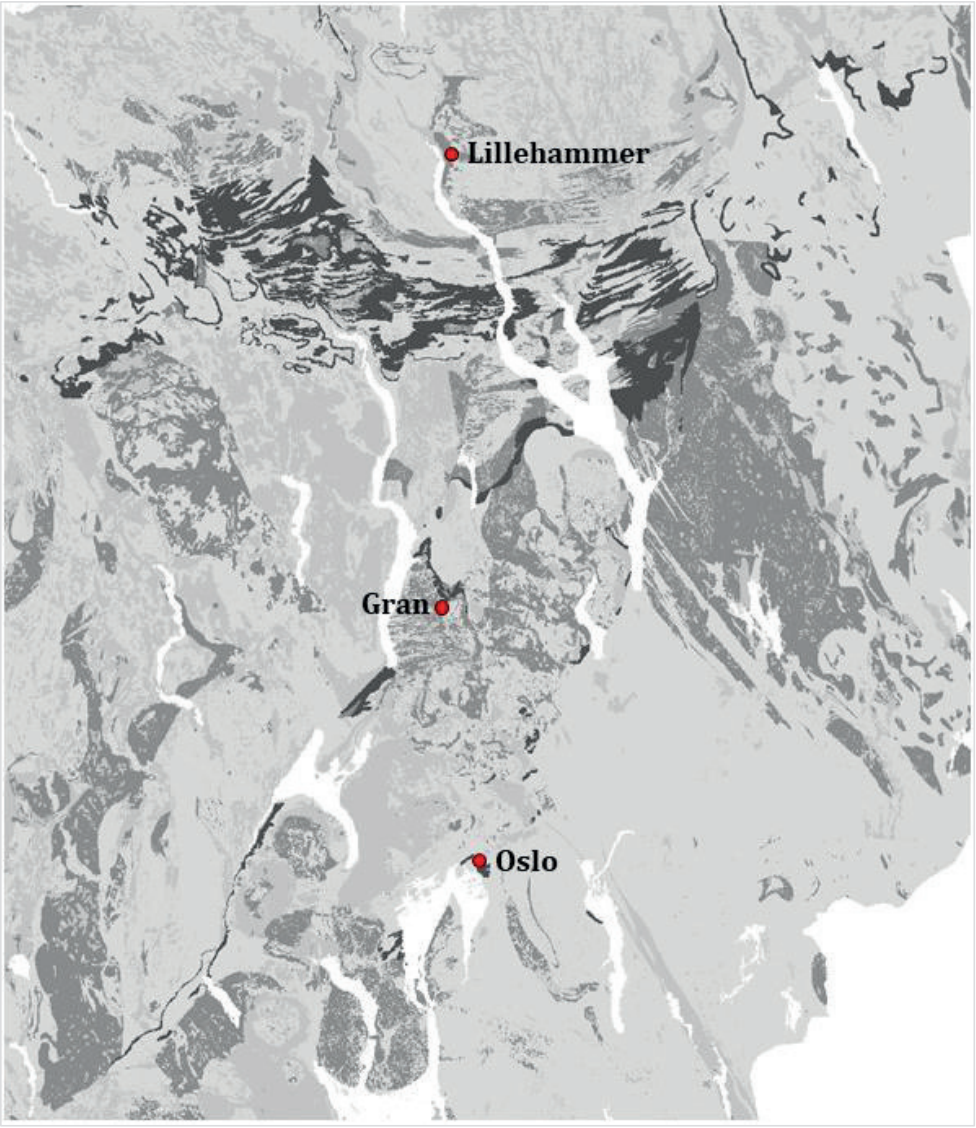

Figure 1: Map for radon risk, eastern Norway. Alum shale areas are marked in dark grey (extra high radon risk, (NGU, 2016)). Modified from NGU (2019).

There is a lot of construction activity going on in alum shale, e.g., in the Oslo area and further north on both sides of Lake Mjøsa to Lillehammer. Projects like the new governmental quarters (NGI, 2019b) and train tunnel from Ski to Oslo (Follobanen) (NGI,

2019a) generate large amounts of excavated alum shale that need to be handled and stored properly. The Norwegian Environmental Agency has published guidelines for characterization, handling and storage of acid-producing rock (Endre & Sørmo, 2015; Sørmo et al., 2015). The deposition of alum shale from construction work is also regulated in Norwegian law. The Pollution Control Act (Forurensningsforskriften, § 2-3) (2004) defines contaminated ground as soil or bedrock that produces acid or other substances that can cause contamination in contact with water and/or air. Following amendments performed in 2011, the regulation also applies to NORM. For material containing natural ^{238}U in secular equilibrium with all daughter nuclides, the limit for radioactive waste is 1 Bq ^{238}U g^{-1} ($\approx$ 80 mg U kg^{-1}) (Strålevernsforskriften, 2016). Norwegian alum shales have been found to have about 20-400 mg U kg^{-1} (Pabst et al., 2016) and Alloway (2013) reports concentrations up to 1,250 mg U kg^{-1} for black shales worldwide.

In this work, leaching from alum shale under different storage conditions is investigated in the context of the potential impact of release of trace elements and NORM from such storage sites on the local environment. Emphasis is given to radionuclides, because of the more limited availability of information on their behaviour in comparison to trace elements. This is particularly true for ^{226}Ra, for which there is little knowledge in the literature on leaching from black shales over time under relevant storage conditions.

The tunnel construction at Gran has been used as a case study, and information from related fieldwork and experiments investigating bioavailability of radionuclides and stable elements in the alum shale and their effects on biota are included in the discussion.

1.1 Research aims and hypotheses

The overarching aim of this thesis was to assess the potential release and mobility of key radionuclides and stable elements in alum shale under different storage conditions. Particular focus was directed toward NORM as the available information is limited.

The aims for this work can be summarized as:

1. Develop a method for quick and efficient quantitative determination of ^{226}Ra to better assess environmental consequences
2. Investigate the leaching of NORM and stable elements from alum shale when stored in water under atmospheric and low oxygen conditions

3. Investigate the effect of exchange of water and periods of drying on the leaching of NORM and stable elements from alum shale
4. Investigate how the buffer capacity of stored debris is affected by different processes under varying storage conditions

Furthermore, some hypotheses were formulated:

1. Even without a pH drop, there will be considerable leaching of elements that are soluble at a circumneutral pH, resulting in potentially harmful water concentrations
2. Drying of the debris between periods of submersion will lead to greater pyrite oxidation and increased leaching of a range of elements
3. Exchange of water will lead to faster depletion of the buffer capacity of the debris
4. Ra will follow Ba and be limited by $BaSO_4$ solubility, and thus have lower mobility as pyrite oxidation increases
5. Exchange of water will increase the mobility of elements that are limited by solubility constraints, like ^{226}Ra and Ba

To enable detailed investigations of the mobility of ^{226}Ra in alum shale, a method was developed for direct measurement of ^{226}Ra in water and digested samples in Paper I. In Paper II, the leaching of stable and radioactive elements from alum shale debris in atmospheric and low oxygen conditions was investigated. In Paper III, the effect of exchanging water and drying of debris on the leaching of stable and radioactive elements from alum shale was investigated.

2 Background

2.1 Alum shale

Figure 2: Unweathered alum shale from the tunnel construction at Gran.

Alum shale (Figure 2) is a sedimentary rock formed from sediments deposited under reducing conditions. It is a black shale (black mudrock) formed in the Cambro-Ordovician period, i.e., about 500 million years ago (Owen et al., 1990; Pipkin et al., 2008). Black shales are found throughout the world, with particularly large deposits in Northern Europe as well as Russia, USA, Canada, Australia, China and Brazil (Alloway, 2013). In general, alum shales are an acid producing type of rock, causing acid rock drainage (ARD) (Pabst et al., 2016). In Norway, alum shale is mainly found in the Oslo Region (Endre & Sørmo, 2015). However, acid-producing rock can be encountered in large parts of the country (Endre & Sørmo, 2015). The Ordovician successions of the Oslo region have been described by Owen et al. (1990). Here, the somewhat simplified lithological grouping of Pabst et al. (2016) is used. The different horizons have variable compositions and thus different potential for acid production and leaching of NORM and stable elements. The alum shale formation comprises horizons 1 to 3a, where the lowermost horizon, i.e., horizon 1, mainly consists of (not-acid-producing) sandstone, while horizons 2 and 3a have high content of organic matter and sulphides, and are the focus of this work. The alum shale formation ranges in thickness from about 20 to almost 100 metres (Owen et al., 1990).

The main use of alum shale has been for production of alum salt (hydrated aluminium sulphate, most commonly with potassium, $KAl(SO_4)\times 12\ H_2O$), which historically has been

used for multiple purposes including tanning of hide, fixing of colours in the textile industry and in pharmaceuticals (Andersson et al., 1985). The kerogen of the alum shale has been used for oil production in Sweden (Andersson et al., 1985), and 23 % of gas production in the US in 2010 was extracted from shales with fracking (Erlström, 2014). Alum shale has also been mined for metals, for example U and V (Andersson et al., 1985).

2.1.1 Mineralogy

Alum shale consists of silicate minerals, organic matter (kerogen), sulphides and carbonates (Falk et al., 2006; Owen et al., 1990; Pabst et al., 2016). The sulphide minerals, for example pyrite (FeS_2) and pyrrhotite (FeS), are formed due to the reducing conditions during sedimentation and formation of the rock, and is the source of the acid-producing capacity of the rock. The carbonate in alum shale is often calcite ($CaCO_3$), and can be present in the form of nodules, giving a very uneven distribution of the carbonates in the rock (Owen et al., 1990; Pabst et al., 2016). Kerogen is incompletely decomposed organic matter from sedimentation and is responsible for the characteristic black colour (Tourtelot, 1979).

2.1.2 Pyrite oxidation and acid neutralization

Pyrite can be oxidized by various oxidizing agents, for example oxygen and ferric iron (Fe^{3+}), and the overall process can be described by four equations (Chandra & Gerson, 2010; Singer & Stumm, 1970):

$$FeS_2(s) + \frac{7}{2}O_2\,(aq) + H_2O \rightleftharpoons Fe^{2+} + 2\,SO_4^{2-} + 2H^+ \qquad \textit{Equation 1}$$

$$Fe^{2+} + \frac{1}{4}O_2\,(aq) + H^+ \rightleftharpoons Fe^{3+} + \frac{1}{2}H_2O \qquad \textit{Equation 2}$$

$$Fe^{3+} + 3H_2O \rightleftharpoons Fe(OH_3)(s) + 3H^+ \qquad \textit{Equation 3}$$

$$FeS_2(s) + 14Fe^{3+} + 8H_2O \rightleftharpoons 15\,Fe^{2+} + 2SO_4^{2-} + 16H^+ \qquad \textit{Equation 4}$$

Equation 1 describes the oxidation of pyrite by oxygen and water. The produced ferrous iron (Fe^{2+}) is not stable, and its oxidation to ferric iron is shown in equation 2. As long as the pH is circumneutral, the solubility of ferric iron is very low, and it precipitates as iron (oxy)hydroxides, illustrated with $Fe(OH_3)$ in equation 3. This represents another source of acid, and the net production in equations 1-3 is 4 moles of protons per mole of pyrite. As long as oxygen is available and pH is circumneutral, equations 1-3 are constantly relevant. When the pH drops below ~4, solubility of ferric iron increases and the ferric

iron starts oxidizing pyrite (equation 4) (Appelo & Postma, 2010). Equation 4 represents a propagation of pyrite oxidation as pH decreases: ferric iron ions speeds up the oxidation. Also note that when the pH decreases, equation 3 will shift to the left, and this mechanism will no longer be a source of H^+. Fe^{3+} in solution is also important for transport of acid: as acid rock drainage meets neutral stream water, precipitation of Fe (oxy)hydroxides will cause a delayed release of acid. When the pH decreases, acid reacts with the rock causing increased weathering rates and concomitant release of radioactive and stable elements.

Biological activity can catalyse pyrite oxidation (Appelo & Postma, 2010; Parbhakar-Fox & Lottermoser, 2015). However, assessing the effect of the biological activity was outside the scope of this work due to practical limitations.

In extreme cases, pyrite oxidation can cause negative pH values (Appelo & Postma, 2010). The presence of carbonates in the rock can buffer the produced acid, but the pH will drop if all the carbonate is used or not readily available for neutralization. Calcite dissolution and carbonate equilibrium can be described with the following equations (vanLoon & Duffy, 2011):

$CaCO_3 \rightleftharpoons Ca^{2+} + CO_3^{2-}$	$K_{SP} = 5 \times 10^{-9}$	*Equation 5*
$CO_3^{2-} + H_3O^+ \rightleftharpoons HCO_3^- + H_2O$	$pK_{a2} = 10.32$	*Equation 6*
$HCO_3^- + H_3O^+ \rightleftharpoons CO_2(aq) + 2H_2O$	$pK_{a1} = 6.3$	*Equation 7*
$CO_2(aq) \rightleftharpoons CO_2(g)$	$K_H = 3.3 \times 10^{-7}$	*Equation 8*

Note that equation 7 is also including the step via carbonic acid (H_2CO_3), but this concentration will be minor compared to dissolved CO_2, and the equations are thus simplified (vanLoon & Duffy, 2011).

Silicate minerals, like muscovite and quartz, are more stable and will degrade very slowly unless aggressive weathering conditions (i.e., lower pH) prevail (Appelo & Postma, 2010). Silicate weathering will buffer the acid, but this process is extremely slow relative to neutralization by for example calcite, and areas with mainly silicate rocks are susceptible for acidification from pyrite oxidation, and also to acid rain (Appelo & Postma, 2010).

A very important property of excavated rock materials is the acidification potential (AP) compared to the (acid) neutralization potential (NP), see Equation 9. The AP of a rock is estimated by assuming that all S in the rock comes from sulphides behaving like pyrite, and the NP is estimated from the content of carbonates, assuming these behave like calcite (Lawrence & Wang, 1996; Pabst et al., 2016).

$$\frac{Neutralization\ potential}{Acidification\ potential}$$

Equation 9

If this ratio is <1, the rock will usually be acid producing, while if it is above 3 it is classified as neutralizing (Pabst et al., 2016). Due to uncertainties in the assumptions for estimating sulphide and calcite content, rocks having a ratio between 1 and 3 fall into the uncertainty zone where one cannot be certain that the rock is not acid producing. However, even without a pH drop to increase leaching, radionuclides and stable elements incorporated in the pyrite materials can be released during oxidation, or contaminants can be released from other minerals and from organic matter in the rock, giving *neutral rock drainage* (NRD) (Alloway, 2013; Appelo & Postma, 2010; Bierens de Haan, 1991).

Figure 3: Weathered alum shale.

Comparing the fresh alum shale rock in Figure 2 with the weathered sample in Figure 3 illustrates the weathering of alum shale. In Figure 3, note the expansion of the layers while the structure of the rock is broken down – the rock itself is in the process of fragmenting. The yellow precipitate is iron sulphates.

2.1.3 Stable elements

The formation of black shales in shallow seawater with a reducing environment is partly responsible for the enrichment of a number of trace elements (Alloway, 2013). As mentioned, alum shale is enriched in a range of trace elements including Cd, Co, Cu, As, Ni, Zn, V, Mo, Ba and U (Falk et al., 2006; Owen et al., 1990; Pabst et al., 2016). These can leach into the nearby aquatic environment or become enriched in soils developed on the alum shale.

As alum shale is weathered, a number of processes may result in release of potentially harmful amounts of a variety of elements. Physical breakdown of rock at, e.g., a construction site will increase surface area and create reactive surfaces with a high potential for leaching (Bierens de Haan, 1991). By contact with water, soluble minerals will start dissolving, and if oxygen is present, redox-sensitive components will start to change. As pyrite is oxidized, elements present as impurities in the mineral itself, particularly As, Co, Ni and Sb, but also a range of other elements, will be released (Abraitis et al., 2004; Bierens de Haan, 1991). Impurities in carbonates will also be released as the carbonates dissolve to neutralize the produced acid. These mechanisms can cause release of harmful levels of elements that are soluble by neutral pH, such as As, Cd, Co, Mo, Ni, Sb, U and Zn, giving neutral rock drainage (NRD) (Alloway, 2013; Endre & Sørmo, 2015; Jeng, 1992; Lavergren et al., 2009; Lydersen et al., 2002). Other elements have a limited solubility at circumneutral pH, or are not released from the minerals before more aggressive weathering conditions prevail, and are not expected to cause major problems unless pH is reduced.

The ferric (oxy)hydroxides resulting from pyrite oxidation at circumneutral pH (equation 3 above) represent an important scavenging agent, and can limit the mobility of a number of elements in the environment (Appelo & Postma, 2010; Braunschweig et al., 2013). As and Sb are, for example, typically associated with iron (oxy)hydroxides (Appelo & Postma, 2010; Okkenhaug, 2012). If the pH of the system drops, the scavenging effect from the precipitation of the Fe (oxy)hydroxides ceases as equation 3 shifts to the left.

Furthermore, already precipitated iron (oxy)hydroxides can dissolve to buffer the pH change, releasing the scavenged contaminants once more (Parbhakar-Fox & Lottermoser, 2015).

Another mechanism that limits mobility of elements is precipitation of oversaturated compounds. One such compound is the salt $BaSO_4$, and its low solubility limits the leaching of Ba in sulphate-rich acid rock drainage, as well as of the heavier alkaline earth metal Ra which is co-precipitated, see section 2.1.4.2.

Many elements that remain fixed by sorption or in minerals at circumneutral pH are mobilized as the water becomes more acidic (Appelo & Postma, 2010). Al becomes soluble when pH drops below about 5, and a potentially major environmental problem (Appelo & Postma, 2010; Endre, 2013; Rayner-Canham & Overton, 2006). Inorganic monomeric Al can have a detrimental impact on aquatic life (Rosseland et al., 1992). From the disposal sites of sulphide-bearing rock from road construction in southern Norway, 90 tons of S leaches into the downstream fjord Kaldvellfjorden each year, together with 18 tons of Al, and 4.5 tons of Mn (Hindar, 2013). In addition, co-leached elements such as Ni, Zn, Co, Cu and Cd are released.

Another important factor can be the presence of organic matter in the disposal site, which is important for speciation and mobility of e.g., Ni, Zn, Cd and U (Appelo & Postma, 2010; Moulin et al., 2004). In the alum shale disposal site at Gran, an excavated bog, interactions with organic matter can be important. Organic matter can either reduce mobility of the elements by stabilizing them in the disposal site, or increase mobility of otherwise insoluble elements through complexation and transport in dissolved organic matter. The effect of organic matter on the mobility of elements in the disposal site at Gran was considered to be outside the scope of this work.

2.1.4 Naturally occurring radioactive material (NORM)

NORM is present everywhere on earth, and can, in some places, reach harmful concentrations, resulting from natural processes or human activities. Sources of NORM include tailings from mining of both uranium and stable metals, coal mining and combustion, mineral fertilizers, scales and produced water from oil and gas extraction, water and wastewater treatment residuals, mineral sands and waste rock from

construction work (Landa, 2007). NORM contributes the main part of the ionizing radiation dose to the general human population (UNSCEAR, 2018).

In alum shale, the most important radionuclides are associated with the decay chain of ^{238}U (see Figure 4). The age of the rock ensures secular equilibrium between ^{238}U and daughter nuclides in bedrock, at least until the noble gas ^{222}Rn, which can escape through cracks in the bedrock (Sheppard et al., 2006). Once alum shale has been weathered, secular equilibrium cannot be assumed anymore as the different elements in the decay chain have different chemical properties, and thus environmental behaviours. However, because of tedious measurement procedures for most ^{238}U daughter nuclides, secular equilibrium is often (erroneously) assumed in risk assessments. For example, for natural ^{238}U the limit for radioactive waste in Norway is 1 Bq L^{-1}, assuming secular equilibrium with all daughter nuclides (Strålevernsforskriften, 2016). However, several studies illustrates the different behaviour of the radionuclides in nature, resulting in different distribution between compartments. Navas Izquierdo et al. (2005) measured the depth profile distribution of ^{238}U, ^{226}Ra and ^{210}Pb in a natural soil where the content of the given isotopes are assumed to originate from the parent bedrock. ^{238}U was found to be depleted in the upper layers of all soils, and enriched in deeper layers, while ^{226}Ra showed a homogeneous distribution down the soil depth profiles. ^{210}Pb was found to decrease with depth in three of five sites, suggesting a relation to physical properties like soil particle movement and deposition, for example by radon emanation and deposition of daughters. An example from Norway is the work by Thørring et al. (in prep.), where ^{238}U, ^{226}Ra, ^{210}Pb and ^{210}Po was measured in soil and plant samples from a NORM rich area. In most samples, the relation between the radionuclides was far from secular equilibrium.

While the mechanisms and reactions mentioned for stable elements also affects radionuclides, there are some special considerations for this latter group: As an unstable atom – such as ^{238}U – disintegrates, other elements (daughters/progeny) are formed with differing chemical properties, with the result that the tendency of the atom to stay in various compartments of the environment, changes. Thus, to predict the mobility, transport, biological transfer and resulting effect on biota of radionuclides in a specific site, the properties of all the daughters must be considered. A short overview of some of the radionuclides important for this work is presented below.

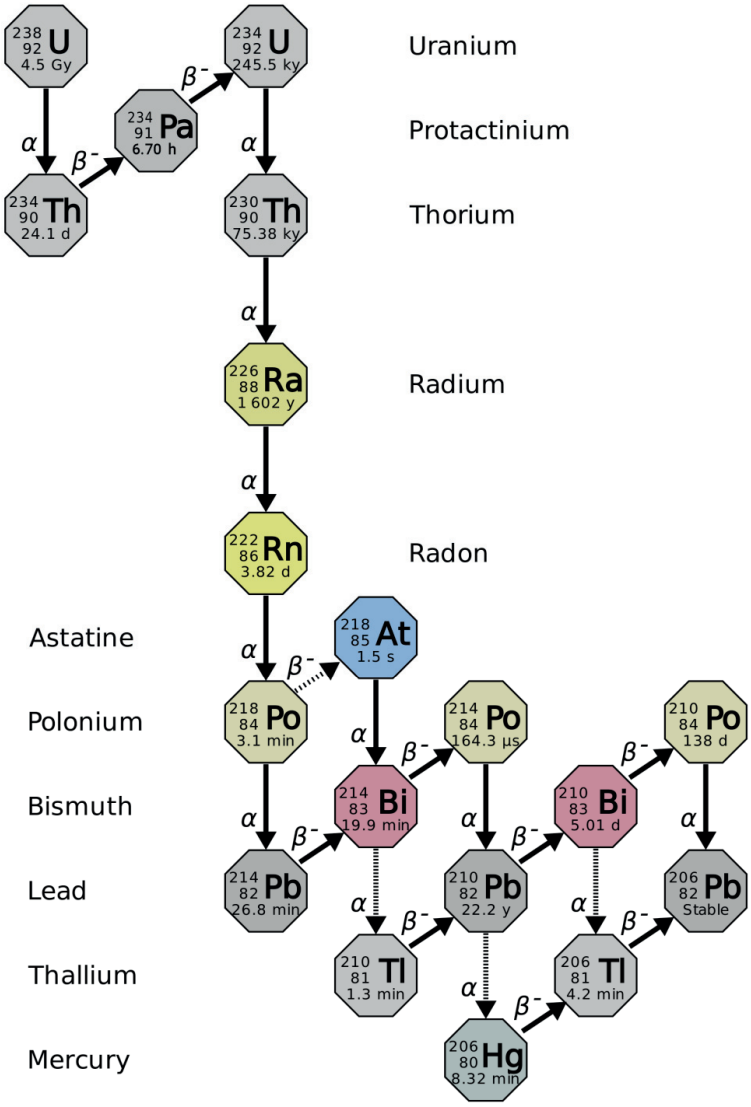

Figure 4: Decay chain of ^{238}U. The major decay routes are marked with solid arrows, while the less probable decay routes are marked with broken arrows. Information about ^{234}Pa has been modified from Wikimedia (2014) according to information from IAEA (2019). The figure is reused under the Creative Commons Attribution 3.0 Unported license.

2.1.4.1 Uranium (U)

Of the naturally occurring uranium isotopes, ^{238}U (99.27 %) is far more abundant than ^{235}U (0.72 %) and ^{234}U (0.005 %). While being known for being radioactive, the chemical toxicity of ^{238}U ($t_{½} = 4.46 \times 10^9$ y) is higher than the radiotoxicity. This is reflected in lower

drinking water guidelines when considering chemical properties (30 μg L^{-1}) than when considering radiochemical properties (10 Bq L^{-1} ≈ 800 μg L^{-1}) (WHO, 2017).

Common oxidation states are IV and VI, e.g., as uranous (U^{4+}) and uranyl (U^{6+}) ions, with the latter being much more soluble and thus important for uranium mobility, and also the prevailing state by oxidizing conditions in nature (Landa, 2007). However, in bedrock U is often present as U^{IV}, such as in uraninite (UO_2) – a primary U ore mineral (Alloway, 2013).

As black shales are formed in shallow, reducing seawater, U can accumulate in the sediments by reduction of the highly soluble uranyl ion to the poorly soluble uranous ion, together with complexation by organic matter (Alloway, 2013). Swanson (1961) summarizes three processes for enrichment of U in black shales: Sorption by organic matter from river and sea water, direct precipitation of U (likely as uraninite) in reducing conditions and precipitation by phosphate. The dominating process will depend on the conditions during formation of the black mud (Swanson, 1961). Organic matter is partly responsible in all these processes, as decomposition of organic matters causes the reducing conditions and the phosphate is likely biogenic, and as a result, marine shales with low organic matter generally contain less U than shales with > 2 % organic matter (black shales) (Swanson, 1961).

Uranium sorption to soil has been found to be highest between pH 5 and 8.5 (Landa, 2007). Organic soils have been found to have the highest K_d values for U (Sheppard et al., 2006; Vandenhove et al., 2009), humic ligands are found to be important for U speciation (Moulin et al., 2004) and U has increased solubility in carbonate rich water (Seder-Colomina et al., 2018; Stanley & Wilkin, 2019). Furthermore, amorphous iron (like freshly formed iron oxyhydroxides from pyrite oxidation) can be important for sorption of U (Braunschweig et al., 2013). All these factors can be important for the mobility of U in the disposal site at Gran.

2.1.4.2 Radium (Ra)

The Ra isotope found in the ^{238}U decay chain, and thus the most important in alum shale, is ^{226}Ra ($t_{½}$ = 1600 y). As a heavy calcium analogue with high mobility in the environment and accumulation in bone in vertebrates, ^{226}Ra is one of the most radiotoxic naturally

occurring radionuclides and is of relevance from both an environmental and a human radiation protection perspective (IAEA, 2014).

As an alkaline earth metal, Ra is found in nature in the oxidation state +II. At the pH of most natural waters, dissolved Ra will be present primarily as the uncomplexed Ra^{2+} cation (IAEA, 2014). While not directly sensitive to changing redox conditions, the mobility of Ra can be influenced by dissolution or precipitation of sorbing phases (Landa, 2007). Ra forms soluble salts with chloride, bromide and nitrate. The alkaline earths are often found in insoluble deposits, with silicates, phosphates, sulphates and carbonates being important, and Ra is easily co-precipitated with barium due to the similar chemical behaviour (Mitchell et al., 2013). As Ra sulphate has very low solubility ($K_{SP} = 4.25 \times 10^{-11}$, Kirby and Salutsky (1964)), and because Ra is co-precipitated with $BaSO_4$, Ra is not expected to leach extensively in acid rock drainage as many other elements (Landa, 2007). Ra can sorb to clay minerals, chalky soil, colloidal silicic acid, Mn and Fe (oxy)hydroxides and organic matter (IAEA, 2014; Landa, 2007; Lieser, 1995). Groundwater low in sulphate, with high ionic strength and high contents of Ca^{2+} and Ba^{2+}, are conducive to the transport of Ra.

Furthermore, ^{226}Ra is the precursor to radionuclides that are major contributors to the dose to the general population, like the radon daughters ^{210}Pb and ^{210}Po (UNSCEAR, 2018). Thus, monitoring ^{226}Ra is important for dose and risk assessments. In emergency situations, there is also a pronounced need for rapid analyses of drinking water and other sample matrices (Maxwell & Culligan, 2012).

The drinking water limit for ^{226}Ra set by the U.S. Environmental Protection Agency (USEPA) is 5 pg L^{-1} (0.2 Bq L^{-1}) (*National Primary Drinking Water Regulations*, 2009), and in the EU, the Euratom Drinking Water Directive indicates a value of 14 pg L^{-1} (0.5 Bq L^{-1}) (EU, 2013). In both cases, the required detection limit (DL) for the analysis of ^{226}Ra in drinking water is 1 pg L^{-1} (0.04 Bq L^{-1}) (EU, 2013; GPO, 2012).

Determination of ^{226}Ra in environmental samples usually involves lengthy, work-intensive procedures before measurement by liquid scintillation counting, alpha or gamma spectrometry (Hou & Roos, 2008; IAEA, 2010; Köhler et al., 2002). The analysis of one sample can take days to weeks. Accelerator Mass Spectrometry (AMS), Thermal Ionization Mass Spectrometry (TIMS) and Inductively Coupled Plasma Mass

Spectrometry (ICP-MS) have also been used for ^{226}Ra determination, and offer faster analysis time than the radioanalytical techniques. However, the developed methods still require tedious concentration and separation procedures prior to analysis in order to increase Ra concentration and/or remove interferences (Becker, 2005; Hou & Roos, 2008; IAEA, 2010, 2014; Lagacé et al., 2017; Maxwell & Culligan, 2012; Morvan et al., 2001; Zhang et al., 2015). Direct measurements of ^{226}Ra have until recently been limited to methods with insufficient detection limits, as discussed in Paper I (Wærsted et al., 2018).

For geological samples, such as soils and rocks, there is an additional challenge for Ra determination by ICP-MS, which is to achieve complete recovery of the element from the sample matrix. Sulphates of Sr, Ba and rare earth elements (REE) are very difficult to dissolve, and Ra can be present as inclusions in such minerals (Abbasi et al., 2016; IAEA, 2010; Ulrich et al., 2012). For Ra determination, digestion with HNO_3, HF, HCl or combinations of these are commonly used (IAEA, 2014). However, this may not necessarily result in a complete recovery of Ra from the sample (Melgård, 2017), and consequently lead to underestimation of the Ra content.

2.1.4.3 Thorium (Th)

^{232}Th ($t_{½} = 1.4 \times 10^{10}$ y) constitutes the "parent" of another, natural decay chain. Although this radionuclide is not as abundant as ^{238}U in alum shale, it can still be present in smaller amounts. Th exists in nature as a tetravalent ion (Landa, 2007). Most Th compounds have low solubility, and Th is easily sorbed to clay and humic material or precipitated, giving a low mobility and low concentrations in water. Humic substances are considered particularly important for adsorption of Th, while the presence of inorganic anions such as carbonate, fluoride, phosphate, chloride and nitrate can increase the solubility by formation of complexes (EPA, 1999). The binding to dissolved organic matter can increase the mobility of Th (Moulin et al., 2004). Solubility is greatly enhanced when pH falls below 2-3, and substantial leaching from U tailings can occur due to acid rock drainage (Landa, 2007).

2.1.5 Other concerns

In addition to the environmental threat from the acidic, toxic leachate from alum shale investigated in this work, there are several other challenges associated with this and similar rock types. The acidic leachate aggressively attacks construction materials such

as concrete and steel, and can shorten the service life of constructions (Endre & Sørmo, 2015). Another challenge that is encountered is formation of sulphate minerals as sulphides are oxidized. These take up to several times greater volume than the former sulphide minerals, and swelling of the rock can occur, causing damage to building foundations and other constructions (Endre, 2013; Endre & Sørmo, 2015). This is illustrated above in Figure 3, wherein both precipitates and expansion of the layers of the alum shale are clearly seen. Undisturbed alum shale bedrock can also cause a human health hazard, as ^{222}Rn, one of the U daughters, is a radioactive noble gas and leaks into households, increasing the risk for lung cancer in humans (UNSCEAR, 2018). Lastly, the pyrite oxidation is an exothermic reaction, and large amounts of improperly stored alum shale can self-ignite (Endre & Sørmo, 2015). A notable example is provided by the case of the railway line from Jaren (a few kilometres from Gran, our study site) to Randsfjorden: At the end of the 19th century, alum shale was used as foundation for this 7 km railway stretch, and exothermic reactions of the rock caused the railroad to be free of snow for several years after construction (Løken, 2007).

2.2 Speciation, bioavailability and multiple stressors

The source and release scenario can determine the physico-chemical form (speciation) of elements, and thus mobility and bioavailability of the contaminants after a release (Salbu et al., 2004). Species of low molecular mass are assumed to be more mobile and potentially bioavailable than colloids and particles. Particles/solids can, on the other hand, act as sources for contamination over time, depending on the properties and weathering rates of the solid. Thus, information on source characterization and behaviour in different media are needed to estimate the long-term environmental impact of various types of contamination. ARD exemplifies the importance of the source and resulting matrix of the contaminant, as the formation of acid and a subsequent dramatic drop in pH will greatly enhance leaching of several stable and radioactive elements (Appelo & Postma, 2010). Mechanical breakdown of alum shale will lead to formation of everything from submicron-sized particles to large rock fragments. Finely crushed alum shale can be transported by water unless the debris is properly contained, and especially by high water discharge large amounts of particles can be washed away.

The mobility of various elements in the rock depends on their speciation, which changes as the rock is exposed to water and oxygen. Once released, the speciation of elements in

solution depends on a number of factors such as pH, ionic strength, alkalinity and the presence of inorganic ligands and dissolved organic matter (Landa, 2007; Lydersen et al., 2002; Moulin et al., 2004; Rosseland et al., 1992). Thus the acid from ARD is not only a problem because it reacts with the rock and thereby increases leaching, but also because the acid changes solubility and speciation of many elements. Potential effects on the environment can thus be greater, as certain elements will be more soluble by lower pH, and some elements are also more bioavailable by lower pH, and is taken up to a greater extent – and causes a greater effect. The low pH itself can also be harmful for biota.

For stable elements, uptake in an organism is necessary to cause a biological effect, while for radionuclides effects can also be caused by external radiation exposure. For α-emitters like ^{238}U and ^{226}Ra, that emit only low energy γ-radiation alongside α-particles, internal dose is, however, by far the most important (Loveland et al., 2006; UNSCEAR, 2018). High alkalinity and content of base cations like Ca^{2+} and Mg^{2+} can reduce mobility of trace elements in soil and compete for uptake in aquatic organisms, thus reducing uptake of certain elements (Lydersen et al., 2002).

When assessing effects on organisms in the laboratory, single elements or compounds are usually considered. These results are then used for assessing environmental risks and determining environmental quality standards for each contaminant individually. However, in nature, organisms will often experience a *mixed toxicity scenario* where the sum of the stressors can be additive (1+1 = 2), synergistic (1+1 = 3) or antagonistic (1+1 = 0.5), and the combined effect on biota can be difficult to predict (Eggen et al., 2004; Salbu et al., 2019). When exposed to alum shale leachate, organisms will likely experience stress from multiple stable and radioactive elements.

Alum shale is nutrient rich, and soils developed on alum shales are often fertile, though with elevated levels of unwanted stable and radioactive elements. Potentially harmful levels of trace elements have been found in food products grown on soils developed on black shales (Alloway, 2013).

2.3 Case study: Gran

When building the tunnel at Gran, Hadeland, Norway (Figure 5), black shales with potential for ARD were expected in the excavated bedrock, both from the alum shale formation (horizons 2-3a) and from the Galgeberg horizon (3bβ) (Endre, 2013; Owen et

al., 1990). The Galgeberg horizon is a part of the Tøyen formation, which was formed later in the Cambro-Ordovician period than the alum shale formation, and can thus be expected higher up in the succession (Owen et al., 1990; Pabst et al., 2016).

Figure 5: Tunnel construction at Gran.

Proper storage of acid-producing rock can be difficult and expensive to achieve, and consequences of improper storage can be detrimental for the local environment (Pipkin et al., 2008; Sørmo et al., 2015). In 2013, the Norwegian Public Roads Administration (NPRA – Statens Vegvesen) got permission to reuse black shale in the road foundation at Gran (Fjermestad et al., 2018). The local situation at Gran is unusual from the perspective of several factors important for avoiding ARD by the chosen storage conditions (Fjermestad et al., 2018). Of special importance were the geological formations surrounding the excavated bog, making it a suitable disposal site, and that the rock masses that were to be disposed were mainly unweathered, reducing the reactivity. Local storage is preferable to avoid large transportation costs and oxidation of debris during transit. Detailed investigations, risk analyses and preparations were made; see Fjermestad et al. (2018).

As a part of the 4-year research and development program NORWAT (Nordic Road Water) at NPRA, a project was initiated to examine the effects on biota from the construction work at Gran (Skipperud et al., 2016a). The project included fieldwork before and during the construction work as well as various laboratory experiments, and results from this project are included in the discussion.

3 Materials and methods

3.1 Developing a method for the determination of ^{226}Ra

Figure 6: ICP-QQQ (left) and high sample throughput of ^{226}Ra (right).

An Agilent 8900 triple quadrupole inductively coupled plasma mass spectrometry (ICP-QQQ, Figure 6) was used for developing a new detection method for ^{226}Ra. The instrument has an octopole collision-reaction cell positioned between two quadrupole mass filters (Q1 and Q2) (Figure 7). Nitrous oxide (N_2O) was used as reaction gas. The first quadrupole (Q1) of the instrument was set to introduce only mass 226 into the collision-reaction cell, where an oxygen atom transfers from N_2O to Ra^+. The last quadrupole (Q2) then selects mass 242 ($^{226}Ra^{16}O^+$). In this way, spectral interferences are excluded and the mass spectre is free of noise. This detection method for ^{226}Ra was first developed for samples that had been separated and concentrated with cation exchange (Melgård, 2017). In the present work, the method was adapted to direct measurements of a sample without concentration or separation.

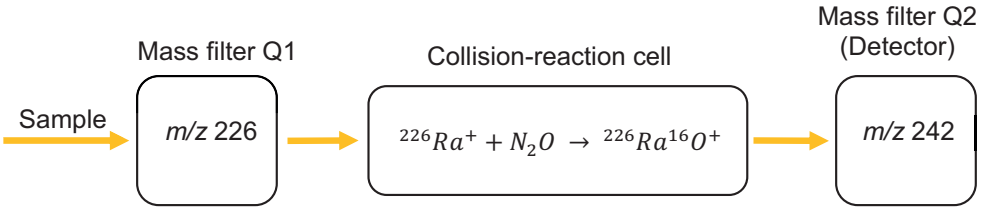

Figure 7: Overview of the measurements process of ^{226}Ra in the ICP-QQQ.

The full method is described in Paper I.

3.1.1 Analysis of more complex matrices

In order to study the effect of high total dissolved solids (TDS) on the sensitivity of the ICP-QQQ measurements of Ra, formation water from a Silesian underground coalmine

was tested. The samples were analysed after 30 times dilution. This formation water was used in an interlaboratory comparison conducted in 2015 by the Silesian Centre for Environmental Radioactivity, Central Mining Institute (GIG, Poland) (Bonczyk & Michalik, 2016).

Soil and rock samples were analysed after digesting 0.2-0.3 g sample with 2 mL HNO_3 + 4 mL H_3PO_4 in a Milestone UltraWAVE at 260 °C for 40 minutes. This acid combination was chosen based on results from Melgård (2017). The digested sample was diluted to 50 mL, left over night for sedimentation and further diluted 1+9 or 1+14 with 5 % (V/V) HNO_3 before analysis with the same method as water samples. The reason for the second dilution is to reduce the total dissolved solids (TDS) introduced into the instrument. The accuracy of the method was verified by the use of certified reference material (CRM) IAEA-448 (Radium-226 in soil from oil field) and reference material IAEA-314 (226Ra, Th and U in stream sediment), and found to be satisfying when the sample was measured the day after digestion. However, for the CRM IAEA-448, the measured concentration of ^{226}Ra in the digested sample was substantially lower when the sample was measured again after 12 weeks (Table 1). This was likely caused by a (co)precipitation or sorption to sedimented particle, as no decrease was seen when the sample was shaken to include the precipitate in the aliquot taken out for dilution. To avoid this problem completely, 2 mL of HBF_4 can be included in the acid mix used for digestion, see Table 1. Addition of 1 mL HBF_4 was not sufficient.

Table 1: Measured ^{226}Ra in digested CRM IAEA-448 with time after digestion, with or without including the bottom precipitate. Certified activity concentration is 19.05 ± 0.26. All samples were digested on the same day and measured on the same day 12 weeks later. N=3.

Dilution	**2 mL HNO_3 + 4 mL H_3PO_4 (kBq kg^{-1})**	**2 mL HNO_3 + 4 mL H_3PO_4 + 2 mL HBF_4 (kBq kg^{-1})**
On digestion day, w/precipitate	17.73 ± 0.02	17.7 ± 0.6
12 w after digestion, w/o precipitate	0.8 ± 0.2	17.3 ± 0.5
12 w after digestion, w/precipitate	18.6 ± 0.9	18 ± 1

To summarize, the acid mix used in Paper I (2 mL HNO_3 + 4 mL H_3PO_4) is adequate if the sample is diluted to the final volume for measurement shortly after digestion, or shaken before the final dilution to ensure inclusion of precipitates. The problem with precipitations is eliminated if 2 mL HBF_4 is used in the digestion; there were in fact no visible precipitations in the samples digested with this acid mix. The use of HBF_4 does

however come with greater health risk than the HNO_3+H_3PO_4 acid mix, and necessitates extra precautions to ensure a safe working environment.

3.2 Site description

At Gran (Figure 8), large amounts of alum shale were excavated during tunnel construction, and the debris was used to fill a bog situated at the southern entrance of the tunnel (Figure 9), partly serving as foundation for the new road. Debris from tunnel blasts containing > 10 % alum shale were stored in the disposal site (Fjermestad et al., 2018). Overall, 66 500 m^3 of alum shale (horizon 2-3a) and 10 500 m^3 black shale from the Galgeberg horizon (3bβ) were placed in the bog (Fjermestad et al., 2018). Most of the black shale was taken directly from the tunnel to storage in the disposal site to minimize oxidation and avoid further breaking down of rock during off/on loading for temporary storage (Fjermestad et al., 2018). Increased fragmentation of the rock would result in smaller particles with increasing surface area and thereby higher reactivity (Bierens de Haan, 1991).

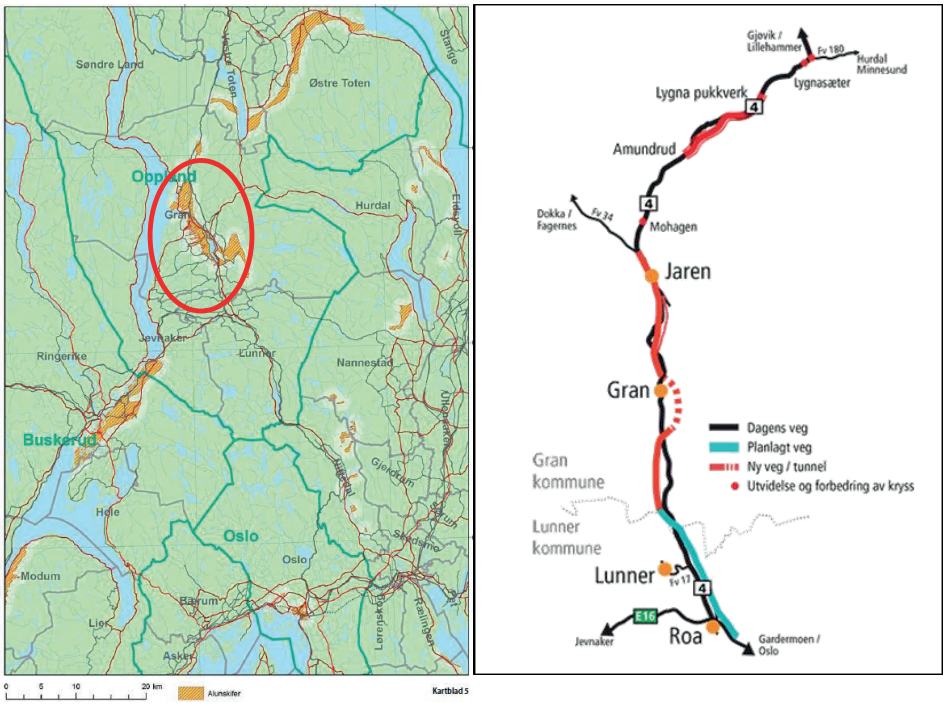

Figure 8: Left: Areas north of Oslo with alum shale (orange), the circle indicates the position of Gran (NRPA & NGU, 2011). Right: Plan for the building of the new road and tunnel (Rv. 4) (www.vegvesen.no).

Measures were taken to keep the debris submerged in water, and the disposal site was covered with a surface coating to reduce access to air.

Figure 9: Disposal site at Gran.

3.3 Sampling and sample treatment

Alum shale samples from tunnel: Alum shale excavated in the tunnel construction at Gran was used for leaching experiments (Papers II and III). About 10 kg unweathered alum shale debris was collected 19.05.2015 directly from a tunnel blast in the alum shale formation (chainage 9354), executed the same day. Handheld XRF (Niton™ XL3t GOLDD+ from Thermo Scientific) was used to ensure that U-rich material was collected. Alum shale from this batch was also used for uptake experiments with earthworms (Schöpke, 2017).

Water samples from disposal site: For comparison with experimental results, water in the disposal site was sampled in the period where disposal of masses in the site was ongoing, and the site was still an open pond. Sampling was performed 19/05/2015, 1 year and 2 months after the tunnel construction started, and thus also the storage of

masses. 1-2 months later the tunnel excavations were finished and the site was sealed. Conductivity and pH were measured *in situ,* directly in the disposal site, with handheld multi-meter in the Multi series from WTW. Unfiltered water samples were taken for analysis of anions. The water in the disposal site was sampled untreated for total analysis, and fractionated *in situ*: the water was filtrated (0.45 µm membrane filters, Millipore) for analysis of the dissolved fraction and ultrafiltrated (Amicon hollow fibre, nominal cut off 10 kDa) for analysis of the low molecular mass (LMM) fraction. A combined size and charge fractionation system was applied using hollow fibre interfaced with ion chromatography (cation resin Chelex and anion resin AG) (Barnes, 1975; Driscoll, 1984; Teien, 2005). The samples intended for ICP-MS analysis were acidified with 5 % (V/V) ultrapure HNO_3. All water samples were taken in triplicates, stored in the dark at 4 °C, and analysed as described in sections 3.6 and 3.7.

Figure 10: Alum shale used for the experiments (before crushing, left), jaw crusher for crushing of alum shale debris (middle) and sieving of alum shale through 2 mm (right).

Sample handling: The collected alum shale was stored until experiments were initiated; six months for the AOC and LOC treatments, and 1.5 years for the DRY and WET treatments. To get fresh rock surface, pieces larger than 1-2 cm were selected and crushed with a jaw crusher (Figure 10), sieved through a 2 mm mesh, and stored under nitrogen until experiment start-up (1-3 days). The debris was crushed in air, as this best simulates what happens in construction work.

3.4 Alum shale characterization

The alum shale debris (crushed as described in section 3.3) was characterized before and after the leaching experiments of Paper II and Paper III.

Total element concentrations were determined by ICP-MS (see section 3.7) after digestion. 0.25 g of debris in triplicates was digested at 260 °C for 40 min in a Milestone UltraCLAVE with the following acid mixtures: 5 mL HNO_3 (for Li, P, S, Ca and Fe), 5 mL HNO_3 + 1 mL HF (Mn, Cu, Zn, As, Mo, Cd, Sn, Sb and U), and 2 mL HNO_3 + 4 mL H_3PO_4 (Be, Na, Mg, Al, K, V, Cr, Co, Ni, Sr, Ba, La, Ce, Pr, Nd, Sm, Eu, Gd, Dy, Ho, Er, Tm, Yb, Lu, Pb, ^{226}Ra and Th). Rh was added as internal standard. Digested samples were diluted to 50 mL. Certified reference materials were digested and measured in parallel to the alum shale: NIST 2709a San Joaquin Soil and NSC ZC 73007 soil (all three digestions), NIST 2710a Montana I soil (only HNO_3 digestion), and NSC DC 73325 soil (only HF digestion). When determining ^{226}Ra content, reference materials IAEA-314 (sediment) and IAEA-448 (soil) were used. Results for all reference materials where within the uncertainties of certified values.

The pH of the debris was measured at room temperature in a 1+2 V/V mix of debris and water left overnight, with a handheld multi-meter in the Multi series from WTW. Organic matter was estimated from loss on ignition (550 °C overnight). Total organic (TOC) and inorganic (TIC) carbon in the debris were measured by coulometry. The TOC was only measured in the starting material and used for geochemical characterization (see section 3.9). Particle size distribution was determined for a 10 g sample, where organic matter had been removed by heating with H_2O_2, by wet sieving through 0.06 mm (removing the sand fraction) and separating silt and clay (<0.002 mm) by sedimentation according to Stokes' law. Mineral composition was determined by powder X-ray diffraction (XRD) on a D8 Discover (Bruker). The XRD diffractograms were analysed with TOPAS software for peak identification using a reference spectra library, and quantified by the Rietveld refinement technique.

Elemental maps of alum shale debris were obtained by micro X-ray fluorescence spectroscopy (μ-XRF) using a Bruker M4 Tornado (Bruker Nano GmBH) equipped with a Rh target excitation source operated at 50 kV, 200 μA and 25 μm spot size, and a dual XFlash® silicon drift detector. A small container was filled with alum shale debris and the surface was pressed and flattened with an iron spatula. A 7.0 mm × 5.6 mm area was

mapped under vacuum (20 mbar) using a 20 μm step size, dwell time of 10 ms pixel^{-1}, and 4 measuring cycles.

3.5 Leaching experiments: experimental design

The leaching experiments were designed to investigate the effect of different storage conditions on the leaching from alum shale, investigating varying access to oxygen, drying of the debris and concentrations effects. Two different experiments were performed, with a total of four different treatments (Figure 11). The specifics for each experiment are described in the subchapters below.

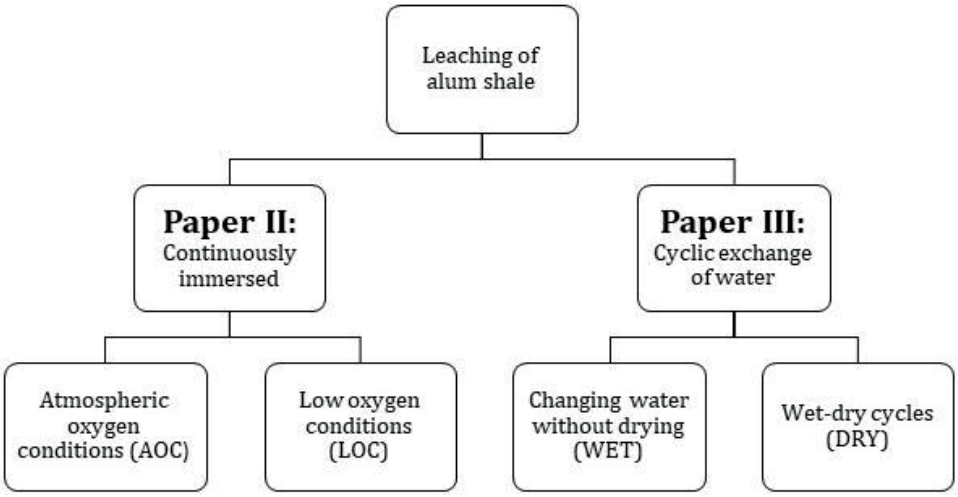

Figure 11: The different treatments in the leaching experiments.

All treatments were performed with 1 part alum shale to 10 parts leachant (synthetic rainwater). Synthetic rainwater was prepared with the same quality as rain falling in Hurdal, a meteorological station in a 27 km radius from the alum shale sampling point (Aas et al., 2015). The average ion concentrations and pH (4.93) of the rainwater in 2010-2014 was used. One sample consisting of only artificial rainwater (no debris) was kept in parallel to each treatment as a blank, and treated, sampled and analysed in the exact same way to monitor contamination and other unintended effects in the experiment.

Jeng (1991) observed a significant effect of temperature on the leaching from alum shale. The batch experiments were performed at 10 °C (Figure 12) as this is an environmentally relevant temperature in Scandinavia. The samples were kept dark to exclude the effect of photodegradation.

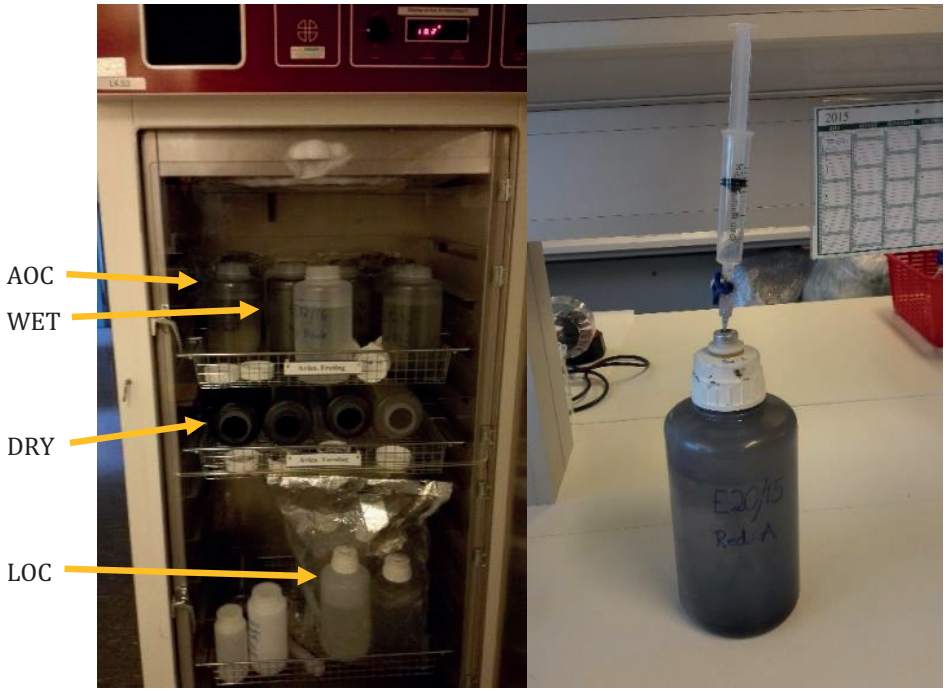

Figure 12: Leaching samples kept at 10 degrees with different access to air (left), gas sampling from LOC treatment (right).

All samples were shaken by hand 2-3 times per week to get all of the debris in contact with the leachant. This was preferred over continuous shaking or rolling of samples, as that could cause physical breakdown of particles giving an observed increase of element concentrations in the colloidal fraction unrelated to leaching processes.

Leachate aliquots were taken out as a function of contact time (Table 2) for leachate analyses as described in sections 3.6 and 3.7. The sampled volume was replaced with synthetic rainwater.

Table 2: Duration and sampling points of leaching experiments. Blue: Submerged, low oxygen. Yellow: Submerged, atmospheric oxygen, Red: drying of debris in air. Sampling points are approximately marked by X.

Week	1	2	3	4	5	6	7	8	9	10	11	12	13	14	15	16	17	18	19	20	21	22	23	24	25	26	27	28	…	52
LOC	xxx			x								x																x		x
AOC	xxx			x								x																x		x
WET	xxx		x		x	xxx		x		x	xxx		x		x	xxx		x		x	xxx		x		x	xxx		x		
DRY	xxx		x			xxx		x			xxx		x			xxx		x			xxx		x			xxx		x		

3.5.1 Paper II: Continuously immersed, AOC and LOC treatments

Batch experiments were chosen to mimic the storage conditions applied at Gran. For all samples, 150 g crushed rock was used to 1.5 L synthetic rainwater, and the experiment lasted for 1 year. Two treatments were used:

AOC: Three samples were kept continuously immersed in synthetic rainwater and open to the atmosphere (atmospheric oxygen conditions, AOC), contained in 2 L Nalgene polypropylene bottles (Thermo Scientific).

LOC: Three samples were kept continuously immersed in synthetic rainwater under low oxygen conditions (LOC), contained in 2 L heavy-duty polypropylene vacuum bottles (Nalgene, Thermo Scientific) inside bags of oxygen-excluding material (FireDebris Tubular Rollstock from Ampac). The samples were handled and stored under a N_2 atmosphere, and had septa installed in the lid for sampling of the gas phase (Figure 12). The synthetic rainwater used for this treatment was flushed with nitrogen for about 1.5 hours before use, and the oxygen content was measured to 0.01 mg L^{-1}. The setup did not completely exclude oxygen, and thus measurements of oxygen in both water and gas phase are presented in section 4.2.2.

Water aliquots were sampled at 1 hour, 24 hours and at 1, 4, 12, 28 and 52 weeks after first mixing of water and rock (Table 2).

The AOC and LOC treatments (Paper II) were chosen to investigate two possible scenarios of relevance to the storage site at Gran, depending on how successful the design of the storage site is in excluding oxygen. The two treatments could also mimic situations that might occur at different time points after establishing the site, or at the same time with increasing oxygen access in the upper part of the site and gradual depletion downwards.

3.5.2 Paper III: Cyclic exchange of water, WET and DRY treatments

The effect of exchange of water on the leaching from the alum shale was investigated in another batch experiment. Crushed alum shale (180 g) was mixed with synthetic rainwater (1.8 L) in 2 L Nalgene polypropylene bottles. Two treatments were used:

DRY: Four samples were exposed to wet and dry cycles where the debris was kept alternately in water (3 weeks) and air (2 weeks). The wet cycle was repeated 6

times with dry periods between. In the dry periods, the debris was dry after a bit more than a week.

WET: The water of four samples was changed every 5 weeks without drying the debris. The cycles were going in parallel to the DRY samples, and there were thus 5 cycles of 6 weeks and a last cycle of 3 weeks.

At the end of each wet period, water was carefully lifted off the sedimented alum shale debris using a peristaltic pump to minimize loss of particles.

The treatments with cyclic exchange of water (Paper III) were included to investigate what happens in the case of poor or uncontrolled storage conditions. The DRY treatment mimics what could occur in the upper part of the storage site, e.g., in an especially dry summer giving fluctuating ground water level. The WET treatment mimics the conditions that could occur in the storage site if water is frequently exchanged, but below fluctuations of the groundwater level, like during snowmelt or heavy rain.

The WET and DRY treatments lasted for a total of 28 weeks. Aliquots for analysis of leachate quality were taken out at 1 h, 24 h, 1 and 3 weeks after starting a cycle (mixing debris with synthetic rainwater) for all samples, and additionally at 5 weeks for the WET samples (see Table 2).

3.6 Leachate analysis

Leachate aliquots were collected with a syringe and split for different analyses. Oxygen concentration (with a FDO® 925 Optical Dissolved Oxygen Sensor), conductivity, oxidation-reduction potential (ORP) and pH were measured immediately after sampling on untreated aliquots with handheld multi-meter in the Multi series from WTW. E_h was calculated from ORP by adding 207 mV, according to instructions from producer.

Samples for ICP-MS analyses, alkalinity, dissolved organic carbon (DOC) and anion chromatography were immediately filtered by 0.45 µm polyethersulfone membrane syringe filters (VWR), and selected subsamples were also filtered by 10 kDa Amicon® Ultra-15 centrifugal filter devices from Merck Millipore for analysis of low molecular mass (LMM) components by ICP-MS. The samples were stored in the dark at 4 °C. Prior to measurements, samples for ICP-MS were acidified with 5 % (V/V) ultrapure HNO_3. Alkalinity was measured by colorimetry according to ISO 9963-1:1994 with titration

down to pH 4.5. Anions were quantified by ion chromatography using a Lachat IC5000 system equipped with a Dionex™ IonPac™ AS22-Fast IC column and a Dionex AMMS™ 300 ion suppressor, both from Thermo Scientific. DOC was determined with a TOC-VCPN analyser from Shimadzu, but all samples were below the detection limit (DL) (1.8 mg L^{-1}).

When sampling the leachate from the two leaching experiments, samples were collected of the dissolved fraction (<0.45 µm) and for certain time points also of the low molecular mass fraction (<10 kDa, LMM). This allowed for the identification of the colloidal fraction (= dissolved fraction – LMM fraction) in addition to the two measured fractions. Unfiltered water, giving the total concentrations, was not sampled. This would include the particulate fraction, which would mainly depend on the size of the crushed alum shale added to the experiment and the time since the sample was last agitated.

3.7 ICP-MS analysis

Water samples from fieldwork, synthetic rainwater, leachate and digested alum shale were analysed for Li, Be, Na, Mg, Al, P, S, K, Ca, V, Cr, Mn, Fe, Co, Ni, Cu, Zn, As, Sr, Mo, Cd, Sn, Sb, Ba, La, Ce, Pr, Nd, Sm, Eu, Gd, Dy, Ho, Er, Tm, Yb, Lu, Pb, ^{232}Th and ^{238}U with Agilent 8800 or 8900 Triple Quadrupole ICP-MS. Ge, In, Ir and Bi were added online as internal standards. The instrument was switched between He, O_2 and no gas in the collision/reaction chamber to remove interferences. On each analysis day, an in-house standard covering all analysed elements except Sn was measured for quality control.

^{226}Ra was measured in samples as described in section 3.1 and Paper I.

3.8 Gas-phase measurements

Samples of the gas phase of the LOC treatment (Paper II) were analysed with an Agilent 7890A Network Gas Chromatograph to determine the levels of O_2, N_2, CH_4 and CO_2. The results are, however, only semi-quantitatively described as the gas phase was exchanged with N_2 during each water sampling.

3.9 Statistics and data treatment

Figures and tables show average ± one standard deviation of replicate samples. T-tests were used for identifying significant differences between treatments (Miller & Miller, 2005). Grubbs test was used for identifying outliers.

In the sampling at 28 weeks, one of the LOC samples showed an unexpectedly high level of oxygen in both the water and the gas phase, which was reflected in higher concentrations of several elements making the sample more similar to the AOC samples. Thus, for the two last sampling points, data from this sample were considered as outliers and were omitted, and the presented LOC data represents only two samples.

In the AOC-LOC experiment, the leachate concentrations at 12 months and the concentrations in the alum shale starting material were used to calculate the relative mass fraction (%) of each element that leached during the experiment. In the cyclic experiment, the mass in solution at the end of each wet period were summed for each sample individually. This mass was used together with the concentration in the starting material to calculate the leached fraction of an element.

Geochemical characterization of the alum shale sample was provided by the Norwegian Geotechnical Institute (NGI). The characterization was made by comparing data from whole-rock analysis (elemental composition, TIC and TOC) and calculated acidification and neutralization potentials with an existing database of Cambro-Ordovician black mudrocks from the Oslo region (Norway), as described by Pabst et al. (2016). The acidification potential (AP) of the debris was estimated by assuming that all S in the rock comes from sulphides behaving like pyrite, and the neutralization potential (NP) was estimated from the TIC, assuming these carbonates behave like calcite (Lawrence & Wang, 1996; Pabst et al., 2016).

For comparison with measured alkalinity, the solubility of calcite was used to estimate the alkalinity at the prevailing conditions in the experiments, as described by vanLoon and Duffy (2011). For the LOC samples, measured CO_2 concentrations were used for the calculations, while for the AOC samples the atmospheric concentration of 390 ppm was used (Hartmann et al., 2013).

4 Results and discussion

The results and discussion are based on the attached papers. In Paper I, a new method for direct determination of ^{226}Ra in water and digested geological samples is described. In Papers II and III, alum shale collected at Gran is characterized and mobility of radionuclides and stable elements from the debris is investigated under different conditions.

4.1 High throughput, direct determination of ^{226}Ra in water and digested geological samples – Paper I

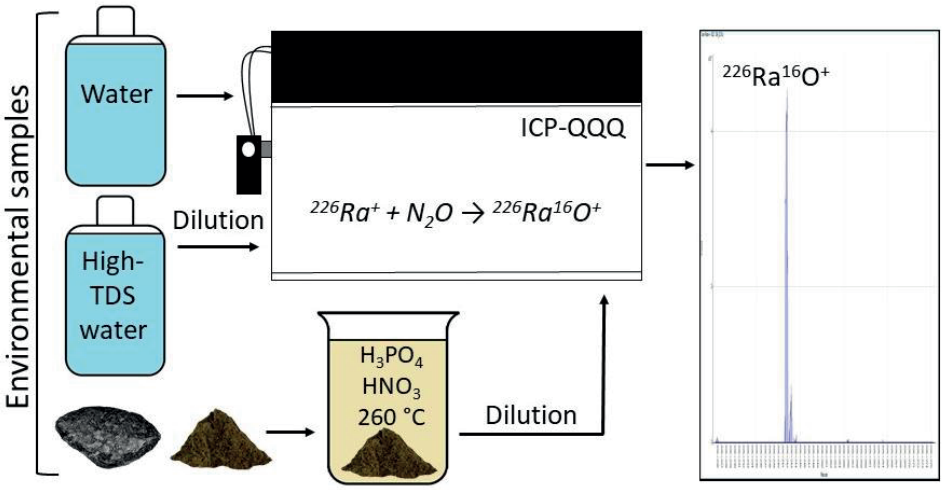

Figure 13: Overview of the developed method for analysis of ^{226}Ra in environmental samples (Paper I: Wærsted et al., 2018).

In order to handle efficiently the large number of ^{226}Ra-determinations required for this study, a method was developed for direct measurements of ^{226}Ra in water samples with triple quadrupole Inductively Coupled Plasma Mass Spectrometry (ICP-QQQ) as described in materials and methods (section 3.1) and Paper I (Wærsted et al., 2018); see overview in Figure 13. The use of N_2O as reaction gas introduced a highly chemoselective step into the process to ensure that no separation before analysis was necessary. Analysis of water samples was achieved within 2 minutes on a running instrument. To the authors' knowledge, no other methods provide results for ^{226}Ra as fast and simple as the proposed method, for neither water nor geological samples. The preparation of geological samples is subject to microwave digestion capacity, and with our instrumentation, preparation and analysis of 15 samples can be completed in 3 hours.

The detection limit (DL) for water samples was 0.42 pg L^{-1} (15 mBq L^{-1}). Samples with lower concentrations can be concentrated before analysis, e.g., according to Lagacé et al. (2017) or Zhang et al. (2015). However, the DL achieved with direct measurements is compliant with the specifications for methods used for routine analysis of drinking water quality according to European and U.S. regulations (DL of 1 pg L^{-1}). This means that drinking water quality can be better monitored as more samples can be analysed and results are available almost immediately. Water samples with high total dissolved solids (TDS) were measured after dilution, with accordingly higher DL. Using methods for concentration and separation developed for high-TDS samples before analysis could substantially lower the DL, see e.g. Lagacé et al. (2017) or Zhang et al. (2015).

Soil and rock samples were measured with the same method as used for water samples, after acid (HNO_3 + H_3PO_4) digestion and dilution, resulting in a limit of detection of 0.75 ng kg^{-1} (27 Bq kg^{-1}) for the original sample material. For some samples, reduction in dissolved ^{226}Ra was observed after storage of a digested sample. This seemed to be related to (co)precipitation or sorption to sedimented particles in the sample. If digested samples are to be stored before analysis, this issue can be avoided by a) diluting the sample to the final volume and acid concentration for measurement right after digestion (storage was then not a problem), b) shaking the stored sample vigorously before the final dilution, to ensure inclusion of sedimented particles, or c) including HBF_4 in the acid mix used for digestion. The estimated average of ^{226}Ra in the continental crust is about 33 Bq kg^{-1} (IAEA, 2014), although actual background levels vary by location. Soil ^{226}Ra concentrations in areas with normal background (i.e., not areas of high natural background) vary from 3.7 to 126 Bq kg^{-1} (IAEA, 2014). Thus, the developed method is sufficiently sensitive to detect elevated concentrations of ^{226}Ra in rock and soil.

For samples with about 5 pg ^{226}Ra L^{-1}, the relative standard deviation (RSD) of repeated measurements (precision) was about 10 %, but varied with the complexity of the sample matrix, and the RSD decreased as sample concentration increased (see Tables 3 and 4 in Paper I). The accuracy of the method was tested with digested soil reference materials and found to be adequate, see Table 5 in Paper I.

A brief summary of the method for the different sample types is provided in Table 3. The key advantages of this direct analysis method are short preparation time, low labour intensity, low sample input (2 mL for water samples, 0.2 g for geological material), high

sample throughput (2 min sample to sample, > 150 samples measured in 8 h) and use of standard ICP-QQQ hardware. Considering the opportunity for processing large numbers of samples with minimal effort, in a wider context, the method may prove indispensable for improving emergency preparedness, environmental monitoring and collection of large datasets for the purpose of environmental modelling.

Table 3: Overview of the proposed methods for detecting ^{226}Ra in water, water with high total dissolved solids (TDS) and geological samples. Detection limit (DL) and quantification limit (QL) are calculated as 3 and 10 times the standard deviation of the blank concentrations, respectively (Paper I; Wærsted et al., 2018).

	Water	**High-TDS water**	**Geological material**
Sample size needed	2 mL (8 mL)	< 1 mL	0.2 g
Sample preparation	Acidification	Acidification Dilution (30×)	Acid digestion (1.5 h/15 samples) Dilution
Analysis time (sample to sample)	2 min	2 min	2 min
Sample throughput	> 150 samples/8 h > 400 samples/24 h	> 150 samples/8 h > 400 samples/24 h	For digested samples: > 150 samples/8 h > 400 samples/24 h
Detection limit	0.42 pg L^{-1} 15 mBq L^{-1}	17 pg L^{-1} 0.61 Bq L^{-1}	0.75 ng kg^{-1} 27 Bq kg^{-1}
Quantification limit	1.4 pg L^{-1} 51 mBq L^{-1}	56 pg L^{-1} 2.1 Bq L^{-1}	2.5 ng kg^{-1} 91 Bq kg^{-1}

The described method was successfully applied to water and alum shale samples from the leaching experiments (Paper II and III). The use of this method allowed for collection of detailed information on the behaviour of ^{226}Ra in the leaching experiments, which would not be (practically) possible using traditional methods requiring large sample volumes and work-intensive sample preparation.

4.2 Mobility of NORM and stable elements in alum shale – Paper II & III

4.2.1 Characterization of the alum shale

Values of pH, total inorganic carbon (TIC), loss on ignition, total organic carbon (TOC) and particle size distribution for the alum shale used as starting material in the two experiments and of the debris after the experiment are presented in Table 4. The TIC concentrations of both the untreated and treated samples were similar to what has been found in other alum shales in Norway, and in the lower range of other Cambro-Ordovician black shales in Norway (Pabst et al., 2016). The particle size distribution is important as size of particles are determining for the surface area and thus reactivity and weathering rates. The particle size distribution was quite similar in the two experiments with the

main part of the debris being sand sized, a smaller fraction silt sized and little debris in the clay fraction.

The most marked changes can be seen for the cyclic experiment, where the pH of the debris was reduced with almost a unit from before the experiment to after, and the TIC was reduced to less than half of the original value in both treatments ($p < 0.0009$).

Table 4: pH, total inorganic carbon (TIC), loss on ignition (LOI), total organic carbon (TOC) and particle size distribution in alum shale debris before and after leaching under atmospheric (AOC) or low (LOC) oxygen conditions, or with cyclic exchange of water either with (DRY) or without (WET) periods of drying.

	n	pH	TIC	LOI	TOC	Sand	Silt	Clay
						2-0.06 mm	60-2 µm	<2 µm
			%	%	%	%	%	%
AOC-LOC exp.								
Starting mat.	1	7.31	0.29	13	8.9	86.6	12.2	1.2
AOC	3	7.48 ± 0.01	0.25 ± 0.06	13.1 ± 0.3	-	-	-	-
LOC	3	7.36 ± 0.03	0.25 ± 0.01	13.1 ± 0.1	-	-	-	-
Cyclic exp.								
Starting mat.	1[a]	7.53	0.22 ± 0.02	12.3	7.8	90.4	8.5	1.1
WET	4	6.62 ± 0.07	0.09 ± 0.01	12.6 ± 0.2	-	-	-	-
DRY	4	6.65 ± 0.30	0.10 ± 0.01	12.7 ± 0.2	-	-	-	-

[a] For the TIC analysis of the starting material for the cyclic experiment, n=2.
- : samples have not been measured

The concentrations of selected elements determined with ICP-MS in the unleached alum shale used for the two leaching experiment are presented in Table 5. In general, the starting material for the two experiments had quite similar concentrations of most elements. The greatest differences was seen for Ca which was 50 % higher in the debris used for the AOC-LOC experiment compared to the cyclic experiment. Differences above 15 % were seen for Cr, Mn, Ni, Sr, Mo, Ba and ^{226}Ra. Most of these differences are not significant ($p = 0.05$), but simply reflects the heterogeneity of the material.

Table 5: Total element concentrations of the alum shale used for the leaching experiments, n=3.

		Alum shale AOC-LOC experiment [a]	Alum shale Cyclic experiment	
Group 1	Li	31.3 ± 0.3	32 ± 0.6	mg kg^{-1}
Alkali metals	Na	3.23 ± 0.03	3.3 ± 0.2	g kg^{-1}
	K	42 ± 1	39 ± 3	g kg^{-1}
Group 2	Mg	9.0 ± 0.3	9.2 ± 0.4	g kg^{-1}
Alkaline earth metals	Ca	13 ± 5	8.8 ± 2.3	g kg^{-1}
	Sr	146 ± 7	182 ± 77	mg kg^{-1}
	Ba	0.8 ± 0.1	0.66 ± 0.04	g kg^{-1}
	^{226}Ra	35 ± 2	30 ± 6	ng kg^{-1}
		1.28 ± 0.07	1.1 ± 0.2	kBq kg^{-1}
Groups 4-11	V	3.08 ± 0.08	2.9 ± 0.2	g kg^{-1}
Transition metals	Cr	139 ± 29	118 ± 8	mg kg^{-1}
	Mo	226 ± 4	265 ± 4	mg kg^{-1}
	Mn	272 ± 52	311 ± 12	mg kg^{-1}
	Fe	32 ± 3	33 ± 4	g kg^{-1}
	Co	23.4 ± 0.1	22 ± 2	mg kg^{-1}
	Ni	438 ± 34	366 ± 27	mg kg^{-1}
	Cu	141 ± 5	146 ± 1	mg kg^{-1}
Group 12	Zn	514 ± 36	564 ± 112	mg kg^{-1}
	Cd	11.2 ± 0.8	12 ± 2	mg kg^{-1}
Group 13	Al	79 ± 1	77 ± 4	g kg^{-1}
Group 14	Pb	47 ± 1	47 ± 2	mg kg^{-1}
Group 15	As	88 ± 4	81 ± 1	mg kg^{-1}
	Sb	19.1 ± 0.8	20 ± 0.4	mg kg^{-1}
Group 16	S	31 ± 3	32 ± 4	g kg^{-1}
Actinides	^{232}Th	14.8 ± 0.7	14.1 ± 0.9	mg kg^{-1}
		0.060 ± 0.002	0.0057 ± 0.004	kBq kg^{-1}
	^{238}U	107 ± 2	110 ± 3	mg kg^{-1}
		1.34 ± 0.02	1.37 ± 0.03	kBq kg^{-1}

[a] AOC = atmospheric oxygen conditions, LOC = low oxygen conditions.

Table 6 shows the minerals identified in the alum shale debris, together with the relative fractions (%) that these minerals contribute to the measured content of elements in the debris. Potential impurities in the different minerals are also listed, i.e., what has been found as impurities in such minerals by others. However, which elements that will in fact occur as impurities will vary with the geographic origin of a rock sample as this greatly depends on the local conditions during formation of the material (Abraitis et al., 2004; Botkin & Keller, 2005). Also, this list is not specific for alum shales, but applies to the separate minerals as part of different types of rocks.

Muscovite, quartz, pyrite and calcite were found in the alum shale debris using XRD, as well as about 30 % amorphous material. Slight variations are seen for the debris used for the two leaching experiments, and the biggest difference is seen for calcite. While this difference is likely not significant, similar differences in TIC and Ca concentrations of the samples support that is an actual difference in calcite content.

The measured amorphous material includes about 13 % organic matter. The organic matter in alum shale can originate both from marine and terrestrial sources (Armands, 1972). Terrestrial organic matter will often be humic matter, which is one of the sources of U in the alum shale (Swanson, 1961). Both Armands (1972) and Fjermestad (2013) found U in all fractions tested by using various leaching techniques on alum shale. Armands (1972) found that U was correlated to K-feldspar in the alum shale as well as detrital minerals (zircon, titanite, phosphorite), with organic matter (probably fixed as uranyl humates) and with organic sulphur and pyrite. However, Armands (1972) also hypothesized that some of these relations were simply covariation and that U can occur in alum shale as dispersedly distributed UO_2 or amorphous pitchblende, and not as part of one of the major phases detected by XRD. For alum shale from Gran, advanced microanalytical characterization has shown that U, Th and more elements (Al, V, Pb, Mg, Fe and Si) were associated with high density inclusions in the rock (Skipperud et al., 2016a). This indicates that the radionuclides are present in a different phase than the phases detected with XRD. The results also showed that Ca, Mg and Mn were associated with each other, which might indicate that the three are associated with calcite. Mn followed Ca especially closely.

For the AOC-LOC experiment, no changes in mineral concentrations were measured in the leached debris after the experiment, while in the cyclic experiment the calcite concentration was reduced to about a third after the experiment for both the WET and the DRY treatment (see table 3 in Paper III). Pyrite concentrations did, however, not change in either experiment, despite expected pyrite oxidation.

Table 6: Mineral content of the alum shale starting material used for the leaching experiments, measured by XRD. "Mineral contribution" is the contribution of given mineral to the concentration of given element (measured by ICP-MS). "Potential impurities" lists elements found as impurities in given mineral in other places.

			AOC-LOC experiment [e] (Starting material)		Cyclic experiment (Starting material)			
Mineral	**Structure formulae**	**Elements**	**Content**	**Mineral contribution**	**Content**	**Mineral contribution**	**Potential impurities**	**Reference impurities**
			%	%	%	%		
Muscovite	$KAl_2(AlSi_3O_{10})(F, OH)_2$		43.7		42.2		Cr, Li, Fe, V, Mn, Na, Cs, Rb, Ca, Mg, H_2O	Mindat.org (2019b)
		K		102		106		
		Al		112		111		
Quartz	SiO_2		19.2		20.8		Not expected [b]	Mindat.org (2019d)
Pyrite	FeS_2		3.5		4.3		Ag, As, Au, Bi, Cd, Co, Cu, Hg, Mo, Ni, Pb, Pd, Ru, Sb, Se, Sb, Sn, Te, Tl, V, Zn and U [c]	Abraitis et al. (2004); Armands (1972); Bierens de Haan (1991); Mindat.org (2019c)
		Fe		51		61		
		S		60		72		
Calcite	$CaCO_3$		2.4		1.7		Mn, Fe, Zn, Co, Ba, Sr, Pb, Mg, Cu, Al, Ni, V, Cr, Mo	Appelo and Postma (2010); Mindat.org (2019a)
		Ca		74		76		
		C [a]		100		92		
Amorphous mat.	n.a.	n.a.	30.9	n.a.	31	n.a.	U [c, d]	Armands (1972); Swanson (1961)

[a] Measured TIC is used for C in calcite
[b] Quartz crystals are generally very pure (>99.5 % SiO_2)
[c] Where there is U, the daughters will also be present
[d] U is expected to be associated with organic matter
[e] AOC = atmospheric oxygen conditions, LOC = low oxygen conditions
n.a.: not applicable

Calcite was very heterogeneously distributed in the samples. This is reflected in high standard deviations for Ca in ICP-MS measurements of debris and for calcite in XRD results. It was also confirmed by XRF, see Figure 14. Calcite in alum shale can be present as nodules (Pabst et al., 2016), and that seems to be the case here.

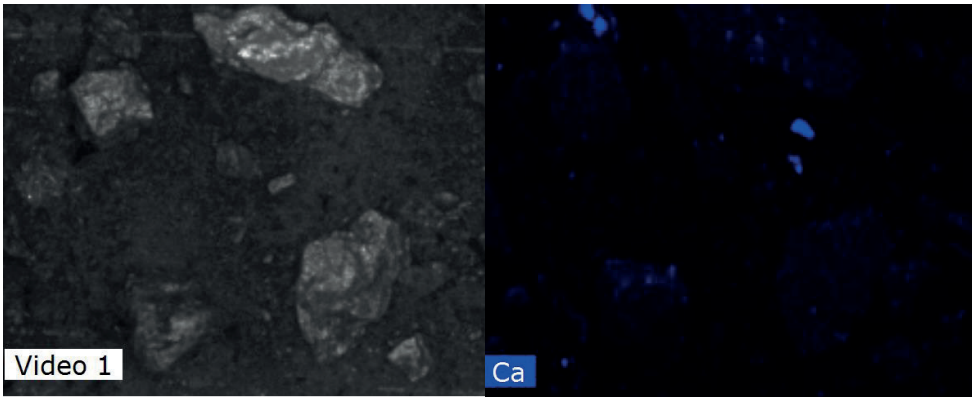

Figure 14: XRF results for alum shale debris from Gran. Left: Picture of the sample analysed. Right: signal for Ca in the same section. The colour intensity reflects the relative fluorescence signal for the given element

4.2.1.1 Geochemical characterization of the alum shale

The method of Pabst et al. (2016) for geochemical characterisation of Norwegian Cambro-Ordovician black mudrocks is based on comparing whole rock analysis with a database containing several hundred samples from the Cambro-Ordovician stratigraphy collected in the Oslo area. Triangular plots as well as plots of acidification potential (AP) vs. neutralization potential (NP) and Fe vs. S are used to see how the sample places itself among the samples in the database.

The geochemical characterization placed the collected alum shale batch in horizon 3a of the alum shale formation, see Figure 15 - Figure 19. Though, for some parameters, the samples position themselves in horizon 2. Horizon 3a (and also horizon 2) is expected to be acid producing, and to have high levels of NORM (U-series) and several stable trace elements (Owen et al., 1990; Pabst et al., 2016). In the figures, the larger symbols represent the measured replicates when characterizing the alum shale used in Paper II (AS1-AS3) and paper III (AS4-AS6), while the other points represent samples from the different horizons in the Cambro-Ordovician stratigraphy, from a database collected by the Norwegian Geotechnical Institute (NGI).

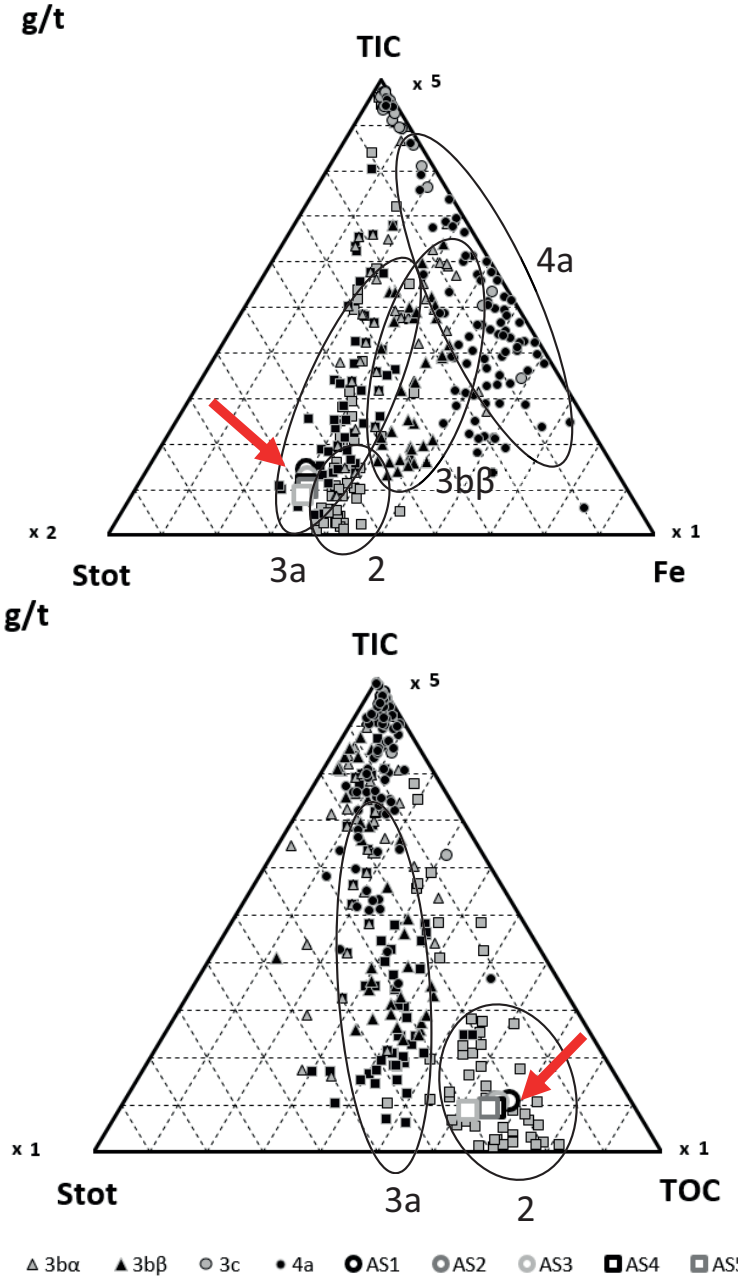

Figure 15: Selected triangular plots of samples from the Cambro-Ordovician stratigraphy in the Oslo area. Black circles show the grouping of the different horizons. AS1-AS3 are replicate measurements of the debris used for the AOC-LOC leaching experiment, and AS4-AS6 of the debris used for the cyclic experiment. The arrow marks the position of these samples. The other points represent samples from the different horizons in the Cambro-Ordovician stratigraphy, from a database by the Norwegian Geotechnical Institute (NGI). Stot = total sulphur content.

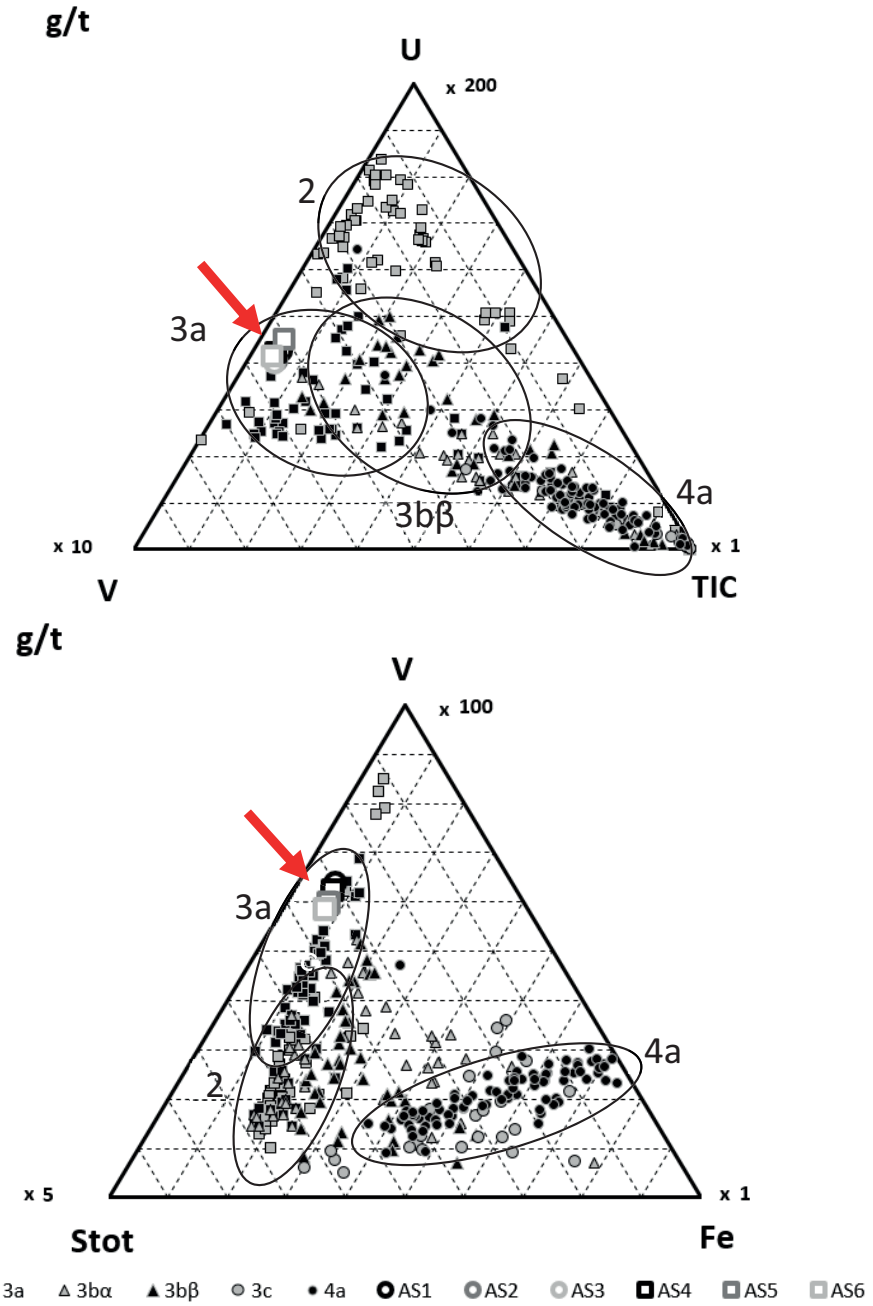

Figure 16: Selected triangular plots of samples from the Cambro-Ordovician stratigraphy in the Oslo area. Black circles show the grouping of the different horizons. AS1-AS3 are replicate measurements of the debris used for the AOC-LOC leaching experiment, and AS4-AS6 of the debris used for the cyclic experiment. The arrow marks the position of these samples. The other points represent samples from the different horizons in the Cambro-Ordovician stratigraphy, from a database by the Norwegian Geotechnical Institute (NGI). Stot = total sulphur content.

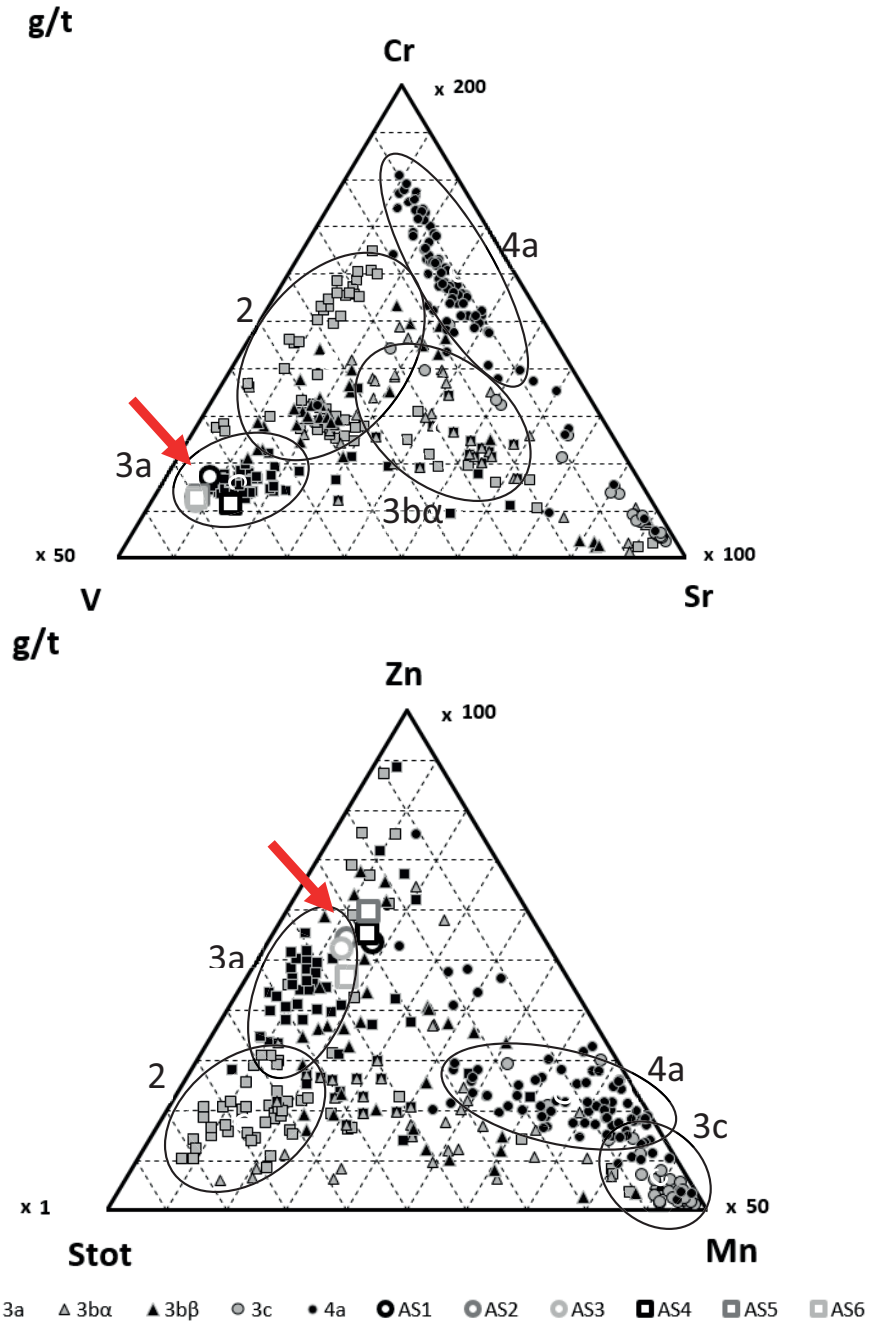

Figure 17: Selected triangular plots of samples from the Cambro-Ordovician stratigraphy in the Oslo area. Black circles show the grouping of the different horizons. AS1-AS3 are replicate measurements of the debris used for the AOC-LOC leaching experiment, and AS4-AS6 of the debris used for the cyclic experiment. The arrow marks the position of these samples. The other points represent samples from the different horizons in the Cambro-Ordovician stratigraphy, from a database by the Norwegian Geotechnical Institute (NGI). Stot = total sulphur content.

For the TIC, only one replicate of the debris for each experiment was measured. Thus, the three replicates in Figure 18 have different values for AP (estimated from S), but the same for NP (estimated from TIC). For the AOC-LOC experiment (Paper II), the average calculated AP of the debris was 96.5 kg $CaCO_3$ eq t^{-1}, and the NP was 24.4 kg $CaCO_3$ eq t^{-1}, giving a ratio of 0.25. For the cyclic experiment (Paper III), these values were 99.9 kg $CaCO_3$ eq t^{-1}, 18.3 kg $CaCO_3$ eq t^{-1}, and 0.18, respectively. Thus, the debris used for both experiments were clearly expected to be acid producing.

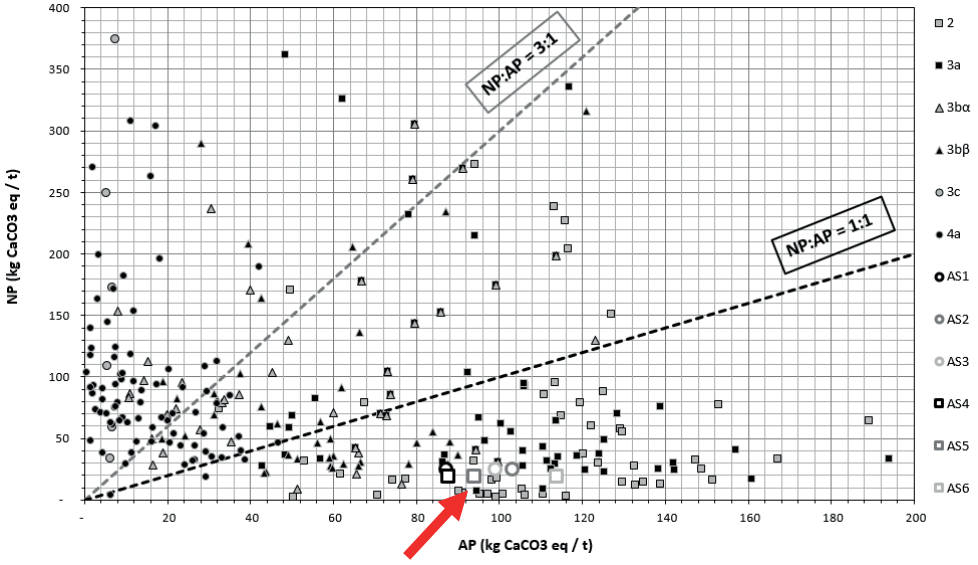

Figure 18: Neutralization potential (NP) vs. acidification potential (AP) in Norwegian Cambro-Ordovician black mudrocks. AS1-AS3 are replicate measurements of the debris used for the AOC-LOC leaching experiment, and AS4-AS6 of the debris used for the cyclic experiment. The arrow marks the position of these samples. The other points represent samples from the different horizons in the Cambro-Ordovician stratigraphy, from a database by the Norwegian Geotechnical Institute (NGI).

A ratio of Fe and S close to 1:2 (Figure 19) indicates that the sulphur in the sample is mainly present as pyrite (FeS_2) (Pabst et al., 2016), as was also indicated by the mineralogy results.

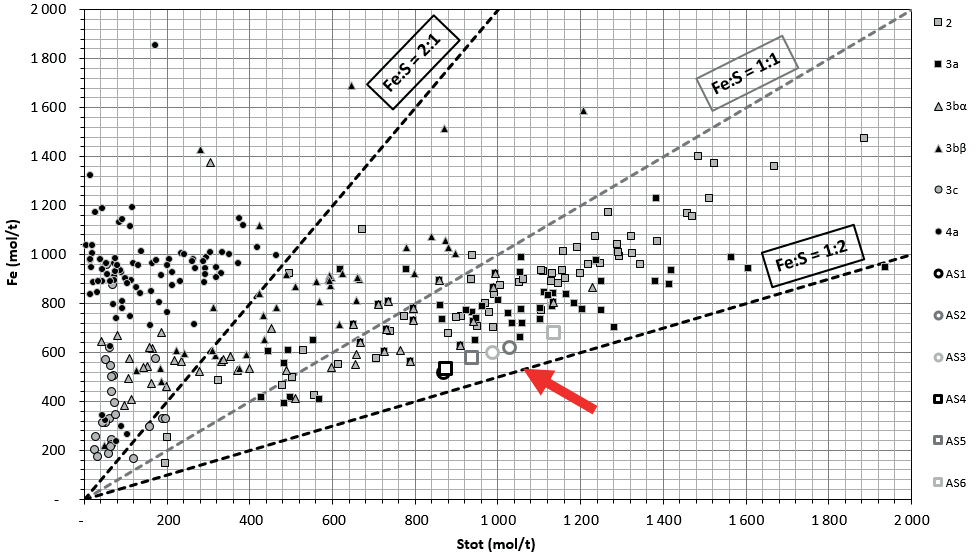

Figure 19: Ratio of Fe to S in Cambro-Ordovician black mudrocks. AS1-AS3 are replicate measurements of the debris used for the AOC-LOC leaching experiment, and AS4-AS6 of the debris used for the cyclic experiment. The arrow marks the position of these samples. Other points represent samples from the different horizons in the Cambro-Ordovician stratigraphy, from a database by the Norwegian Geotechnical Institute (NGI). Stot = total sulphur content.

4.2.2 Leaching as a function of time: Physico-chemical variables

Several physical-chemical variables were monitored in the leachates during the experiments in order to understand the leaching processes. Of special interest was of course the pH, as there was expected to be acid production from pyrite oxidation. The variation in leachate pH with time in the two leaching experiments is presented in Figure 20. The graph on the left represents the AOC-LOC experiment (Paper II), with leaching of alum shale debris under atmospheric (AOC) and low (LOC) oxygen conditions. The inset graph shows the variation in pH for the first week of the experiment as this is difficult to read from the main graph. The graph on the right presents the pH results from the cyclic leaching experiment (Paper III). Each vertical line represents the start of a new cycle, i.e., mixing of the debris with fresh synthetic rainwater. In the DRY treatment, the debris was dried for two weeks before a new cycle started (see section 3.5), while for the WET treatment, fresh synthetic rainwater was added right after removal of the old.

In all treatments of the two experiments, pH increased from 5.0 in the synthetic rainwater to 7.9-9.0 within one hour, with the highest values measured in the LOC treatment. Then, there was a sudden drop to about pH 7.0-7.4 at 24 h in all treatments except the LOC

treatment, before the pH rose again. Similar behaviour was also seen in later cycles in the cyclic experiment. All treatments had a pH of 7.6-7.8 in the end of the experiment– also in all the cycles of the cyclic experiment. The pH values reflects the dissolution of carbonates.

The sudden drop in pH at 24 h in the AOC, WET and DRY treatments could be attributed to precipitation of Fe (oxy)hydroxides, with Fe(III) originating from pyrite oxidation. This is supported by the lack of such a drop in the LOC treatment, where the pyrite oxidation is expected to be more limited.

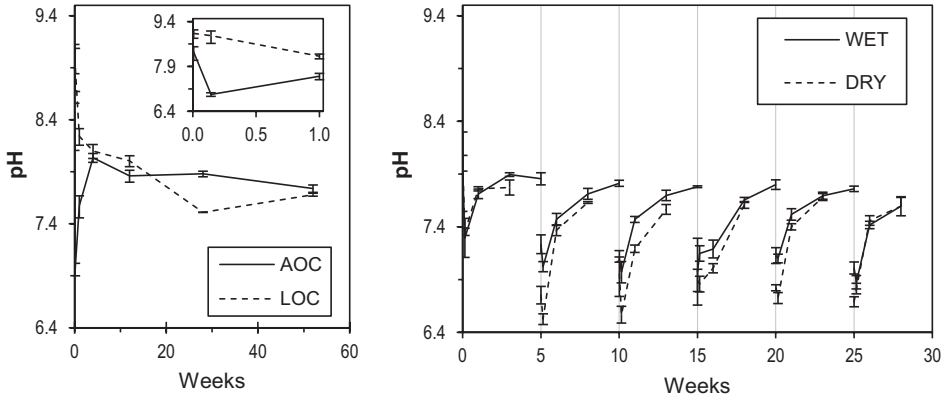

Figure 20: Leachate pH as a function of time in the AOC-LOC experiment (left) and the cyclic leaching experiment (right). The inset graph (left graph) is showing the first week of the experiment. The error bars represent one standard deviation of replicate samples. Full (AOC, WET) and dashed (LOC, DRY) lines are connecting average concentrations of samples. In the graph for the cyclic experiment, each vertical line represents the start of a new cycle. For each sampling point in the AOC-LOC experiment, n=3, except for 28 and 52 weeks of the LOC treatment where n=2. For the cyclic experiment, n=4.

The sulphate concentrations increased with time (Figure 21), and the release rate for all treatments was highest in the beginning of the experiments. This represent most likely both dissolution of soluble sulphate compounds and pyrite oxidation. For the AOC-LOC experiment (Figure 21, left), notice the marked difference between the two treatments, with higher sulphate concentrations in the AOC treatment. This was expected from the higher oxygen access leading to increased pyrite oxidation. In the cyclic experiment (Figure 21, right), there was a marked difference between the treatments with greater sulphate leaching in the DRY treatment. Again, this was expected from higher oxygen access. The measured concentration of S in the leachate corresponded well with the measured SO_4^{2-}. When looking at the leached amount of S as % of the debris content, the

leaching increased in the order LOC < AOC < WET < DRY, i.e., with increasing access to oxygen.

The direct comparison of the two experiments is, however, potentially misleading. The debris used for the two experiments were from the same batch, however, as seen in Table 5, there were small differences in composition of the two subsamples. Probably more important, the debris for the cyclic experiment was stored for a longer time before the experiment was initiated, and the surface of the debris has likely been oxidized to a greater extent. An attempt was made to correct for this by choosing larger pieces and crushing these to get fresh surfaces, but there was nevertheless a certain fraction of the surface that had been exposed to air before the experiment started. The oxidation during storage is reflected in the faster increase in sulphate concentration in the cyclic experiment, with about 260 mg L^{-1} after three weeks, while there was 190 mg L^{-1} after four weeks in the AOC treatment. If the starting point was the same, the AOC, DRY and WET treatments should have been similar in the first few weeks of the experiment.

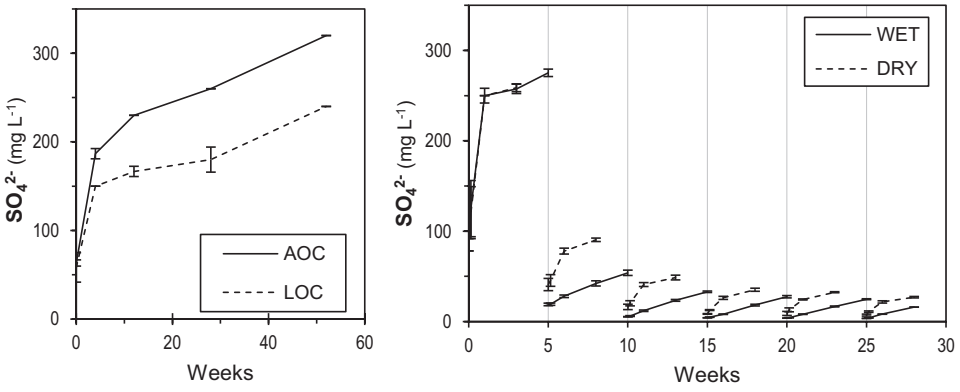

Figure 21: Dissolved (<0.45 µm) sulphate concentrations as a function of time in the AOC-LOC experiment (left) and the cyclic leaching experiment (right). The error bars represent one standard deviation of replicate samples. Full (AOC, WET) and dashed (LOC, DRY) lines are connecting average concentrations of samples. In the graph for the cyclic experiment, each vertical line represents the start of a new cycle. For each sampling point in the AOC-LOC experiment, n=3, except for 28 and 52 weeks of the LOC treatment where n=2. For the cyclic experiment, n=4.

Previous works with leaching experiments under varying experimental conditions have shown that the rate of pyrite oxidation depends on the surface area of the samples, the concentration of oxidizing agent, and only slightly on the initial pH of the leachant (Bierens de Haan, 1991). The Pourbaix diagram in Figure 22 depicts the stable forms of

Fe by different pH and redox conditions. The desired state for storage of acid-producing rock is the area where pyrite is stable, i.e., the area marked with FeS_2 (s).

In the aqueous phase of the leaching experiments, E_h (calculated from measurements of ORP) ranged from 246 to 497 mV, which together with the measured pH (6.5-9.2) places all samples in the stability range of Fe(III) (Grundl et al., 2011). Thus, oxidation of pyrite was expected. The green rectangle in Figure 22 marks the area within which the pH and E_h measurements fall.

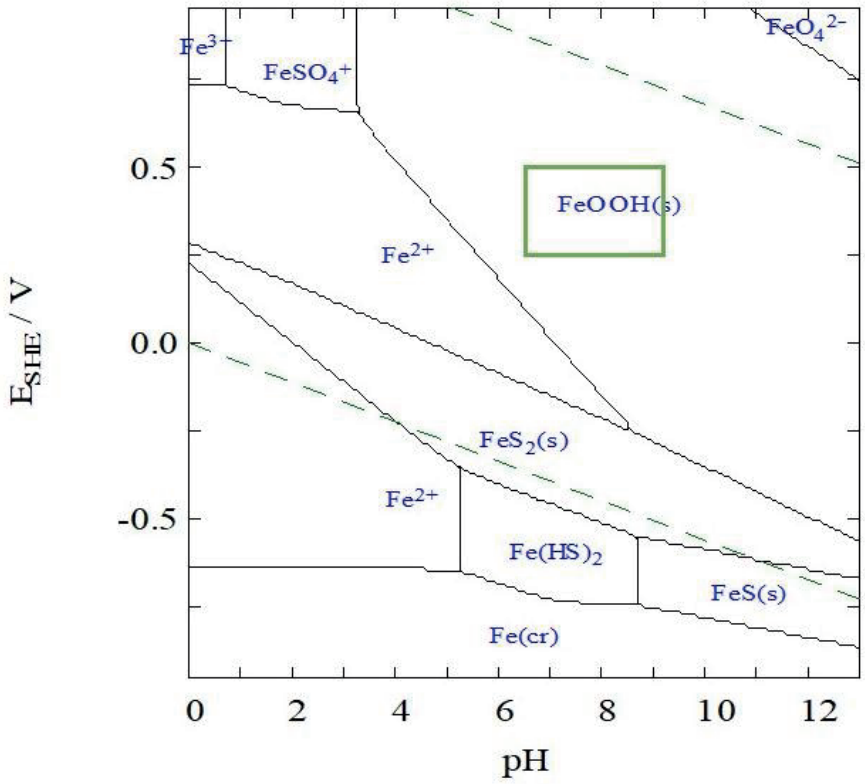

Figure 22: Pourbaix diagram showing the predominant phases of Fe and S with varying E_h and pH values. The conditions in the two leaching experiments fall within the green box. Pyrite is stable in the area marked with FeS_2 (s). The diagram is made in Medusa with the Hydra database. Input conditions are typical for the leaching experiment: 2 mM SO_4^{2-}, 0.1 µM Fe^{3+}, 1 mM CO_3^{2-}, t = 10 °C. Dashed, green lines show the stability range of water.

As mentioned above, the pyrite concentrations in the debris did not change in either experiment, despite expected pyrite oxidation under the prevailing conditions. However, if we look at the total amount of S that leached in the experiments, we see that maximum 5 % of the debris content leached, and some of this was likely from sulphates. Thus,

probably <5 % of the pyrite oxidized in the duration of the experiment, and this was not sufficient to cause a significant change in the debris concentrations detectable by XRD.

For the AOC-LOC experiment, determination of the O_2 levels was important for documenting the conditions, especially in the LOC treatment. Concentrations of O_2 in water are presented in Figure 23, and were substantially lower in the LOC treatment compared to the AOC treatment. In the LOC samples, addition of the alum shale increased dissolved oxygen levels from 0.01 to 0.20 ± 0.07 mg L^{-1} in the first 1 h, likely caused by oxygen bound to the surface of the crushed alum shale. Thereafter the oxygen levels fluctuated between 0.3 and 0.9 mg L^{-1}. The highest levels were observed at the end of the experiment (52 weeks). This was also seen for the O_2 in the gas phase, which increased from about 0.4 % in the first week to around 3.5 % by the end of the experiment, still substantially lower than atmospheric levels (21 %). As the gas phase was completely exchanged every time the water was sampled, the results do not represent development with time and are not presented in any more detail.

For the AOC treatment, the initial O_2 concentration in the leachant was 8.4 mg L^{-1} oxygen, which increased to 9.00 ± 0.02 mg L^{-1} at 1 h due to release from the alum shale and equilibration with air. After this, the O_2 concentration varied between 9.5 and 10.1 mg L^{-1}.

In the cyclic experiment, O_2 concentration was measured at selected time points only, and were similar to the measurements for the AOC treatment, both in the WET and the DRY treatments.

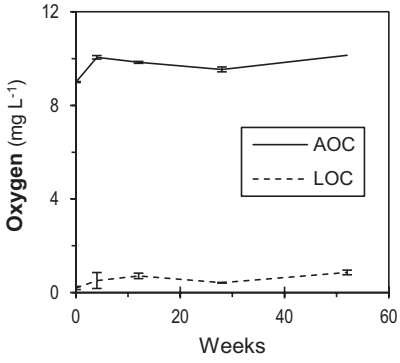

Figure 23: Dissolved oxygen as a function of time in the AOC-LOC experiments. The error bars represent one standard deviation of replicate samples. Full (AOC) and dashed (LOC) lines are connecting average concentrations of samples. For each sampling point, n=3, except for 28 and 52 weeks of the LOC treatment where n=2.

4.2.2.1 Carbonates and buffer capacity

If more pyrite is oxidized and more acid is produced, then more carbonates are expected to dissolve and thereby buffer the pH. Concentration of Ca in solution in the AOC-LOC experiment increased faster in the AOC than the LOC treatment (Figure 24, left) as was also seen for sulphate. Concentrations of Ca increased a bit quicker in the cyclic experiment (Figure 24, right) compared to the in the AOC-LOC experiment, as was also seen for sulphate. Thus, the Ca measurements supports the assumptions made from the sulphate concentrations.

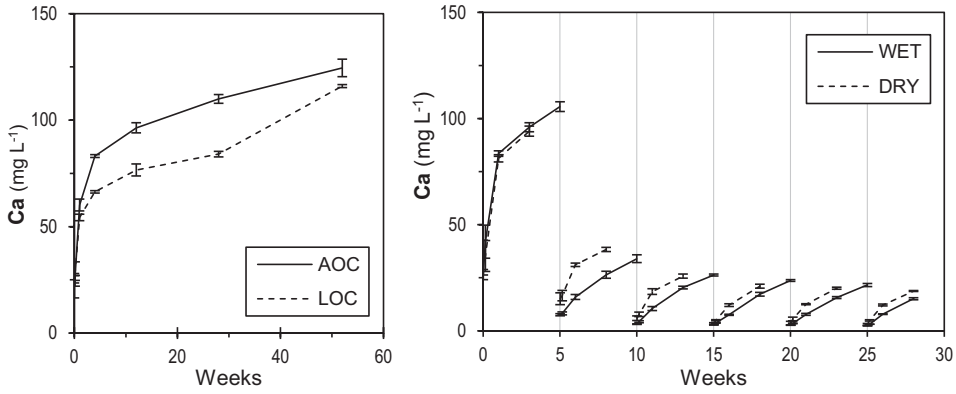

Figure 24: Dissolved (<0.45 µm) leachate concentration of Ca as a function of time in the AOC-LOC experiment (left) and the cyclic leaching experiment (right). The error bars represent one standard deviation of replicate samples. Full (AOC, WET) and dashed (LOC, DRY) lines are connecting average concentrations of samples. In the graph for the cyclic experiment, each vertical line represents the start of a new cycle. For each sampling point in the AOC-LOC experiment, n=3, except for 28 and 52 weeks of the LOC treatment where n=2. For the cyclic experiment, n=4.

At the pH values observed in the two leaching experiments (6.5-9.2), carbonates in the water will mainly be present as bicarbonate (HCO_3^-), and this will be the major part of what is measured as alkalinity. The alkalinity of the leachate likely reflects dissolution of calcite ($CaCO_3$) in the debris. In the AOC-LOC experiment (Figure 25, left), the alkalinity was similar for the two treatments at 1 hour and 4 weeks after initial mixing, then the alkalinity in the LOC samples increased steadily to 1.9 mmol L^{-1} at 52 weeks, while the AOC samples stabilized at about 1.1 mmol L^{-1}. The solubility of calcite increases with higher partial pressure of CO_2 in air (P_{CO2}) (vanLoon & Duffy, 2011). In the LOC treatment, P_{CO2} up to 5 times higher than the atmospheric CO_2 concentration of 390 ppm (Hartmann et al., 2013) was determined in the gas phase (Paper II). Calculations indicated that this

was likely responsible for the higher alkalinity measurements in this treatment (Figure 25, left), and not only differences in pyrite oxidation.

In the cyclic experiment (Figure 25, right), alkalinity gradually decreased from cycle to cycle in the WET treatment, while for the DRY treatment, the alkalinity in cycle 2 was less than half of that in cycle 1, and leachates in following cycles all reached about the same levels (~0.5 mmol L^{-1}). Summing the alkalinity at the end of each cycle gives a total of 29 % less buffer capacity in the DRY leachates compared to the WET ($p = 2e\text{-}8$). While the longer contact time in the WET treatment gave more time for dissolution of calcite, the change in calcite and TIC content of the debris was the same for both treatments (see section 4.2.1), thus, the difference in measured alkalinity was likely caused by greater sulphide oxidation in the DRY treatment.

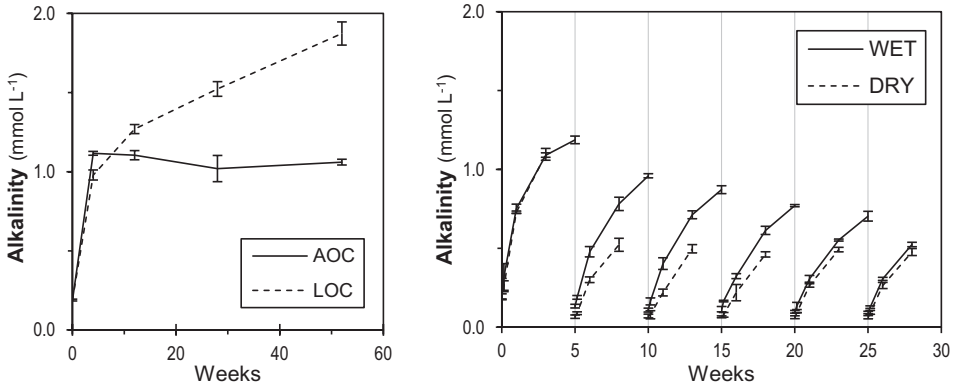

Figure 25: Alkalinity as a function of time in the AOC-LOC experiment (left) and the cyclic leaching experiment (right). The error bars represent one standard deviation of replicate samples. Full (AOC, WET) and dashed (LOC, DRY) lines are connecting average concentrations of samples. In the graph for the cyclic experiment, each vertical line represents the start of a new cycle. For each sampling point in the AOC-LOC experiment, n=3, except for 28 and 52 weeks of the LOC treatment where n=2. For the cyclic experiment, n=4.

As shown in section 4.2.1.1 and Figure 18, the estimated ratios for neutralization potential (NP) to acidification potential (AP) were 0.25 and 0.18 for the AOC-LOC and cyclic experiments, respectively. Thus, the debris used for the leaching experiments was clearly expected to be acid producing.

As mentioned, rock masses with NP:AP < 1 are considered surely acid producing, NP:AP > 3 are considered safe, and rock masses falling in between are in the uncertainty zone (Pabst et al., 2016). However, depending on local regulations, a smaller uncertainty zone can be used, and rock masses with NP:AP > 1.2 can be considered safe (Dold, 2017). At

Gran, a 1:1 relationship was used for classifying rock as safe together with other criteria (Fjermestad et al., 2018). This is further discussed in section 4.3.3.1.

When calculating the AP and NP, all carbonates are assumed to behave like calcite – which fits well with the XRD results in this case – and each mole of calcite is expected to neutralize two moles of protons (Lawrence & Wang, 1996; Pabst et al., 2016). However, because the pK_{a1} for carbonic acid is 6.3 (see section 2.1.2), when all carbonates are spent for neutralization, the pH will be below 6.3. This is often lower than the optimal pH in a disposal site (Dold, 2017) and for leaching from masses considered safe and thus disposed of freely. Thus, Dold (2017) argues that when calculating NP, only one mole of protons should be assumed neutralized per mole of calcite. Using this assumption, the estimated NP to AP ratios are 0.13 and 0.09 for starting materials of the AOC-LOC and cyclic experiments, respectively. This rock debris is considered clearly acid-producing in either case, but if dealing with rock masses close to being considered safe (and especially if 1.2 is used as the "safe" ratio for NP:AP), this difference in calculations can be crucial.

When setting a limit for NP:AP ratios that are acceptable, local conditions are important, and knowledge of the mineralogy is of utmost importance (Dold, 2017). While the molar ratio of NP and AP is important, the reactivity of minerals largely depends on mineral properties and fragmentation of the rock increasing the surface area (Dold, 2017; Parbhakar-Fox & Lottermoser, 2015). The size of mineral grain size depends on the conditions during formation of the mineral/rock. If the pyrite minerals are large, the reactivity is lower and acid production will be slower. One of the problems with alum shale is that fragmentation easily occurs when it is handled (Endre & Sørmo, 2015), causing large surface areas. For storage of acid-producing rock masses, one solution is addition of neutralizing material like shell sand or other carbonate rich material (Dold, 2017; Hindar, 2010). However, it is then of crucial importance that this material is available for acid neutralization: elements released during sulphide oxidation and breakdown of other materials in the rock masses can cause precipitations, and the neutralizing material can be deactivated by precipitations on the surface (Hindar, 2010).

Furthermore, if there is any exchange of water in a disposal site (at a pH where carbonate or bicarbonate is present), the dissolved bicarbonates can be transported out and the buffer capacity is lost. This was demonstrated in the cyclic experiment (Paper III), where water with considerable alkalinity was removed (Figure 25, right) in each cycle, and the

calcite was depleted much faster than in the AOC-LOC experiments of Paper II. This means that a substantial amount of the assumed buffer capacity of calcite can be lost without contributing to neutralization of acid, supporting Dold's (2017) arguments for using 1 mole of H^+ per mole of calcite for calculations of the AP to NP ratio.

Higher P_{CO2} is expected underground due to microbial activity (vanLoon & Duffy, 2011), and CO_2 will also be produced as a result of neutralization of acid by carbonates. Thus, in a storage site like at Gran, higher P_{CO2} and thus increased solubility of calcite can be expected, and if water is exchanged this will lead to an even greater loss of buffer capacity. This could mean that rock masses that are assumed to be neutralizing can turn into acid-producing as the carbonates are washed out, and should be taken into account when estimating a "safe" NP:AP ratio.

4.2.3 Leaching as a function of time: NORM and trace elements

Leaching results for selected elements are presented and discussed here, for more information see Paper II and III. As mentioned, the leaching results from the two different experiments are not directly comparable as the alum shale material used for the two experiments was not identical, and the debris used for the cyclic leaching experiment was likely more oxidized before starting the experiment due to longer storage time.

The concentrations of elements in the dissolved (<0.45 μm) and low molecular mass (LMM, < 10 kDa) fractions were determined by ICP-MS. In the AOC-LOC experiment, all elements where present as > 90 % LMM. The same was true in the cyclic experiment, except for U, as is described in more detail together with the leaching results below. In the cyclic experiment, the LMM fraction of ^{226}Ra was only measured at a few time points (end of cycles 3-6 for WET and 4-6 for DRY), but the results indicated that ^{226}Ra as expected was mainly present as LMM species.

In both experiments, the leaching of most elements was fastest in the beginning. This can be an artefact of the crushing of the rock, causing fresh, reactive surfaces and does not necessarily result from chemical weathering processes.

4.2.3.1 Alkali metals (Group 1)

The relative fraction (%) leached of the different alkali metals are presented in Table 7, and the leaching curves for K are presented in Figure 26. In the AOC-LOC experiment, there seemed to be a slight difference between the two treatments up to 28 weeks, but at

52 weeks this difference disappeared. Looking at the leaching curves for the cyclic experiment, it seems that K was released faster after the drying periods, i.e., that K originated from a phase affected by oxidation. All K in the debris could be accounted for by muscovite (see Table 6), which is not expected to weather before pH drops considerably (Appelo & Postma, 2010). However, as only ~0.3 % of K was released in the experiment, it could also originate from another phase that was too scarce for detection by XRD.

Table 7: Leached alkali metals at the end of the AOC-LOC leaching experiment (52 weeks) and the cyclic leaching experiment (28 weeks). Values are in percent of total debris content. For the AOC treatment, n=3, while it is 2 for the LOC treatment and 4 for the WET and DRY treatments.

	AOC-LOC experiment (Paper II)		Cyclic experiment (Paper III)	
	AOC % leached	LOC % leached	WET % leached	DRY % leached
Li	0.66	0.45	0.98	1.2
Na	1.1	1.0	2.3	2.4
K	0.13	0.13	0.32	0.35

Leaching curves for Li and Na were quite similar to K (though at different concentrations), except that Li leached 50 % more in the AOC treatment compared to the LOC (see Figure 2 in Paper II) and that very little Na was released in cycles 2-6 (see Paper III).

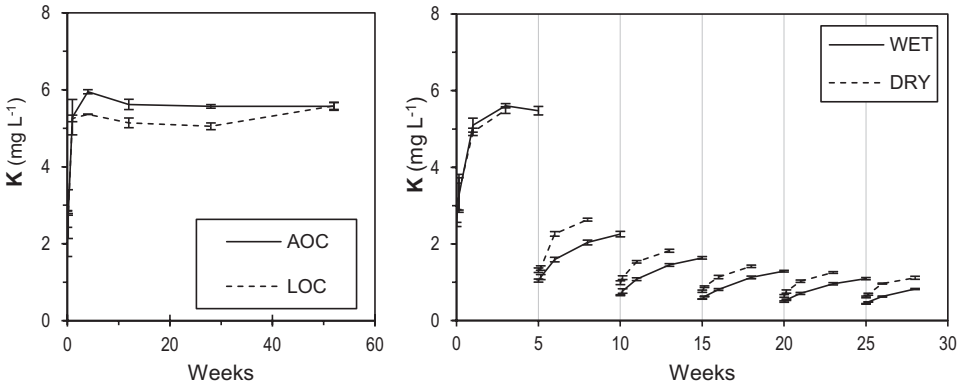

Figure 26 Dissolved (<0.45 μm) K concentrations as a function of time in the AOC-LOC experiment (left) and the cyclic leaching experiment (right). The error bars represent one standard deviation of replicate samples. Full (AOC, WET) and dashed (LOC, DRY) lines are connecting average concentrations of samples. In the graph for the cyclic experiment, each vertical line represents the start of a new cycle. For each sampling point in the AOC-LOC experiment, n=3, except for 28 and 52 weeks of the LOC treatment where n=2. For the cyclic experiment, n=4.

4.2.3.2 Alkaline earth metals (Group 2)

The lighter alkaline earth elements Mg, Ca and Sr were quite soluble in the leaching experiment, and a considerable amount of especially Ca and Sr leached from the debris (Table 8). Leaching figures for Ca were presented earlier in section 4.2.2.1.

Table 8: Leached alkaline earth metals at the end of the AOC-LOC leaching experiment (52 weeks) and the cyclic leaching experiment (28 weeks). Values are in percent of debris content. n = 3 for the AOC treatment, 2 for the LOC treatment and 4 for the WET and DRY treatments.

	AOC-LOC experiment (Paper II)		Cyclic experiment (Paper III)	
	AOC % leached	LOC % leached	WET % leached	DRY % leached
Mg	0.94	0.85	2.0	2.1
Ca	9.5	8.8	26	25
Sr	16	15	22	21
Ba	0.02	0.03	0.38	0.36
^{226}Ra	0.12	0.09	0.63	0.76

The solubility of the heavier alkaline earth elements Ba and ^{226}Ra was generally low, and the fractions leached were less than 1 % of the total debris content in any treatment (Figure 27, Figure 28, Table 8). The most likely explanation for this is precipitation of $BaSO_4$ and co-precipitation of ^{226}Ra, and in the AOC-LOC experiment the K_{SP} of $BaSO_4$ (1.07×10^{-10}, 25 °C (*CRC Handbook of Chemistry and Physics*, 1993)) was slightly exceeded in all sampling points (Figure 27, left). The cyclic leaching experiment was well designed to further investigate the behaviour of Ba and ^{226}Ra; to check how exchange of water would affect the solubility, and specifically if drying of the rock would lead to higher oxidation, higher sulphate concentrations and lower Ba and thus ^{226}Ra solubility.

Solubility calculations indicated that K_{SP} of $BaSO_4$ was exceeded only in certain parts of the cyclic experiment, see Figure 27 (right). The sampling points where the K_{SP} was exceeded coincided with drops in measured ^{226}Ra concentrations (Figure 28, right). As we see in Table 8, 12-19 times more Ba and 5-8 times more ^{226}Ra leached in the cyclic experiment compared to the AOC-LOC experiment. These differences are bigger than for the other elements, and reflect that Ba and ^{226}Ra concentrations are limited by solubility. Thus, the solubility and mobility of both Ba and ^{226}Ra increased markedly with exchange of water, as expected. On the other hand, opposite of the expectations, the leaching of ^{226}Ra was higher in the DRY compared to the WET treatment despite higher sulphate concentrations in the DRY treatment. This reflects that $BaSO_4$ solubility was only exceeded for parts of the experiment, and the faster leaching rate in DRY seen in Figure

28 furthermore suggests that ^{226}Ra leached from a phase that is sensitive to the drying part of the experiment, for example sensitive to oxidation.

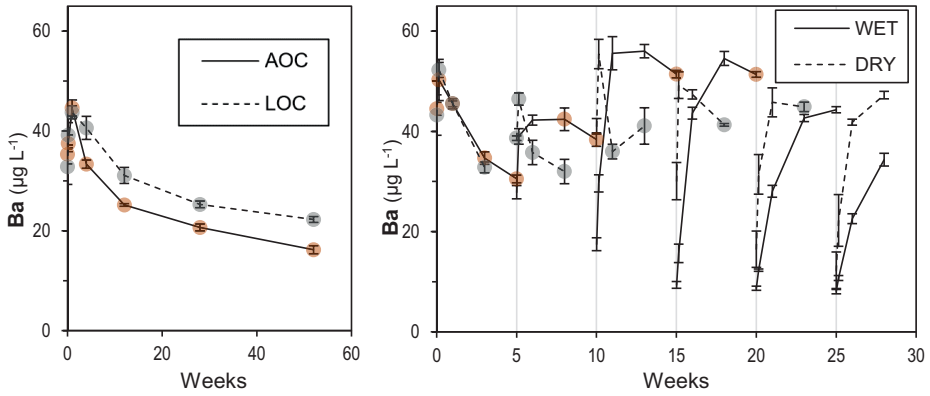

Figure 27: Dissolved (<0.45 µm) Ba concentrations as a function of time in the cyclic leaching experiment. Each vertical line represents the start of a new cycle. Full (AOC, WET) and dashed (LOC, DRY) lines are connecting average concentrations of samples. The error bars represent one standard deviation of replicate samples. Grey (LOC, DRY) and orange (AOC, WET) circles mark the sampling points were K_{SP} for $BaSO_4$ is exceeded. For each sampling point in the AOC-LOC experiment, n=3, except for 28 and 52 weeks of the LOC treatment where n=2. For the cyclic experiment, n=4.

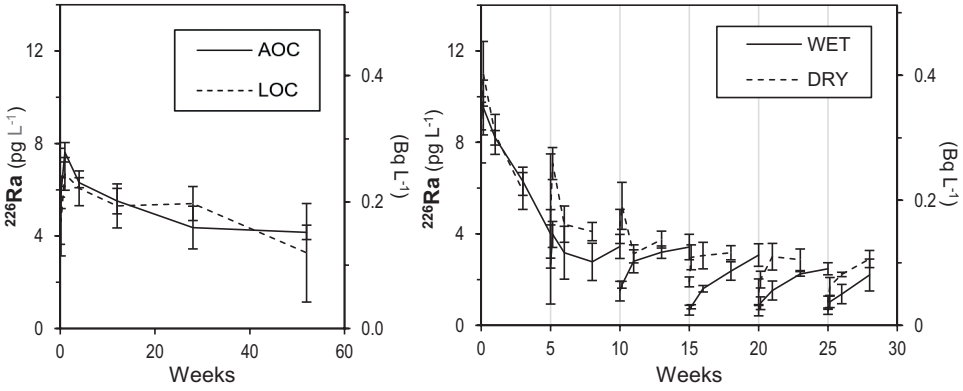

Figure 28: Dissolved (<0.45 µm) ^{226}Ra concentrations as a function of time in the AOC-LOC experiment (left) and the cyclic leaching experiment (right). The error bars represent one standard deviation of replicate samples. Full (AOC, WET) and dashed (LOC, DRY) lines are connecting average concentrations of samples. In the graph for the cyclic experiment, each vertical line represents the start of a new cycle. For each sampling point in the AOC-LOC experiment, n=3, except for 28 and 52 weeks of the LOC treatment where n=2. For the cyclic experiment, n=4.

4.2.3.3 Transition metals (Groups 4-11)

The solubility and behaviour varied substantially between the different transition metals (Table 9). Despite what can be assumed from Table 9, the solubility of Co and Ni did not seem to increase because of the water exchange. The difference between the two

experiments was caused by a high release rate in the first cycle of the cyclic experiment (see Figures S9 and S10 in the supporting information for Paper III), similar to what is described for Cd in section 4.2.3.4, and was thus not related to the exchange of water or the drying period. The solubility in cycles 2-6 was rather low.

Leaching curves for Mn (Figure 2 in Paper II and Figure 2 in Paper III) in all treatments were similar to the ones presented for Ca in section 4.2.2.1, just at lower concentrations. Mn generally had a high mobility, and the same was seen by Fjermestad et al. (2017) and Helmers (2013), while Hjulstad (2015) observed quite low Mn concentrations in her leaching experiments.

Table 9: Leached transition metals at the end of the AOC-LOC leaching experiment (52 weeks) and the cyclic leaching experiment (28 weeks). Values are in percent of alum shale debris content. n = 3 for the AOC treatment, 2 for the LOC treatment and 4 for the WET and DRY treatments.

	AOC-LOC experiment (Paper II)		Cyclic experiment (Paper III)	
	AOC % leached	LOC % leached	WET % leached	DRY % leached
V	0.0006	0.0002	0.00097	0.0013
Cr	0.0001	0.0001	<0.004	<0.003
Mo	22	7.1	14	18
Mn	6.3	5.6	8.9	8.6
Fe	0.00009	0.0001	<0.0002	<0.0001
Co	0.78	0.33	1.59	1.64
Ni	1.2	1.4	2.6	2.5
Cu	0.007	0.004	<0.1	<0.1

The leaching of Mo (Figure 29) was similar for all four treatments in the beginning of the experiments. After four weeks, the concentration of Mo was about 1300 µg L^{-1} in both the AOC and LOC treatment, while the WET and DRY treatments had concentration of about 1200 µg L^{-1} at 3 weeks and the WET treatment had almost 1400 µg Mo L^{-1} after 5 weeks. After 4 weeks, the concentration of Mo in the AOC treatment increased linearly, while the concentrations in the LOC treatment stabilized at ~1600 µg L^{-1}. In the cyclic experiment, Mo kept leaching substantial amounts in cycle after cycle, and there was a marked higher leaching rate in the DRY treatment compared to the WET. Overall, 28 % more leached in the DRY treatment ($p = 3\times10^{-6}$) – the difference between the treatments was reduced by the longer contact time in the WET treatment. Results in both experiments indicated that Mo leached from a phase that was sensitive to oxidation, but the similarity of the first weeks of the two experiments indicated that Mo was not affected by oxidation during storage before start-up of the cyclic leaching experiment, as was likely the case for Cd (see below). The conditions in the AOC treatment and WET treatment should be the same,

except the exchange of water. At 28 weeks, 14.0 % of the Mo had leached in the WET treatment and 14.5 % in the AOC treatment – thus leaching of Mo did not seem to be affected by the concentration of Mo or other elements in the leachate, only by the contact time and the access to oxygen.

The observed high mobility of Mo in alum shale from Gran is in accordance with findings by Fjermestad et al. (2017), Santos (2014) and Hjulstad (2015), and in other alum shales (Lavergren et al., 2009).

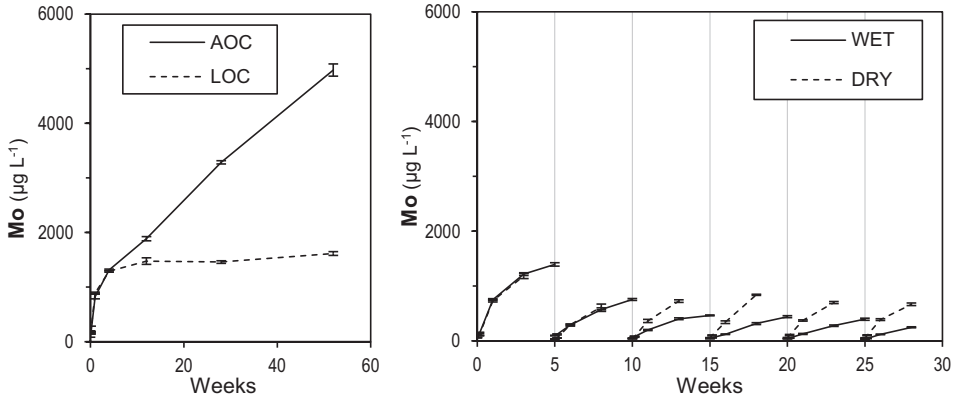

Figure 29: Dissolved (<0.45 µm) Mo concentrations as a function of time in the AOC-LOC experiment (left) and the cyclic leaching experiment (right). The error bars represent one standard deviation of replicate samples. Full (AOC, WET) and dashed (LOC, DRY) lines are connecting average concentrations of samples. In the graph for the cyclic experiment, each vertical line represents the start of a new cycle. For each sampling point in the AOC-LOC experiment, n=3, except for 28 and 52 weeks of the LOC treatment where n=2. For the cyclic experiment, n=4.

The other transition metals are further discussed in Paper II (Wærsted et al., in prep.-a) and Paper III (Wærsted et al., in prep.-b).

4.2.3.4 Group 12

Zn and Cd were both quite mobile under the experimental conditions, with 0.4-4.4 % leached in the different treatments (Table 10).

Table 10: Leached group 12 elements at the end of the AOC-LOC leaching experiment (52 weeks) and the cyclic leaching experiment (28 weeks). Values are in percent of alum shale debris content. For the AOC treatment, n=3, while it is 2 for the LOC treatment and 4 for the WET and DRY treatments.

	AOC-LOC experiment (Paper II)		Cyclic experiment (Paper III)	
	AOC % leached	LOC % leached	WET % leached	DRY % leached
Zn	1.8	0.43	1.1	1.2
Cd	2.6	0.82	4.0	4.4

Cd exhibited quite different behaviour in the two leaching experiments (Figure 30). The linear leaching curve in the AOC treatment of the AOC-LOC experiment indicated that the element would leach at a constant rate for a prolonged time by atmospheric oxygen conditions, while the solubility under lower oxygen conditions was much more limited – indicating a sensitivity to oxidation. The pattern observed in the cyclic experiment was, however, very different. The leaching rate was much higher in the first cycle of the cyclic experiment and reached higher concentrations in 1 week than the AOC treatment reached in 52 weeks. If the starting points for the two experiments were the same, AOC, WET and DRY treatments should have been similar in the first few weeks. As the concentration of Cd in the debris for both experiments was quite similar (Table 5), one explanation for the difference between the two experiments is that the debris was oxidized during storage, before the onset of the cyclic experiment. This underlines the importance of relocating alum shale debris to appropriate storage conditions within a short period time after excavation. The difference between the two treatments in the AOC-LOC experiment and the effect of storage indicated that Cd leached from a mineral that is sensitive to oxidation, while there seemed to not be so much effect of the drying periods.

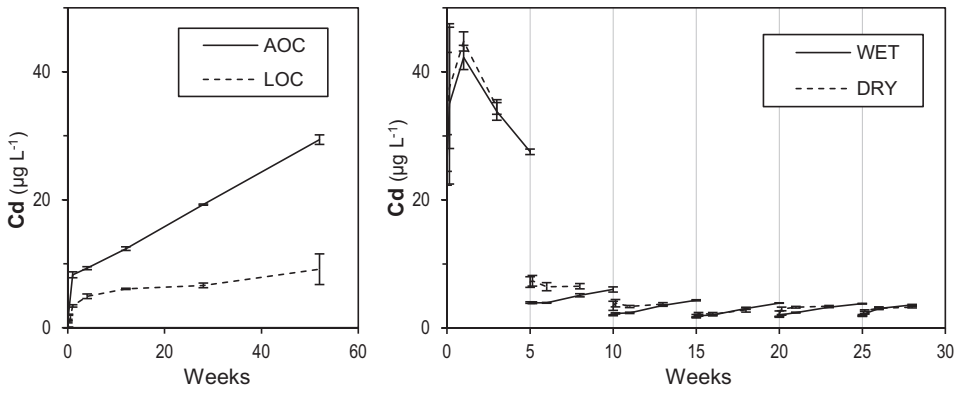

Figure 30: Dissolved (<0.45 µm) Cd concentrations as a function of time in the AOC-LOC experiment (left) and the cyclic leaching experiment (right). The error bars represent one standard deviation of replicate samples. Full (AOC, WET) and dashed (LOC, DRY) lines are connecting average concentrations of samples. In the graph for the cyclic experiment, each vertical line represents the start of a new cycle. For each sampling point in the AOC-LOC experiment, n=3, except for 28 and 52 weeks of the LOC treatment where n=2. For the cyclic experiment, n=4.

The reason for the sudden drop in Cd concentrations after 1 week in the first cycle is unknown, but the same behaviour was seen for Co, Ni and Zn (see Figures S9, S10 and

S11 in SI to Paper III). Co and Zn also had similar leaching curves as Cd in the AOC-LOC experiment, while Ni deviated (see Figure 2 of Paper II).

Leaching of Cd from alum shale collected at Gran observed by Hjulstad (2015) was much lower, with 0.09 µg L^{-1} after a seven weeks batch experiment. As in the presented work, all dissolved Cd was low molecular mass (LMM) species. Of this, Hjulstad (2015) observed that about 80 % of Cd was cationic and the rest anionic or neutral. Fjermestad et al. (2017) observed up to about 18 µg L^{-1} Cd in containers with alum shale from Gran left open to precipitation over an eight month period, which is more similar to the results in Figure 30.

4.2.3.5 Groups 13-16

Elements in group 13, 14 and 15 generally exhibited low solubility (Table 11). Leachate concentrations of S in the leaching experiment corresponded to the measured sulphate concentrations, see Figure 21.

Table 11: Leached elements from the groups 13-16 at the end of the AOC-LOC leaching experiment (52 weeks) and the cyclic leaching experiment (28 weeks). Values are in percent of alum shale debris content. For the AOC treatment, n=3, while it is 2 for the LOC treatment and 4 for the WET and DRY treatments.

		AOC-LOC experiment (Paper II)		Cyclic experiment (Paper III)	
		AOC	LOC	WET	DRY
		% leached	% leached	% leached	% leached
Group 13	Al	0.000009	0.00003	0.00025	0.00026
Group 14	Pb	0.0004	0.0004	<0.009	<0.009
Group 15	As	0.009	0.003	0.018	0.019
	Sb	0.70	1.0	1.7	1.3
Group 16	S	3.3	2.5	4.4	5.0

After 4 weeks there was about 20 µg L^{-1} Sb in the leachates from both the AOC and the LOC treatments (Figure 31), then the concentrations decreased in the AOC treatment, while in the LOC treatment the concentrations peaked at about 25 µg L^{-1} at 12 weeks before decreasing. Sb was slowly released during the first weeks of the cyclic experiment giving ~8 µg L^{-1} at 3-5 weeks, and it might have been affected by oxidation during storage of the debris. Solubility of Sb was in general higher in the treatments with less oxygen. However, more Sb was released in total in the cyclic experiment – likely because the exchange of water removed some solubility restrictions like precipitation or co-precipitation. Low Sb solubility can be caused by scavenging by Fe (oxy)hydroxides, for which Sb has a high affinity (Braunschweig et al., 2013; Okkenhaug, 2012), which could explain the lower solubility with more oxygen in the system.

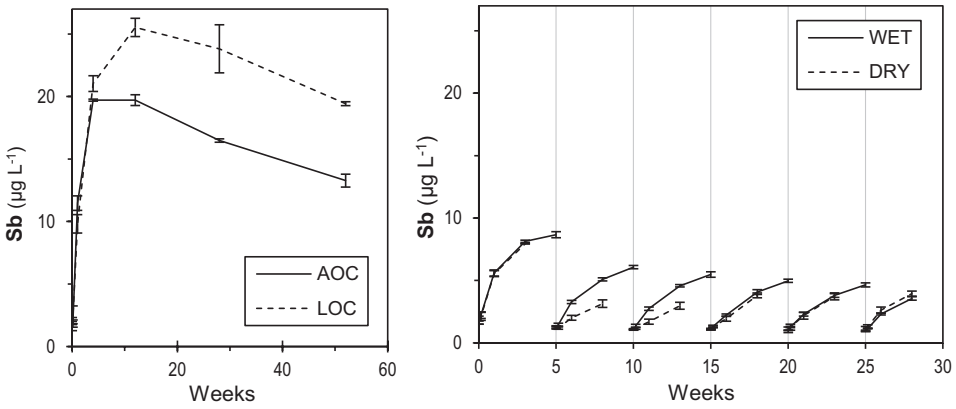

Figure 31: Dissolved (<0.45 µm) Sb concentrations as a function of time in the AOC-LOC experiment (left) and the cyclic leaching experiment (right). The error bars represent one standard deviation of replicate samples. Full (AOC, WET) and dashed (LOC, DRY) lines are connecting average concentrations of samples. In the graph for the cyclic experiment, each vertical line represents the start of a new cycle. For each sampling point in the AOC-LOC experiment, n=3, except for 28 and 52 weeks of the LOC treatment where n=2. For the cyclic experiment, n=4.

4.2.3.6 Actinides

The relative fractions (%) of actinides in the different leaching treatments are presented in Table 12. The mobility of ^{238}U was clearly higher under the tested conditions than the mobility of the other radionuclides, ^{226}Ra (section 4.2.3.2) and ^{232}Th.

Table 12: Leached actinides at the end of the AOC-LOC leaching experiment (52 weeks) and the cyclic leaching experiment (28 weeks). Values are in percent of alum shale debris content. For the AOC treatment, n=3, while it is 2 for the LOC treatment and 4 for the WET and DRY treatments.

	AOC-LOC experiment (Paper II)		Cyclic experiment (Paper III)	
	AOC % leached	LOC % leached	WET % leached	DRY % leached
^{232}Th	<0.00004	0.0002	<0.006	<0.001
^{238}U	4.0	4.9	3.3	2.3

^{238}U was relatively soluble, and 2.3-4.9 % of the total concentrations in the debris leached in the different treatments (Table 12). The leaching of ^{238}U was quite similar in the first weeks of all four treatments (Figure 32). At four weeks, concentrations were 192 and 221 µg L^{-1} in the AOC and LOC treatments, respectively. In the WET treatment, concentrations were 175 µg L^{-1} at three weeks and 242 µg L^{-1} at five weeks, and in the DRY treatment the concentration was 195 µg L^{-1} at three weeks.

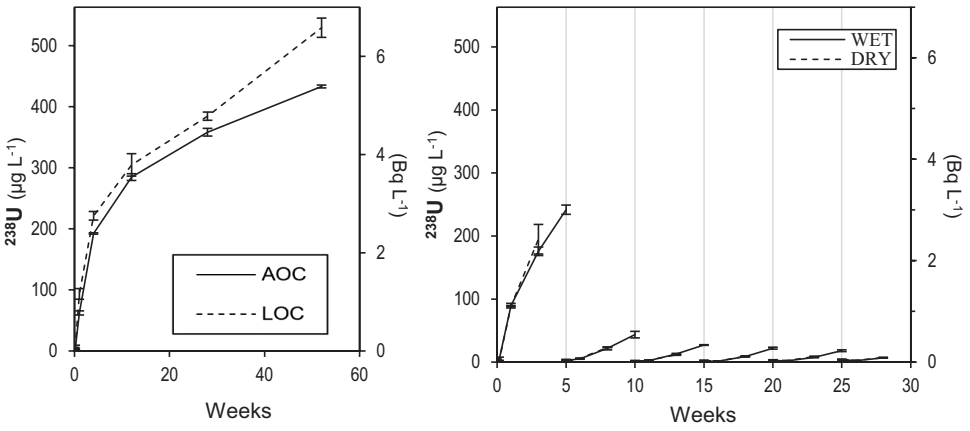

Figure 32: Dissolved (<0.45 µm) ^{238}U concentrations as a function of time in the AOC-LOC experiment (left) and the cyclic leaching experiment (right). The error bars represent one standard deviation of replicate samples. Full (AOC, WET) and dashed (LOC, DRY) lines are connecting average concentrations of samples. In the graph for the cyclic experiment, each vertical line represents the start of a new cycle. For each sampling point in the AOC-LOC experiment, n=3, except for 28 and 52 weeks of the LOC treatment where n=2. For the cyclic experiment, n=4.

The fastest U leaching rate was observed in the LOC treatment. This is not a direct effect of the lower oxygen conditions, as the less oxidized U^{IV} is less soluble than U^{VI}. One hypothesis is less scavenging by Fe (oxy)hydroxides formed from pyrite oxidation, as U has a high affinity for these (Braunschweig et al., 2013; Vandenhove et al., 2007). Based on the measured sulphate concentrations, the relative rate of pyrite oxidation for the different treatments is expected to have been DRY > WET > AOC > LOC. However, if Fe (oxy)hydroxides was important for the U concentration, leaching rates should have been slower in DRY compared to WET. While less U leached in total in the DRY treatment (Table 12), the rate of leaching in the two treatments was the same – seen by the overlapping curves in Figure 32. Thus, ^{238}U seemed to leach from a phase that was unaffected by the drying periods, and the difference between the leaching of ^{238}U in the WET and DRY treatments seemed to be caused by difference in contact time. Another reason for the faster leaching in the LOC treatment could be increased solubility of U in carbonate rich water (Seder-Colomina et al., 2018; Stanley & Wilkin, 2019), as the measured alkalinity was higher in this treatment.

If the leaching of U under atmospheric oxygen conditions was mainly controlled by contact time, the leaching in the AOC and WET treatments should be similar. The total leached amount of U in the WET treatment was 3.3 % after a total of 28 weeks leaching,

and the same value was seen for U in the AOC treatment at 28 weeks. The exchange of water thus seemed to have no effect on the leaching of ^{238}U.

The leaching behaviour of U was unlike any other measured element, possibly reflecting a different source phase in the rock than the other measured elements. The daughter ^{226}Ra was expected to be in the same phases as the mother nuclide ^{238}U, but has a completely different chemical behaviour, thus, similar leaching curves were not expected.

Hjulstad (2015) also observed high mobility of U in alum shale from Gran, and measured concentrations of 118 µg L^{-1} U after seven weeks in a batch leaching experiment similar to the AOC treatment. Fjermestad et al. (2017) measured up to 5,000 µg L^{-1} U in containers with alum shale left open to precipitation over an eight month period.

In the cyclic experiment, up to 90 % of U was present in the colloidal fraction at the beginning of the cycles, though < 10 % in the end of the cycles (Figure 33). This cyclic variation can mainly be ascribed to lower dissolved concentrations of ^{238}U in the leachate in the beginning of the cycles, but there was also a decreasing trend in colloidal concentrations in each cycle with 1-3 µg L^{-1} in the beginning of a cycle and about 0.5 µg L^{-1} later in the cycle – except in cycle 1, where calculated colloidal concentrations were up to 18 µg L^{-1}. Colloids in the leachates could for example be newly formed precipitation products or results from flocculation and scavenging by Fe.

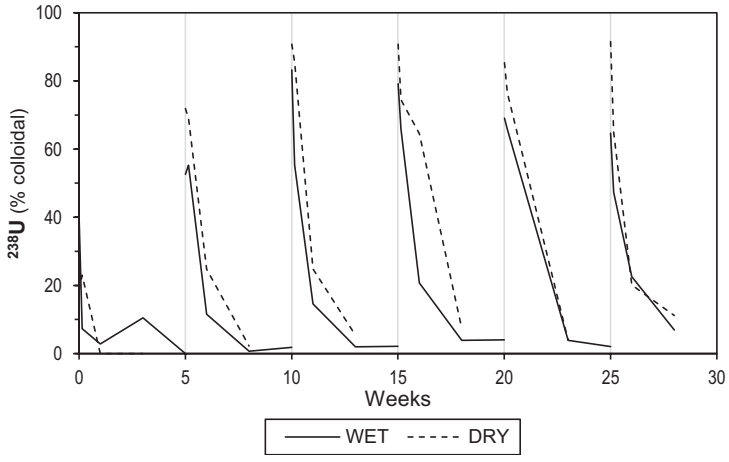

Figure 33: Percentage colloidal fraction of ^{238}U as a function of time in the cyclic leaching experiment. For all data points, n=4.

In her leaching experiments with alum shale from Gran, Hjulstad (2015) observed that all the dissolved U was LMM species, and of that, almost 75 % were in the anionic + neutral fraction, while the remaining 25 % were cationic.

As expected, Th exhibited low solubility (Table 12). Also in the disposal site and other leaching experiments with alum shale from Gran, Th has shown low solubility (Fjermestad et al., 2017; Skipperud et al., 2016a). However, solubility of Th is greatly enhanced when pH falls below 2-3, and substantial leaching from U tailings can occur due to acid rock drainage (Landa, 2007). Thus, if there is a pH drop in the storage site at Gran, increased mobility of Th might be the result.

4.2.4 Comparison with the disposal site

The concentration of elements in the water in the disposal site at Gran is compared with the results from the end (52 weeks) of the AOC-LOC experiment in Table 13. The pH values and the concentrations of sulphate, Mg and Ca were quite similar, indicating a similar overall water quality. The higher conductivity in the disposal site is likely explained mainly by the higher concentrations of NO_3^-, Cl^- and Na and the somewhat higher concentration of SO_4^{2-}.

Nitrate was at least 2,000 times higher in the disposal site than in the experiment, which is likely related to residuals from explosives in the disposed tunnel debris (Fjermestad et al., 2018). As NO_3^- is an important electron acceptor, the high levels could contribute to pyrite oxidation (Appelo & Postma, 2010) and delay the onset of anoxic or reducing conditions in the disposal site.

Several of the elements (Mo, Mn, Ni, Zn, Cd and U) that are expected to be high in alum shale was much higher in the leachate from the experiment than in the disposal site water. This might reflect that the experiment used pure alum shale and the disposal site was filled with tunnel blast having > 10 % black shales, and thus contains substantial amounts of other rocks (Fjermestad et al., 2018). Ni, Zn and Cd were more than 100 times higher in the experiment than in the disposal site water, while Mn and Co were more than 10 times higher. Mo and U were also several times higher in the experiment leachates.

One the other hand, the alkali metals where generally higher in the disposal site water compared to both treatments, except Li that was quite similar. High Na concentrations likely originate from salting of roads in the area, which is reflected in the high Cl^-

concentration. The elements V, As and Sb, which all showed limited solubility in the AOC-LOC leaching experiment, were present in higher concentration in the disposal site. Furthermore, exchange of water seemed to increase the solubility and thus mobility of V, As and Sb in the cyclic experiments, which can be important if there is extensive water exchange in the disposal site.

Table 13: Water quality and element concentrations in water collected at the disposal site at Gran (average ± one standard deviation) and concentration ratios to the measurements obtained for experiment leachates from atmospheric (AOC) and low (LOC) oxygen conditions. For the disposal site, n=1 for pH and conductivity and 3 for the rest of the measurements. For the AOC treatment, n=3 for all measurements, and for the LOC treatment n=2. Element concentrations were measured in samples filtered through 0.45 µm*. The table is modified from Wærsted et al. (in prep.-a) (Paper II).

		Disposal site		AOC (52 w) / disposal site	LOC (52 w) / disposal site
Water quality	pH	7.65		1.0	1.0
	Conductivity	1236	µS cm^{-1}	0.55	0.48
	SO_4^{2-} *	340	mg L^{-1}	0.94	0.71
	NO_3^- *	186	mg L^{-1}	≤0.0005	≤0.0005
	Cl^- *	23	mg L^{-1}	0.043	0.026
Group 1	Li	20 ± 0.2	µgL^{-1}	1.0	0.71
(Alkali metals)	Na	99 ± 1	mg L^{-1}	0.035	0.033
	K	13 ± 0.1	mg L^{-1}	0.43	0.43
Group 2	Mg	12 ± 0.4	mg L^{-1}	0.70	0.63
(Alkaline earth metals)	Ca	110 ± 4	mg L^{-1}	1.1	1.1
	Sr	1.40 ± 0.03	mg L^{-1}	1.6	1.5
Transition metals	V	2.4 ± 0.06	µg L^{-1}	0.76	0.25
	Cr	0.14 ± 0.03	µg L^{-1}	0.14	0.11
	Mo	850 ± 0.4	µg L^{-1}	5.9	1.9
	Mn	97 ± 2	µg L^{-1}	18	16
	Fe	4.4 ± 0.7	µg L^{-1}	0.64	1.0
	Co	0.48 ± 0.07	µg L^{-1}	38	16
	Ni	4.3 ± 0.2	µg L^{-1}	117	140
	Cu	0.26 ± 0.02	µg L^{-1}	3.8	1.9
Group 12	Zn	<2.6	µg L^{-1}	≥354	≥85
	Cd	0.13 ± 0.006	µg L^{-1}	226	70
Group 13	Al	7.8 ± 0.4	µg L^{-1}	0.091	0.26
Group 14	Sn	0.12 ± 0.002	µg L^{-1}	0.058	0.025
	Pb	0.042 ± 0.0007	µg L^{-1}	0.48	0.40
Group 15	As	3.7 ± 0.07	µg L^{-1}	0.21	0.071
	Sb	90 ± 0.4	µg L^{-1}	0.15	0.22
Rare earth elements	La	0.0087 ± 0.002	µg L^{-1}	1.1	1.3
Actinides	Th	<0.004	µg L^{-1}	†	>0.8
	U	73 ± 0.4	µg L^{-1}	5.9	7.2

* Anions were measured in unfiltered water from the disposal site, but in filtered (0.45 µm) experiment leachates.

† For Th, concentrations in AOC and the disposal site could not be compared as both measurements were below QL.

Ba and ^{226}Ra were not measured in water from the disposal site, but as SO_4^{2-} levels in the disposal site water were similar to the experiment leachates, we expect low release and mobility of these elements. However, the cyclic experiment demonstrated that exchange of water in the disposal site can significantly increase the solubility of Ba and ^{226}Ra.

Overall, it seemed like the AOC and LOC treatments were more similar to each other than either of them were to the disposal site water. The most important reason for this can be that the disposed rock masses has a great variation in composition, while the debris used for the experiment was part of one tunnel blast crushed down and thoroughly mixed before the experiment, and the two treatments therefore had a shared starting point that was not shared by the disposal site. Also, the debris-to-water relationship was lower in the experiments than in the disposal site, where the ratio would change as the pond was gradually filled with debris. Furthermore, in addition to natural drainage, water was pumped out from the disposal site during the disposal period, which could lead to a situation similar to later cycles of the WET treatment. Another important factor can be the presence of organic matter in the disposal site, which is important for speciation and mobility of e.g. Ni, Zn, Cd and U (Appelo & Postma, 2010; Moulin et al., 2004).

When sampling the disposal site, fractionation by size and charge was made. Fractionation results for selected elements are presented in Table 14. Note that the results for the anionic and cationic LMM fractions are given as relative fraction (%) of the LMM, not of the total. In some cases these two fraction added up to more than a 100 % because the *in situ* fractionation was performed on water continuously pumped from the disposal site and the incoming water quality could thus vary with time during the sampling process.

The colloidal fraction was small for all tested elements, while several elements had a considerable particulate fraction. Fractionation of the water in the disposal site showed that S, Ca, Mo, Sb and U mainly were present in the LMM fraction, while Fe and Th were present as particles. This fits with the results from the leaching experiment where Fe and Th were very low in the dissolved fraction, and the other mentioned elements mainly were in the LMM fraction.

Sulphur was almost exclusively present in the anionic LMM fraction, as expected, and Ca was mainly in the cation LMM fraction. Only minor fractions of Sb was measured to be in

the anionic or the cationic LMM fraction, meaning that it was mainly present as neutral LMM. Mo was mainly present as anions, while U was divided between the anionic and cationic fractions. Cd had close to 60 % particular fraction, a minor colloidal fraction and the rest LMM. Of the Cd present as LMM, almost 90 % was anionic.

Table 14: Fractionation results for the water in the disposal site at Gran. Anionic and cationic low molecular mass (LMM) fractions are as % of the LMM, not of the total. For all measured fractions, n=3.

	S	Ca	Fe	Mo	Cd	Sb	Th	U
	%	%	%	%	%	%	%	%
Total	100	100	100	100	100	100	100	100
Particles	0	8	100	0	59	0.0	98	5
Colloidal	3	0	0	5	3	0	0	1
Low molecular mass (LMM)	97	92	0	95	38	100	2	94
Anionic LMM	100	0	0	100	89	1	0	100
Cationic LMM	4	100	0	7	17	2	0	60

In the leaching experiments, the unfiltered samples were not measured. The amount of particles would mainly reflect the time since the last agitation of the sample, and was thus not considered interesting.

4.3 Implications for storage of acid-producing rock in water

4.3.1 Mobility of NORM and stable elements from alum shale

Several elements in the alum shale were relatively mobile even at neutral pH, and greater leaching would be expected if a pH drop occurs. The elements that were mobile at circumneutral pH in the leaching experiments included Mo, Mn, Ni, Zn, Cd and U. Also, high leaching of Ca, SO_4^{2-}, K and Mg was seen, which is important for the water quality. In the disposal site water at Gran, high concentrations were also seen for Ca, SO_4^{2-}, K, Mg, Mo and U.

This mix of elements, stable and radioactive, is expected to give a multiple stressor scenario if leached into downstream waterbodies in sufficient amounts.

4.3.2 Bioavailability and effects of NORM and toxic elements in alum shale

In Paper II, concentrations in the leachates from the AOC-LOC experiment at 52 weeks are compared with environmental quality standards (see Table 3 in Paper II). Mo, Ni, Zn, Cd and U are 22-322 times higher than the limits, and can be expected to pose a serious environmental risk at such concentrations.

Bioavailability of several elements in the alum shale from Gran has been demonstrated in several laboratory experiments in related projects. Uptake and effect have also been observed in the field in the vicinity to the disposal site.

Field investigations in the area around Gran revealed a negative effect from the construction work on the benthic macroinvertebrate communities in the downstream affected streams and brooks compared to unaffected sites (Engelstad, 2016). The effect could also be linked to element levels in mayflies, especially Al, Ni, Cd, Mn, Co and As, but was also correlated to Ca, Fe, Cr, Th, Pb, S, Zn and U.

Brown trout was sampled in the Vigga River before (2013) and during (2015) the construction work at Gran (Skipperud et al., 2016a). No effect on the fish could be seen, as both element concentrations in measured organs (gills, kidney and liver) and condition factor[1] (Ricker, 1975) were unchanged. Normal physiological values were observed in blood, and the concentrations levels of Cd, Mo and U in the sampled organs were lower than what would expectedly give a negative effect (Skipperud et al., 2016a). There was, however, higher Cd and Mo concentrations in gills of fish further downstream Vigga River compared to the upstream control site, but this was ascribed to existing conditions and did not seem to be related to the tunnel construction work.

Two experiments exposing brown trout (*Salma trutta*) to leachate from alum shale collected during the tunnel construction at Gran were performed in the laboratory to investigate uptake of leached elements and effects on the fish from the leachate (Skipperud et al., 2016a). One experiment investigated uptake with time (Hjulstad, 2015). There was clear uptake of U in both gills and liver, and well as Cd, Mo and Ni in gills. Most of the uptake was seen during the first 96 h, and the difference from 96 h to 264 h was small. Other elements were not found to be taken up in the 264 h experiment. The leachate pH was about 7.8 and Ca^{2+} concentrations about 38 mg L^{-1}. In the other fish experiment, the dose-response with different dilutions of alum shale leachate was investigated (Skipperud et al., 2016a). Leachate prepared by contact with alum shale was diluted with varying amounts of control water with the same pH and major ion concentrations, and the brown trout was exposed to the leachates for 192 h. U, Mo and Cd were again taken up by the fish, and other elements not. Increasing concentrations of

[1] The condition factor is $K = \frac{100 \times w}{l^3}$ where w is the weight of the fish and l is the length.

U and Mo were identified in gills, liver and kidney with increasing leachate concentrations, while for Cd this was only seen in gill. Bioconcentration factors (concentration in organ divided by concentration in water) in the dose-response experiment in gills were 0.7-0.8 for Mo, 4-7 for U and 1,000-2,800 for Cd. For Cd and U, the experimental bioconcentration factors were quite similar to observations in the field, while for Mo the bioconcentration factor was 1-2 orders of magnitude higher in the field (Skipperud et al., 2016a). In this experiment, pH was about 7.4 and Ca concentrations about 32 mg L^{-1}. The pH and Ca levels in the leachates of both experiments will have had a protective effect on the fish, and have likely contributed to the limited uptake of many of the elements in solution. Negative effects on the fish where not seen in either experiment. Higher uptake of several elements and pronounced effect on fish would be expected by a lower pH (Lydersen et al., 2002; Rosseland et al., 1992).

Laboratory experiments with the earthworm *Eisenia hortensis* were performed with 0, 5 and 25 % alum shale from Gran mixed into the soil (Schöpke, 2017). The alum shale debris used in the experiments was from the same batch as the debris used for the leaching experiments in this work. Uptake from the added alum shale was seen for several elements, and was especially clear for Cd with concentration ratios (CR)[2] above 10. Other elements that were taken up included V, Ni, Mo, Zn, Sb and U. The worms in the 25 % alum shale treatment had lower reproduction than both the 0 and 5 % treatments, and 16 % mortality was also observed in this treatment. Both the mortality and reproduction results indicated that the levels of NORM and/or stable elements reached toxic levels in the treatment with 25 % alum shale. Schöpke (2017) also investigated the transfer of elements from adult worms to cocoons, and saw that especially Zn, Sb, Cu, Mn and U were transferred in substantial amounts (CR 0.7-1.5).

Soils developed on black shales have been shown to have elevated concentrations of several trace elements, and crops grown on such soils have been found to have elevated levels of Cd and Mo (Alloway, 2013).

The major part of the elements determined in the aqueous phase of the leaching experiments were assumed to be bioavailable, as they were present as low molecular

[2] $CR = \frac{concentration\ in\ organism}{concentration\ in\ media}$ where media is the exposure media the organism is in, e.g. soil or water.

mass species. As mentioned, pH and Ca^{2+} concentrations are also important for the toxicity of the leachate to biota (Lydersen et al., 2002; Rosseland et al., 1992). Dilution of leachate from the disposal site with water having neutral pH and high concentration of base cations like Ca^{2+} will thus reduce the toxicity, while dilution with, e.g., rainwater might not have the same effect on toxicity as the protection from base cations is reduced. Surface water sampled in the Gran area had Ca^{2+} concentrations of 40-130 mg L^{-1} and a pH of 7.5-8.8 (Skipperud et al., 2016a), which can reduce the uptake in biota – a protection that cannot be expected everywhere. pH in lakes in Norway is commonly as low as 5.0, and Ca^{2+} concentrations in some regions are on average below 0.6 mg L^{-1} (Skjelkvåle et al., 2012). The protection from high Ca^{2+} and pH values can be reduced if ARD starts.

For effects on the downstream environment, the volume of contaminated water leaching from the disposal site and the downstream dilution factor are important, in addition to the water quality. As water exchange in the disposal site is sought to be minimized, the dilution factor is expected to be high. So far, Vigga River seems to be only marginally affected by the leaching from the disposal site (Greipsland et al., 2019).

The abovementioned field and laboratory investigations have demonstrated potential bioavailability of both stable and radioactive elements in the alum shale, both for soil-dwelling organisms and aquatic organisms exposed to leached elements. Furthermore, a potential multiple stressor scenario is identified. Based on concentrations measured in the field, a cumulative risk assessment for the trace elements at Gran was performed. Depending on which field station data were used and the organism in focus, U, Ni, Al and Zn were identified as main risk drivers (Skipperud et al., 2016a; Skipperud et al., 2016b).

At Gran and in similar cases, adaptation of the local life can be of importance. The potential effects on the local ecosystems from the disposal of alum shale can be lower than expected because the area is naturally rich in these contaminants and the local life has had time to adapt to somewhat elevated levels of contaminants (Skipperud et al., 2016a; Walker et al., 2012).

4.3.3 Storage of alum shale and other acid producing rock – reflections about the storage site at Gran

4.3.3.1 Selecting rock masses for storage

The guidelines from the Norwegian Environmental Agency for storage of acid producing rock states that if the NP to AP ratio is in the uncertainty zone, i.e., between 1 and 3, further investigations should be done (Endre & Sørmo, 2015). At Gran, several criteria were used for deciding which rock masses should go into the disposal site and which masses should be considered safe (Fjermestad et al., 2018). Firstly, all alum shale and other black shales that had a similar composition (determined by XRF) were put in the disposal site independent of other criteria, and tunnel blasts with down to 10 % alum shale were treated accordingly. For other rock masses, a limit of 10 g S kg^{-1} was used as a minimum limit for (estimated) sulphide content making disposal necessary. Furthermore, if the rock masses had a Ca:S ratio above 2, they were not considered acid producing. Assuming that all Ca is originating from calcite and all S is from pyrite, this translates to a NP:AP of 1. Furthermore, to be required for disposal, the rock masses should have a combined content of Mo, Pb, As, Zn, U and Cu above 320 mg kg^{-1}. See Fjermestad et al. (2018) for a more detailed overview of the requirements.

The criteria from Gran *cannot* be generally applied, and decisions to make such criteria have to be based on a good knowledge regarding local conditions and the geology of the material to be disposed of – not only on the total element concentrations, but on the mineral composition (Dold, 2017; Fjermestad et al., 2018). In mining situations, the geology will often be thoroughly investigated for exploitation purposes, and this knowledge should be used also in the work with classifying the masses for disposal (Dold, 2017). In construction work, separate investigations regarding mineralogy will often have to be made. In the case at Gran, the local geology was quite well investigated and acid tests were made to justify the assumption that the Ca in the rocks represented calcite, in addition to some XRD analyses and leaching tests (Fjermestad et al., 2018). Furthermore, the rock masses that were considered safe were reused locally in the construction of the road (pers. comm. Halldis Fjermestad, 2019), and as the area is naturally rich in chalk, minor acid production is not expected to be a problem (pers. comm. Per Hagelia, 2019).

As mentioned, rock masses at Gran that did not have a high content of trace elements were considered safe even if they were acid producing. While leaking of potentially harmful trace elements is one of the important aspects of acid rock drainage (ARD), leaking of acid water with high content of Al and Fe would be detrimental for downstream aquatic life (Hindar, 2010; Rosseland et al., 1992). The Pollution Control Act (2004) also specifically states that acid-producing masses are considered contaminated ground. Using the assumptions of Dold (2017) (discussed in section 4.2.2.1), the ratio Ca:S of 2 used at Gran translates to a NP:AP ratio of 0.5. Furthermore, one cannot be certain that all Ca is from calcite, or that all S is from sulphides. Most of the excavated rock masses that were not alum shale had however a Ca:S ratio far above 2 and were from horizons not expected to produce acid (Fjermestad et al., 2018; Owen et al., 1990), such as limestone. Thus, most of the rock masses that were considered safe, likely had a high neutralizing capacity, and this can likely make up for small amounts of excavated masses with some acid-producing capacity.

Detailed knowledge about local conditions and geology leads to greater certainty when determining which rock masses need special handling and storage to avoid acid-production and leaching of stable and radioactive elements. In turn, this means that safety margins could be smaller, and likely that a smaller amount of rock masses have to be stored under special conditions. Thus, a greater amount of excavated rock masses could be disposed of freely. This has practical and economical benefits, but also environmental, as less rock masses have to be transported and less resources have to be put into treatment and storage strategies. However, some results from this work should be taken into consideration for assessing rock masses as safe. Firstly, the potential for acid production is not the only criteria that should be considered, as leaching of many elements reach potentially harmful levels even without a pH drop. Secondly, wash-out of buffer capacity can potentially transform net neutralizing rocks into net acid-producing rocks. The potential for wash-out of buffer capacity under different conditions and for different rock types should therefore be further investigated.

4.3.3.2 Storage of acid producing rock in water

Earlier leaching experiments (for up to 1 year and 2 months) with alum shale from this area have not shown any reduction in pH in oxidizing conditions (Fjermestad et al., 2017; Helmers, 2013; Hjulstad, 2015) due to inherent carbonates providing buffering, and slow

kinetics. The same was observed in the present work. However, development of ARD can take many years, and whether and when such development will happen can be difficult to predict correctly (Dold, 2017; Endre & Sørmo, 2015; Parbhakar-Fox & Lottermoser, 2015). Results in this work for NP:AP ratios and changes in carbonate content after leaching experiments clearly indicate that ARD will develop at Gran unless the conditions in the disposal site are strictly controlled. To avoid ARD, the exchange of water and intrusion of air in the disposal site must be minimal.

At Gran, the disposal site was thought to have a slow exchange of water and to drain mainly to the small Vigga River (Fjermestad et al., 2018). Measures were taken to keep the debris submerged in water, and the disposal site was covered with a surface coating to reduce access to air. Crushed rock was used for surface coating (Fjermestad et al., 2018), while ideally clay should have been used to minimize permeability (Appelo & Postma, 2010; Sørmo et al., 2015). If the disposal site has not been completely sealed, oxygenated water will enter and contaminated water will leach out into the downstream river Vigga, with potential effects on the local environment. As discussed above, another effect of exchange of water is the loss of carbonate buffer capacity, which can speed up the onset of ARD. Alkalinity measurements in the storage site at Gran were several times higher than in the leaching experiments (Fjermestad et al., 2018; Greipsland et al., 2019), likely due to higher pH and/or higher P_{CO2}. Thus, exchange of water in the disposal site can remove even more buffer capacity than demonstrated in the cyclic leaching experiment.

Storage in a bog means that the alum shale is stored below the groundwater table, reducing access to oxygen. During a drought, the groundwater level can decline, and the disposed masses can be exposed to air. This can give a cyclic oxidation and leaching scenario for the stored masses. At Gran, acid producing rock was stored 1 m below what was considered natural fluctuations in the groundwater level, and the higher levels of the disposal site was filled with rock that is not acid producing (Fjermestad et al., 2018). In the unusually dry summer of 2018, the water levels in the storage site were still sufficiently high to cover the alum shale (Greipsland et al., 2019). During snow melt and high precipitation, the upper part of the storage site have shown increased exchange of water, while the deeper parts of the storage site seem to be less vulnerable and more stable (Fjermestad et al., 2018). Thus, the results from the WET treatment could possibly

be illustrative for processes in the upper part of the storage site, while the lower masses could be more like the AOC or LOC treatments. The DRY treatment could illustrate what happens in the top part of the disposal site, where rock masses considered not to be acid producing are stored. In Norway, climate change is expected to increase the frequency of both severe droughts and heavy rainfalls (Andreassen et al., 2016) both of which can make the safe storage of acid-producing rock more challenging. At Gran, zones were established around the disposal site where special considerations are required to avoid unintentional lowering of the groundwater level from construction work etc. (Fjermestad et al., 2018).

At Gran, a surveillance program monitoring the conditions in the disposal site, movements of water (both via wells) and conditions in downstream water bodies (surface water sampling) is planned until 2020 (Fjermestad et al., 2018). A gradual decrease in pH in the disposal site has been seen from the disposal site was established, but as of November 2018, almost all pH measurements so far are above pH 7 (Fjermestad et al., 2018; Greipsland et al., 2019). Elevated levels of SO_4^{2-} in the disposal site indicates ongoing sulphide oxidation. Satisfyingly reducing conditions in the disposal site have not yet been established. E_h values measured in the wells have been measured down to about -300 mV, which is satisfying (see Figure 22), but most measurements have been higher and indicated conditions allowing for pyrite oxidation (Greipsland et al., 2019). Concentrations of nitrate were 0.6 mg L^{-1} or lower in the wells in measurements from 2017-2018 (Greipsland et al., 2019), thus the high amounts of NO_3 measured in 2016 (see section 4.2.4) are likely either consumed (by biological processes or oxidation reactions) or washed out, and NO_3^- is likely not important for pyrite oxidation anymore.

Wells downstream the disposal site showed elevated concentrations of SO_4^{2-}, Ni, Zn and U compared to upstream, indicating pyrite oxidation in the disposal site and leaking of contaminated water (Greipsland et al., 2019). Looking at the downstream recipient waterbodies, concentrations of Ni and U have shown a slight increasing tendency from 2014 to 2018, while Zn seem to have decreased the last years (Greipsland et al., 2019). The water quality in these water bodies with regard to As, Cd, Cr, Cu, Ni, Pb, Zn and U is good, according to classifications from the Norwegian Environmental Agency (2016), for the stable elements, and Canadian water quality guidelines for protection of aquatic life, for U (Canadian Council of Ministers of the Environment, 2018).

Results so far indicate that storage conditions in the disposal site are stable and according to plan (Greipsland et al., 2019). Measurements of the groundwater level and temperature in the disposal site indicate nevertheless that water exchange increases during heavy precipitation events and snowmelt (Fjermestad et al., 2018; Greipsland et al., 2019). This showed that a scenario as tested in the WET treatment of the leaching experiment should be realistic, and the experiment results indicated that exchange of water in the disposal site could cause depletion of the buffer capacity, in addition to increased oxygen availability and leaking of contaminated water.

The alum shale at Gran has been found to have a lower concentration of sulphides compared to alum shales further south in the Oslo Region (Endre, 2013). This, together with the inherent buffer capacity from carbonates, has likely limited the short-term potential for leaching, and has probably been important in keeping the pH circumneutral and minimizing the leaching from the disposal site during construction and in the time after.

Of special interest in alum shale is the presence of NORM. In the leaching experiments, solubility of U was demonstrated, implying that U was oxidized to U^{VI} either during excavation, storage or experiment. While some of the U on the surface of the debris is likely to be oxidized to soluble U^{VI} during excavation of rock masses, the main part of U in the rock would likely be present as U^{IV}. Thus, keeping anoxic or reducing conditions in a disposal site is expected keep the main part of U immobile, and reducing conditions can also reduce U^{VI} back to U^{IV} (Alloway, 2013). Other factors of importance for U mobility is sorption to organic matter, and increased solubility in water with high carbonate concentrations (Seder-Colomina et al., 2018; Sheppard et al., 2006; Stanley & Wilkin, 2019; Vandenhove et al., 2009). In the conditions tested in the cyclic leaching experiment, exchange of water seemed to have no effect on leaching of U.

On the other hand, ^{226}Ra could become more mobile in anoxic or reducing conditions as the sulphate concentrations would be reduced. Groundwater low in sulphate, with high ionic strength and high contents of Ca^{2+} and Ba^{2+}, are conducive to the transport of Ra (Landa, 2007). The cyclic leaching experiments demonstrated increased solubility of ^{226}Ra when water was exchanged. Other studies have investigated the release of Ba and ^{226}Ra from $BaSO_4$ by sulphate-reducing bacteria. Phillips et al. (2001) measured release of Ba and ^{226}Ra from an oil-field sample containing barite scale, but the release was not

stoichiometric with the production of sulphide, and >99.9 % of Ba and ^{226}Ra was retained in the solids. On the other hand, Landa et al. (1986) measured release of 20 % of the ^{226}Ra inventory in U mill tailings when exposed to sulphate-reducing bacteria. Thus, there is likely a considerable potential for remobilization of ^{226}Ra if the conditions are favourable.

5 Uncertainties

Essentially, all models are wrong, but some are useful, George Box (1987)

In environmental sciences, we are trying to understand processes in nature. As most ecosystems are immensely complex with a multitude of chemical, biological, physical and geological processes going on intertwined, one approach is simplification and simulation of a certain process in the laboratory – a model. For example, this work set out to investigate the effect of varying oxygen conditions, exchange of water and drying of debris on the leaching from alum shale through laboratory leaching experiments. While simplification is useful or even necessary to isolate the effects of a single parameter or process, translation of the results into implications in "the real world" is often a challenge. This contributes to conceptual uncertainty (Salbu, 2016).

The environmental systems are always more complex than our models, and there may be factors that are equally or more important for determining processes than the factors investigated in the laboratory. In the leaching experiments, the goal was not to exactly mimic the conditions in the disposal site at Gran, but rather to investigate the effect of certain parameters of relevance to leaching. Greater variation in E_h values were observed in the disposal site than was investigated in the experiments. Other potentially important factors that were not investigated includes the presence of organic matter (which affects the speciation and mobility of a range of elements) and biological activity in the disposal site. Biological activity can catalyse the pyrite oxidation, and the high methane and CO_2 concentrations observed in the LOC samples of the cyclic experiment (Paper II) could indicate such activity. Furthermore, water quality can change dramatically when percolating through the ground from the disposal site until entering the downstream water bodies. Sorption to soils, sediments and other materials can reduce the levels of contaminants before and after the water reaches Vigga River. While protecting the aquatic life, this can have adverse effects on soil and sediment fauna. As the water move downstream, the pH and redox is likely to change, which means possible changes in speciation and mobility of the leached elements.

Input uncertainty includes uncertainty in laboratory measurements as well as representativeness of sampling (Salbu, 2016). In this work, the measurement uncertainties associated with determination of element concentrations in samples were

assumed to be rather low. Of greater importance is the chosen sampling strategy: Collection of alum shale for leaching experiments was performed to get a sample with high content of uranium, not to get a representative sample of the rock masses stored in the disposal site. Thus, the sampling was biased. Furthermore, when comparing the results from the laboratory experiments to the disposal site water, it is important to remember that the measurements from the disposal site represent a snapshot of the conditions.

When generalizing findings in this work to other situations in other places, even greater uncertainties arise. Most importantly, it must be kept in mind that local variations in mineralogy could drastically change the outcome of the experiments. Thus, detailed information about local conditions and geology is crucial when applying the results of this work in a different context.

6 Conclusions

The newly developed method for measuring ^{226}Ra was rapid and simple, and allowed for direct determination in water and digested geological samples. The method allowed for collection of detailed information of the behaviour of ^{226}Ra in the leaching experiments, and is a useful tool for determining ^{226}Ra in elevated soil samples as well as for assessing drinking water quality.

In the leaching experiments with alum shale from Gran, pyrite oxidation with concomitant acid production was expected by the given conditions, and sulphate concentrations indicated that it occurred. However, the buffer capacity of the debris was not exceeded in either of the treatments, and this was reflected in a leachate pH of 7.6-7.7 at the end of the experiment for all treatments. The debris content of calcite was, however, reduced by two thirds in the experiment with cyclic exchange of water, and the experiment illustrated how the buffer capacity of the rock can be washed out without contributing to neutralizing acid.

High mobility of several elements in alum shale, including Mo, Mn, Ni, Zn, Cd and U, was observed in the leaching experiments. Mo and U also showed high concentrations in the disposal site, and Ni, Zn and U have been measured in elevated concentrations in downstream wells. Unless exchange of water in the disposal site is kept at a minimum, these elements can likely leach in significant amounts to downstream water bodies. If acid rock drainage develops in the disposal site, higher mobility of also other elements can be expected.

Of the measured radionuclides in the experiments, ^{238}U was clearly the most mobile, and 2-5 % of the debris content leached in the different treatments. The highest mobility was seen in the treatment with low oxygen conditions. ^{232}Th generally had very low solubility by the given conditions, while solubility of ^{226}Ra increased markedly with exchange of water, but still <1 % of the debris content leached.

The results underline the importance of minimizing water exchange if alum shale or other acid producing rock are stored submerged in water.

6.1 Evaluation of hypotheses

The following hypotheses where formulated (see the introduction, section 1.1):

1. Even without a pH drop, there will be considerable leaching of elements that are soluble at a circumneutral pH, resulting in potentially harmful water concentrations

The concentrations in the leachates were high for many elements, and greatly exceeded environmental quality standards for several elements. Thus, for organisms directly exposed to these leachates, adverse effects can be expected. However, downstream the disposal site at Gran there will likely be substantial dilution, which reduces the chances of environmental effects.

2. Drying of the debris between periods of submersion will lead to greater pyrite oxidation and increased leaching of a range of elements

Based on higher sulphate concentrations in the DRY treatment, the drying periods can be assumed to have increased pyrite oxidation. However, there were no measureable changes in pyrite concentrations of the tested rock debris. The leaching of many elements in the DRY treatment was statistically significantly higher than in the WET treatment, but the actual differences were rather small for most of them. Thus, there was no great increase in leaching after drying periods. However, if the experiment had been continued until the buffer capacity was depleted, and there was a pH drop, this hypothesis might have been supported.

3. Exchange of water will lead to faster depletion of the buffer capacity of the debris

More than half of the calcite and carbonates in the alum shale debris was dissolved at the end of the cyclic leaching experiment, in both treatments. The alkalinity measurements indicated that a significant part of the dissolved carbonates have been removed without contributing to acid neutralization when the water was exchanged. Thus, this hypothesis seemed to be supported. Furthermore, this result should be seen in combination with results from the LOC treatment, where increased P_{CO2} likely caused increased solubility of calcite. Thus, by high P_{CO2} (as can be expected in an underground storage site), exchange of water will deplete the buffer capacity even faster.

4. Ra will follow Ba and be limited by $BaSO_4$ solubility, and thus have lower mobility as pyrite oxidation increases

The general trends for Ba and ^{226}Ra were similar in both experiment, and when the K_{SP} for $BaSO_4$ was exceeded, leachate concentrations of both elements decreased, indicating co-precipitation of ^{226}Ra. However, when the K_{SP} for $BaSO_4$ was not exceeded, the leaching rate of ^{226}Ra was higher in the DRY treatment with assumed greater (pyrite) oxidation than the WET treatment. This indicates that ^{226}Ra was leaching from a phase that was sensitive to oxidation.

5. Exchange of water will increase the mobility of elements that are limited by solubility constraints, like ^{226}Ra and Ba

This hypothesis was supported by the results. Higher release of elements like V, As, Ba, and ^{226}Ra was seen in the cyclic experiment compared to the AOC-LOC experiment.

6.2 Further work

The experimental work included only some important factors that would influence leaching of NORM and stable elements from alum shale. Other factors that could be investigated to shed further light on important processes include a greater variation in pH and E_h values, where the mobility of ^{226}Ra by strictly anoxic or reducing conditions would be especially interesting, as well as continuation of oxic leaching experiments in the time after a pH drop has occurred. The effect of the variation in pH and E_h on the speciation of the elements should also be investigated. A more thorough characterization of the alum shale using advanced technology such as synchrotron-radiation based techniques could identify the source phases of the trace elements in the rock, making prediction of behaviour easier. Investigations of the microbial community in the disposal site at Gran could provide useful information about the effect of these on the leaching. Furthermore, as none of the abovementioned fieldwork or investigations of bioavailability and effect included any measurements for ^{226}Ra, this would be a very interesting step in continuation of this work. The potential for wash-out of carbonate buffer capacity for different kinds of rock under different conditions should be investigated.

7 References

Aas, W., Platt, S., Solberg, S., & Yttri, K. E. (2015). *Monitoring of long-range transported air pollutants in Norway, annual report 2014* (M-367).

Abbasi, S., Lamb, D. T., Palanisami, T., Kader, M., Matanitobua, V., Megharaj, M., & Naidu, R. (2016). Bioaccessibility of barium from barite contaminated soils based on gastric phase in vitro data and plant uptake. *Chemosphere, 144*, 1421-1427. doi:https://doi.org/10.1016/j.chemosphere.2015.10.031

Abraitis, P. K., Pattrick, R. A. D., & Vaughan, D. J. (2004). Variations in the compositional, textural and electrical properties of natural pyrite: a review. *International Journal of Mineral Processing, 74*(1), 41-59. doi:https://doi.org/10.1016/j.minpro.2003.09.002

Alloway, B. J. (2013). *Heavy Metals in Soils: Trace Metals and Metalloids in Soils and their Bioavailability* (B. J. Alloway & J. T. Trevors Eds., 3rd ed.): Springer.

Andersson, A., Dahlman, B., Gee, D. G., & Snäll, S. (1985). *The Scandinavian Alum Shales*. Uppsala: Sveriges Geologiska Undersökning.

Andreassen, L. M., Beldring, S., Bjune, A., Breili, K., Dahl, C. A., Dyrrdal, A. V., Isaksen, K., Haakenstad, H., Haugen, J. E., Hygen, H. O., Langehaug, H. R., Lauritzen, S.-E., Lawrence, D., Melvold, K., Mezghani, A., Ravndal, O. R., Risebrobakken, B., Roald, L., Sande, H., Simpson, M. J. R., Skagseth, Ø., Skaugen, T., Skogen, M., Støren, E. N., Tveito, O. E., & Wong, W. K. (2016). *Klima i Norge 2100. Kunnskapsgrunnlag for klimatilpasning oppdatert i 2015* (2/2015). I. Hanssen-Bauer, E. J. Førland, I. Haddeland, H. Hisdal, S. Mayer, A. Nesje, J. E. Ø. Nilsen, S. Sandven, A. B. Sandø, A. Sorteberg, & B. Ådlandsvik (Eds.), www.klimaservicesenter.no:

Appelo, C. A. J., & Postma, D. (2010). *Geochemistry, groundwater and pollution* (2nd ed.): CRC press.

Armands, G. (1972). *Geochemical Studies of Uranium, Molybdenum and Vanadium in a Swedish Alum Shale.* (Ph.D.), University of Stockholm, Stockholm Contributions in Geology, Volume XXVII.

Barnes, R. B. (1975). The determination of specific forms of aluminum in natural water. *Chemical Geology, 15*(3), 177-191. doi:http://dx.doi.org/10.1016/0009-2541(75)90018-2

Becker, J. S. (2005). Inductively coupled plasma mass spectrometry (ICP-MS) and laser ablation ICP-MS for isotope analysis of long-lived radionuclides. *International Journal of Mass Spectrometry, 242*(2), 183-195. doi:https://doi.org/10.1016/j.ijms.2004.11.009

Bierens de Haan, S. (1991). A review of the rate of pyrite oxidation in aqueous systems at low temperature. *Earth-Science Reviews, 31*(1), 1-10. doi:http://dx.doi.org/10.1016/0012-8252(91)90039-I

Bonczyk, M., & Michalik, B. (2016). *Radium isotopes in water – interlaboratory comparison (ILC)*.

Botkin, D. B., & Keller, E. A. (2005). *Environmental Science - Earth as a living planet* (5th ed.). United States of America: John Wiley & Sons.

Box, G. E. P., & Draper, N. R. (1987). *Empirical Model-Building and Response Surfaces*: John Wiley & Sons.

Braunschweig, J., Bosch, J., & Meckenstock, R. U. (2013). Iron oxide nanoparticles in geomicrobiology: from biogeochemistry to bioremediation. *New Biotechnology, 30*(6), 793-802. doi:https://doi.org/10.1016/j.nbt.2013.03.008

Canadian Council of Ministers of the Environment. (2018). Water Quality Guidelines for the Protection of Aquatic Life. on 25.06.2019

Chandra, A. P., & Gerson, A. R. (2010). The mechanisms of pyrite oxidation and leaching: A fundamental perspective. *Surface Science Reports, 65*(9), 293-315. doi:http://dx.doi.org/10.1016/j.surfrep.2010.08.003

CRC Handbook of Chemistry and Physics. (1993). (D. R. Lide Ed., 74th ed.). U.S.A.: CRC.

Dold, B. (2017). Acid rock drainage prediction: A critical review. *Journal of Geochemical Exploration, 172*, 120-132. doi:https://doi.org/10.1016/j.gexplo.2016.09.014

Driscoll, C. T. (1984). A procedure for the fractionation of aqueous aluminium in dilute acidic waters. *International Journal of Environmental Analytical Chemistry, 16*(4), 267-283.

Eggen, R. I., Behra, R., Burkhardt-Holm, P., Escher, B. I., & Schweigert, N. (2004). Challenges in ecotoxicology. *Environmental Science & Technology, 38*(3), 58a-64a.

Endre, E. (2013). *Identifisering og karakterisering av skiferhorisonter i tunneltraséen* (20120110-R=1).Norwegian Geotechnical Institute:

Endre, E., & Sørmo, E. (2015). *Identifisering og karakterisering av syredannende bergarter: Veileder for miljødirektoratet M-310* (M-310). N. G. Institute (Eds.), miljodirektoratet.no:

Engelstad, J. G. (2016). *Ecological Implications of Road Construction in an Alum Shale Bedrock Area - A State Highway (Rv4) Case Study.* (M. Sc.), Norwegian University of Life Sciences

EPA. (1999). *Understanding variation in partition coefficient, K_d, values. Volume II: Review of geochemistry and available K_d values for cadmium, cesium, chromium, lead, plutonium, radon, strontium, thorium, tritium (^3H) and uranium*.Washington, USA:

Erlström, M. (2014). *Skiffergas och biogen gas i alunskiffern i Sverige, förekomst och geologiska förutsättningar – en översikt* (19).Uppsala:

Laying down requirements for the protection of the health of the general public with regard to radioactive substances in water intended for human consumption, (2013).

Falk, H., Lavergren, U., & Bergbäck, B. (2006). Metal mobility in alum shale from Öland, Sweden. *Journal of Geochemical Exploration, 90*(3), 157-165. doi:http://dx.doi.org/10.1016/j.gexplo.2005.10.001

Fjermestad, H. (2013). *Mobility of Uranium and other metals in bedrock materials from Gran, Norway - Implications for tunnel construction.* (MSc), Norwegian University of Life Sciences, Ås, Norway.

Fjermestad, H. (2019). [Personal communication via E-mail].

Fjermestad, H., Gundersen, E., Hagelia, P., Moen, A. B., & Torp, M. (2018). *National Road 4, utilization of black shale - Final report and experiences gathered* (333). Retrieved from www.vegvesen.no/

Fjermestad, H., Hagelia, P., & Thomassen, T. (2017). *Large-scale leaching experiment with black shale from National Road 4, Hadeland* (665). Retrieved from www.vegvesen.no

Analytical methods for radioactivity, 40 CFR 141.25 § 141.25 (2012).

Greipsland, I., Skrutvold, J., & Roseth, R. (2019). *Rv. 4 Gran - Jaren. Etterundersøkelser av vannkjemi i grunnvann og resipienter* (5/34/2019).www.nibio.no:

Grundl, T. J., Haderlein, S., Nurmi, J. T., & Tratnyek, P. G. (2011). Introduction to Aquatic Redox Chemistry. In *Aquatic Redox Chemistry* (Vol. 1071, pp. 1-14): American Chemical Society.

Hagelia, P. (2019). Personal communication via E-mail.

Hartmann, D. L., Tank, A. M. G. K., Rusticucci, M., Alexander, L. V., Brönnimann, S., Charabi, Y., Dentener, F. J., Dlugokencky, E. J., Easterling, D. R., Kaplan, A., Soden, B. J., Thorne, P. W., Wild, M., & Zhai, P. M. (2013). *Observations: Atmosphere and Surface.* T. F. Stocker, D. Qin, G.-K. Plattner, M. Tignor, S.K. Allen, J. Boschung, A. Nauels, Y. Xia, V. Bex and P.M. Midgley (Eds.), Cambridge University Press,

Cambridge, United Kingdom and New York, NY, USA.: Retrieved from https://www.ipcc.ch/report/ar5/wg1/

Helmers, T. A. (2013). *The mobility of uranium from U-containing bedrock materials as a function of pH: Implications for tunnel construction.* (MSc), Norwegian University of Life Sciences, Ås, Norway.

Hindar, A. (2010). *Highway E18 Grimstad-Kristiansand; effects and quantification of acid runoff from deposits of sulphide-bearing rock*. Retrieved from http://brage.bibsys.no

Hindar, A. (2013). E18 Grimstad-Kristiansand gjennom sulfidholdige bergarter – syreproduksjon og effekter på avrenningsvann. *Vann, 48*(1), 97-103.

Hjulstad, M. (2015). *Leaching, Uptake and Effects in Brown Trout (Salmo trutta) of Radionuclides and Metals from Black Shales and Sulphur Bearing Gneiss* (MSc), Norwegian University of Life Sciences, Ås, Norway.

Hou, X., & Roos, P. (2008). Critical comparison of radiometric and mass spectrometric methods for the determination of radionuclides in environmental, biological and nuclear waste samples. *Analytica Chimica Acta, 608*(2), 105-139. doi:https://doi.org/10.1016/j.aca.2007.12.012

IAEA. (2010). *Analytical Methodology for the Determination of Radium Isotopes in Environmental Samples* (19).Vienna:

IAEA. (2014). *The environmental behaviour of radium: Revised edition* (476).Vienna: Retrieved from https://www-pub.iaea.org/books/iaeabooks/series/80/Technical-Reports-Series

IAEA. (2019). Live Chart of Nuclides. Retrieved from https://www-nds.iaea.org/relnsd/vcharthtml/VChartHTML.html on 05.07.2019

Jeng, A. S. (1991). Weathering of Some Norwegian Alum Shales. I. Laboratory simulations to study acid generation and the release of sulfate and metal cations (calcium, magnesium, and potassium). *Acta Agriculturae Scandinavica, 41*(1), 13-35. doi:10.1080/00015129109438580

Jeng, A. S. (1992). Weathering of Some Norwegian Alum Shales, II. Laboratory Simulations to Study the Influence of Aging, Acidification and Liming on Heavy Metal Release. *Acta Agriculturae Scandinavica, Section B — Soil & Plant Science, 42*(2), 76-87. doi:10.1080/09064719209410203

Kirby, H. W., & Salutsky, M. L. (1964). *The Radiochemistry of Radium* (NAS-NS 3057).

Köhler, M., Preuße, W., Gleisberg, B., Schäfer, I., Heinrich, T., & Knobus, B. (2002). Comparison of methods for the analysis of 226Ra in water samples. *Applied Radiation and Isotopes, 56*(1), 387-392. doi:https://doi.org/10.1016/S0969-8043(01)00219-6

Lagacé, F., Foucher, D., Surette, C., & Clarisse, O. (2017). Quantification of 226Ra at environmental relevant levels in natural waters by ICP-MS: Optimization, validation and limitations of an extraction and preconcentration approach. *Talanta, 167*, 658-665. doi:https://doi.org/10.1016/j.talanta.2017.02.031

Landa, E. R. (2007). Naturally occurring radionuclides from industrial sources: characteristics and fate in the environment. In S. George (Ed.), *Radioactivity in the Environment* (Vol. 10, pp. 211-237): Elsevier.

Landa, E. R., Miller, C. L., & Updegraff, D. M. (1986). Leaching of 226Ra From U Mill Tailings by Sulfate-reducing Bacteria. *Health Phys, 51*(4), 509-518.

Lavergren, U., Åström, M. E., Falk, H., & Bergbäck, B. (2009). Metal dispersion in groundwater in an area with natural and processed black shale – Nationwide perspective and comparison with acid sulfate soils. *Applied Geochemistry, 24*(3), 359-369. doi:https://doi.org/10.1016/j.apgeochem.2008.11.022

Lawrence, R. W., & Wang, Y. (1996). *Determination of Neutralization Potential for Acid Rock Drainage Prediction* (MEND Project 1.16.3). Retrieved from http://mend-

nedem.org/mend-report/determination-of-neutralization-potential-for-acid-rock-drainage-prediction/
Lieser, K. H. (1995). Radionuclides in the Geosphere: Sources, Mobility, Reactions in Natural Waters and Interactions with Solids. *Radiochimica acta., 70-71*, 355.
Loveland, W., Morrissey, D. J., & Seaborg, G. T. (2006). *Modern Nuclear Chemistry*: John Wiley & Sons.
Lydersen, E., Löfgren, S., & Arnesen, R. T. (2002). Metals in Scandinavian Surface Waters: Effects of acidification, Liming, and Potential Reacidification. *Critical Reviews in Environmental Science and Technology, 32*(2), 73-295. doi:https://doi.org/10.1080/10643380290813453
Løken, T. (2007). Alunskifer/svartskifer - den forurensende bergarten. *Vann, 42*(2), 211-218.
Maxwell, S. L., & Culligan, B. K. (2012). Rapid determination of 226Ra in environmental samples. *Journal of Radioanalytical and Nuclear Chemistry, 293*(1), 149-156. doi:10.1007/s10967-012-1627-z
Melgård, M. D. (2017). *Determination of Ra-226 in Environmental Samples using ICP-QQQ after Cation Exchange-Separation.* (MSc), Norwegian University of Life Sciences, Ås.
Miller, J. N., & Miller, J. C. (2005). *Statistics and Chemometrics for Analytical Chemistry*. Great Britain: Pearson Education Limited.
Mindat.org. (2019a). Calcite. Retrieved from https://www.mindat.org/min-859.html on 22.06.2019
Mindat.org. (2019b). Muscovite. Retrieved from https://www.mindat.org/min-2815.html on 22.06.2019
Mindat.org. (2019c). Pyrite. Retrieved from https://www.mindat.org/min-3314.html on 22.06.2019
Mindat.org. (2019d). Quartz. Retrieved from https://www.mindat.org/min-3337.html on 09.07.2019
Mitchell, N., Perez-Sanchez, D., & Thorne, M. C. (2013). A review of the behaviour of U-238 series radionuclides in soils and plants. *J Radiol Prot, 33*(2), R17-48. doi:10.1088/0952-4746/33/2/r17
Morvan, K., Andres, Y., Mokili, B., & Abbe, J.-C. (2001). Determination of Radium-226 in Aqueous Solutions by α-Spectrometry. *Analytical Chemistry, 73*(17), 4218-4224. doi:10.1021/ac0015220
Moulin, V., Amekraz, B., Barre, N., Planque, G., Mercier, F., Reiller, P., & Moulin, C. (2004). The role of humic substances in trace element mobility in natural environments and applications to radionuclides. In E. A. Ghabbour & G. Davies (Eds.), *Humic Substances: Nature's Most Versatile Materials* (pp. 275-286): Taylor & Francis.
National Primary Drinking Water Regulations. (EPA 816-F-09-004). (2009). EPA 816-F-09-004: U.S. Environmental Protection Agency.
Navas Izquierdo, A., Machín Gayarre, J., & Soto, J. (2005). Mobility of natural radionuclides and selected major and trace elements along a soil toposequence in the Central Spanish Pyrenees. *Soil Science, 170*, 743-757.
NGI. (2019a). Follobanen. Retrieved from www.ngi.no/Prosjekter/Follobanen on 10.07.2019
NGI. (2019b). Regjeringskvartalet på alunskifer. Retrieved from www.ngi.no/Prosjekter/Regjeringskvartalet-paa-alunskifer on 10.07.2019
NGU. (2016). *PRODUKTARK: Nasjonalt aktsomhetskart for radon* Norwegian Geological Survey: Retrieved from https://register.geonorge.no/data/documents/Produktark_Radon%20aktsomhet_v2_produktark-radonaktsomhet_.pdf
NGU. (2019). Radon aktsomhetskart. Retrieved from http://geo.ngu.no/kart/radon/ on 11.07.2019

Norwegian Environmental Agency. (2016). *Quality standards for water, sediment and biota*. (M-608).
NRPA, & NGU. (2011). *Alunskiferkart for vurdering av hensynssoner i henhold til plan of bygningsloven*. Retrieved from https://www.ngu.no/upload/Aktuelt/Nyheter%202011/alunskifer_jan_11_web.pdf
Okkenhaug, G. (2012). *Mobility and solubility of antimony (Sb) in the environment.* (PhD), Norwegian University of Life Sciences, Ås. (2012:34)
Owen, A. W., Bruton, D. L., Bockelie, J. F., & Bockelie, T. G. (1990). *The Ordovician successions of the Oslo Region, Norway*. D. Roberts (Eds.), Geological survey of Norway (NGU): Retrieved from http://paleoarchive.com/
Pabst, T., Sørmo, E., & Endre, E. (2016). Geochemical characterisation of Norwegian Cambro-Ordovician black mudrocks for building and construction use. *Bulletin of Engineering Geology and the Environment, 76*(4), 1577–1592. doi:https://doi.org/10.1007/s10064-016-0941-z
Parbhakar-Fox, A., & Lottermoser, B. G. (2015). A critical review of acid rock drainage prediction methods and practices. *Minerals Engineering, 82*, 107-124. doi:https://doi.org/10.1016/j.mineng.2015.03.015
Phillips, E. J. P., Landa, E. R., Kraemer, T., & Zielinski, R. (2001). Sulfate-Reducing Bacteria Release Barium and Radium from Naturally Occurring Radioactive Material in Oil-Field Barite. *Geomicrobiology Journal, 18*(2), 167-182. doi:10.1080/01490450120549
Pipkin, B., Trent, D. D., Hazlett, R., & Bierman, P. (2008). *Geology and the environment* (P. Adams Ed., 5th ed.). USA: Thomson Brooks/Cole.
Pollution Control Act (Forurensningsforskriften), FOR-2004-06-01-931 (2004).
Rayner-Canham, G., & Overton, T. (2006). *Descriptive inorganic chemistry* (J. Fiorillo Ed., 4th ed.). Houndmills, England: W. H. Freeman and Company.
Ricker, W. E. (1975). Computation and interpretation of biological statistics of fish populations. *Bulletin of the Fisheries Research Board of Canada, 191*(1).
Rosseland, B. O., Blakar, I. A., Bulger, A., Kroglund, F., Kvellstad, A., Lydersen, E., Oughton, D. H., Salbu, B., Staurnes, M., & Vogt, R. (1992). The mixing zone between limed and acidic river waters: complex aluminium chemistry and extreme toxicity for salmonids. *Environmental Pollution, 78*(1–3), 3-8. doi:http://dx.doi.org/10.1016/0269-7491(92)90003-S
Salbu, B. (2016). Environmental impact and risk assessments and key factors contributing to the overall uncertainties. *Journal of Environmental Radioactivity, 151*, 352-360. doi:https://doi.org/10.1016/j.jenvrad.2015.09.001
Salbu, B., Lind, O. C., & Skipperud, L. (2004). Radionuclide speciation and its relevance in environmental impact assessments. *Journal of Environmental Radioactivity, 74*(1–3), 233-242. doi:http://dx.doi.org/10.1016/j.jenvrad.2004.01.008
Salbu, B., Teien, H. C., Lind, O. C., & Tollefsen, K. E. (2019). Why is the multiple stressor concept of relevance to radioecology? *Int J Radiat Biol*, 1-10. doi:10.1080/09553002.2019.1605463
Santos, S. H. (2014). *Potential Mobility of Radionuclides and Trace Elements in Bedrock Materials and in the Deposition Area at a Tunnel Construction Site RV4 Gran, Hadeland.* (MSc), Norwegian University of Life Sciences, Ås, Norway.
Schöpke, C. (2017). *Uranium and toxic metal uptake by the earthworm Eisenia hortensis in contaminated soils.* (MSc), Norwegian University of Life Sciences, Ås.
Seder-Colomina, M., Mangeret, A., Stetten, L., Merrot, P., Diez, O., Julien, A., Barker, E., Thouvenot, A., Bargar, J., Cazala, C., & Morin, G. (2018). Carbonate Facilitated Mobilization of Uranium from Lacustrine Sediments under Anoxic Conditions.

Environmental Science & Technology, 52(17), 9615-9624. doi:10.1021/acs.est.8b01255

Sheppard, S. C., Sheppard, M. I., Tait, J. C., & Sanipelli, B. L. (2006). Revision and meta-analysis of selected biosphere parameter values for chlorine, iodine, neptunium, radium, radon and uranium. *Journal of Environmental Radioactivity, 89*(2), 115-137. doi:http://dx.doi.org/10.1016/j.jenvrad.2006.03.003

Singer, P. C., & Stumm, W. (1970). Acidic Mine Drainage: The Rate-Determining Step. *Science, 167*(3921), 1121-1123. doi:10.2307/1728684

Skipperud, L., Alvarenga, E., Lind, O. C., Teien, H.-C., Tollefsen, K. E., Salbu, B., & Wærsted, F. M. (2016a). *Construction works in areas with sulphide containing rock. Case: Effects and environmental risks related to alum shale disposal site* (651).Norwegian Public Roads Administration: Retrieved from www.vegvesen.no

Skipperud, L., Gomes, T., Teien, H.-C., Tollefsen, K. E., & Wærsted, F. M. (2016b). *Challenges with naturally ocurring radioactive material (NORM) in road- and tunnel construction.* Paper presented at the 6th Norwegian Environmental Toxicology Symposium, Oslo, Norway.

Skjelkvåle, B. L., Aas, W., Manø, S., Solberg, S., Yttri, K. E., Skancke, L. B., Garmo, Ø. A., Høgåsen, T., Fjellheim, A., Halvorsen, G. A., Schartau, A. K., Jensen, T. C., Walseng, B., Saksgård, R., Hesthagen, T., Andreassen, K., Timmermann, V., Clarke, N., Framstad, E., Aarrestad, P. A., Bakkestuen, V., Bruteig, I. E., Evju, M., Kålås, J. A., & Nygård, T. (2012). *Overvåking av langtransporterte forurensninger 2011. Sammendragsrapport*. B. L. Skjelkvåle (Eds.),

Stanley, D. M., & Wilkin, R. T. (2019). Solution equilibria of uranyl minerals: Role of the common groundwater ions calcium and carbonate. *Journal of Hazardous Materials, 377*, 315-320. doi:https://doi.org/10.1016/j.jhazmat.2019.05.101

Forskrift om strålevern og bruk av stråling (strålevernforskriften), FOR-2016-12-16-1659 (2016).

Swanson, V. E. (1961). *Geology and Geochemistry of Uranium in Marine Black Shales, A Review. Uranium in Carbonaceous Rocks*.https://pubs.usgs.gov:

Sørmo, E., Breedveld, G., & Pabst, T. (2015). *Deponering av syredannende bergarter. Grunnlag for veileder.* (M-385).

Teien, H.-C. (2005). *Transformation of Aluminium Species in Unstable Aquatic Mixing zones - Mobility and Bioavailability towards Fish.* (PhD), Norwegian University of Life Sciences (2005:1)

Thørring, H., Wærsted, F. M., Raaness, A., Skipperud, L., & Jensen, L. K. (in prep.). *Elevated natural radioactivity in undisturbed forest and mountain areas of arctic Norway – local geology, soil characteristics, and transfer to biota*. Norwegian Radiation and Nuclear Safety Authority.

Tourtelot, H. A. (1979). Black shale - its deposition and diagenesis. *Clays and Clay Minerals, 27*(5), 313-321.

Ulrich, M., Bureau, S., Chauvel, C., & Picard, C. (2012). Accurate Measurement of Rare Earth Elements by ICP-MS after Ion-Exchange Separation: Application to Ultra-Depleted Samples. *Geostandards and Geoanalytical Research, 36*(1), 7-20. doi:doi:10.1111/j.1751-908X.2011.00116.x

UNSCEAR. (2018). *Sources, Effects and Risks of Ionizing Radiation. UNSCEAR 2017. Report to the General Assembly, with Scientific Annexes*.New York: Retrieved from http://www.unscear.org/docs/publications/2017/UNSCEAR_2017_Report.pdf

Vandenhove, H., Gil-García, C., Rigol, A., & Vidal, M. (2009). New best estimates for radionuclide solid–liquid distribution coefficients in soils. Part 2. Naturally occurring

radionuclides. *Journal of Environmental Radioactivity, 100*(9), 697-703. doi:http://dx.doi.org/10.1016/j.jenvrad.2009.03.014

Vandenhove, H., Van Hees, M., Wouters, K., & Wannijn, J. (2007). Can we predict uranium bioavailability based on soil parameters? Part 1: Effect of soil parameters on soil solution uranium concentration. *Environmental Pollution, 145*(2), 587-595. doi:http://dx.doi.org/10.1016/j.envpol.2006.04.011

vanLoon, G. W., & Duffy, S. J. (2011). *Environmental Chemistry - a global perspective* (3rd ed.). New York: Oxford University Press.

Walker, C. H., Sibly, R. M., Hopkin, S. P., & Peakall, D. B. (2012). *Principles of Ecotoxicology* (4th ed.). Boca Raton, FL: Taylor & Francis Group.

WHO. (2017). *Guidelines for drinking-water quality: fourth edition incorporating the first addendum* (Licence: CC BY-NC-SA 3.0 IGO.).Geneva:

Wikimedia. (2014, 11.06.2015). Uranium-238 decay chain diagram. Retrieved from https://commons.wikimedia.org/wiki/File:Decay_chain(4n%2B2,_Uranium_series).svg on 19.06.2019

Wærsted, F. M., Jensen, K. A., Reinoso-Maset, E., & Skipperud, L. (2018). High Throughput, Direct Determination of 226Ra in Water and Digested Geological Samples. *Analytical Chemistry, 90*(20), 12246-12252. doi:10.1021/acs.analchem.8b03494

Wærsted, F. M., Reinoso-Maset, E., Salbu, B., & Skipperud, L. (in prep.-a). *Rainwater leaching of alum shale debris under atmospheric and low oxygen conditions*. Faculty of Environmental Science and Natural Resource Management. Norwegian University of Life Sciences.

Wærsted, F. M., Riss, P. J., & Skipperud, L. (in prep.-b). *The effect of water exchange on the leaching of alum shale*. Faculty of Environmental Science and Natural Resource Management. Norwegian University of Life Sciences.

Zhang, T., Bain, D., Hammack, R., & Vidic, R. D. (2015). Analysis of Radium-226 in High Salinity Wastewater from Unconventional Gas Extraction by Inductively Coupled Plasma-Mass Spectrometry. *Environmental Science & Technology, 49*(5), 2969-2976. doi:10.1021/es504656q

Errata

Side	Line	Original text	Corrected text
xi	6-7	Følgelig er riktig lagring av alunskifermasser og andre syredannende bergarter avgjørende for å unngå negative effekter på miljøet.	*Moved to end of p. xiii*
xii	4	svovel	sulfat
xiii	5	og	samt
3	10	1 Bq g^{-1}	1 Bq ^{238}U g^{-1}
7	28	relative to for example calcite	relative to neutralization by for example calcite
9	14	cause	create
27	20	The experiment was kept dark	The samples were kept dark
30	17	samples.	samples (see Table 2).
32	5	, thus the	, and the
32	24	the atmospheric concentration was used.	the atmospheric concentration of 390 ppm was used (Hartmann, 2013).
48	8	Figure 22 was changed for the same figure with better resolution	
50	16	(6.47-9.16)	(6.5-9.2)
52	3	to be calcite	to behave like calcite
71	4	(Walker et al. 2012).	(Skipperud et al. 2016a; Walker et al. 2012)

Paper I

analytical chemistry

Article

Cite This: *Anal. Chem.* 2018, 90, 12246−12252

pubs.acs.org/ac

High Throughput, Direct Determination of ^{226}Ra in Water and Digested Geological Samples

F. M. Wærsted,* K. A. Jensen, E. Reinoso-Maset, and L. Skipperud

Centre for Environmental Radioactivity (CERAD), Faculty of Environmental Sciences and Natural Resource Management, Norwegian University of Life Sciences, P.O. Box 5003, N-1432 Ås, Norway

Supporting Information

ABSTRACT: A method was developed for direct measurements of ^{226}Ra in water samples with triple quadrupole inductively coupled plasma mass spectrometry (ICP-QQQ). The limit of detection was 0.42 pg L^{-1} ^{226}Ra (15 mBq L^{-1}, 0.42 pCi L^{-1}), which is compliant with the specifications for methods used for routine analysis of drinking water quality according to European and U.S. regulations. The use of N_2O as reaction gas ensured that no separation before analysis was necessary. Water samples with high total dissolved solids (conductivity >100 mS cm^{-1}) were also successfully analyzed after a simple dilution, yet the associated detection limit was higher (17 pg L^{-1}, 0.61 Bq L^{-1}, 16 pCi L^{-1}). ^{226}Ra content in soil and rock samples was determined with the same method after acid (HNO_3 + H_3PO_4) digestion and dilution, resulting in a limit of detection of 0.75 ng kg^{-1} (27 Bq kg^{-1}, 0.74 nCi L^{-1}). Analysis of water samples was achieved within 2 min on a running instrument, while the preparation and analysis of 15 geological samples can be completed in 3 h. The key advantages of this direct analysis method are short preparation time, low labor intensity, low sample input (2 mL for water samples, 0.2 g for geological material), high sample throughput (2 min sample to sample, >150 samples measured in 8 h), and use of standard ICP-QQQ hardware. Overall, the proposed method offers a new opportunity for measuring a large number of samples with minimal effort and, in turn, for improving emergency preparedness, environmental monitoring, and data collection for environmental modeling.

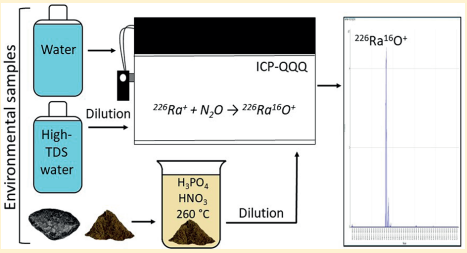

Radium-226 (^{226}Ra, $t_{1/2}$ = 1600 a), a radionuclide in the uranium-238 (^{238}U) decay chain, can be found in terrestrial, freshwater, and marine environments all over the world. Spreading of ^{226}Ra can be augmented by human activities like uranium mining, phosphate industry, and oil, gas, and coal production.[1] As a heavy calcium homologue with high mobility in the environment and accumulation in bone in vertebrates, ^{226}Ra is one of the most radiotoxic naturally occurring radionuclides and is of relevance from both an environmental and a human radiation protection perspective.[1] The drinking water limit for ^{226}Ra set by the U.S. Environmental Protection Agency (USEPA) is 5 pg L^{-1} (0.2 Bq L^{-1}, 5 pCi L^{-1}),[2] and in the EU, the Euratom Drinking Water Directive indicates a value of 14 pg L^{-1} (0.5 Bq L^{-1}, 14 pCi L^{-1}).[3] In both cases, the required limit of detection (LOD) for the analysis of ^{226}Ra in drinking water is 1 pg L^{-1} (0.04 Bq L^{-1}, 1 pCi L^{-1}).[3,4] In emergency situations, the need for rapid analyses of drinking water and other sample matrices is even more pronounced.[5]

Measurements of ^{226}Ra in environmental samples usually involves lengthy, work-intensive procedures before measurement by liquid scintillation counting or alpha or gamma spectrometry.[6−8] Counting time in these common radioanalytical techniques is typically hours to days for one sample, which together with the potential need for prior concentration, radiochemical separation, and/or waiting for equilibration with daughter nuclides for up to 30 days notoriously impedes rapid processing of samples. Accelerator mass spectrometry (AMS), thermal ionization mass spectrometry (TIMS), and inductively coupled plasma mass spectrometry (ICPMS) have also been used for ^{226}Ra determination and offer faster analysis time than radioanalytical techniques. However, the developed methods still require tedious concentration and separation procedures prior to analysis in order to increase the Ra concentration and/or remove interferences.[1,5−7,9−13] For measurements of ^{226}Ra by ICPMS, spectral interferences at m/z 226 can be caused by polyatomic ions like $^{88}Sr^{138}Ba^{+}$, $^{186}W^{40}Ar^{+}$, $^{207}Pb^{19}F^{+}$, $^{208}Pb^{18}O^{+}$ and combinations of Mo and Xe isotopes.[7,14−16]

Direct measurements of ^{226}Ra have to date been limited to methods with insufficient detection limits. For example, van Es et al.[17] analyzed groundwater samples directly by ICPMS using He as an unreactive collision gas for removal of interferences by kinetic energy differentiation (KED). The detection limit was 1 Bq L^{-1} (~27 pg L^{-1}), which is insufficient for evaluating drinking water quality in the US or EU. Evans et al.[16] did an online matrix removal with column chromatography before

Received: August 3, 2018
Accepted: September 14, 2018
Published: October 3, 2018

DOI: 10.1021/acs.analchem.8b03494
Anal. Chem. 2018, 90, 12246−12252

analysis with ICPMS, achieving a LOD of 0.05 pg L^{-1} for treated mine effluent samples in a 10 min procedure, but preparations and troubleshooting are normally more time-consuming for such a system than for direct measurements with ICPMS.

Another option for online removal of interferences with ICPMS is the use of a reaction gas such as O_2, NH_3, or N_2O. Gas reaction is generally more efficient than He-KED for removing interferences, as either the analyte or the interference is displaced to a different mass and better sensitivity is achieved.[14] However, in a single quadrupole ICPMS, there will be a variety of masses introduced into the reaction cell, giving a high number of polyatomic products which can potentially create new interferences. Triple quadrupole ICPMS (ICP-QQQ) eliminates this problem as only the selected mass enters the reaction cell, drastically reducing the possible formed interferences and unwanted side-reactions from lower and higher mass elements.

For geological samples such as soils and rocks, there is an additional challenge for Ra determination by ICPMS, which is to achieve complete recovery of the element from the sample matrix. Sulfates of Sr, Ba, and rare earth elements (REE) are very difficult to dissolve, and Ra can be present as inclusions in such minerals.[6,18,19] For Ra determination, digestion with HNO_3, HF, HCl, or combinations of these are commonly used; however, this may not necessarily result in a complete recovery of Ra from the sample[1,20] and consequently lead to underestimation of the Ra content.

In order to overcome the current limitations of work-intensive, time-consuming, and inaccurate measurement procedures for environmental samples, the main aim of this work was to develop a method for the direct measurement of ^{226}Ra in water samples by ICP-QQQ. Solutions containing common matrix elements were tested to evaluate potential spectral interferences, and more complex waters were analyzed to study the effect of high total dissolved solids on the instrument response. Geological materials were analyzed after a straightforward acid digestion, including certified reference materials to assess the accuracy of the method.

EXPERIMENTAL SECTION

Sample Preparation. *Water.* Water samples containing ^{226}Ra were prepared by leaching of alum shale with synthetic rainwater. Alum shale is a black mudrock with a high natural content of ^{238}U and its daughters, including ^{226}Ra.[1,21] Alum shale was collected in May 2015 from a tunnel blast during construction work in the alum shale formation in Gran, Hadeland, Norway. It was crushed with a jaw crusher and sieved through a 2 mm mesh to remove bigger particles. Synthetic rainwater was prepared with the same quality as rain commonly falling in the sampling area.[22] Leaching experiments were performed with a 1:10 (w/w) crushed rock to synthetic rainwater ratio for up to 1 year. The conductivity of the leachates ranged between 0.02 and 0.7 mS cm^{-1}. The water samples were acidified with 5% (V/V) concentrated, ultrapure HNO_3 prior to ICP-QQQ analysis, and representative samples of environmentally relevant characteristics were used for the evaluation of the method's precision and repeatability.

High-TDS Water. In order to study the effect of high total dissolved solids (TDS) on the sensitivity of the ICP-QQQ measurements, formation water from a Silesian underground coal mine was tested. This formation water was used in an interlaboratory comparison conducted in 2015 by the Silesian Centre for Environmental Radioactivity, Central Mining Institute (GIG) (Poland), which reported a ^{226}Ra content of 0.101 ± 0.026 ng L^{-1} (3.70 ± 0.95 Bq L^{-1}).[23] The conductivity of this formation water is 115 mS cm^{-1}, about twice that of seawater and 3 orders of magnitude higher than the alum shale leachates.

Formation water samples were prepared by diluting a total of eight subsamples from three intercomparison study bottles 30 times with type I water (ASTM D1193-91 standard specifications) followed by acidification (5% V/V HNO_3) and ICP-QQQ analysis. This dilution reduced the TDS of the samples, but it was still 5−200 times higher than the alum shale water leachates.

Geological Material. Three replicates of 0.2−0.3 g of alum shale were weighed into Teflon tubes and digested with a mixture of 2.0 mL of concentrated, ultrapure HNO_3 and 4.0 mL of H_3PO_4 (BioUltra ≥85%, Sigma) at 260 °C for 40 min in a Milestone UltraWAVE. This acid mixture was chosen because heating of phosphoric acid above its boiling point (158 °C) causes formation of pyrophosphate ion, which acts as an excellent complexing agent,[24] enhancing the extraction of matrix elements. Indeed, Melgård[20] demonstrated that this digestion method gives a complete recovery of Ba and REE in various soil reference materials, and a similar recovery was expected for Ra. Digested samples were diluted to 50 mL with type I water, followed by a further 15-fold dilution of a subsample on the analysis day. Concentrated, ultrapure HNO_3 was added to the samples to a final concentration of 5% (V/V). The extra dilution was necessary to reduce the amount of TDS introduced into the instrument. Additionally, triplicates of certified reference material IAEA-448 (Radium-226 in soil from oil field) and reference material IAEA-314 (^{226}Ra, Th and U in stream sediment) were prepared in the same manner as the samples to check the accuracy of the method.

To correct for water content in the geological samples, dry matter was determined by heating 2 g of material at 105 °C overnight. Characterization analyses (see the Supporting Information for details) showed that the alum shale contained 31 g kg^{-1} S, 0.12 g kg^{-1} Sr, and 0.43 g kg^{-1} Ba, which could pose a problem if Ra is present in MSO_4 minerals. Furthermore, ^{238}U activity in this alum shale was 1.34 ± 0.02 kBq kg^{-1}. Alum shale was formed more than 450 million years ago,[21] and secular equilibrium is expected; i.e., the activity of ^{238}U and its daughter ^{226}Ra should be the same.

During this method development, the digested geological samples (50 mL) were left to settle overnight before measurements to prevent undigested particles from clogging the nebulizer. However, if there is an urgent need for results, the samples can be centrifuged or filtered and measured on the same day.

Measurements with ICP-QQQ. *Instrument Settings.* Analyses were performed with an Agilent 8900 triple quadrupole ICPMS, which has an octopole collision-reaction cell positioned between two quadrupole mass filters (Q1 and Q2). The instrument was equipped with a MicroMist nebulizer (0.4 mL min^{-1}) and standard lenses and sample introduction system (x-lens, nickel sample and skimmer cones, and a Scott double pass (quartz) spray chamber).

Nitrous oxide (N_2O) was used as reaction gas. The first quadrupole (Q1) of the instrument introduces only mass 226 into the collision-reaction cell, where an oxygen atom is transferred from N_2O to Ra^+. The last quadrupole (Q2) then

DOI: 10.1021/acs.analchem.8b03494
Anal. Chem. 2018, 90, 12246−12252

selects mass 242 ($^{226}Ra^{16}O^+$). In this way, spectral interferences are excluded and the mass spectrum is free of noise. N_2O has an oxygen affinity (OA) of about 1.8 eV and readily donates an oxygen atom.[14] To check the probability of the reaction to occur, a product ion scan (PIS) was performed by setting Q1 to mass 226 and Q2 to scan all masses from 226 to 275 (instrument settings and PIS are provided in the Supporting Information). The greatest part of ^{226}Ra reacted to mass 242 ($^{226}Ra^{16}O^+$), with only 0.6% left unreacted at mass 226. When O_2 (OA of 5.2 eV) was tested as reaction gas, the reaction efficiency only reached approximately 10%.

Instrument settings are presented in Table 1. Variation in parameters is due to manual optimization of sensitivity on different analysis days. Gas flows were tuned for the highest sensitivity, while plasma conditions were adapted to a somewhat complex matrix. An integration time of 10 s gives one replicate, and 5 replicates constitute one measurement.

Table 1. Instrument Settings for ICP-QQQ Analysis of ^{226}Ra in Water, High-TDS Water, and Digested Geological Samples[a]

parameter	setting
scan type	MS/MS
monitored mass pairs (Q1 → Q2)	169 → 185 ($^{169}Tm^+$ → $^{169}Tm^{16}O^+$)
	226 → 242 ($^{226}Ra^+$ → $^{226}Ra^{16}O^+$)
integration time	10 s for Ra; 0.25 s for Tm
replicates	5
RF power	1600 W
sample depth plasma	7.5 mm
nebulizer gas flow	0.75 L min^{-1}
spray chamber temperature	2 °C
makeup gas flow	0.32−0.38 L min^{-1}
collision-reaction cell	
N_2O flow rate	0.45 mL min^{-1}
octopole bias	−3.0 V
axial acceleration	1 V
energy discrimination	−7.0 V
deflect lens	5.0−5.4 V

[a]Q denotes quadrupole mass filter.

Standard and Test Solutions. Standard solutions of ^{226}Ra (1−2000 pg L^{-1}) were prepared from a ^{226}Ra certified standard solution purchased from National Physics Laboratory (UK) in type I water and 5% (V/V) HNO_3. In addition, Ca^{2+} (2 mg L^{-1}), Sr^{2+} (100 μg L^{-1}), and Ba^{2+} (20 μg L^{-1}) were added to all standard solutions. These elements are expected to have similar adsorption behavior to Ra and thus minimize its adsorption in the sample introduction system. The second highest standard (500 pg L^{-1}) and the calibration blank were measured every 10 samples during the run to correct for instrument drift. Standard solutions were stored in the dark at 4 °C between analysis days and compared to freshly made standards to exclude storage effects.

Thulium (Tm, mass 169) was used as online internal standard. Tm was expected to correct well for physical interferences due to a similar low ionization energy as Ra (6.18 and 5.28 eV, respectively) and the same reaction efficiency for accepting an oxygen atom from N_2O. Tm was therefore measured on mass 185 ($^{169}Tm^{16}O^+$). Solutions of 10 and 30 μg L^{-1} Tm were used for water samples and more complex samples (formation water, and digested soil and rock), respectively. The internal standard was introduced online and mixed with the samples (ca. 17 times dilution) before reaching the nebulizer.

To study possible spectral interferences, solutions containing Sr + Ba (1, 10, and 100 mg L^{-1}), W (0.01, 0.1, 1, and 10 mg L^{-1}), Pb (0.01, 0.1, 1, and 10 mg L^{-1}; with and without 0.1% HF), or 61 different elements (200 μg L^{-1}; prepared from 71A, 71B, and 71D Inorganic Ventures stock solutions) were prepared with type I water and 5% (V/V) HNO_3 and measured in the same manner as ^{226}Ra standard solutions. Moreover, these solutions were also measured with no gas and He in the collision-reaction cell, in both single quadrupole mode (equal to regular ICPMS) and triple quadrupole mode (MS/MS), to compare with N_2O in MS/MS mode (instrument settings provided in the Supporting Information).

Limit of Detection and Quantification. Limits of detection (LOD) and quantification (LOQ) were calculated as 3 and 10 times the standard deviation of the blank concentrations, respectively. In order to assess the capability of the method for use in samples of environmentally relevant matrices, different blanks corresponding to each type of samples were prepared and measured in the same manner and in parallel to the samples. Water blanks (26 replicates) were prepared by acidifying type I water. Formation water blanks (5 replicates) were prepared from type I water and diluted 30 times before acidification, and LOD and LOQ were estimated by calculating back to the original sample volume. Geological sample blanks (8 replicates) were prepared by adding only the acid mixture to empty Teflon vials and then digesting and diluting as carried out with the geological samples. The average mass of the measured samples was used to normalize the LOD and LOQ to dry solid mass.

Additionally, LOD and LOQ for water were calculated from 140 experiment blanks generated during the alum shale leaching experiments. These blanks were synthetic rainwater that had been through the same treatment as the leachate but

Table 2. Background Equivalent Concentration (BEC, in pg L^{-1} ^{226}Ra) Obtained for Interferences When Analyzing Different Test Solutions without ^{226}Ra in No Gas, He, and N_2O Mode and in Single (MS) and Triple (MS/MS) Quadrupole Modes

		BEC (pg L^{-1} ^{226}Ra)				
		no gas		He		N_2O
test solution	suspected interferences	MS	MS/MS	MS	MS/MS	MS/MS
100 mg L^{-1} Sr; 100 mg L^{-1} Ba	$^{88}Sr^{138}Ba^+$	<LOD	<LOD	<LOD	<LOD	<LOD
10 mg L^{-1} W	$^{186}W^{40}Ar^+$	520	4	4	<LOD	<LOD
10 mg L^{-1} Pb	$^{208}Pb^{18}O^+$	89	62	51	22	<LOD
10 mg L^{-1} Pb w/0.1% HF	$^{207}Pb^{19}F^+$, $^{208}Pb^{18}O^+$	130	81	99	49	<LOD
200 μg L^{-1} of 61 elements	above-mentioned, $^{40}Ar_2{}^{146}Nd^+$, $^{87}Sr^{139}La^+$, $^{86}Sr^{140}Ce^+$, $^{209}Bi^{16}O^1H^+$, $^{92+n}Mo^{134-n}Xe^+$, and more	18	7	6	<LOD	<LOD

DOI: 10.1021/acs.analchem.8b03494
Anal. Chem. 2018, 90, 12246−12252

not been in contact with the alum shale and should thus not contain any ^{226}Ra.

RESULTS AND DISCUSSION

Testing for Spectral Interferences. Samples containing high concentrations of Ra can have high Sr and Ba concentrations due to their similar chemical behavior; thus, the formation of $^{88}Sr^{138}Ba^{+}$ was tested with solutions containing up to 100 mg L^{-1}. A further increase in concentrations would likely affect the plasma and reduce the signal causing a physical, not spectral, interference. Other elements, such W and Pb, may not commonly be present in high concentrations in water but can be elevated in digested geological samples. Here, solutions containing up to 10 mg L^{-1} W and Pb were tested. However, if this method is to be used on, for example, Pb or W ore samples, interferences at even higher concentrations should be tested. The background equivalent concentration (BEC) was measured for these and other suspected spectral interferences in no gas, He, and N_2O mode, and the results for the highest tested concentrations are presented in Table 2. The BEC is the level of interference that would be caused by the element(s) at a given concentration, i.e., the apparent concentration of ^{226}Ra.

Despite being mentioned as an important interference in several studies,[12,16] $^{88}Sr^{138}Ba^{+}$ did not cause an interference in any of the gas modes tested here. Interferences from W and Pb caused relatively high BEC for ^{226}Ra (up to 520 pg L^{-1}) in both no gas and He mode, as seen by others,[15,16] but were below the limit of detection in N_2O mode. Similar interference effects were observed for the solution with 61 different elements, i.e., measurable BEC (6−18 pg L^{-1}) in no gas and He mode (MS) but below detection in N_2O mode.

A peculiar note is the higher BEC for some solutions in single quadrupole mode compared to MS/MS mode, especially for the W solution. This indicates that some of the interferences are largely formed after the plasma. If they were formed in the plasma, the BEC should be the same for both single quadrupole and MS/MS as the interference would pass through both quadrupoles in the MS/MS mode. The $^{186}W^{40}Ar^{+}$ interference is assumed to be formed from Ar gas and W^{+}. There will always be some neutral Ar gas present in the vacuum system, and in single MS mode, W^{+} will pass the Q1 and react with Ar in the Q1, in the reaction cell, or in both. In MS/MS mode, W^{+} will not pass the Q1; thus, the reaction can only happen in the plasma or in the ion path of the lenses before Q1. This seems to happen to some extent in our system, as there is a small interference also in no gas MS/MS mode (4 pg L^{-1} ^{226}Ra), but the higher interference level in no gas single MS mode (520 pg L^{-1} ^{226}Ra) implies that the reaction happens to a greater extent in the Q1 and/or reaction cell.

Overall, these results demonstrate the advantage of using N_2O as a reaction gas for measuring ^{226}Ra. The counts per second measured for interference test solutions were no higher than for the calibration blank; thus, using N_2O as a reaction gas efficiently removed all the tested polyatomic interferences that caused a problem in no gas or He mode. This is because it was not thermodynamically favorable for the interferences to perform the same mass shift as Ra.

Linearity, Precision, and Repeatability. The response of the method on a 3 orders of magnitude ^{226}Ra concentration range (Table 3) was linear ($R^2 = 1$), even when only the lowest standards (1 and 5 pg L^{-1}) were considered ($R^2 = 0.9996$). The high relative standard deviation (RSD; 32%) of repeated measurements of the lowest standard (1 pg L^{-1}) reflects that it is just below the quantification limit of 1.4 pg L^{-1} for water (see Overview of the Method).

Table 3. Concentrations of Standard Solutions and Instrument Response for Measurements of ^{226}Ra by ICP-QQQ[a]

prepared standard concentrations		measurements		
activity (Bq L^{-1})	concentration (pg L^{-1})	n	concentration (pg L^{-1})	RSD (%)
0.037	1	7	1.1 ± 0.4	32
0.18	5	6	4.6 ± 0.3	7
0.73	20	13	20.4 ± 1.5	7
3.7	100	14	104 ± 8	8
18	500	98	497 ± 16	3
73	2000	9	2058 ± 85	4

[a]The results are an average of measured concentrations from different analysis days, some of which were months apart, with errors representing one standard deviation of the measurements (n), and RSD is the relative standard deviation.

The repeatability of the method was investigated with repeated measurements of the same vials of two water, one formation water, and two digested reference material samples (Table 4). The vials were chosen to represent the range of sample matrices but otherwise randomly. The two water samples (A and B) were taken at the same time point from two different containers of the leaching experiments; thus, similar matrix and ^{226}Ra content were expected. At concentrations of 5−7 pg L^{-1}, the RSDs of the water and digested soil were about 10%, which is acceptable for such low concentrations. The RSD decreased to 3.6% for the 108 pg L^{-1} digested soil. The high RSD obtained for the formation water (25%) demonstrates the challenges associated with high TDS content, even after 30 times dilution. Lower RSD could be achieved by diluting the samples further or by including a simple separation step before analysis to reduce TDS.

Table 4. Average of ^{226}Ra Concentrations for Repeated Measurements (n) of Selected Vials with Representative Water, High-TDS Formation Water, and Digested Reference Material Soil Samples[a]

		^{226}Ra concentration in solution	
sample matrix	n	average (pg L^{-1})	RSD (%)
water (sample A)	3	6.5 ± 0.8	12
water (sample B)	3	6.0 ± 0.5	8.4
diluted formation water	5	4.0 ± 1.0	25
digested soil (IAEA-314)	10	5.0 ± 0.4	8.3
digested soil (IAEA-448)	10	108 ± 4	3.6

[a]The errors represent one standard deviation, and RSD is the relative standard deviation.

Accuracy. The ^{226}Ra concentrations measured in the formation water and digested alum shale samples were 0.12 ± 0.02 ng L^{-1} (4.5 ± 0.6 Bq L^{-1}, $n = 8$) and 35 ± 2 ng kg^{-1} (1.28 ± 0.07 kBq kg^{-1}, $n = 3$), respectively. These values are in good agreement with the interlaboratory comparison results for the formation water (0.101 ± 0.026 ng L^{-1}; 3.70 ± 0.95 Bq L^{-1}) and the alum shale ^{226}Ra activity concentration estimated from secular equilibrium with ^{238}U (1.34 ± 0.02 kBq kg^{-1}). The reference activity concentrations of the IAEA materials are within the 95% confidence interval of the measured activity

DOI: 10.1021/acs.analchem.8b03494
Anal. Chem. 2018, 90, 12246−12252

concentrations for ^{226}Ra (Table 5). All together, these results demonstrate that the chosen microwave-assisted digestion conditions (40 min, 260 °C, HNO_3 + H_3PO_4) and ^{226}Ra determination methodology are suitable for determining accurate ^{226}Ra concentrations in water as well as in geological materials.

Table 5. Reference and Measured (n = 3) ^{226}Ra Activity Concentrations (kBq kg^{-1}) of Two IAEA Reference Materials

		measured values (kBq kg^{-1})	
reference material	reference activity concentration (kBq kg^{-1})	activity concentration	95% confidence interval
IAEA-314	0.732	0.63 ± 0.07	0.47–0.79
IAEA-448	19.05 ± 0.26	18.3 ± 0.7	16.6–19.9

Overview of the Method. A summary of the methods for the different sample matrices is presented in Table 6. The resulting method is fast, with 2 min of analysis time sample to sample, and gives the opportunity for analyzing more than 150 samples in an 8 h working day. In fact, more than 250 samples from the alum shale leaching experiment were measured in 12 h.

For geological samples, the limiting step is the digestion. The UltraWAVE has capacity for 15 samples at a time, and the total runtime of the digestion is about 1.5 h including cooling down; thus, digestion and analysis of these samples can be completed in about 3 h if they are filtered or centrifuged before analysis instead of waiting for remaining undigested particles to settle.

The samples size needed for analysis is small compared to most radiochemical methods: 2 mL of the sample solution was used for one measurement. For water samples, collection of a larger sample volume (e.g., 8 mL) should however be considered to allow for retesting. If the sample solution is limited, using a total consumption nebulizer would reduce the sample volume required for analysis to 0.2 mL or lower.[11,14,25] For water with high TDS (e.g., seawater, produced water, or formation water), <1 mL is sufficient as the sample must be diluted. For geological samples with limited available sample size, less than 0.2 g can be used with correspondingly lower acid and dilution volumes. The proposed method for geological samples can be applied to biological samples, but HNO_3 would suffice for the digestion as sulfate minerals are not present. Furthermore, LOD and LOQ are expected to be lower for biological samples due to lower TDS in the digested sample solution, allowing for about 15 times lower dilution.

The detection limit for the water samples in Table 6 corresponds to the instrumental detection limit. Higher instrument sensitivity and thus lower instrumental LOD could be achieved with other plasma settings and a more efficient sample introduction system[14,25] but only for samples with lower TDS.

Evaluating the Limits of Detection. *Detection Limits for Water.* The achieved limit of detection for water samples at 0.42 pg L^{-1} (15 mBq L^{-1}) is complying with the requirements for methods used for analysis of drinking water established by the USEPA[4] and the EU[3] at 1 pg L^{-1} (0.04 Bq L^{-1}). The detection and quantification limits (Table 6) were calculated using 26 acidification blanks, i.e., a rather simple matrix. Nonetheless, when using experimental blanks (n = 140) with properties closer to real environmental sample matrices, the LOD and LOQ were about the same at 0.55 and 1.8 pg L^{-1} ^{226}Ra, respectively.

These low detection limits mean that water can be evaluated for drinking water quality for ^{226}Ra with direct measurements, with no concentration or separation methods, and with the possibility for measuring several hundred samples per day. For investigations that require even lower detection limits, the sample can be concentrated and/or purified in a separation step prior to analysis.

Several methods have been developed for concentration and separation of ^{226}Ra in samples before analysis by ICPMS, online or offline.[9,12,15−17,26] These methods are often more complicated than what is necessary before our detection method, as the reaction with N_2O in the ICP-QQQ means that specific interferences, such as Sr and Ba that chemically follow Ra, do not need to be removed. To lower the detection limit of water samples with the presented method, a simple separation or concentration procedure, e.g., cation exchange separating monovalent from divalent cations, is thus expected to be sufficient. The method of Kim et al.[26] was successfully applied to water samples in our laboratory.[20] However, this method was not specific enough to eliminate other divalent cations, which can become a problem for more complex samples like formation water where concentrations can be high enough to cause physical interferences like ionization suppression in the plasma. In this case, more sophisticated separation and concentration methods would be needed. For example, both

Table 6. Overview of the Proposed Methods for Water, High-TDS Water, and Geological Samples[a]

	water	high-TDS water	geological material
sample size needed	2 mL (8 mL)	<1 mL	0.2 g
sample preparation	acidification	acidification	acid digestion (1.5 h/15 samples)
		dilution (30×)	dilution
analysis time (sample to sample)	2 min	2 min	2 min
sample throughput	>150 samples/8 h	>150 samples/8 h	for digested samples:
	>400 samples/24 h	>400 samples/24 h	>150 samples/8 h
			>400 samples/24 h
limit of detection	0.42 pg L^{-1}	17 pg L^{-1}	0.75 ng kg^{-1}
	15 mBq L^{-1}	0.61 Bq L^{-1}	27 Bq kg^{-1}
limit of quantification	1.4 pg L^{-1}	56 pg L^{-1}	2.5 ng kg^{-1}
	51 mBq L^{-1}	2.1 Bq L^{-1}	91 Bq kg^{-1}

[a]Limits of detection (LOD) and quantification (LOQ) are calculated as 3 and 10 times the standard deviation of the blank concentrations, respectively.

DOI: 10.1021/acs.analchem.8b03494
Anal. Chem. 2018, 90, 12246−12252

Lagacé et al.[9] and Zhang et al.[12] present methods that effectively removed divalent cations (except Ra) from seawater and high salinity wastewater, respectively, and should hence work for more complex samples before analysis with the suggested method.

The International Atomic Energy Agency (IAEA) lists absolute detection limits for different methods for determining ^{226}Ra.[1] The absolute LOD for water obtained with the method described in this work is 0.84 fg (equal to 2.2×10^6 atoms or 31 μBq), which is as low as the listed LOD for the most sensitive method (TIMS, 37 μBq). This absolute LOD was calculated using the sample volume (2 mL). With a total consumption nebulizer, the volume consumed for analysis could easily be lowered to 0.2 mL or lower,[11,14,25] giving correspondingly lower absolute LOD. Combined with concentration or separation procedures, as described above, the absolute detection limits could be further reduced.

Detection Limits for Formation Water. Formation water, seawater, or other samples with high content of total dissolved solids (TDS) must be diluted before measurements to avoid physical interferences in the plasma, but as a consequence, the concentration of ^{226}Ra may be reduced to below the instrumental LOD. In our study, 30 times dilution was used and the achieved limit of detection was 17 pg L^{-1} (0.61 Bq L^{-1}) for the original sample, which is ca. 40 times higher than for water that does not need dilution. The method for high-TDS samples is hence only sufficiently sensitive for samples with high content of ^{226}Ra, like Marcellus Shale Wastewater,[12] the formation water measured in this work, or similar. The formation water had about twice the salinity of seawater; thus, seawater samples could be diluted only 15 times before measurements, meaning that lower concentrations can be detected. Methods for concentration and separation of Ra in samples for ICPMS measurements have been developed for high-TDS samples[9,12] and could be applied before measurements with the proposed method to reduce detection limits.

Detection Limits for Geological Samples. The achieved limit of detection of 0.75 ng kg^{-1} (27 Bq kg^{-1}) for geological samples is higher than in several other methods used for the determination of ^{226}Ra, such as liquid scintillation counting and alpha and gamma spectrometry,[6,7] yet the proposed method is well suited for evaluation of environmental quality. The estimated average of ^{226}Ra in the continental crust is ~0.90 ng kg^{-1} (33 Bq kg^{-1}), and soil concentrations in areas with normal background (i.e., not areas with high natural background) vary from 0.10 to 3.44 ng kg^{-1} (3.7 to 126 Bq kg^{-1}).[1] Therefore, the proposed method is sensitive enough to detect any elevated concentration of ^{226}Ra in soil and rock and, being significantly quicker and simpler than other methods commonly used,[1,5,7] is excellent for emergency preparedness where the goal is to quickly identify contaminated samples. It is also suitable for determining whether a material should be treated as radioactive waste, e.g., in Norway the limit for ^{226}Ra is 27 ng kg^{-1} (1000 Bq kg^{-1}). Nonetheless, as the sample size in this method is relatively small, care must be taken to ensure that the determined concentration is representative of the larger sample, e.g., by running replicates. Alternatively, larger sample containers can be used in the Milestone UltraWAVE, allowing for larger sample size, however, at the expense of sample throughput as fewer containers can be run simultaneously.

As mentioned, if a limited amount of sample is available, less than 0.2 g of material can be used with correspondingly lower acid and dilution volumes, without affecting the detection limits. Table 6 reports LOD for samples diluted 15 times more after digestion to a total volume of 750 mL. A lower dilution (10 times, 500 mL final volume) gave the same RSD for repeated measurements (data not shown), which would have lowered the LOD. Nonetheless, the higher dilution was chosen for these specific samples to reduce instrument drift. As for formation water, methods for separation and concentration of Ra from high-TDS samples can be applied after digestion to lower the limit of detection.

CONCLUSIONS

The proposed method using N_2O as a reaction gas in an ICP-QQQ can be used for environmental and public health related monitoring of ^{226}Ra, and the short analysis time enables a quicker response to unexpected high levels in, e.g., drinking water. To the authors' knowledge, no other methods provide results for ^{226}Ra as fast and simple as the proposed method, for neither water nor geological samples.

The use of microwave-assisted digestion with phosphoric acid in combination with nitric acid resulted in a complete recovery of ^{226}Ra from the tested geological matrices, and the achieved limit of detection was sufficiently low to detect any ^{226}Ra concentrations above background levels. The method for geological materials could be easily adapted to biological samples with an expected lower limit of detection.

The absence of concentration or separation steps eliminates a source of uncertainty in the results that is associated with most methods for ^{226}Ra determination. In case of unexpected instrumental problems, the small sample volume needed (ca. 2 mL) usually allows for reanalysis of a sample, something that is often not possible when using techniques that require the concentration of a large sample volume. Moreover, as the method is rapid and requires low sample volume, it can be used for screening a large number of samples and identifying which are below the detection limit and need to be reanalyzed after concentration and/or separation or, alternatively, using radiochemical methods.

Additionally, the proposed method is expected to work for ^{228}Ra with a similar limit of detection when measured in mass concentration (pg L^{-1}). Nevertheless, because of the shorter half-life of ^{228}Ra (5.6 a), the detection limit in activity concentration (Bq L^{-1}) will be considerably higher, and interferences including ^{228}Th reacting to $^{228}Th^{16}O^+$ will have to be investigated.

ASSOCIATED CONTENT

Supporting Information

The Supporting Information is available free of charge on the ACS Publications website at DOI: 10.1021/acs.analchem.8b03494.

Details of alum shale characterization and elemental composition (S, Sr, Ba, and ^{238}U) analyses; ICP-QQQ instrument settings for testing spectral interferences in no gas and He and N_2O gas modes and associated product ions scans in N_2O mode (PDF)

AUTHOR INFORMATION

Corresponding Author

*E-mail: frwa@nmbu.no.

DOI: 10.1021/acs.analchem.8b03494
Anal. Chem. 2018, 90, 12246−12252

ORCID
F. M. Wærsted: 0000-0003-3526-0235

Notes

The authors declare no competing financial interest.

■ ACKNOWLEDGMENTS

This study has been funded by the Norwegian Research Council through its Centre of Excellence (CoE) funding scheme (Project 223268/F50). The authors thank the Silesian Centre for Environmental Radioactivity, Central Mining Institute (GIG), Poland, for providing the formation water samples and the evaluation report of the interlaboratory comparison exercise.

■ REFERENCES

(1) IAEA. *The environmental behaviour of radium*, Revised ed.; Technical report series 476; International Atomic Energy Agency: Vienna, 2014.
(2) U.S. Environmental Protection Agency. *National Primary Drinking Water Regulations*; EPA 816-F-09-004; U. S. EPA: Washington, DC, 2009.
(3) EU. *Council Directive 2013/51/Euratom: Official Journal of the European Union*; 2013.
(4) GPO. *Analytical Methods for Radioactivity*; 40 CFR 141.25; U.S. governmental publishing office: Washington DC, 2012.
(5) Maxwell, S. L.; Culligan, B. K. *J. Radioanal. Nucl. Chem.* **2012**, *293*, 149−156.
(6) IAEA. *Analytical Methodology for the Determination of Radium Isotopes in Environmental Samples*; IAEA Analytical Quality in Nuclear Applications Series 19; International Atomic Energy Agency: Vienna, 2010.
(7) Hou, X.; Roos, P. *Anal. Chim. Acta* **2008**, *608*, 105−139.
(8) Köhler, M.; Preuße, W.; Gleisberg, B.; Schäfer, I.; Heinrich, T.; Knobus, B. *Appl. Radiat. Isot.* **2002**, *56*, 387−392.
(9) Lagacé, F.; Foucher, D.; Surette, C.; Clarisse, O. *Talanta* **2017**, *167*, 658−665.
(10) Morvan, K.; Andres, Y.; Mokili, B.; Abbe, J.-C. *Anal. Chem.* **2001**, *73*, 4218−4224.
(11) Becker, J. S. *Int. J. Mass Spectrom.* **2005**, *242*, 183−195.
(12) Zhang, T.; Bain, D.; Hammack, R.; Vidic, R. D. *Environ. Sci. Technol.* **2015**, *49*, 2969−2976.
(13) Tims, S. G.; Hancock, G. J.; Wacker, L.; Fifield, L. K. *Nucl. Instrum. Methods Phys. Res., Sect. B* **2004**, *223*−*224*, 796−801.
(14) Tanner, S. D.; Baranov, V. I.; Bandura, D. R. *Spectrochim. Acta, Part B* **2002**, *57*, 1361−1452.
(15) Dalencourt, C.; Michaud, A.; Habibi, A.; Leblanc, A.; Larivière, D. *J. Anal. At. Spectrom.* **2018**, *33*, 1031−1040.
(16) Evans, R. D.; Izmer, A.; Benkhedda, K.; Toms, A.; Fernando, A.; Wang, W. *Can. J. Chem.* **2015**, *93*, 1226−1231.
(17) van Es, E. M.; Russell, B. C.; Ivanov, P.; Read, D. *Appl. Radiat. Isot.* **2017**, *126*, 31−34.
(18) Ulrich, M.; Bureau, S.; Chauvel, C.; Picard, C. *Geostand. Geoanal. Res.* **2012**, *36*, 7−20.
(19) Abbasi, S.; Lamb, D. T.; Palanisami, T.; Kader, M.; Matanitobua, V.; Megharaj, M.; Naidu, R. *Chemosphere* **2016**, *144*, 1421−1427.
(20) Melgård, M. D. *Determination of Ra-226 in Environmental Samples using ICP-QQQ after Cation Exchange-Separation*. Master Thesis, Norwegian University of Life Sciences, Ås, 2017.
(21) Owen, A. W.; Bruton, D. L.; Bockelie, J. F.; Bockelie, T. G. *The Ordovician successions of the Oslo Region, Norway*; The NGU Special Publication series; Geological survey of Norway (NGU): Trondheim, Norway, 1990.
(22) Aas, W.; Platt, S.; Solberg, S.; Yttri, K. E. *Monitoring of long-range transported air pollutants in Norway, annual report 2014*; M-367; Norwegian Institute for Air Research: Kjeller, 2015.
(23) Bonczyk, M.; Michalik, B. *Radium isotopes in water − interlaboratory comparison (ILC)*; JRP IND57 MetroNORM internal report; Central Mining Institute (GIG), Silesian Centre for Environmental Radioactivity: Katowice, 2016.
(24) Wang, Y.; Baker, L. A.; Helmeczi, E.; Brindle, I. D. *Analytical Chemistry Research* **2016**, *7*, 17−22.
(25) Becker, J. S.; Dietze, H.-J.; McLean, J. A.; Montaser, A. *Anal. Chem.* **1999**, *71*, 3077−3084.
(26) Kim, Y.-J.; Kim, C.-K.; Kim, C.-S.; Yun, J.-Y.; Rho, B.-H. *J. Radioanal. Nucl. Chem.* **1999**, *240*, 613−618.

DOI: 10.1021/acs.analchem.8b03494
Anal. Chem. 2018, 90, 12246−12252

Paper I: Supporting information

Supporting information for

High throughput, direct determination of ^{226}Ra in water and digested geological samples

Wærsted, F. M*[†]., Jensen, K.A.[†], Reinoso-Maset, E.[†], and Skipperud, L.[†]

[†]Centre for Environmental Radioactivity (CERAD), Faculty of Environmental Sciences and Natural Resource Management, Norwegian University of Life Sciences, P.O. Box 5003, N-1432, Ås, Norway

Table of Contents

Alum shale characterisation analysis

The concentration of S, Sr, Ba and ^{238}U were determined in the alum shale samples used in the method development. For determining total element concentrations in alum shale, ca. 0.25 g of the debris were weighed into Teflon tubes and 5 mL of concentrated, ultrapure HNO_3 (when measuring S and Sr) or a mixture of 5 mL HNO_3 + 1 mL HF (when measuring Ba and U) were added. At this stage, an aliquot of an internal standard solution (Rh) was also added. Samples were digested at 260 °C for 40 minutes in a Milestone UltraCLAVE and diluted to 50 mL with type I waters.

The digested samples were analysed with an Agilent 8800 Triple Quadrupole ICP-MS, switching between He, O_2 and no gas in the reaction chamber to remove different interferences and determine content of S, Sr, Ba and ^{238}U (Table S-1).

Table S-1: Elemental composition of the alum shale used in the leaching experiments. Concentrations represent average measurements ± one standard deviation.

Element	Sample concentration	
S	31 ± 3	g kg^{-1}
Sr	0.12 ± 0.01	g kg^{-1}
Ba	0.43 ± 0.02	g kg^{-1}
^{238}U	1.34 ± 0.02	Bq kg^{-1}

Instrument settings for product ion scans

Product ion scans (PIS) were performed with N_2O as reaction gas with the settings presented in Table S-2.

Table S-2: Instrument settings when performing product ion scans (PIS) by ICP-QQQ.

Parameter	Setting
Scan type	MS/MS
Monitored mass pairs	226 → 226 226 → 227 … 226 → 275
Q2 peak pattern	20 points
Integration time	0.3 s
Replicates	3
RF Power	1600 W
Sample depth plasma	7.5 mm
Nebulizer gas flow	0.75 L min^{-1}
Spray chamber temperature	2 °C
Makeup gas flow	0.39 L min^{-1}
Collision-reaction cell:	
N_2O flow rate	0.45 mL min^{-1}
Octopole bias	-3.0 V
Axial acceleration	1 V
Energy discrimination	-7.0 V
Deflect lens	5.0 – 5.4 V

Product ion scans (PIS)

Product ion scans (PIS) were performed in N_2O gas mode from mass 226 to 275 for the following solutions: 10 ng L^{-1} ^{226}Ra, 100 mg L^{-1} Sr + 100 mg L^{-1} Ba (testing for interference from $^{88}Sr^{138}Ba^{+}$), 10 mg L^{-1} W ($^{186}W^{40}Ar^{+}$), 10 mg L^{-1} Pb ($^{208}Pb^{18}O^{+}$) and 10 mg L^{-1} Pb + 0.1 % HF ($^{207}Pb^{19}F$).

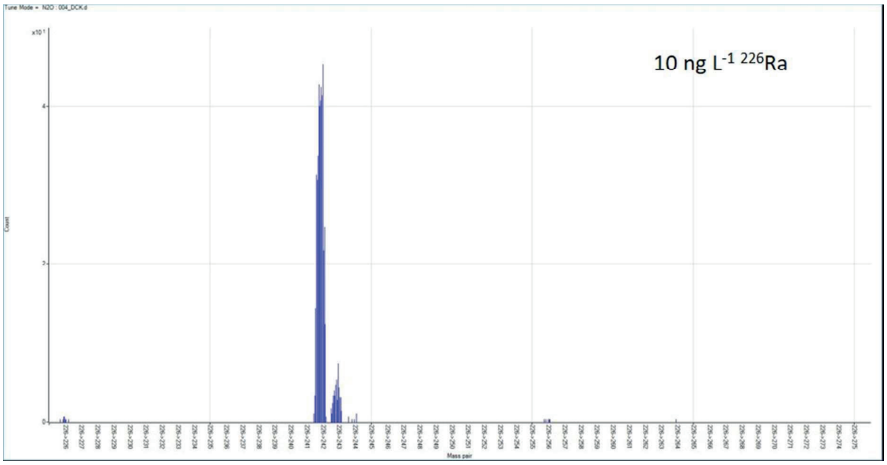

Figure S-1: Product ion scan for a solution with 10 ng L^{-1} ^{226}Ra. The main peak is found at mass 242 ($^{226}Ra^{16}O^{+}$). A smaller peak appears at 243 (possibly $^{226}Ra^{16}O^{1}H^{+}$) and 0.6 % of the signal is left at mass 226.

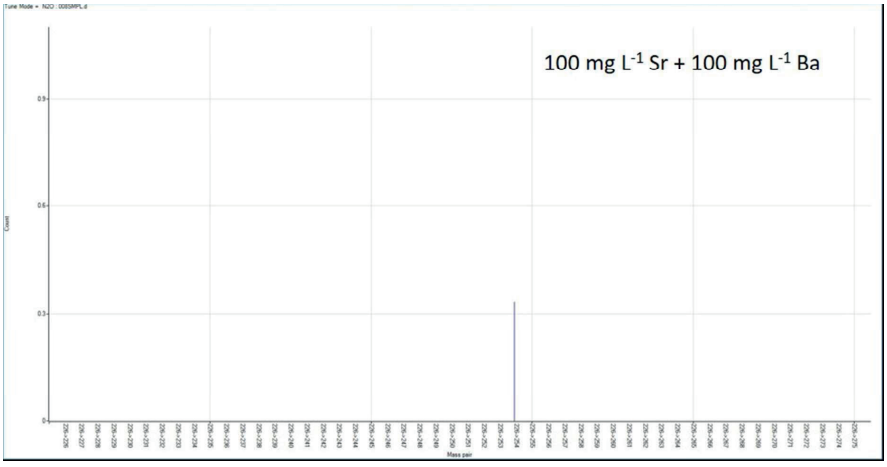

Figure S-2: Product ion scan for a solution with 100 mg L^{-1} Sr + 100 mg L^{-1} Ba. Noise seen at mass 254 was considered insignificant, otherwise no signal is observed between mass 226 and 275.

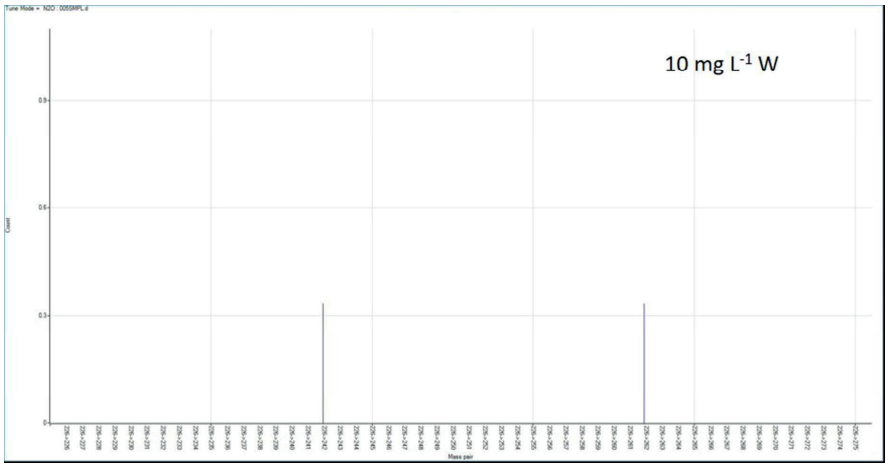

Figure S-3: Product ion scan for a solution with 10 mg L^{-1} W. Insignificant noise is seen at masses 242 and 262, otherwise no signal is observed at other masses.

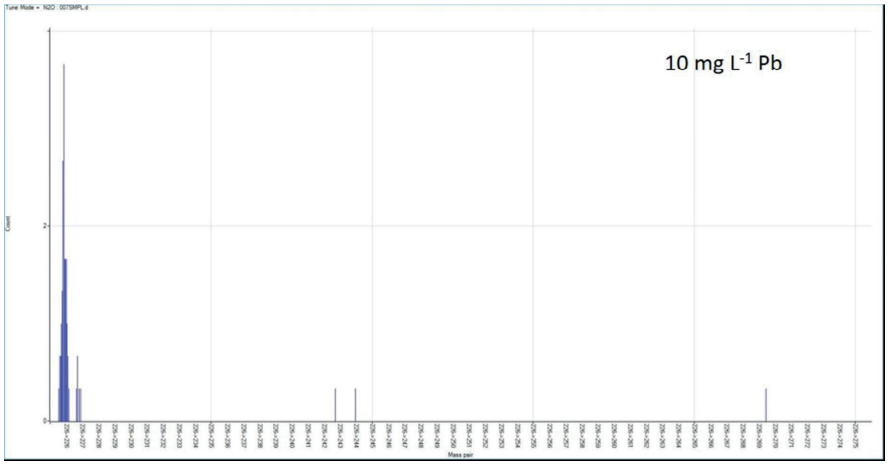

Figure S-4: Product ion scan for a solution with 10 mg L^{-1} Pb. The peak at mass 226 would cause interferences if ^{226}Ra was measured without mass displacement. No interference is observed at mass 242. A minor peak is seen at mass 227, and noise seen at mass 243, 244 and 269 is considered insignificant.

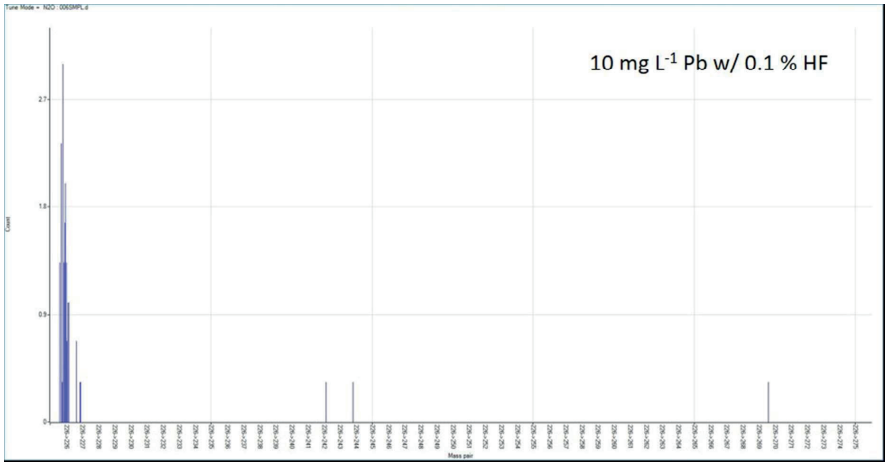

Figure S-5: Product ion scan for a solution with 10 mg L^{-1} Pb with 0.1 % HF. The peak at mass 226 would cause interferences if ^{226}Ra was measured without mass displacement. Noise seen at masses 242, 244 and 270 is considered insignificant, while a few more counts are seen at mass 227.

Instrument settings for testing of interferences in no gas and He mode

ICP-QQQ instrument settings used for testing spectral interferences on $^{226}Ra^{+}$ with He as a collision gas and with no gas added in the collision-reaction chamber, in single quadrupole (MS) and triple quadrupole (MS/MS) mode, are presented in Table S-3.

Table S-3: Instrument settings for no gas and He mode ICP-QQQ analyses used with test solutions containing suspected spectral interferences.

Parameter	No gas	No gas	He	He
Scan type	MS	MS/MS	MS	MS/MS
Monitored mass pairs		169 → 169 226 → 226		
Integration time		4 s for Ra; 0.25 s for Tm		
Replicates		3		
RF Power		1600 W		
Sample depth plasma		7.5 mm		
Nebulizer gas flow		0.75 L min^{-1}		
Spray chamber temperature		2 °C		
Makeup gas flow		0.38 L min^{-1}		
Collision-reaction cell:				
He flow rate	-	-	5.5 mL min^{-1}	5.5 mL min^{-1}
Octopole bias	-8.0 V	-8.0 V	-18.0 V	-18.0 V
Axial acceleration	0 V	0 V	1 V	1 V
Energy discrimination	5.0 V	5.0 V	5.0 V	5.0 V
Deflect lens	16.2 V	15.2 V	-1 V	-0.8 V

Paper II

Rainwater leaching of alum shale debris under atmospheric and low oxygen conditions

F. M. Wærsted*, E. Reinoso-Maset, B. Salbu and L. Skipperud

Centre for Environmental Radioactivity (CERAD), Faculty of Environmental Sciences and Natural Resource Management, Norwegian University of Life Sciences, P.O. Box 5003, N-1432 Ås, Norway

*Corresponding author email: frwa@nmbu.no

Abstract

When construction works are performed in alum shale areas, potentially acid-producing debris will be exposed to rainwater and air. To investigate the leaching potential of alum shale debris with respect to trace metals and radionuclides, one-year batch leaching experiments were performed using rock material obtained from tunnel construction and synthetic rainwater under atmospheric oxygen conditions (AOC) and low oxygen conditions (LOC). Measurements of pH, E_h and sulphate indicated pyrite oxidation, especially in the AOC, but the buffer capacity of the rock was not surpassed after 52 weeks and pH in both treatment leachates was ~7.7. The leaching of 38 stable elements and the radionuclides ^{226}Ra, ^{232}Th and ^{238}U varied with chemical and mineralogical properties, from 0.000009 % of Al to 22 % of Mo with respect to initial alum shale content. In particular, leached Mo, Ni, Zn, Cd and U raised an environmental concern, as the concentrations were 20-322 times higher than environmental quality standards. The AOC treatment increased the leaching of Co, Cd, Mo and Zn 2-4 times compared to LOC, while the leaching of ^{238}U was about 20 % higher in the LOC treatment with lower O_2. The ^{226}Ra and Ba concentrations peaked after one week followed by a decrease, likely due to (co-)precipitation of $BaSO_4$ as the sulphate concentrations in the leachate increased. In general, the leaching rates decreased with lower O_2 concentrations (LOC storage conditions). When comparing these results to concentrations measured in water samples from the road construction disposal site, the concentrations of Mn, Co, Ni, Zn, Cd and U in the experiment leachates were 1-2 orders of magnitude higher, while the concentrations

of NO_3^-, Cl^-, Na, As and Sb were 1-3 orders of magnitude lower. Nevertheless, these findings confirm the importance of a proper waste disposal planning and managing of alum shale and other acid-producing rock masses at construction sites. From this work, we recommend to minimize oxygen access when storing such debris in water, and monitoring pH, E_h, alkalinity and SO_4^{2-} and Ca levels for detecting changes in the storage conditions that could lead to increased acid production and leaching of trace metals and radionuclides.

Keywords
Alum shale, black shale, NORM, trace elements, acid rock drainage, neutral rock drainage

1 Introduction

Crushed rock produced in mining and construction work is a potential source to harmful levels of naturally occurring radioactive materials (NORM) and stable trace elements to the environment. Processing and storage of the rock alter its chemical and physical properties, potentially increasing mobility, runoff and, ultimately, bioavailability of harmful elements. Proper storage of acid-producing rock can be difficult and expensive to achieve, and consequences of improper storage can be detrimental for the local environment (Pipkin et al., 2008). Local storage is preferable in order to avoid large transportation costs and oxidation of debris during transit. At Gran, Hadeland, Norway, alum shale from tunnel construction was re-used locally to fill an excavated bog (Fjermestad et al., 2018). Measures were taken to keep the debris submerged in water, and the disposal site was covered with a surface coating to reduce access to air. However, if the disposal site has not been completely sealed, oxygenated water will enter and contaminated water will leach out into the downstream river (Vigga), with potentially large effects on the local environment.

Alum shale is a Cambro-Ordovician black mudrock (sedimentary rock) formed under reducing conditions, which contains silicate minerals, organic matter (kerogen), sulphides (such as pyrite, FeS_2, and pyrrhotite, FeS) and carbonates (Falk et al., 2006; Owen et al., 1990; Pabst et al., 2016). Alum shale is enriched in several trace elements including Cd, Co, Cu, As, Ni, Zn, V, Mo, Ba and U. Uranium in unweathered alum shale is in secular equilibrium with its daughter nuclides, and ^{226}Ra (a highly radiotoxic radionuclide) is thus present in the same activity concentrations as ^{238}U (IAEA, 2014).

Alum shales are typically acid-generating rocks, i.e., its neutralization potential (NP) to acidification potential (AP) ratio is lower than 1 (Pabst et al., 2016). The NP is mainly provided by carbonates, while the AP is normally originating from sulphide-containing minerals like pyrite and pyrrhotite (Lawrence & Scheske, 1997). When alum shale is exposed to air and water, oxidation of sulphide minerals will produce acid that can attack the rock, resulting in acid rock drainage (ARD) with elevated levels of trace elements and NORM. Therefore, the weathering of alum shale will depend on the storage conditions, where higher release of harmful elements to water is expected to occur under atmospheric oxygen conditions compared to when limited oxygen is available. Presence of carbonates can buffer acid production from pyrite oxidation, but the pH will drop if all the carbonate is consumed. Nevertheless, even without a pH drop, radionuclides and metals incorporated in alum shale can be released during oxidation, leading to neutral rock drainage (NRD) (Alloway, 2013; Appelo & Postma, 2010; Bierens de Haan, 1991).

This study aimed to investigate potential releases of relevance to man and the environment from the reuse of alum shale in road construction, by assessing the leaching potential of alum shale under different storage conditions. Unweathered, crushed alum shale from Gran was leached with synthetic rainwater under atmospheric oxygen conditions (AOC) and low oxygen conditions (LOC), and the leaching behaviour of 41 elements was investigated. Furthermore, leachate results from the two treatments were compared to measured concentrations in the disposal site at Gran.

2 Materials and methods

2.1 Site description and sampling

At Gran, Hadeland, Norway, alum shale from tunnel construction was disposed of by use as filling material under the planned road at the southern entrance of the tunnel (Fjermestad et al., 2018). The disposal site is an excavated bog and thus below groundwater level, chosen to ensure continuous submerging of the disposed alum shale. The disposal site is thought to have a slow exchange of water and to drain mainly to the small river Vigga. Tunnel blasts with >10 % alum shale were stored in the disposal site. In total, about 66 500 m^3 of alum shale and 10 500 m^3 of other black shale were placed in the bog.

Alum shale debris was collected on 19/05/2015 from a tunnel blast in the alum shale formation executed on the same day. Handheld XRF (Niton™ XL3t GOLDD+, Thermo Scientific) was used to ensure that U-rich material was collected. The material was stored for 6 months before the leaching experiments. Moreover, for comparison with laboratory experiments, water from the disposal site was also sampled. At this time, i.e., 1 year and 2 months after the tunnel construction and storage of masses started, disposal of masses was still ongoing and the site was an open pond. Conductivity and pH were measured directly in the pond with a handheld multi-meter (Multi series, WTW). Unfiltered samples were taken for analysis of anions, and for elemental analysis with inductively coupled plasma mass spectrometry (ICP-MS), water was filtered *in situ* with 0.45 µm membrane filters (Millipore) and acidified to 5 % (V/V) with ultrapure HNO_3. All water samples were stored in the dark at 4 °C until analysis.

2.2 Chemicals

All chemicals used were analytical grade unless otherwise noted. Type I water (ASTM D1193-91 standard specifications) was used for all applications. Synthetic rainwater was prepared with the same quality as rain falling in Hurdal, 27 km in straight line from the alum shale sampling point (Aas et al., 2015). The average ion concentrations and pH (4.93) of the rainwater from 2010-2014 were used (Table S-1 in supporting information).

2.3 Experimental set-up

Alum shale pieces greater than 2 cm were selected and crushed with a jaw crusher to get fresh rock surface, sieved through a 2 mm mesh, and stored in nitrogen over the weekend before the start of the experiment. The debris was crushed in air, as this best simulates what happens during construction works.

Batch experiments were performed with 150 g crushed rock to 1.5 L synthetic rainwater. Three samples were kept open to the atmosphere (atmospheric oxygen conditions, AOC) in 2 L Nalgene polypropylene bottles (Thermo Scientific). Another three were kept under a nitrogen atmosphere (low oxygen conditions, LOC) in heavy-duty vacuum bottles of the same size and material (Thermo Scientific) inside bags of oxygen-excluding material (FireDebris Tubular Rollstock from Ampac). Septa were installed in the lids for sampling of the LOC gas phase. The leachant for the LOC treatment was flushed with nitrogen for about 1.5 hours before use, and the O_2 concentration was measured (0.01 mg L^{-1}).

Start-up of the experiment and sampling of water was performed in a nitrogen tent. The setup did not completely exclude oxygen; thus, measurements of oxygen in both water and gas phase are presented in section 3.2. One sample consisting of only artificial rainwater (no debris) was prepared in parallel to each treatment, and treated, sampled and analysed in the exact same way. These served as experiment blanks to monitor contamination and other unintended effects in the experiment.

The samples were kept in the dark at 10 °C for 52 weeks and shaken by hand 2-3 times per week to get all of the debris in suspension, i.e., in contact with the leachant. Water aliquots for leachate quality analyses were taken out at 1 h, 24 h and at 1, 4, 12, 28 and 52 weeks after first mixing of water and rock, and the sampled volume was replaced with synthetic rainwater. In the duration of the experiment, a total of 20 % of the leachant was sampled and replaced. The gas phase of the LOC-samples was sampled before water sampling and at additional time points using a syringe through the septum installed in the bottle lids. Subsamples of the starting material (crushed alum shale) and leached debris (air-dried at the end of the experiment) were characterized as described in section 2.4.

2.4 Chemical analysis

2.4.1 Alum shale characterization

Total element concentrations were determined by ICP-MS after digesting (260 °C, 40 min, Milestone UltraCLAVE) 0.25 g of debris in triplicate, with Rh added as internal standard. The following acid mixtures were used: 5 mL HNO_3 (for Li, P, S, Ca and Fe), 5 mL HNO_3 + 1 mL HF (Mn, Cu, Zn, As, Mo, Cd, Sn, Sb and U), and 2 mL HNO_3 + 4 mL H_3PO_4 (Be, Na, Mg, Al, K, V, Cr, Co, Ni, Sr, Ba, La, Ce, Pr, Nd, Sm, Eu, Gd, Dy, Ho, Er, Tm, Yb, Lu, Pb, Ra and Th). Digested samples were diluted to 50 mL with ultrapure water. Certified reference materials NIST 2709a San Joaquin Soil and NSC ZC 73007 soil (all three digestions), NIST 2710a Montana I soil (only HNO_3 digestion), and NSC DC 73325 soil (only HF digestion) were digested and measured in parallel to the alum shale. When determining ^{226}Ra, reference materials IAEA-314 (sediment) and IAEA-448 (soil) were used. Results for all reference materials where within the uncertainties of certified values.

pH was measured in a 1+2 V/V mix of debris and water left overnight (handheld multi-meter, Multi series, WTW). Organic matter (OM) was estimated from loss on ignition (LOI, 550 °C, overnight). Total organic (TOC) and inorganic (TIC) carbon in the debris were

measured by coulometry. The TOC was only measured in the starting material and used for geochemical characterization (see section 2.5). Particle size distribution was determined for a 10 g sample, where organic matter had been removed by heating with H_2O_2, by wet sieving through 0.06 mm (sand fraction) and separating silt and clay by sedimentation according to Stokes' law. Mineral composition was determined by powder X-ray diffraction (XRD) on a D8 Discover (Bruker). The XRD diffractograms were analysed for peak identification with TOPAS software using a reference spectra library and quantified by the Rietveld refinement technique.

2.4.2 Leachate analysis

Leachate aliquots were collected using a syringe and divided into different subsamples. Oxygen concentrations (FDO® 925 Optical Dissolved Oxygen Sensor), conductivity, oxidation-reduction potential (ORP) and pH were measured immediately after sampling on untreated aliquots (handheld multi-meter, Multi series, WTW). E_h was calculated from ORP according to instructions from producer. Samples for ICP-MS, alkalinity, dissolved organic carbon (DOC) and anion chromatography were immediately filtered using 0.45 µm polyethersulfone membrane syringe filters (VWR). Subsamples from 1 h and 4, 12, 28 and 52 weeks were also filtered through 10 kDa Amicon® Ultra-15 centrifugal filters (Merck Millipore) for analysis of low molecular mass components by ICP-MS. Samples for ICP-MS were acidified to 5 % (V/V) ultrapure HNO_3, and all samples were stored in the dark at 4 °C until analysis. Alkalinity was measured by colorimetry by titration to pH 4.5 (ISO 9963-1:1994). Anions were quantified by ion chromatography (Lachat IC5000 system, Dionex™ IonPac™ AS22-Fast IC column, Dionex AMMS™ 300 ion suppressor, Thermo Scientific). DOC was determined with a TOC-VCPN analyser (Shimadzu), but all samples were below the detection limit (DL) (1.8 mg L^{-1}).

2.4.3 ICP-MS analysis

Water samples from the disposal site, synthetic rainwater, alum shale leachates and digested alum shale were analysed for Li, Be, Na, Mg, Al, P, S, K, Ca, V, Cr, Mn, Fe, Co, Ni, Cu, Zn, As, Sr, Mo, Cd, Sn, Sb, Ba, La, Ce, Pr, Nd, Sm, Eu, Gd, Dy, Ho, Er, Tm, Yb, Lu, Pb, ^{232}Th and ^{238}U using an Agilent 8800 Triple Quadrupole ICP-MS. Ge, In, Ir and Bi were added online as internal standards. The instrument was switched between He, O_2 and no gas in the collision/reaction chamber to remove interferences. On each analysis day, an in-house standard covering all analysed elements except Sn was analysed to check the

accuracy of the analysis method. ^{226}Ra was measured in the leachates and digested alum shale with an Agilent 8900 Triple Quadrupole ICP-MS using N_2O as reaction gas to eliminate interferences. Full method details are described in Wærsted et al. (2018).

2.4.4 Gas-phase measurements

Gas phase samples were analysed with an Agilent 7890A Network Gas Chromatograph to determine the levels of O_2, N_2, CH_4 and CO_2. Results are only semi-quantitatively described since the gas phase was exchanged with N_2 during each water sampling.

2.5 Data treatment

Element concentrations of the starting material and 52-weeks leachate were used to calculate the leached mass percentage of each element. For comparison with measured alkalinity, the solubility of calcite (K_{sp} = 5×10^{-9}) and measured (LOC samples) or atmospheric (AOC samples) CO_2 concentrations were used to estimate the alkalinity at the experimental conditions (vanLoon & Duffy, 2011). The acidification and neutralization potentials (AP and NP) of the debris were estimated by assuming that all S in the rock comes from sulphides behaving like pyrite, that the carbonates measured as TIC behave like calcite, and that each mole of calcite can neutralize two moles of protons (Lawrence & Wang, 1996; Pabst et al., 2016). Geochemical characterization of the alum shale was performed by comparing AP, NP and whole-rock analysis data (elemental composition, TIC and TOC) with an existing database of Cambro-Ordovician black mudrocks from the Oslo region (Norway) (Pabst et al., 2016).

Analyses of experiment blank samples showed a contamination of Zn, V and Ba; therefore, the average concentrations of the blanks were subtracted from the concentration of the samples of the corresponding treatment. Moreover, one of the LOC samples showed an unexpectedly high level of oxygen in both water and gas phases at 28 weeks. This was associated with high concentrations of several elements, similar to the AOC samples. Thus, data for this replicate was omitted for the two last sampling points, i.e., LOC data for 28 and 52 weeks is the average of only two replicate samples.

Significant differences between treatments were evaluated by t-tests performed in excel.

3 Results and discussion

3.1 Alum shale characterization

The organic matter (OM) concentration of the alum shale debris did not change during the experiments (Table 1). Measured TOC of the starting material was 8.9 %, somewhat higher than estimated from LOI (7.5 %). Measured TIC levels were similar to other acid-production black shales in Norway (Pabst et al., 2016), and decreased from 0.29 % to ~0.25% after both leaching treatments. Since TIC represent the main part of the buffer capacity of the debris, this slight concentration change reflects carbonate dissolution and/or consumption by acid production. The pH rose from 7.31 in the starting material to 7.48 in the AOC and 7.36 in the LOC, thus increasing with the exposure to oxygen. While the change was rather small, it was the opposite of what was expected.

Table 1: Loss on ignition (LOI), total inorganic carbon (TIC) and pH in the alum shale before (untreated) and after 52 weeks leaching (AOC and LOC). Average ± one standard deviation of replicate samples is shown.

Treatment	n	LOI (%)	TIC (%)	pH
Untreated	1	13.0	0.29	7.31
AOC	3	13.1 ± 0.3	0.25 ± 0.06	7.48 ± 0.01
LOC	3	13.1 ± 0.1	0.25 ± 0.01	7.36 ± 0.03

Measured elemental composition of the alum shale (Table 2) generally falls within the rather wide range of concentrations found in other Scandinavian locations (Falk et al., 2006; Jeng, 1991, 1992; Lavergren et al., 2009; Pabst et al., 2016). The high standard deviation for Ca (36 %) can be caused by the presence of carbonate nodules in the rock (Pabst et al., 2016). The concentrations of Cr, Ni, Cu, Zn, As and Cd exceeded the Norwegian limits for contaminated ground (Pollution Control Act, 2004), and since the U concentration is above the 81 mg kg^{-1} (1 Bq g^{-1}) limit, the alum shale is considered low-level radioactive waste (Radiation Protection Act, 2016). The measured activity concentration of ^{226}Ra in the debris (1.28 ± 0.08 kBq kg^{-1}) corresponds well to the estimate obtained assuming secular equilibrium with ^{238}U (1.34 ± 0.02 kBq kg^{-1}).

Table 2 : Elemental composition (average ± one standard deviation) of the untreated alum shale used in the leaching experiments, percentage of the elements leached from the alum shale into solution under atmospheric (AOC) and low (LOC) oxygen conditions after 52 weeks reaction, and concentration ratio of AOC and LOC treatments at 52 weeks. For all analyses, n = 3.

		Alum shale total concentration		AOC leachate % of rock	LOC leachate % of rock	AOC/LOC[a]
Group 1	Li	31.3 ± 0.3	mg kg^{-1}	0.66	0.45	1.5***
Alkali metals	Na	3.23 ± 0.03	g kg^{-1}	1.1	1.0	1.1
	K	42 ± 1	g kg^{-1}	0.13	0.13	1.0
Group 2	Be	6.7 ± 0.2	mg kg^{-1}	<0.0007	0.0008	†
Alkaline earth metals	Mg	9.0 ± 0.3	g kg^{-1}	0.94	0.85	1.1
	Ca	13 ± 5	g kg^{-1}	9.5	8.8	1.1*
	Sr	0.146 ± 0.007	g kg^{-1}	16	15	1.1
	Ba	0.8 ± 0.1	g kg^{-1}	0.02	0.03	0.73***
	^{226}Ra	35 ± 2	ng kg^{-1}	0.12	0.09	1.3
		1.28 ± 0.07	kBq kg^{-1}			
Group 4-11	V	3.08 ± 0.08	g kg^{-1}	0.0006	0.0002	3.0***
Transition metals	Cr	0.14 ± 0.03	g kg^{-1}	0.0001	0.0001	1.1†
	Mo	0.226 ± 0.004	g kg^{-1}	22	7.1	3.1***
	Mn	0.27 ± 0.05	g kg^{-1}	6.3	5.6	1.1*
	Fe	32 ± 3	g kg^{-1}	0.00009	0.0001	0.62*
	Co	23.4 ± 0.1	mg kg^{-1}	0.78	0.33	2.4***
	Ni	0.44 ± 0.03	g kg^{-1}	1.2	1.4	0.84*
	Cu	0.141 ± 0.005	g kg^{-1}	0.007	0.004	2.0***
Group 12	Zn	0.51 ± 0.04	g kg^{-1}	1.8	0.43	4.2***
	Cd	11.2 ± 0.8	mg kg^{-1}	2.6	0.82	3.2***
Group 13	Al	79 ± 1	g kg^{-1}	0.000009	0.00003	0.35**
Group 14	Sn	3.67 ± 0.06	mg kg^{-1}	0.002	0.0008	2.2†
	Pb	47 ± 1	mg kg^{-1}	0.0004	0.0004	1.0
Group 15	P	0.81 ± 0.05	g kg^{-1}	0.0003	0.0009	0.31†
	As	88 ± 4	mg kg^{-1}	0.009	0.003	2.9***
	Sb	19.1 ± 0.8	mg kg^{-1}	0.70	1.0	0.68***
Group 16	S	31 ± 3	g kg^{-1}	3.3	2.5	1.3**
Rare earth elements	La	50 ± 1	mg kg^{-1}	0.0001	0.0002	0.57*
Lanthanides and group 3	Ce	92 ± 2	mg kg^{-1}	0.00007	0.0002	0.36**
	Pr	12.9 ± 0.4	mg kg^{-1}	0.00009	0.0002	0.48**
	Nd	47 ± 2	mg kg^{-1}	0.0001	0.0002	0.58
	Sm	9.4 ± 0.2	mg kg^{-1}	0.0003	0.0004	0.79
	Eu	1.8 ± 0.1	mg kg^{-1}	0.001	0.001	1.1†
	Gd	9.1 ± 0.3	mg kg^{-1}	0.0007	0.0007	0.94
	Dy	8.5 ± 0.3	mg kg^{-1}	0.001	0.002	0.87
	Ho	1.88 ± 0.05	mg kg^{-1}	0.002	0.002	1.1
	Er	5.0 ± 0.2	mg kg^{-1}	0.002	0.002	1.1
	Tm	0.75 ± 0.01	mg kg^{-1}	0.002	0.003	0.83
	Yb	4.35 ± 0.04	mg kg^{-1}	0.002	0.002	1.2
	Lu	0.66 ± 0.01	mg kg^{-1}	0.002	0.002	0.99
Actinides	^{232}Th	14.8 ± 0.7	mg kg^{-1}	<0.00004	0.0002	†
		0.060 ± 0.002	kBq kg^{-1}			
	^{238}U	107 ± 2	mg kg^{-1}	4.0	4.9	0.82***
		1.34 ± 0.02	kBq kg^{-1}			

[a] Significance levels for t-test between AOC and LOC concentrations: *p < 0.1, **p < 0.05, ***p < 0.01, † t-test not performed as at least one replicate was below the detection limit

Geochemical characterization (see supporting information) places the sampled debris in the 3a layer of the alum shale formation (Owen et al., 1990; Pabst et al., 2016), a layer that is expected to be acid producing and have high concentrations of several trace elements and NORM (U-series). Estimated NP and AP were 24 and 97 kg $CaCO_3$ eq t^{-1}, respectively, resulting in a NP to AP ratio of 0.25. This means that if the debris is stored in contact with air and water, a pH drop is expected to occur when oxidation of sulphides have consumed all the carbonates.

Particle size distribution analysis revealed that 86.6 % of the starting material was sand, 12.2 % was silt and 1.2 % was clay. Mineral composition derived from XRD analyses showed no significant changes before and after leaching. Muscovite ($KAl_2(AlSi_3O_{10})(F,OH)_2$, 43.7 %), quartz ($SiO_2$, 19.2 %), pyrite ($FeS_2$, 3.5 %) and calcite ($CaCO_3$, 2.4 %) were the main mineral phases. Amorphous material (30.9 %) was also detected, and about half of it is accounted for by OM. The content of muscovite corresponds to the measured K and Al in the debris, while the calcite accounts for the TIC and ¾ of the Ca. The pyrite concentration (3.5 %) is somewhat lower than what Jeng (1991) measured in three unweathered, Norwegian alum shales (4.3-13.3 %), but higher than the weathered sample they measured (0.8 %). Pyrite accounts for 50 and 60 % of the Fe and S found in the alum shale. The molar relationship between Fe and S was close to 1:2, confirming that pyrite (FeS_2) is more dominant than pyrrhotite (FeS). The remaining S can be present as sulphates and/or other sulphides (e.g., pyrrhotite, sulphides with other cations than Fe).

3.2 Changes in physical-chemical variables

In the LOC samples, addition of the alum shale increased dissolved oxygen levels from 0.01 to 0.20 ± 0.07 mg L^{-1} in the first 1 hour, likely caused by oxygen bound to the surface of the crushed alum shale (Figure 1 a). Thereafter, the oxygen levels fluctuated between 0.3 and 0.9 mg L^{-1}, with the highest levels observed at 52 weeks. This was also seen for the gas phase O_2 (data not shown), which increased from about 0.4 % in the first week to ~3.5 % by the end of the experiment. Yet, it is still substantially below atmospheric levels (21 %). For the AOC treatment, the initial leachant concentration was 8.4 mg L^{-1} O_2, which increased to 9.00 ± 0.02 mg L^{-1} at 1 hour due to surface-bound oxygen release and equilibration with air. After this, the O_2 concentrations varied between 9.5 and 10.1 mg L^{-1}.

Within the first hour, the leachate pH increased from 4.97 in the synthetic rainwater to 8.4 and 9.0 in the AOC and LOC treatments, respectively (Figure 1 b). The pH in the AOC treatment dropped suddenly to 7.0 at 24 hours, followed by an increase to 8.0 at 4 weeks before slowly decreasing to 7.7 at 52 weeks. The early pH drop can be due to precipitation of Fe released from pyrite oxidation as (oxy)hydroxides, removing OH^- from solution. This early pH drop was also observed by Wærsted et al. (in prep.) in other oxic leaching experiments with the same alum shale batch, but was not seen in the LOC treatment samples, possibly due to less Fe release from pyrite oxidation. Yet, the two leaching treatments had similar pH from 4 weeks onwards, since the LOC treatment also showed a slow decrease from pH 8.2 to 7.7 between 1 and 52 weeks.

Together with the measured pH, calculated E_h (ranging from 246 to 497 mV) placed all leaching systems in the stability range of Fe(III) (Grundl et al., 2011), thus pyrite oxidation was expected. In the duration of this experiment, calcite provided sufficient buffering to keep pH circumneutral, and similar pH values have been observed in other leaching experiments with alum shale from Gran (Fjermestad et al., 2017; Hjulstad, 2015; Wærsted et al., in prep.). Based on the low NP to AP ratio for this alum shale, we would expect a pH drop in the long term, but these results demonstrated that it could be postponed, or even avoided, by minimizing access to air and exchange of water in the disposal site. Leaching experiments with other Scandinavian alum shales have resulted in pH levels down to 2-3 (Falk et al., 2006; Jeng, 1991; Yu et al., 2014). In a 14 weeks batch experiment, Jeng (1991) measured decreasing pyrite content of a calcareous alum shale together with increased leaching of SO_4^{2-} and Ca during weathering experiments, but no change in pH because of neutralization of the acid, as we see here.

The alkalinity of the leachate likely reflects dissolution of calcite ($CaCO_3$) in the debris. The alkalinity was similar for the two treatments at 1 hour and 4 weeks after initial mixing, followed by a steady increase to 1.9 mmol L^{-1} in the LOC samples during 52 weeks, while the AOC samples stabilized at ~1.1 mmol L^{-1} (Figure 1 c). This difference may indicate a greater production of acid in the AOC samples due to pyrite oxidation. However, the P_{CO2} in the gas phase of the LOC treatment also increased with time (data not shown). At the end of the experiment, when the bottles had been closed for 24 weeks (i.e., no gas phase exchange), measured P_{CO2} was about 5 times higher than the 390 ppm atmospheric CO_2 (Hartmann et al., 2013). Solubility calculations indicate that dissolved

309 HCO_3^- concentrations in both treatments were limited by solubility of calcite. Therefore,
310 the higher alkalinity in the LOC samples was likely due to the P_{CO2} increase, which
311 increases the solubility of calcite (vanLoon & Duffy, 2011), while the CO_2 produced in the
312 open AOC samples equilibrated with air. Besides carbonate dissolution, increasing P_{CO2}
313 can indicate chemical or biological oxidation of organic matter in the presence of oxygen
314 (vanLoon & Duffy, 2011). Since the samples were not sterilized, biological activity could
315 have occurred in these systems, as also suggested by the elevated methane
316 concentrations measured in the gas phase (data not shown) (vanLoon & Duffy, 2011).
317 The highest methane concentrations (~1000 ppm) appeared between 4 and 28 weeks,
318 and were substantially higher than the ~2 ppm atmospheric P_{CH4} (Hartmann et al., 2013).
319 After 28 weeks, methane concentrations were lower despite longer periods between
320 sampling points and thus exchange of the gas phase.

321 The conductivity reflects the total amount of ions in solution, and thus gives an indication
322 of the total leaching into the water under different oxygen conditions. From 4 weeks, the
323 conductivity in the AOC treatment was about 15 % higher than in the LOC treatment,
324 indicating greater leaching with higher access to oxygen (Figure 1d), as expected.

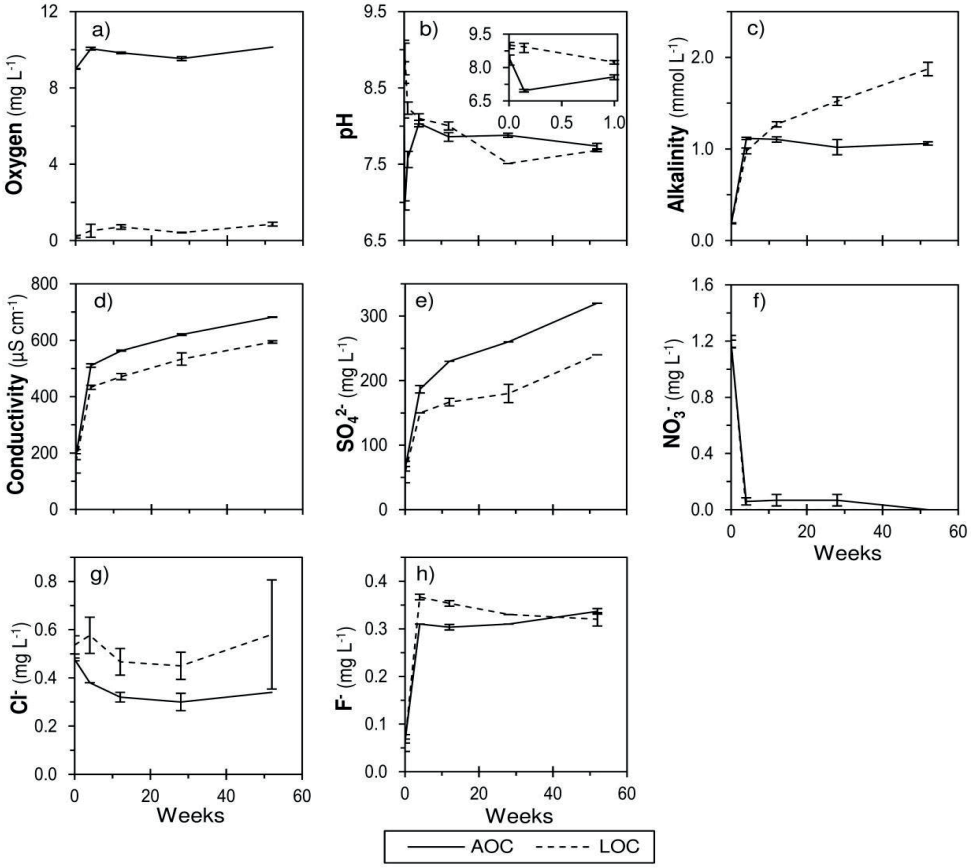

Figure 1: Water quality parameters (a-d) and anions (e-h) in alum shale leachates of atmospheric oxygen conditions (AOC) and low oxygen conditions (LOC) over time. Full (AOC) and dashed (LOC) lines are connecting average concentrations, and the error bars represent one standard deviation of replicate samples. For all data points, n = 3, except 28 and 52 weeks for the LOC treatment where n =2. The inset graph in b) shows the pH in the first week.

Sulphate was, together with carbonates, the dominating anion in the leachate (Figure 1 e). Leaching of sulphate is expected from both dissolution of sulphates and oxidation of sulphides present in the debris. Sulphate increased greatly in both treatments up to four weeks, then continued increasing at a slower rate. Concentrations were about 30 % greater in the AOC than in the LOC experiments, indicating higher oxidation rates of sulphides with greater access to oxygen. At 52 weeks, 3.3 % of the total S in the debris had leached in the AOC treatment and 2.5 % in the LOC (Table 2).

A slight nitrate reduction from 1.3 to ~1.2 mg L^{-1} was observed already after 1 hour in both treatments (Figure 1 f), and after 4 weeks concentrations were below or within error of the detection limit (0.09 mg L^{-1}). Nitrate was likely used by microorganisms, as

it is an important nutrient, or consumed by reactions such as pyrite oxidation (Appelo & Postma, 2010; vanLoon & Duffy, 2011). Chloride in the AOC treatment decreased to about 0.3 mg L^{-1} from the starting concentration of 0.46 mg L^{-1}, while the LOC treatment concentrations were within error of 0.5 mg L^{-1} (Figure 1 g). Fluoride increased from <0.04 mg L^{-1} in the starting water to about 0.30-0.35 mg L^{-1} in both treatments (Figure 1 h). One possible source of F^- is the muscovite.

3.3 Leaching of elements under different oxygen conditions

In general, the leachate concentrations of most elements increased abruptly in the first hour after mixing, independently of the treatment. This can be an artefact of the crushing of the alum shale, creating very reactive, fresh surfaces. At 52 weeks, more than 1 % of the total debris content of Na, Ca, Sr, Mo, Mn, Ni, Zn, Cd, S and U had been released to the aqueous phase (Table 2). Other elements, such as K, leached a smaller percentage of the debris content, but still reached high concentrations in the leachate due to high rock concentration. Elemental S concentrations in the leachate matched well the sulphate concentrations (Figure 1) at all time-points, suggesting that all S in the leachates was present as sulphate.

Leaching over time for selected elements is presented in Figure 2 and discussed in the next sections. Measurements of the < 10 kDa fraction at 1 hour, 4, 12, 28 and 52 weeks showed that ≥ 90 % of these selected elements were present as low molecular mass species in the leachate. Be, Cr, Fe, Cu, P and ^{232}Th together with group 13, 14 and rare earth elements (Table 2) leached in concentrations close to detection limits, resulting in fractionation measurements associated with high uncertainties, and these results are thus not presented.

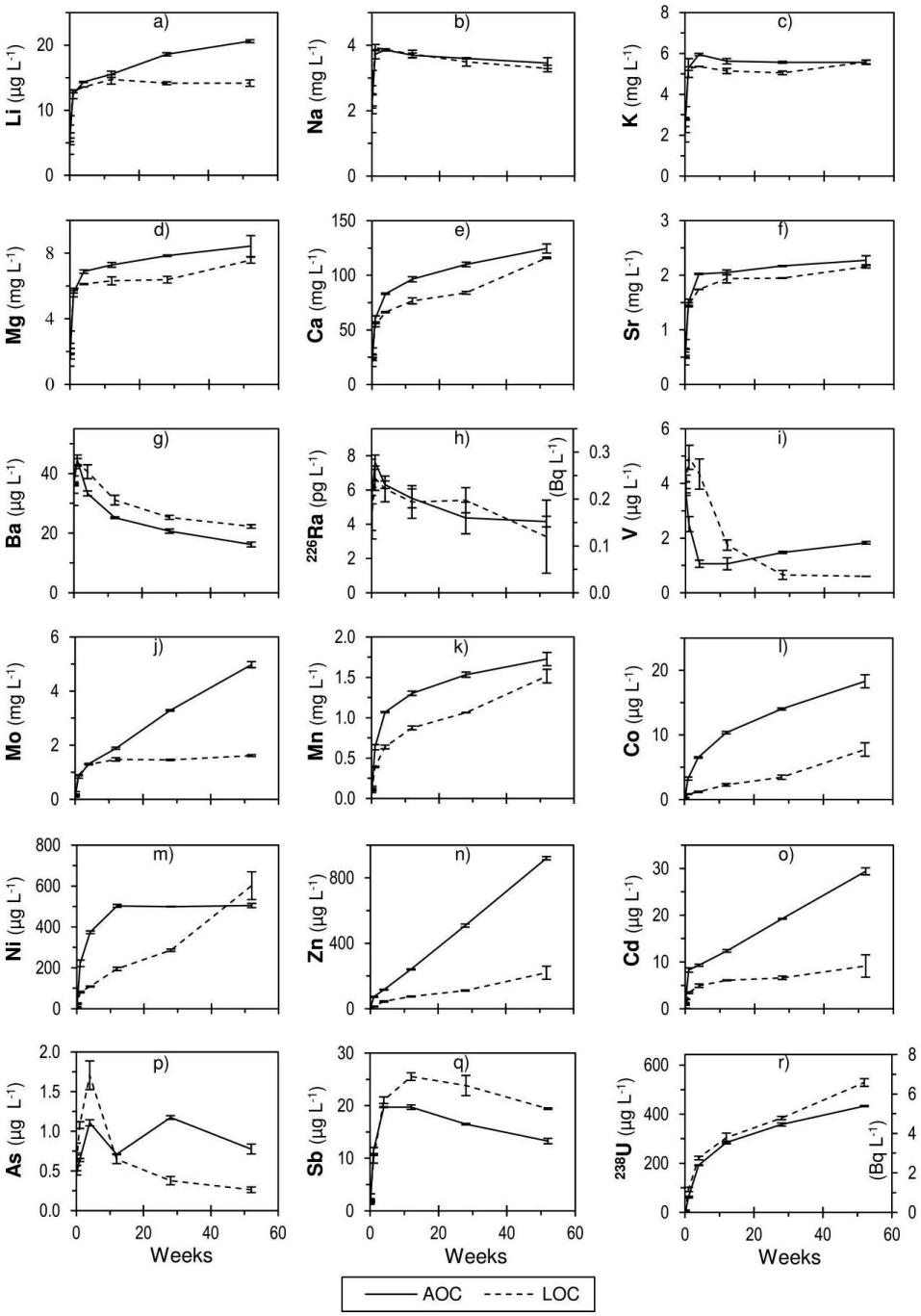

Figure 2: Dissolved (<0.45 µm) concentrations of selected elements leached from alum shale over time, under atmospheric (AOC) and low (LOC) oxygen conditions. Full (AOC) and dashed (LOC) lines connect average concentrations, and error bars represent one standard deviation of replicate samples (n = 3, except 28 and 52 weeks of LOC treatment where n = 2). For the radionuclides (h and r), the secondary y-axis shows activity concentrations (Bq L^{-1}).

3.3.1 Group 1 (Alkali metals)

Leached Li concentrations (Figure 2 a) were similar in the two treatments until 4 weeks, and then the concentrations stabilized in the LOC and continued to increase in the AOC treatment. At 52 weeks, Li was 46 % higher in the AOC than the LOC ($p = 0.0002$). Comparing the aqueous concentration at 52 weeks to the elemental composition of the debris, less than 1 % of Li leached in both treatments (Table 2).

The concentrations of Na and K (Figure 2 b and c) increased greatly the first week, then stabilized or even slightly declined. Leaching of Na seemed to be unaffected by oxygen access, while for K there were only small differences between treatments. K concentrations (5-6 mg L^{-1}) were almost twice as high as Na concentrations (3-4 mg L^{-1}). K in the debris is likely exclusively contributed by muscovite, and is thus not readily available for dissolution, reflected in that only 0.13 % of the K in the debris was released in either treatment. The quick release in the first week can be an artefact from the crushing of the debris causing damages to the clay structure. More K will be released in the event of a pH drop, because the acid attacks the clay minerals, as seen by (Yu et al., 2014).

3.3.2 Group 2 (Alkaline earth metals)

The concentrations of Mg, Ca and Sr increased quickly the first week, and then continued to increase at a slower rate (Figure 2 d-f). Leaching curves of Mg and Ca (Figure 2 d and e) resembled that of SO_4^{2-} (Figure 1 e), likely due to calcite dissolution. Mg, Sr and Ba can be expected as impurities in calcite (Appelo & Postma, 2010; Gabitov et al., 2013), but can also originate in other phases in the debris. The differences between the two treatments were smaller for Mg and Ca than what was seen for sulphate, probably because the solubility of calcite was higher in the LOC treatment due to the higher P_{CO2}. At 52 weeks, almost 10 % of the Ca debris content had dissolved, but less than 1 % of the Mg (Table 2). This, and the very similar leaching curves of the two elements, could indicate that the fraction of Mg that has dissolved comes from Mg substituting Ca in calcite, while the greater fraction of Mg in the debris is in another, less soluble, phase.

Leaching of Sr was a bit slower in the LOC compared to the AOC treatment, but the concentrations in both treatments were about 2200 µg L^{-1} in the last sampling point. The solubility product of $SrSO_4$ is 3.44×10^{-7} (25 °C) (*CRC Handbook of Chemistry and Physics*, 1993) which was not exceeded for either treatments in the duration of the experiment.

At 52 weeks, the aqueous concentration of Sr in the AOC treatment corresponded to 16 % of the total Sr in the debris and in the LOC treatment 15 %, and Sr was after Mo the element that leached the greatest fraction of the debris content.

Concentrations of Ba and ^{226}Ra peaked at 1 week before decreasing, likely due to precipitation of $BaSO_4$ and co-precipitation of ^{226}Ra (Figure 2 g and h). The concentration of Ba decreased somewhat slower in the LOC treatment – likely due to the slower release of SO_4^{2-}. The solubility product K_{sp} ($BaSO_4$) = 1.07×10^{-10} (25 °C) (*CRC Handbook of Chemistry and Physics*, 1993) was exceeded at every time point in both treatments. ^{226}Ra followed a very similar trend to Ba, but bigger standard deviations make it difficult to say anything about differences of the two treatments beyond assuming that the true curves may be similar to those of Ba. At 52 weeks, Ba was 27 % lower in the AOC compared to the LOC ($p = 0.003$). Of the total debris content, ^{226}Ra leached a higher percentage than Ba (Table 2), but still only 0.12 % and 0.09 % in the AOC and LOC treatment, respectively.

3.3.3 Transition metals

The transition metals V (Figure 2 i), Cr, Fe and Cu showed very limited solubility with <0.01 % leached at 52 weeks, while Co, Ni, Mn and Mo (Figure 2 j-m) leached 0.33 - 22 %. Jeng (1992) observed very limited leaching of Cu and Fe from different alum shales when pH was > 3. Fe^{3+} is produced in the pyrite oxidation, but will precipitate as Fe (oxy)hydroxides by the prevailing pH and E_h. Amorphous iron (oxy)hydroxides have a great potential for scavenging a variety of other elements (Appelo & Postma, 2010; Braunschweig et al., 2013), thus Fe is likely very important for the processes in the leaching experiments even if dissolved concentrations are low.

Concentrations of V peaked early in the experiment and decreased quickly, potentially linked to scavenging by iron (oxy)hydroxides (Braunschweig et al., 2013). The decrease was quickest in the AOC treatment, but after 12 weeks the concentrations started increasing again and at the 52 weeks sampling, the V concentration in the AOC was three times that of the LOC ($p = 5e\text{-}5$).

Concentrations of Mo increased almost linearly in the AOC treatment, while the concentrations in the LOC treatment stabilized at about 1600 µg L^{-1}. At 52 weeks the concentrations of Mo in the AOC was 3 times that of the LOC ($p = 4e\text{-}5$). Of the total Mo in the debris, 22 % leached in the AOC treatment and 7.1 % in the LOC treatment. The

approximately linear curve for the AOC treatment indicates that the leaching could continue at the same rate for a prolonged time, and given that the greatest part of the element is still in the rock, concentrations in a prolonged experiment would be expected to be considerably higher.

Mn had very similar leaching curves to Ca and Mg, likely because it is often present as a doubly charged ion and is a common impurity in calcite (Appelo & Postma, 2010; Rayner-Canham & Overton, 2006). From 4 weeks onwards, leached Mn concentrations were between 68 % ($p = 6e-6$) and 14 % ($p = 0.07$) higher in the AOC treatment than under LOC. Concentrations increased logarithmically in both treatments following a similar trend. At 52 weeks, 6.3 % of the total Mn in the debris had leached out in the AOC treatment, and 5.6 % in the LOC.

There was a faster increase of Co in the AOC than the LOC treatment, but neither of the treatments seemed to reach a stable concentration level in the duration of the experiment. At 52 weeks, concentrations in the AOC treatment was 140 % higher than in the LOC treatment ($p = 0.001$), and the aqueous concentrations corresponded to 0.78 % and 0.33 % of the total Co concentration in the debris, respectively.

In the AOC treatment, Ni concentrations increased quickly in the beginning and stopped abruptly at 12 weeks, where AOC concentrations were 160 % greater than LOC concentrations ($p = 9e-7$). The concentrations in the LOC treatment increased slower, but were 16 % higher than the AOC at 52 weeks ($p = 0.08$). At 52 weeks, 1.2 % of the Ni had leached to the aqueous phase of the AOC treatment, and 1.4 % to the LOC.

3.3.4 Group 12

Zn and Cd exhibited similar behaviour to Mo (group 6), and the release rates were much higher in the AOC compared to the LOC treatment (Figure 2 n and o). Indeed, these elements exhibited the greatest concentration difference between the two treatments. At 52 weeks, the concentrations of Zn and Cd were, respectively, more than 4 ($p = 7e-5$) and 3 ($p = 0.0007$) times higher in the AOC than in the LOC leachate. The total Zn and Cd leached was, respectively, 1.8 % and 2.6 % (AOC) and 0.4 % and 0.8 % (LOC).

3.3.5 Group 15

The group 15 elements P, As (Figure 2 p) and Sb (Figure 2 q) were behaving similarly by having limited solubility or decreasing concentrations as a main characteristic of the time

trend, possibly caused by scavenging by iron (oxy)hydroxides formed during pyrite oxidation (Braunschweig et al., 2013; Okkenhaug, 2012). The solubility of the elements increased with mass, and for Sb up to 1 % of the total element concentration in the debris was in the aqueous phase at 52 weeks. The solubility of the group 15 elements in the disposal site might increase if pH decreases and scavenging by Fe ceases. The group 5 element V, which have a similar electron configuration, was also characterized by limited solubility and decreasing concentrations.

3.3.6 Actinides

Activity concentrations of ^{238}U (Figure 2 r) in the leachates reached much higher than those of its daughter ^{226}Ra (Figure 2 h), except at 1 and 24 hours where the activity concentration of ^{226}Ra in the leachate was higher than the one of ^{238}U. After 4 weeks, the rate of U release decreased, but concentrations were still increasing at the end of the experiment and seemed to increase faster in the LOC samples. One explanation can be less scavenging by Fe (oxy)hydroxides due to less pyrite oxidation, or increased solubility because of the higher carbonate concentrations in the LOC treatment (Seder-Colomina et al., 2018; Stanley & Wilkin, 2019). The concentration at 52 weeks was 22 % higher in the LOC treatment ($p = 0.001$). 3.7 % and 4.5 % of the total U in the debris had leached to the aqueous phase at 52 weeks, in the AOC and LOC treatment, respectively.

3.4 Environmental relevance of results

The leaching experiment demonstrated neutral rock drainage (NRD). Even with a neutral pH, several elements were leaching to concentration levels of concern, but if the debris is oxidized to the point of a pH drop, the leaching of several elements is expected to accelerate (Falk et al., 2006; Jeng, 1992). Falk et al. (2006) collected weathered and unweathered alum shale in the field in Öland, Sweden. They found substantially higher concentrations of Cd, Cu, Ni, Zn and As in the unweathered rock compared to the weathered, indicating that a great part of these elements has been released to the environment. The greatest difference was found for Zn and Cd, where 80-85 % was presumably lost. A leaching experiment with the unweathered rock, including a pH drop to about 3, gave 10 times higher Ni, Zn and Cd concentrations than found in the present work and 1000 times higher Cu. The concentrations especially increased after the pH dropped below ~5. Solubility of Th is also greatly enhanced when pH falls below 2-3, and substantial leaching from U tailings can occur due to acid rock drainage (Landa, 2007).

The slower release of elements in calcareous alum shales is largely caused by less weathering, and this will accelerate when the pH drops and acid attacks the rock and the ferric ion (Fe^{3+}) propagates the pyrite oxidation (Jeng, 1992; Singer & Stumm, 1970). Furthermore, scavenging effects of Fe (oxy)hydroxides will cease, and elements that have precipitated or been scavenged may become soluble as the pH decreases, causing a sudden release of contaminants. When pH drops below about 5, Al becomes soluble, and a possible major environmental problem (Endre, 2013; Rayner-Canham & Overton, 2006). An estimated 18 tons of dissolved Al leaches yearly into the fjord Kaldvellfjorden, Southern Norway, from an upstream disposal site of acid-producing rock (Hindar, 2013). Al can have a detrimental impact on aquatic life (Lydersen et al., 2002; Rosseland et al., 1992)

Concentrations in the leachates at 52 weeks are compared with environmental quality standards in Table 3. Mo, Ni, Zn, Cd and U are all much higher than the limits, and can be expected to pose a serious environmental risk in such concentrations. These elements were also still increasing in concentrations at the end of the experiment, except Mo in the LOC treatment and Ni in the AOC treatment. While the increasing concentration curves can indicate that concentrations will continue to increase for a long time, this also depends on the binding of the elements in the rock minerals: if the remaining part of the element is bound in minerals with lower reactivity or solubility, the leaching will slow down. At some point, high concentrations in the aqueous phase might also slow down the release rate, but exchange of water in the disposal site or decreasing pH can contribute to keeping the rate of release high.

Table 3: Environmental quality standards for selected elements and ratio of the leachate concentrations of 52 weeks for the atmospheric (AOC) and low (LOC) oxygen conditions to the standard. For leachate concentrations exceeding the environmental quality standard, the ratio is emphasized in bold.

Element	Limit	Unit	AOC/Limit	LOC/Limit	Country[a]	Reference
Cr	3.4	µg L^{-1}	0.006	0.005	NO	[b]
Mo	73	µg L^{-1}	**68**	**22**	CA	[c]
Ni	4	µg L^{-1}	**126**	**150**	NO+EU	[b, d]
Cu	7.8	µg L^{-1}	0.1	0.1	NO	[b]
Zn	11	µg L^{-1}	**83**	**20**	NO	[b]
Cd[e]	0.09	µg L^{-1}	**322**	**102**	NO+EU	[b, d]
Pb	1.2	µg L^{-1}	0.02	0.01	NO	[b]
As	0.5	µg L^{-1}	**1.6**	0.5	NO	[b]
^{238}U	15	µg L^{-1}	**29**	**35**	CA	[c]

[a] For the limits for Norway (NO) and EU, the annual average environmental quality standard (AA-EQS) values are used. For the Canadian (CA) limits, the long-term concentration from the water quality guidelines for protection of aquatic life is used.
[b] (Norwegian Environmental Agency, 2016)
[c] (Canadian Council of Ministers of the Environment, 2018)
[d] (EU, 2013)
[e] Limits for Cd depends on measured $CaCO_3$ concentrations

Concentrations of Cr, Cu and Pb were all below what is of environmental concern. For As, it could be assumed that dilution downstream of the disposal site would make the As concentrations of no concern outside the disposal site. While the AOC treatment seemed to be the better choice regarding leaching of U, a strictly anoxic or reducing environment keeping U in the IV oxidation state would severely limit solubility and mobility of U (Lieser, 1995).

At Gran and similar sites, it can be assumed that water draining from the disposal site will be diluted quite quickly downstream. Even so, concentrations after a 10 times dilution would still raise concern for Mo, Ni, Zn, Cd and U, and even a 100 times dilution might not be enough to mitigate the situation for Cd and Ni. Combined with already elevated concentrations of these elements in the area of the disposal site (Skipperud et al., 2016), the effect of dilution might not be enough to avoid environmental consequences downstream of the disposal site.

The major part of the measured elements are assumed bioavailable, as they were present as low molecular mass species. Bioavailability of several elements also greatly depends on pH and ionic strength, and the effects on biota are often greater as pH and ionic strength are reduced (Lydersen et al., 2002; Rosseland et al., 1992). Thus, dilution of the leachate with water having neutral pH and high concentration of base cations like Ca is

expected to decrease the toxicity, while dilution with e.g. rainwater might not have a considerable effect. The water sampled in streams and lakes around the disposal site at Gran has Ca concentrations of 40-130 mg L^{-1} and pH of 7.9-8.7 (Skipperud et al., 2016). This is high compared to many places in Norway as pH is often down to 5.0 and Ca concentrations in lakes in some regions are on average below 0.6 mg L^{-1} (Skjelkvåle et al., 2012). Thus, the Gran area is likely less vulnerable to biological effects of alum shale disposal than other regions with different conditions. Even so, if ARD develops, the toxicity of the leachate can be greatly increased due to both increased leaching and the lower pH.

3.4.1 Comparison with disposal site

Comparing concentrations at 52 weeks in the leaching experiment with water in the disposal site gives some interesting results (Table 4). Measurements of pH, sulphate, Mg and Ca were quite similar, indicating a similar overall water quality. The higher conductivity in the disposal site is likely explained mainly by the higher concentrations of NO_3^-, Cl^- and Na and the somewhat higher concentration of SO_4^{2-}.

Nitrate was at least 2000 times higher in the disposal site than in the experiment, which is likely related to residuals from explosives in the disposed tunnel debris (Fjermestad et al., 2018). As NO_3^- is an important electron acceptor, the high levels can contribute to pyrite oxidation (Appelo & Postma, 2010) and delay the onset of anoxic or reducing conditions in the disposal site.

Table 4: Water quality and element concentrations measured in water collected at the disposal site at Gran (average ± one standard deviation; n = 1 for pH and conductivity, n = 3 for the rest of the measurements). Concentration ratios to experimental measurements obtained under atmospheric (AOC, n=3) and low (LOC, n=2) oxygen conditions are also presented. Concentrations were measured in samples filtered through 0.45 µm, except for anions in disposal site water that were measured in unfiltered samples.

		Disposal site		AOC (52 w) / disposal site	LOC (52 w) / disposal site
Water quality	pH	7.65		1.0	1.0
	Conductivity	1236	µS cm^{-1}	0.55	0.48
	SO_4^{2-}	340	mg L^{-1}	0.94	0.71
	NO_3^-	186	mg L^{-1}	≤0.0005	≤0.0005
	Cl^-	23	mg L^{-1}	0.043	0.026
Group 1	Li	20 ± 0.2	µgL^{-1}	1.0	0.71
Alkali metals	Na	99 ± 1	mg L^{-1}	0.035	0.033
	K	13 ± 0.1	mg L^{-1}	0.43	0.43
Group 2	Mg	12 ± 0.4	mg L^{-1}	0.70	0.63
Alkaline earth metals	Ca	110 ± 4	mg L^{-1}	1.1	1.1
	Sr	1.40 ± 0.03	mg L^{-1}	1.6	1.5
Group 4-11	V	2.4 ± 0.06	µg L^{-1}	0.76	0.25
Transition metals	Cr	0.14 ± 0.03	µg L^{-1}	0.14	0.11
	Mo	850 ± 0.4	µg L^{-1}	5.9	1.9
	Mn	97 ± 2	µg L^{-1}	18	16
	Fe	4.4 ± 0.7	µg L^{-1}	0.64	1.0
	Co	0.48 ± 0.07	µg L^{-1}	38	16
	Ni	4.3 ± 0.2	µg L^{-1}	117	140
	Cu	0.26 ± 0.02	µg L^{-1}	3.8	1.9
Group 12	Zn	<2.6	µg L^{-1}	≥354	≥85
	Cd	0.13 ± 0.006	µg L^{-1}	226	70
Group 13	Al	7.8 ± 0.4	µg L^{-1}	0.091	0.26
Group 14	Sn	0.12 ± 0.002	µg L^{-1}	0.058	0.025
	Pb	0.042 ± 0.0007	µg L^{-1}	0.48	0.40
Group 15	As	3.7 ± 0.07	µg L^{-1}	0.21	0.071
	Sb	90 ± 0.4	µg L^{-1}	0.15	0.22
Rare earth elements	La	0.0087 ± 0.002	µg L^{-1}	1.1	1.3
Actinides	U	73 ± 0.4	µg L^{-1}	5.9	7.2

Several of the elements (Mo, Mn, Ni, Zn, Cd and U) that we expect to be high in alum shale were much higher in the leachate from the experiment than in the disposal site. This might be reflecting that the experiment had pure alum shale and the disposal site is filled with tunnel blast having > 10 % black shales, and thus includes other rocks (Fjermestad et al., 2018). Ni, Zn and Cd were more than 100 times higher in the experiment than in the disposal site, while Mn and Co were more than 10 times higher. Mo and U were also several times higher in the experiment leachates.

One the other hand, the alkali metals where generally higher in the disposal site compared to both treatments, except Li that was quite similar. High Na concentrations

likely originate from salting of roads in the area, which is reflected in the high Cl^- concentration. V, As and Sb, which all showed limited solubility in the AOC-LOC leaching experiment, were present in higher concentrations in the disposal site. This might indicate lower oxygen conditions leading to less pyrite oxidation and less scavenging by Fe (oxy)hydroxides in the disposal site compared to the experiments, however, the high sulphate concentrations indicate the opposite.

Be, Cr, Fe, Cu, Al, Sn, Pb, La and Th were all low in the disposal site, as also seen in the laboratory experiment. Be and Th were around detection limits in both the disposal site and in the experiment, and are not included in the table. Ba and ^{226}Ra were not measured in water from the disposal site, but as SO_4^{2-} levels in the disposal site water were similar to the experiment leachates, we expect low release and mobility of these elements.

Overall, it seems that the AOC and LOC treatments are more similar to each other than either of them are to the disposal site. The most important reason for this can be that the disposed rock masses has a great variation in content, while the debris used for the experiment was part of one tunnel blast crushed down and thoroughly mixed before the experiment, and the two treatments therefore had a shared starting point that was not shared by the disposal site. Also, the debris-to-water relationship is higher in the disposal site than in the experiments. Another important factor can be the presence of organic matter in the disposal site, which is important for speciation and mobility of e.g. Ni, Zn, Cd and U (Appelo & Postma, 2010; Moulin et al., 2004).

4 Conclusions

Improperly stored alum shale and other acid-producing rock can leach harmful amounts of NORM and stable elements to the environment. The leaching experiments confirmed the importance of storage under low oxygen conditions to protect the environment, as the leaching of most elements was enhanced in atmospheric oxygen conditions. On the other hand, Sb, Ba and U were released quicker in the low oxygen conditions, but for these elements, the concentration differences were not so prominent. If sulphate concentrations gets low, Ba and ^{226}Ra mobility might increase due to reduced precipitation of $BaSO_4$.

Lower concentrations of sulphate under the low oxygen conditions (LOC) indicated less oxidation of sulphides and thus lower production of acid compared to the atmospheric

oxygen conditions (AOC). The buffering capacity of the tested alum shale prohibited a pH drop over 52 weeks. As long as oxygen is available, acid rock drainage can however be expected eventually, as the estimated neutralization potential of the debris was lower than the acidification potential. This will in turn lead to substantially greater leaching of several elements.

When choosing to store acid-producing rock submerged like in this case, careful consideration of the specific site and rock is necessary to confirm the presence of desired properties. The buffer capacity of the debris seen in this experiment can be crucial for avoiding a pH drop in the disposal site while reducing conditions are establishing. Great care should be made to avoid exchange of water in the Gran disposal site and similar sites, both to reduce oxygen availability and to avoid spreading of contaminated water. Even if the deposited alum shale is not kept absolutely oxygen free, the experiments with limited access to oxygen demonstrated considerably slower leaching of several environmentally important elements.

Supporting information

Synthetic rainwater concentrations. Plots for geochemical characterization. XRD results and diffractograms for alum shale analyses.

Acknowledgements

This study has been funded by the Norwegian Public Road Administration through the NORWAT (Nordic Road Water) programme and by the Norwegian Research Council through its Centre of Excellence (CoE) funding scheme (Project 223268/F50). We thank Erlend Sørmo at the Norwegian Geotechnical Institute (NGI) for providing the geochemical characterization of the alum shale used for the experiment.

5 References

Aas, W., Platt, S., Solberg, S., & Yttri, K. E. (2015). *Monitoring of long-range transported air pollutants in Norway, annual report 2014* (M-367).

Alloway, B. J. (2013). *Heavy Metals in Soils: Trace Metals and Metalloids in Soils and their Bioavailability* (B. J. Alloway & J. T. Trevors Eds., 3rd ed.): Springer.

Appelo, C. A. J., & Postma, D. (2010). *Geochemistry, groundwater and pollution* (2nd ed.): CRC press.

Bierens de Haan, S. (1991). A review of the rate of pyrite oxidation in aqueous systems at low temperature. *Earth-Science Reviews, 31*(1), 1-10. doi:http://dx.doi.org/10.1016/0012-8252(91)90039-I

644 Braunschweig, J., Bosch, J., & Meckenstock, R. U. (2013). Iron oxide nanoparticles in
645 geomicrobiology: from biogeochemistry to bioremediation. *New Biotechnology, 30*(6),
646 793-802. doi:https://doi.org/10.1016/j.nbt.2013.03.008
647 Canadian Council of Ministers of the Environment. (2018). Water Quality Guidelines for the
648 Protection of Aquatic Life. on 25.06.2019
649 Chandra, A. P., & Gerson, A. R. (2010). The mechanisms of pyrite oxidation and leaching: A
650 fundamental perspective. *Surface Science Reports, 65*(9), 293-315.
651 doi:http://dx.doi.org/10.1016/j.surfrep.2010.08.003
652 *CRC Handbook of Chemistry and Physics*. (1993). (D. R. Lide Ed., 74th ed.). U.S.A.: CRC.
653 Endre, E. (2013). *Identifisering og karakterisering av skiferhorisonter i tunneltraséen* (20120110-
654 R=1).Norwegian Geotechnical Institute:
655 Directive 2013/39/EU of the european parliament and of the council, (2013).
656 Falk, H., Lavergren, U., & Bergbäck, B. (2006). Metal mobility in alum shale from Öland, Sweden.
657 *Journal of Geochemical Exploration, 90*(3), 157-165.
658 doi:http://dx.doi.org/10.1016/j.gexplo.2005.10.001
659 Fjermestad, H., Gundersen, E., Hagelia, P., Moen, A. B., & Torp, M. (2018). *National Road 4,*
660 *utilization of black shale - Final report and experiences gathered* (333). Retrieved from
661 www.vegvesen.no/
662 Fjermestad, H., Hagelia, P., & Thomassen, T. (2017). *Large-scale leaching experiment with black*
663 *shale from National Road 4, Hadeland* (665). Retrieved from www.vegvesen.no
664 Gabitov, R. I., Gagnon, A. C., Guan, Y., Eiler, J. M., & Adkins, J. F. (2013). Accurate Mg/Ca, Sr/Ca, and
665 Ba/Ca ratio measurements in carbonates by SIMS and NanoSIMS and an assessment of
666 heterogeneity in common calcium carbonate standards. *Chemical Geology, 356*, 94-108.
667 doi:https://doi.org/10.1016/j.chemgeo.2013.07.019
668 Grundl, T. J., Haderlein, S., Nurmi, J. T., & Tratnyek, P. G. (2011). Introduction to Aquatic Redox
669 Chemistry. In *Aquatic Redox Chemistry* (Vol. 1071, pp. 1-14): American Chemical Society.
670 Hartmann, D. L., Tank, A. M. G. K., Rusticucci, M., Alexander, L. V., Brönnimann, S., Charabi, Y.,
671 Dentener, F. J., Dlugokencky, E. J., Easterling, D. R., Kaplan, A., Soden, B. J., Thorne, P. W.,
672 Wild, M., & Zhai, P. M. (2013). *Observations: Atmosphere and Surface.* T. F. Stocker, D. Qin,
673 G.-K. Plattner, M. Tignor, S.K. Allen, J. Boschung, A. Nauels, Y. Xia, V. Bex and P.M. Midgley
674 (Eds.), Cambridge University Press, Cambridge, United Kingdom and New York, NY, USA.:
675 Retrieved from https://www.ipcc.ch/report/ar5/wg1/
676 Hindar, A. (2013). E18 Grimstad-Kristiansand gjennom sulfidholdige bergarter – syreproduksjon
677 og effekter på avrenningsvann. *Vann, 48*(1), 97-103.
678 Hjulstad, M. (2015). *Leaching, Uptake and Effects in Brown Trout (Salmo trutta) of Radionuclides*
679 *and Metals from Black Shales and Sulphur Bearing Gneiss* (MSc), Norwegian University of
680 Life Sciences, Ås, Norway.
681 IAEA. (2014). *The environmental behaviour of radium: Revised edition* (476).Vienna: Retrieved
682 from https://www-pub.iaea.org/books/iaeabooks/series/80/Technical-Reports-Series
683 Jeng, A. S. (1991). Weathering of Some Norwegian Alum Shales. I. Laboratory simulations to
684 study acid generation and the release of sulfate and metal cations (calcium, magnesium,
685 and potassium). *Acta Agriculturae Scandinavica, 41*(1), 13-35.
686 doi:10.1080/00015129109438580
687 Jeng, A. S. (1992). Weathering of Some Norwegian Alum Shales, II. Laboratory Simulations to
688 Study the Influence of Aging, Acidification and Liming on Heavy Metal Release. *Acta*
689 *Agriculturae Scandinavica, Section B — Soil & Plant Science, 42*(2), 76-87.
690 doi:10.1080/09064719209410203
691 Landa, E. R. (2007). Naturally occurring radionuclides from industrial sources: characteristics
692 and fate in the environment. In S. George (Ed.), *Radioactivity in the Environment* (Vol. 10,
693 pp. 211-237): Elsevier.
694 Lavergren, U., Åström, M. E., Falk, H., & Bergbäck, B. (2009). Metal dispersion in groundwater in
695 an area with natural and processed black shale – Nationwide perspective and comparison
696 with acid sulfate soils. *Applied Geochemistry, 24*(3), 359-369.
697 doi:https://doi.org/10.1016/j.apgeochem.2008.11.022

Lawrence, R. W., & Scheske, M. (1997). A method to calculate the neutralization potential of mining wastes. *Environmental Geology, 32*(2), 100-106. doi:10.1007/s002540050198

Lawrence, R. W., & Wang, Y. (1996). *Determination of Neutralization Potential for Acid Rock Drainage Prediction* (MEND Project 1.16.3). Retrieved from http://mend-nedem.org/mend-report/determination-of-neutralization-potential-for-acid-rock-drainage-prediction/

Lieser, K. H. (1995). Radionuclides in the Geosphere: Sources, Mobility, Reactions in Natural Waters and Interactions with Solids. *Radiochimica acta., 70-71*, 355.

Lydersen, E., Löfgren, S., & Arnesen, R. T. (2002). Metals in Scandinavian Surface Waters: Effects of acidification, Liming, and Potential Reacidification. *Critical Reviews in Environmental Science and Technology, 32*(2), 73-295. doi:https://doi.org/10.1080/10643380290813453

Miller, J. N., & Miller, J. C. (2005). *Statistics and Chemometrics for Analytical Chemistry*. Great Britain: Pearson Education Limited.

Moulin, V., Amekraz, B., Barre, N., Planque, G., Mercier, F., Reiller, P., & Moulin, C. (2004). The role of humic substances in trace element mobility in natural environments and applications to radionuclides. In E. A. Ghabbour & G. Davies (Eds.), *Humic Substances: Nature's Most Versatile Materials* (pp. 275-286): Taylor & Francis.

Norwegian Environmental Agency. (2016). *Quality standards for water, sediment and biota*. (M-608).

Okkenhaug, G. (2012). *Mobility and solubility of antimony (Sb) in the environment.* (PhD), Norwegian University of Life Sciences, Ås. (2012:34)

Owen, A. W., Bruton, D. L., Bockelie, J. F., & Bockelie, T. G. (1990). *The Ordovician successions of the Oslo Region, Norway*. D. Roberts (Eds.), Geological survey of Norway (NGU): Retrieved from http://paleoarchive.com/

Pabst, T., Sørmo, E., & Endre, E. (2016). Geochemical characterisation of Norwegian Cambro-Ordovician black mudrocks for building and construction use. *Bulletin of Engineering Geology and the Environment, 76*(4), 1577–1592. doi:https://doi.org/10.1007/s10064-016-0941-z

Pipkin, B., Trent, D. D., Hazlett, R., & Bierman, P. (2008). *Geology and the environment* (P. Adams Ed., 5th ed.). USA: Thomson Brooks/Cole.

Pollution Control Act (Forurensningsforskriften), FOR-2004-06-01-931 (2004).

Radiation Protection Act (Strålevernsforskriften), FOR-2016-12-16-1659 (2016).

Rayner-Canham, G., & Overton, T. (2006). *Descriptive inorganic chemistry* (J. Fiorillo Ed., 4th ed.). Houndmills, England: W. H. Freeman and Company.

Rosseland, B. O., Blakar, I. A., Bulger, A., Kroglund, F., Kvellstad, A., Lydersen, E., Oughton, D. H., Salbu, B., Staurnes, M., & Vogt, R. (1992). The mixing zone between limed and acidic river waters: complex aluminium chemistry and extreme toxicity for salmonids. *Environmental Pollution, 78*(1–3), 3-8. doi:http://dx.doi.org/10.1016/0269-7491(92)90003-S

Seder-Colomina, M., Mangeret, A., Stetten, L., Merrot, P., Diez, O., Julien, A., Barker, E., Thouvenot, A., Bargar, J., Cazala, C., & Morin, G. (2018). Carbonate Facilitated Mobilization of Uranium from Lacustrine Sediments under Anoxic Conditions. *Environmental Science & Technology, 52*(17), 9615-9624. doi:10.1021/acs.est.8b01255

Singer, P. C., & Stumm, W. (1970). Acidic Mine Drainage: The Rate-Determining Step. *Science, 167*(3921), 1121-1123. doi:10.2307/1728684

Skipperud, L., Alvarenga, E., Lind, O. C., Teien, H.-C., Tollefsen, K. E., Salbu, B., & Wærsted, F. M. (2016). *Construction works in areas with sulphide containing rock. Case: Effects and environmental risks related to alum shale disposal site* (651).Norwegian Public Roads Administration: Retrieved from www.vegvesen.no

Skjelkvåle, B. L., Aas, W., Manø, S., Solberg, S., Yttri, K. E., Skancke, L. B., Garmo, Ø. A., Høgåsen, T., Fjellheim, A., Halvorsen, G. A., Schartau, A. K., Jensen, T. C., Walseng, B., Saksgård, R., Hesthagen, T., Andreassen, K., Timmermann, V., Clarke, N., Framstad, E., Aarrestad, P. A., Bakkestuen, V., Bruteig, I. E., Evju, M., Kålås, J. A., & Nygård, T. (2012). *Overvåking av langtransporterte forurensninger 2011. Sammendragsrapport*. B. L. Skjelkvåle (Eds.),

752 Stanley, D. M., & Wilkin, R. T. (2019). Solution equilibria of uranyl minerals: Role of the common
753 groundwater ions calcium and carbonate. *Journal of Hazardous Materials, 377*, 315-320.
754 doi:https://doi.org/10.1016/j.jhazmat.2019.05.101
755 vanLoon, G. W., & Duffy, S. J. (2011). *Environmental Chemistry - a global perspective* (3rd ed.). New
756 York: Oxford University Press.
757 Wærsted, F. M., Jensen, K. A., Reinoso-Maset, E., & Skipperud, L. (2018). High Throughput, Direct
758 Determination of 226Ra in Water and Digested Geological Samples. *Analytical Chemistry,*
759 *90*(20), 12246-12252. doi:10.1021/acs.analchem.8b03494
760 Wærsted, F. M., Riss, P. J., & Skipperud, L. (in prep.). *The effect of water exchange on the leaching*
761 *of alum shale*. Faculty of Environmental Science and Natural Resource Management.
762 Norwegian University of Life Sciences.
763 Yu, C., Lavergren, U., Peltola, P., Drake, H., Bergbäck, B., & Åström, M. E. (2014). Retention and
764 transport of arsenic, uranium and nickel in a black shale setting revealed by a long-term
765 humidity cell test and sequential chemical extractions. *Chemical Geology, 363*, 134-144.
766 doi:http://dx.doi.org/10.1016/j.chemgeo.2013.11.003

767

Paper II: Supporting information

Supporting information to
Rainwater leaching of alum shale debris under atmospheric and low-oxygen conditions

F. M. Wærsted*, E. Reinoso-Maset, B. Salbu and L. Skipperud

Centre for Environmental Radioactivity (CERAD), Faculty of Environmental Sciences and Natural Resource Management, Norwegian University of Life Sciences, P.O. Box 5003, N-1432 Ås, Norway

*Corresponding author email: frwa@nmbu.no

Table of Contents

1.1 Synthetic rainwater concentrations

Table S 1: Synthetic rainwater used for the leaching experiment, imitating rain in Hurdal 2010-2014 (Aas et al., 2015)

SO_4^{2-} mg L^{-1}	NO_3^+ mg L^{-1}	NH_4^+ mg L^{-1}	Ca^{2+} mg L^{-1}	Mg^{2+} mg L^{-1}	Na^+ mg L^{-1}	Cl^- mg L^{-1}	K^+ mg L^{-1}	pH
0.73	1.31	0.43	0.12	0.04	0.32	0.54	0.11	4.97

1.2 Geochemical characterization

The method of Pabst et al. (2016) for geochemical characterisation of Norwegian Cambro-Ordovician black mudrocks is based on comparing whole rock analysis with a database containing several hundred samples from the Cambro-Ordovician stratigraphy collected in the Oslo area. Triangular plots as well as plots of acidification potential (AP) vs. neutralization potential (NP) and Fe vs. S are used to see how the sample places itself among the samples in the database.

The figures below show some examples of the plots used for geochemical characterisation of the alum shale used for the experiment. The geochemical characterization placed the collected alum shale batch in the 3a layer of the alum shale formation, see Figure S 1 - Figure S 5. Though, for some parameters, the samples position themselves in the 2 layer. In the figures, the bigger symbols represents the measured replicates when characterizing the alum shale batch used in this experiment (AS1-AS6), while the other points represent samples from the different horizons in the Cambro-Ordovician stratigraphy, from a database collected by the Norwegian Geotechnical Institute (NGI).

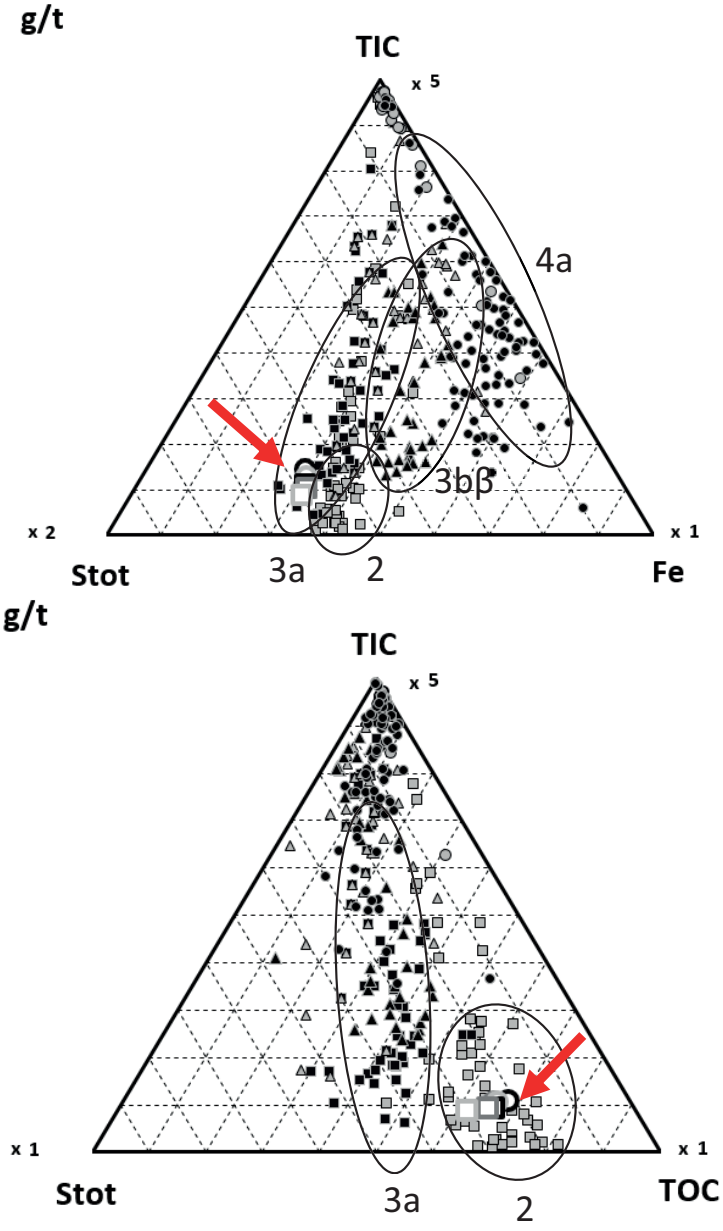

Figure S 1: Selected triangular plots of samples from the Cambro-Ordovician stratigraphy in the Oslo area. Black circles show the grouping of horizons. AS1-AS3 are replicate measurements of the debris used for the AOC-LOC leaching experiment, and AS4-AS6 of the debris used for the cyclic experiment. The arrow marks the position of these samples. The other points represent samples from the different horizons in the Cambro-Ordovician, from a database by the Norwegian Geotechnical Institute (NGI). Stot = total sulphur content.

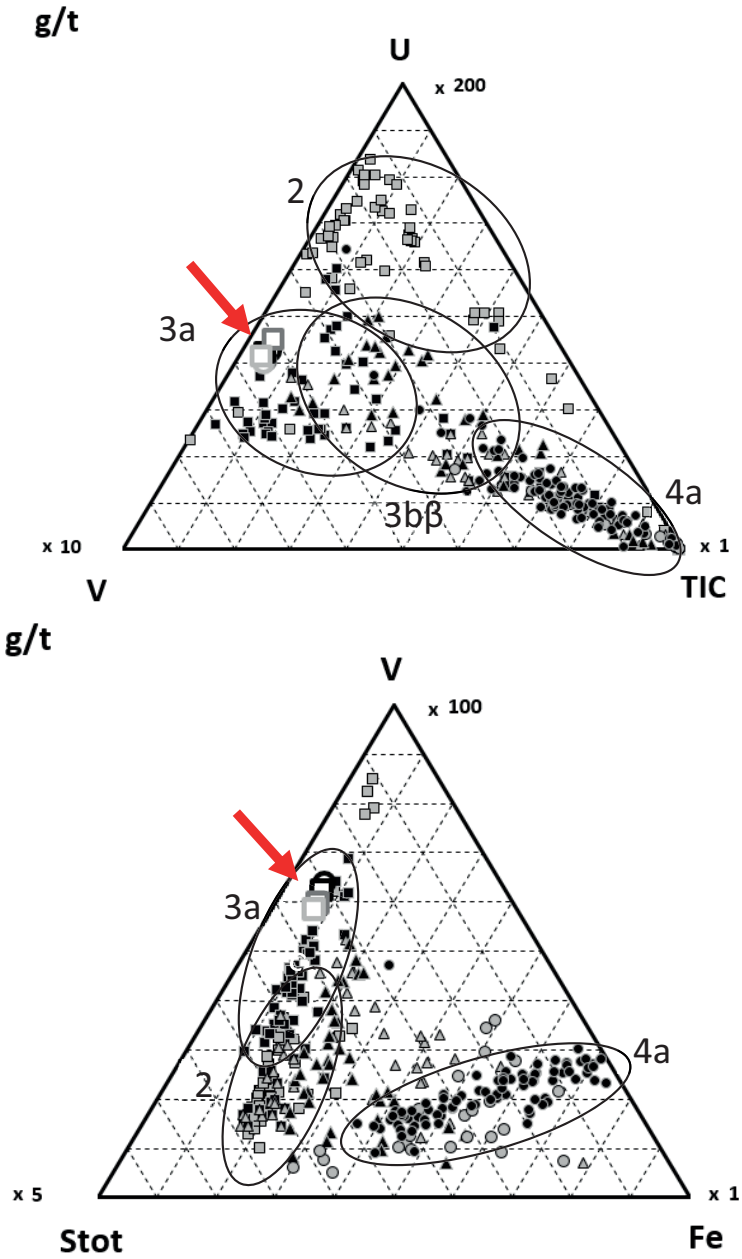

Figure S 2: Selected triangular plots of samples from the Cambro-Ordovician stratigraphy in the Oslo area. Black circles show the grouping of the different horizons. AS1-AS3 are replicate measurements of the debris used for the AOC-LOC leaching experiment, and AS4-AS6 of the debris used for the cyclic experiment. The arrow marks the position of these samples. The other points represent samples from the different horizons in the Cambro-Ordovician, from a database by the Norwegian Geotechnical Institute (NGI). Stot = total sulphur content.

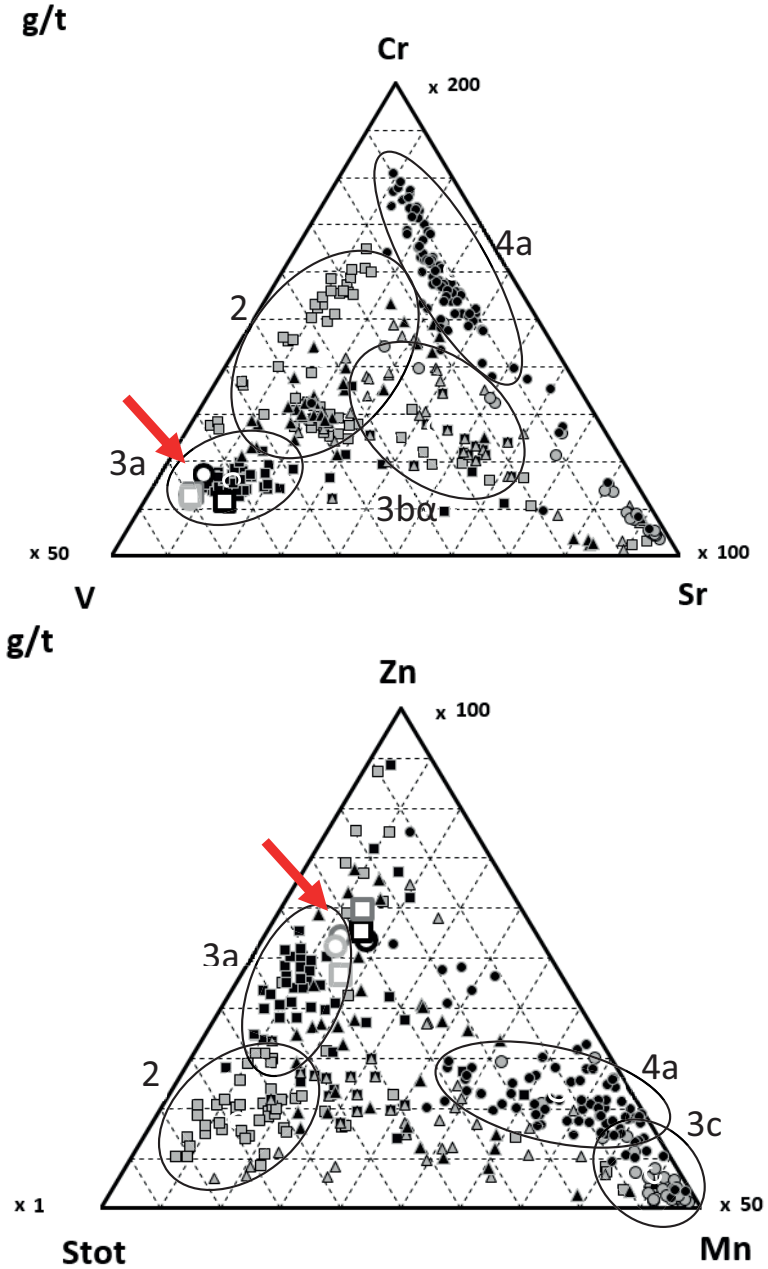

Figure S 3: Selected triangular plots of samples from the Cambro-Ordovician stratigraphy in the Oslo area. Black circles show the grouping of the different horizons. AS1-AS3 are replicate measurements of the debris used for the AOC-LOC leaching experiment, and AS4-AS6 of the debris used for the cyclic experiment. The arrow marks the position of these samples. The other points represent samples from the different horizons in the Cambro-Ordovician, from a database by the Norwegian Geotechnical Institute (NGI). Stot = total sulphur content.

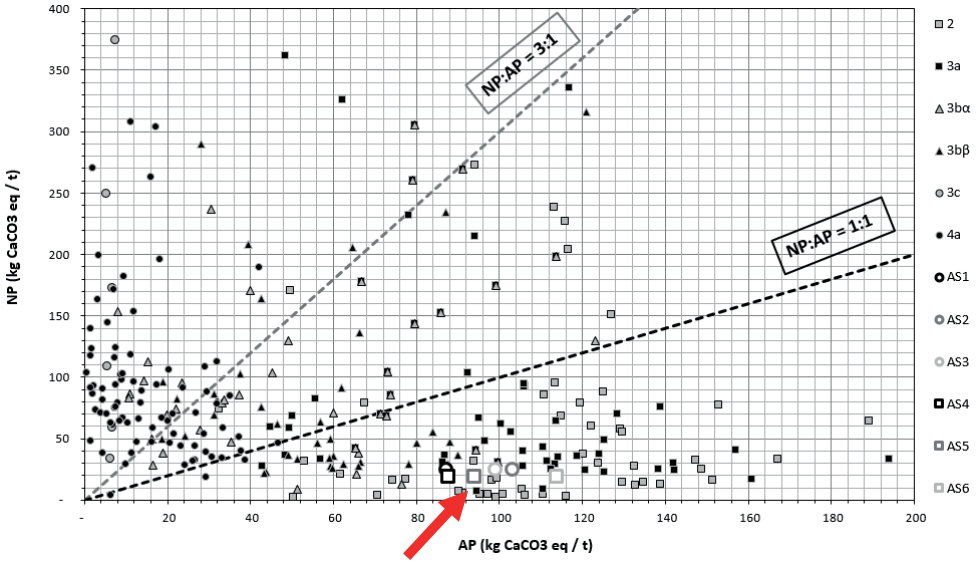

Figure S 4: Neutralization potential (NP) vs. acidification potential (AP) in Norwegian Cambro-Ordovician black mudrocks. AS1-AS3 are replicate measurements of the debris used for the AOC-LOC leaching experiment, and AS4-AS6 of the debris used for the cyclic experiment. The arrow marks the position of these samples. The other points represent samples from the different horizons in the Cambro-Ordovician, from a database by the Norwegian Geotechnical Institute (NGI).

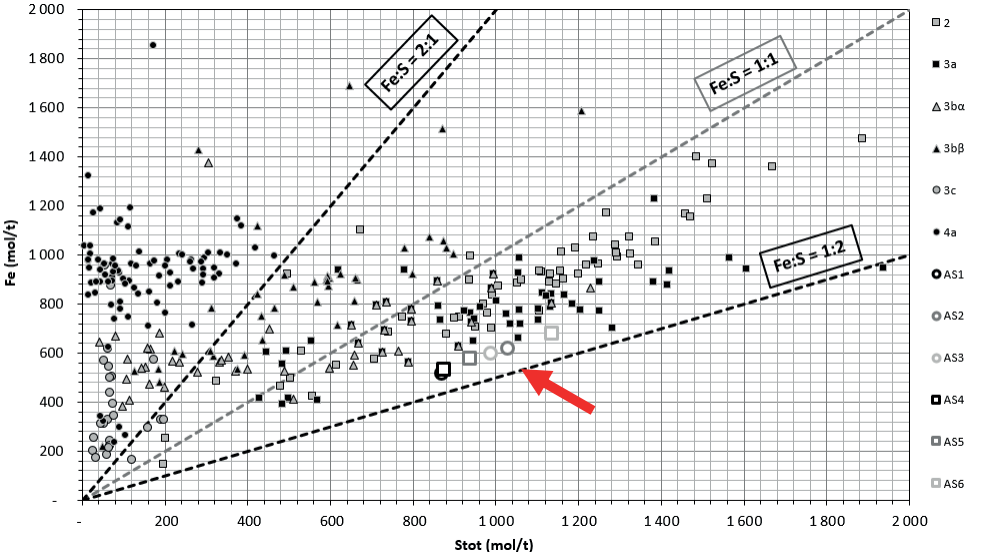

Figure S 5: Ratio of Fe to S in Cambro-Ordovician black mudrocks. AS1-AS3 are replicate measurements of the debris used for the AOC-LOC leaching experiment, and AS4-AS6 of the debris used for the cyclic experiment. The arrow marks the position of these samples.other points represent samples from the different horizons in the Cambro-Ordovician, from a database by the Norwegian Geotechnical Institute (NGI). Stot = total sulphur content.

1.3 XRD results including X-ray diffractograms

Results below show the XRD spectrum (blue line) and the fitted line for quantification (red line). Results are in % of crystalline material, and thus higher than the results in the article that are in % of weight.

The results for takovite were excluded from the article, as the concentration was very low, the mineral composition did not fit with the measured elemental composition of the debris and the mineral was not expected to be found in this area (Mindat.org, 2019).

1.3.1 Starting material

R-Values

```
Rexp : 9.51     Rwp : 17.83     Rp  : 13.79  GOF : 1.87
Rexp`: 23.38    Rwp`: 43.83     Rp` : 44.60  DW  : 0.65
```

Quantitative Analysis - Rietveld

```
   Phase 1  : "Muscovite 2M1"                63.2(10) %
   Phase 2  : Quartz                         27.8(8) %
   Phase 3  : Takovite                       0.4(5) %
   Phase 4  : Pyrite                         5.1(3) %
   Phase 5  : Calcite                        3.5(4) %
```

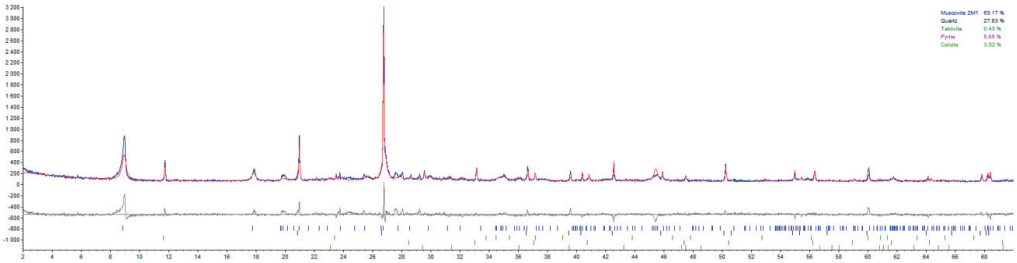

Figure S 6: XRD spectrum of the alum shale starting material used for the leaching experiment.

1.3.2 AOC replicate A

R-Values

```
Rexp : 8.58     Rwp : 18.07     Rp  : 13.81  GOF : 2.11
Rexp`: 21.73    Rwp`: 45.77     Rp` : 46.96  DW  : 0.52
```

Quantitative Analysis - Rietveld

```
   Phase 1  : "Muscovite 2M1"                63.8(10) %
   Phase 2  : Quartz                         27.9(8) %
   Phase 3  : Pyrite                         5.7(3) %
   Phase 4  : Calcite                        2.6(4) %
```

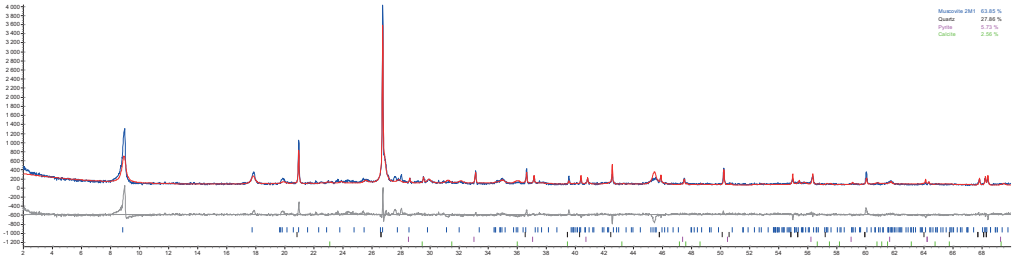

Figure S 7: XRD spectrum of alum shale from one sample after AOC treatment.

1.3.3 AOC replicate B

R-Values

Rexp : 9.35 Rwp : 17.68 Rp : 13.51 GOF : 1.89
Rexp`: 21.80 Rwp`: 41.19 Rp` : 40.19 DW : 0.65

Quantitative Analysis - Rietveld

Phase 1	: "Muscovite 2M1"	62.7(9) %
Phase 2	: Quartz	26.6(7) %
Phase 3	: Pyrite	5.3(3) %
Phase 4	: Calcite	5.4(4) %

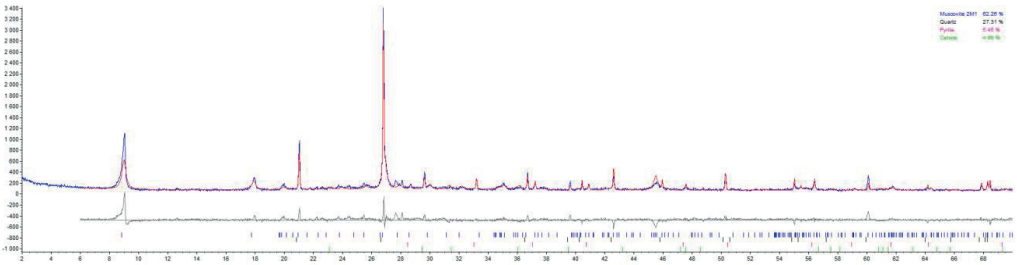

Figure S 8: XRD spectrum of alum shale from one sample after AOC treatment.

1.3.4 AOC replicate C

R-Values

Rexp : 9.30 Rwp : 17.87 Rp : 13.68 GOF : 1.92
Rexp`: 21.48 Rwp`: 41.27 Rp` : 40.50 DW : 0.59

Quantitative Analysis - Rietveld

Phase 1	: "Muscovite 2M1"	62.3(9) %
Phase 2	: Quartz	27.3(7) %
Phase 3	: Pyrite	5.4(3) %
Phase 4	: Calcite	5.0(4) %

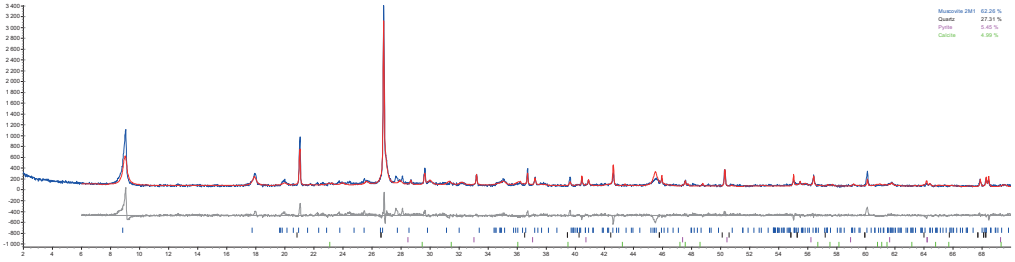

Figure S 9: XRD spectrum of alum shale from one sample after AOC treatment.

1.3.5 LOC replicate A

R-Values

Rexp : 9.16 Rwp : 18.06 Rp : 13.69 GOF : 1.97
Rexp`: 21.64 Rwp`: 42.67 Rp` : 41.67 DW : 0.59

Quantitative Analysis - Rietveld

Phase 1	: "Muscovite 2M1"	65.3(10) %
Phase 2	: Quartz	26.5(7) %
Phase 3	: Takovite	0.1(5) %
Phase 4	: Pyrite	5.4(3) %
Phase 5	: Calcite	2.7(5) %

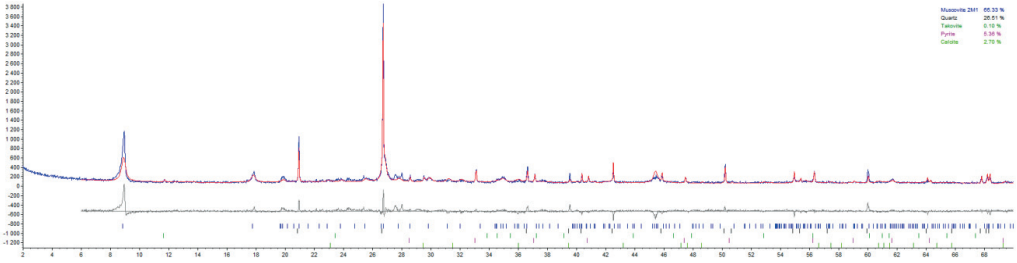

Figure S 10: XRD spectrum of alum shale from one sample after LOC treatment.

1.3.6 LOC replicate B

R-Values

Rexp : 10.17 Rwp : 17.48 Rp : 13.54 GOF : 1.72
Rexp`: 24.01 Rwp`: 41.28 Rp` : 41.13 DW : 0.77

Quantitative Analysis - Rietveld

Phase 1	: "Muscovite 2M1"	64.5(9) %
Phase 2	: Quartz	27.8(7) %
Phase 3	: Pyrite	5.6(3) %
Phase 4	: Calcite	2.1(4) %

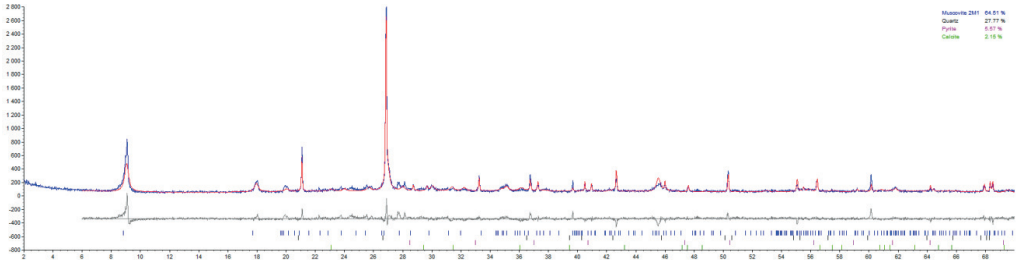

Figure S 11: XRD spectrum of alum shale from one sample after LOC treatment.

1.3.7 LOC replicate C

R-Values

```
Rexp : 9.65     Rwp : 17.36     Rp  : 13.47  GOF : 1.80
Rexp`: 23.78    Rwp`: 42.80     Rp` : 43.92  DW  : 0.69
```

Quantitative Analysis - Rietveld

Phase 1	: "Muscovite 2M1"	63.8(9) %
Phase 2	: Quartz	28.5(7) %
Phase 3	: Pyrite	5.4(3) %
Phase 4	: Calcite	2.3(4) %

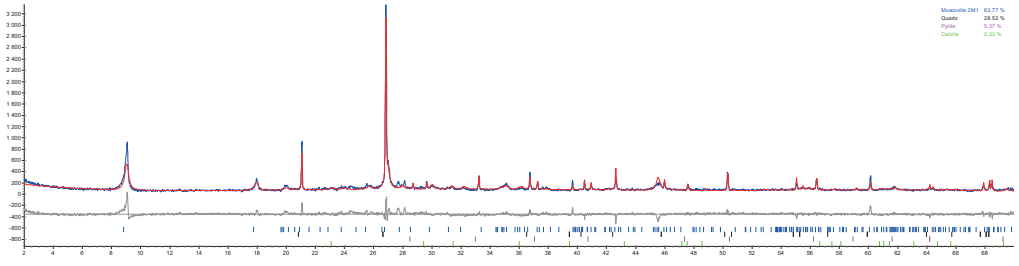

Figure S 12: XRD spectrum of alum shale from one sample after LOC treatment.

1.4 References

Aas, W., Platt, S., Solberg, S., & Yttri, K. E. (2015). *Monitoring of long-range transported air pollutants in Norway, annual report 2014* (M-367).

Mindat.org. (2019). Takovite. Retrieved from https://www.mindat.org/min-3874.html on 27.06.2019

Pabst, T., Sørmo, E., & Endre, E. (2016). Geochemical characterisation of Norwegian Cambro-Ordovician black mudrocks for building and construction use. *Bulletin of Engineering Geology and the Environment*. doi:10.1007/s10064-016-0941-z

Paper III

The effect of water exchange on the leaching of alum shale

F. M. Wærsted*[1], P. J. Riss[2] and L. Skipperud[1]

[1]Centre for Environmental Radioactivity (CERAD), Faculty of Environmental Sciences and Natural Resource Management, Norwegian University of Life Sciences, P.O. Box 5003, N-1432 Ås, Norway

[2]Department of Chemistry, Faculty for Mathematics and Natural Sciences, University of Oslo, Sem Sælands vei 26, N-0371 Oslo, Norway

*Corresponding author email: frwa@nmbu.no

Abstract

In recent years, there has been an increasing focus on the adverse environmental effects from natural occurring radioactive materials (NORM). Acid rock drainage (ARD) produced by debris from mining and construction work is a major environmental issue. ARD can lead to release of both NORM and unwanted stable elements. Batch leaching experiments with alum shale demonstrated that exchange of water will increase leaching of elements whose mobility is limited by concentration effects, such as Ba and the extremely radiotoxic, naturally occurring uranium daughter ^{226}Ra. Periods of drying the alum shale in air increased leaching of Li, V, Mo and ^{226}Ra, increasing their mobility in the environment. Acid production from sulphide oxidation did not cause pH values below 6.4 in the 28 weeks experiment. However, exchange of water lead to depletion of inherent buffer capacity of the alum shale, which will increase the risk of ARD as well as likely reduce the time before onset of ARD.

Keywords: Alum shale, black shale, leaching, acid/neutral rock drainage

1 Introduction

The global population growth and rate of consumption in today's society causes increasing demand for raw materials, leading to extensive mining activity with concomitant environmental issues. Rock debris from mining or construction work can be a major source of naturally occurring radioactive material (NORM) and stable trace elements. Storage conditions for debris from mining or construction work are critical for weathering rates and consequently influence the release of contaminants into the environment. Certain types of rock produce acid when exposed to air and water, which greatly enhances release and mobility of a range of elements in a phenomenon termed *acid rock drainage* (ARD) (Appelo & Postma, 2010; vanLoon & Duffy, 2011).

Alum shale is a sedimentary, Cambro-Ordovician black shale (black mudrock) formed under reducing conditions. Black shales are found throughout the world, with particularly large deposits in Northern Europe as well as Russia, North America, Australia, China and Brazil (Alloway, 2013). Alum shale contains silicate minerals, sulphides, carbonates and organic matter (kerogen), and is enriched with several trace elements including Ba, V, Mo, Co, Ni, Cu, Zn, Cd, and As, as well as the uranium-series (Falk et al., 2006; Owen et al., 1990; Pabst et al., 2016). The primordial NORM ^{238}U in unweathered alum shale is in secular equilibrium with highly radiotoxic daughter nuclides such as ^{226}Ra. As alum shale is excavated and weathering processes start, sulphide minerals (like pyrite and pyrrhotite) in the alum shale can be oxidized, causing production of acid. Carbonates in the rock (such as calcite) can neutralize the acid. Consequently, the ratio of the (acid) neutralization potential (NP) to the acidification potential (AP) is a very important property of rock masses to consider when choosing conditions for storage (Lawrence & Scheske, 1997). Rock masses are considered neutralizing when NP:AP is above 3 and acid-producing when the ratio is below 1, while masses with ratio between 1 and 3 fall into the uncertainty zone (Pabst et al., 2016).

Improper storage of acid-producing rock debris can be detrimental for the local environment (Pipkin et al., 2008). Different approaches can be used for storage to avoid negative effects on the environment, and measures can be divided into active and passive categories (Hindar, 2010). Passive measures are often taken to avoid or reduce weathering of the material, and as such eliminate the generation of ARD. To reduce or avoid weathering of the debris, passive measures will have to strictly limit the availability

of water and/or oxygen as both are needed for the oxidation of sulphides (Appelo & Postma, 2010). In contrast, active measures, such as water treatment, may become necessary when passive measures have failed. Active measures are generally more costly and require a long-term commitment.

One passive option is to store the masses in water, and cover the site with a tight top layer to avoid the intrusion of air (Sørmo, Breedveld, & Pabst, 2015). The water should not be exchanged as that leads to oxygenated water coming in and contaminated water moving out. This requires a completely sealed disposal site. Another passive storage option is to add neutralizing material like shell sand or another source of carbonates to the disposal site (Hindar, 2010). While weathering will occur, this material will neutralize the produced acid and reduce mobility of several trace elements that are more soluble at lower pH (Sørmo et al., 2015). However, even at neutral pH, NORM and stable elements incorporated in the alum shale can be released during oxidation, in a process termed *neutral rock drainage* (NRD) (Alloway, 2013; Appelo & Postma, 2010).

Avoiding exchange of water and intrusion of air can be difficult when storing rock masses submerged in water, both in short and long term perspectives, and even carefully planned disposal sites might not fulfil these criteria. Groundwater levels can fluctuate, and in dry periods masses normally below the groundwater table can be exposed to air. Additionally, debris from older mining and construction work has often been stored without consideration of these issues, and continues to be at multiple sites around the world today (see e.g. Dold, 2017; Falk et al., 2006; Stegnar et al., 2013).

This study investigates effects from improper storage of acid-producing alum shale using batch leaching experiments with debris from construction work. The effect of exchange of water on the leaching of the contaminants was investigated by cyclic exchange of the leachant. Furthermore, the effect of fluctuating water levels in a disposal site was simulated with cyclic drying and submerging of the debris.

2 Materials and methods

2.1 Materials

2.1.1 Sample description and handling

In 2013-2015 a road tunnel was constructed at Gran, Hadeland, Norway, cutting through the alum shale formation (Fjermestad et al., 2018). Alum shale debris used in this study

originates from a tunnel blast in the alum shale formation performed on the 19/05/2015, and was collected on the same day. A handheld XRF instrument (Niton™ XL3t GOLDD+, Thermo Scientific) was used during sampling to ensure that alum shale with high content of U was collected.

The alum shale debris was stored for 18 months before starting the experiment. The day before the beginning of the experiment, approximately 1-2 cm big pieces were selected, crushed with a jaw crusher, sieved (2 mm mesh size), and the finer fraction was collected. The crushed debris was stored under nitrogen overnight until the initiation of the experiment. This was done to obtain fresh rock surface for the experiment.

Geochemical characterization of this alum shale batch was performed earlier (Wærsted et al., in prep.), by comparing whole-rock analysis data (elemental composition, total inorganic carbon (TIC) and total organic carbon (TOC)) as well as calculated acidification and neutralization potentials with an existing database of mudrocks from the Oslo region (Norway), as described by Pabst et al. (2016).

2.1.2 Chemicals

All chemicals used throughout the work were analytical grade unless otherwise noted. Type I water (ASTM D1193-91 standard specifications) was used for all applications.

Synthetic rainwater was prepared to match the specifications of rain falling in Hurdal, a meteorological site within a 27 km radius of the alum shale sampling point (Aas et al., 2015). The average ion concentrations and pH of the rainwater in 2010-2014 was used (Table 1).

Table 1: Synthetic rainwater used for the leaching experiment, modelling rain in Hurdal 2010-2014 (Aas et al., 2015).

SO_4^{2-} mg L^{-1}	NO_3^{+} mg L^{-1}	NH_4^{+} mg L^{-1}	Ca^{2+} mg L^{-1}	Mg^{2+} mg L^{-1}	Na^{+} mg L^{-1}	Cl^{-} mg L^{-1}	K^{+} mg L^{-1}	pH
0.73	1.31	0.43	0.12	0.04	0.32	0.54	0.11	4.97

2.2 Experimental setup

Crushed alum shale (180 g) was mixed with synthetic rainwater (1.8 L) in batch experiments. Four replicates were made for each treatment:

Wet-dry cycles (DRY): Samples were exposed to wet and dry periods where the debris was kept alternately in water (3 weeks) and air (2 weeks). The wet period was repeated six times with dry periods in between (Table 2). During the dry periods, the debris dried completely in about 10 days.

Wet-wet cycles (WET): The water of each sample was exchanged every five weeks without drying the debris.

Samples were kept in the dark at 10 °C in open 2 L polypropylene bottles (Nalgene, Thermo Scientific), covered loosely with plastic foil to reduce evaporation and risk of contamination. All samples were mixed by shaking by hand 2-3 times per week. When sampling intervals allowed it, bottles were shaken 48 h before sampling and left standing to let the debris settle. At the end of each wet period, water was carefully lifted off the solids using a peristaltic pump to minimize loss of particles. One sample consisting of pure artificial rainwater (no debris) kept in parallel to each treatment was treated, sampled and analysed in the exact same way to monitor contamination and other unintended effects in the experiment.

Aliquots for analysis of the leachate were withdrawn at 1 h, 24 h, 1 and 3 weeks after starting a cycle (i.e. after mixing debris with fresh synthetic rainwater) for both treatments, and additionally at 5 weeks for the WET samples. The volume withdrawn during sampling accounted for < 15 % of the total volume in each cycle, and was replaced by synthetic rainwater. Subsamples of the starting material (crushed alum shale) and leached debris (air-dried at the end of the experiment) were characterized as described in section 2.3.

Table 2: Overview of treatment periods. Vertical lines marks the end of a cycle and addition of new leachant. Grey areas represents the dry periods, and white areas the wet periods. Sampling points are approximately marked by crosses.

	Cycle 1					Cycle 2					Cycle 3					Cycle 4					Cycle 5					Cycle 6		
Week	1	2	3	4	5	6	7	8	9	10	11	12	13	14	15	16	17	18	19	20	21	22	23	24	25	26	27	28
WET	xxx		x		x	xxx		x		x	xxx		x		x	xxx		x		x	xxx		x		x	xxx		x
DRY	xxx		x			xxx		x			xxx		x			xxx		x			xxx		x			xxx		x

2.3 Chemical analysis

2.3.1 Alum shale analysis

Total element concentrations were determined by inductively coupled plasma mass spectrometry (ICP-MS) after digesting (260 °C, 40 min, Milestone UltraCLAVE) 0.25 g of debris in triplicate with the following acid mixtures: 5 mL HNO_3 (for Li, S, Ca and Fe), 5 mL HNO_3 + 1 mL HF (Mn, Zn, As, Mo, Cd, Sb and U), and 2 mL HNO_3 + 4 mL H_3PO_4 (Na, Mg, Al, K, V, Co, Ni, Sr, Ba and ^{226}Ra). Rh was added as internal standard. Digested samples were diluted to 50 mL. Certified reference materials were digested and measured in parallel to the samples: NIST 2709a San Joaquin Soil and NSC ZC 73007 soil (all three digestions), NIST 2710a Montana I soil (only HNO_3 digestion), and NSC DC 73325 soil (only HF digestion). When determining ^{226}Ra content, reference materials IAEA-314 (sediment) and IAEA-448 (soil) were used. Results for all reference materials were within the specifications.

The pH (handheld multi-meter, Multi series, WTW) was measured in a 1+2 V/V mix of debris and water left overnight. Organic matter (OM) was estimated from loss on ignition (LOI, 550 °C, overnight). Total inorganic (TIC) and organic (TOC) carbon contents in the debris were determined by coulometry. TOC was only measured in the starting material. Particle size distribution was determined for a 10 g sample, where OM had been removed by heating with H_2O_2, by wet sieving through 0.06 mm (sand fraction) and separating silt and clay (<0.002 mm) by sedimentation according to Stokes' law. Mineral composition was determined by powder X-ray diffraction (XRD) on a D8 Discover (Bruker). The XRD diffractograms were analysed with TOPAS software to identify the peaks using a reference spectra library, and quantified by the Rietveld refinement technique.

2.3.2 Leachate analysis

Leachate aliquots were collected using a syringe, and divided into different subsamples. Conductivity, pH and oxidation-reduction potential (ORP) were measured immediately after sampling on untreated aliquots (handheld multi-meter, Multi series, WTW). E_h was calculated from ORP according to instructions from the manufacturer. Samples for alkalinity, ICP-MS, dissolved organic carbon (DOC) and anion chromatography were immediately filtered through 0.45 µm polyethersulfone membrane syringe filters (VWR), and subsamples for analysis of low molecular mass (LMM) components by ICP-MS were

also filtered through 10 kDa Amicon® Ultra-15 centrifugal filters (Merck Millipore). The samples were stored in the dark at 4 °C. Alkalinity was measured by colorimetry by titration to pH 4.5 (ISO 9963-1:1994). Samples for ICP-MS were acidified with 5 % (V/V) ultrapure HNO_3. Anions were quantified by ion chromatography (Lachat IC5000 system, Dionex™ IonPac™ AS22-Fast IC column, Dionex AMMS™ 300 ion suppressor, Thermo Scientific). DOC was determined with a TOC-VCPN analyser (Shimadzu), but all samples were below the detection limit (DL) (1.8 mg L^{-1}).

2.3.3 ICP-MS analysis

Li, Na, Mg, Al, S, K, Ca, V, Mn, Fe, Co, Ni, Zn, As, Sr, Mo, Cd, Sb, Ba and ^{238}U were determined in synthetic rainwater, leachate and digested alum shale with an Agilent 8800 Triple Quadrupole ICP-MS instrument. Ge, In, Ir and Bi were added online as internal standards within the instrument. Alternately, He, O_2 and no gas were used in the collision/reaction chamber to remove interferences. To check the accuracy of the method, an in-house standard covering all measured elements was analysed on each day of analysis.

Leachate and digested alum shale were analysed for ^{226}Ra with an Agilent 8900 Triple Quadrupole ICP-MS (Agilent Technologies), using the method of Wærsted et al. (2018) that utilizes N_2O as reaction gas to eliminate interferences.

2.3.4 Data treatment

To estimate the total leached mass of each element, the masses in solution at the end of each wet period were summed for each sample individually. This mass was used with the concentration in the starting material to calculate the percentage leached of an element.

The acidification potential (AP) of the debris was estimated by assuming that all S in the rock comes from sulphides behaving like pyrite, and the neutralization potential (NP) was estimated from the TIC, assuming these carbonates behave like calcite (Pabst et al., 2016).

As mentioned, one blank was kept in parallel to each treatment and treated in the same way. There were detectable levels of Zn and Ba in these blanks, but the sample concentrations were well above the detection limit (DL, 3× standard deviation of blank) calculated from these blanks.

All figures and tables show average ± one standard deviation of replicate samples. T-tests were used for finding significant differences between treatments (Miller & Miller, 2005).

3 Results and discussion

3.1 Alum shale characterization

Previous geochemical characterization placed the alum shale batch in the 3a layer of the alum shale formation (Wærsted et al., in prep.). This layer is expected to be acid producing and have a high content of both NORM (U-series) and several stable trace elements of concern (Owen et al., 1990; Pabst et al., 2016).

The minerals muscovite ($KAl_2(AlSi_3O_{10})(F, OH)_2$), quartz ($SiO_2$), pyrite ($FeS_2$) and calcite ($CaCO_3$) were detected in the debris by XRD measurements (Table 3), and 31 % of the material (by weight) was amorphous. The pyrite concentration is in the low range of what Jeng (1991) found in three unweathered, Norwegian alum shales (4.3-13.3 %). The calcite content of the rock decreased to about a third of the starting value in both treatments. No change of the content of the other minerals was observed; also not pyrite despite expected sulphide oxidation. The debris (crushed, as described in section 2.1.1) consisted mainly of sand-sized particles (90.4 %), some silt (8.5 %) and very little clay (1.1 %).

Table 3: Mineral content of alum shale debris before and after leaching. All results are in percent of weight.

Treatment	n	Muscovite %	Quartz %	Pyrite %	Calcite %	Amorphous material %
Untreated	1	42.2	20.8	4.3	1.7	31
WET	4	43 ± 5	22.0 ± 1.2	4.2 ± 0.1	0.5 ± 0.3	31 ± 4
DRY	4	45 ± 1	21.7 ± 0.2	4.2 ± 0.1	0.6 ± 0.4	29 ± 1

The measured TIC (Table 4) corresponded well with carbonate content calculated from calcite content. TIC was reduced to less than half of the original value in both treatments ($p < 0.0009$), supporting the observation of reduced calcite content. The content of TIC and calcite represents the main buffer capacity of the debris, and is reduced by dissolution and consumption by acid. TIC concentrations of both the untreated and treated samples were similar to levels found in other alum shales in Norway, and in the lower range of other Cambro-Ordovician black shales in Norway (Pabst et al., 2016).

The pH of the debris decreased by almost one unit from the starting material to the leached debris for both treatments, likely reflecting acidification via oxidation of sulphides and consumption of carbonate content during the experiment. Organic matter (estimated by LOI) did not change in either treatment. It makes up less than half of the

amorphous material in the sample, which also did not change. Measured TOC in the starting material was 7.8 %, which is quite similar to the estimate from LOI (7.2 %).

Table 4: LOI, TIC and pH of alum shale debris used in the experiment.

Treatment	n	LOI (%)	TIC (%)	pH
Untreated	1[a]	12.3	0.22 ± 0.02	7.53
WET	4	12.6 ± 0.2	0.09 ± 0.01	6.62 ± 0.07
DRY	4	12.7 ± 0.2	0.10 ± 0.01	6.65 ± 0.30

[a]For the TIC analysis of the untreated alum shale, n=2

Estimated AP and NP for the untreated alum shale debris were 99.9 kg $CaCO_3$ eq t^{-1} and 18.3 kg $CaCO_3$ eq t^{-1}, respectively. Thus, the NP to AP ratio is 0.18, and the debris is clearly expected to be acid producing.

The concentration of ^{238}U in the debris (Table 5) was higher than 1 kBq kg^{-1}, therefore, the debris may be classified as (low-level) radioactive waste (in Norway) (Strålevernsforskriften, 2016). Furthermore, the levels of Cr, Ni, Zn, As and Cd exceeded the Norwegian limits for contaminated ground (Pollution Control Act, 2004). Concentrations of the aforementioned elements and other important elements are presented in Table 5, and fall within the rather wide range of concentrations measured in Scandinavian alum shales (Falk et al., 2006; Jeng, 1991, 1992; Lavergren et al., 2009; Pabst et al., 2016). The measured muscovite content corresponds well with the K and Al concentrations in the sample. Pyrite contributes 61 % of Fe and 72 % of S, while 76 % of the Ca in the sample is from calcite. The S in the debris that is not accounted for by pyrite can be present both as sulphates and as other sulphides (e.g. pyrrhotite or sulphides with other cations than Fe), either in amorphous forms or in too low concentration to be detected by the XRD measurements. There was a rapid release of SO_4^{2-} in the beginning (Figure 1 d), presumably indicating that at least some of the S was present as soluble sulphates. As the calculations for estimating AP assume that all S in the debris is present as sulphides behaving like pyrite, the presence of S as sulphates means that the AP has been overestimated to some extent. However, as the environmental consequences of underestimating the AP is greater than overestimating it, total S is commonly used for the estimation (Dold, 2017). Using e.g. pyrite for the calculations could exclude other acid-producing sulphides like pyrrhotite. The presence of pyrrhotite would imply a faster reaction rate than for pyrite (Pratt et al., 1996).

Activity concentration of ^{226}Ra estimated from secular equilibrium with U (1.37 ± 0.03 kBq kg^{-1}) was a bit higher than the measured activity concentration. This is likely caused by one replicate for the ^{226}Ra measurements being substantially lower than the other two, reflecting the heterogeneity of the rock debris. The heterogeneity is also reflected in the measured Ca concentration, with close to 30 % standard deviation, likely due to presence of carbonate nodules in the rock (Pabst et al., 2016).

Table 5: Total element concentrations of the alum shale debris before leaching, together with percent leached in the two treatments and the ratio of the summed leached mass in the treatments. Data for samples filtrated through 0.45 µm is used. For all measurements, n=3.

		Alum shale total concentration	WET % leached	DRY % leached	Ratio DRY/WET
Group 1	Li	32 ± 0.6 mg kg^{-1}	0.98	1.2	1.24****
(Alkali metals)	Na	3.3 ± 0.2 g kg^{-1}	2.3	2.4	1.03**
	K	39 ± 3 g kg^{-1}	0.32	0.35	1.09****
Group 2	Mg	9.2 ± 0.4 g kg^{-1}	2.0	2.1	1.05****
(Alkaline earth metals)	Ca	8.8 ± 2.3 g kg^{-1}	26	25	0.96***
	Sr	182 ± 77 mg kg^{-1}	22	21	0.99
	Ba	656 ± 38 mg kg^{-1}	0.38	0.36	0.96**
	^{226}Ra	30 ± 6 ng kg^{-1}	0.63	0.76	1.22**
		1.1 ± 0.2 kBq kg^{-1}			
Group 4-11	V	2.9 ± 0.2 g kg^{-1}	0.00097	0.0013	1.38****
(Transition metals)	Mo	265 ± 4 mg kg^{-1}	14	18	1.28****
	Mn	311 ± 12 mg kg^{-1}	8.9	8.6	0.96**
	Fe	33 ± 4 g kg^{-1}	<DL	<DL	
	Co	22 ± 2 mg kg^{-1}	1.59	1.64	1.03*
	Ni	366 ± 27 mg kg^{-1}	2.6	2.5	0.98
Group 12	Zn	564 ± 112 mg kg^{-1}	1.1	1.2	1.07*
	Cd	12 ± 2 mg kg^{-1}	4.0	4.4	1.10***
Group 13	Al	77 ± 4 g kg^{-1}	0.00025	0.00026	1.06
Group 15	As	81 ± 1 mg kg^{-1}	0.018	0.019	1.02
	Sb	20 ± 0.4 mg kg^{-1}	1.7	1.3	0.76****
Group 16	S	32 ± 4 g kg^{-1}	4.4	5.0	1.14****
Actinides	^{238}U	110 ± 3 mg kg^{-1}	3.0	2.2	0.71****
		1.37 ± 0.03 kBq kg^{-1}			

Significance levels for t-test testing the difference between % leached in WET and DRY treatments: *p < 0.1, **p < 0.05, ***p < 0.01, ****p <0.001

3.2 Water quality parameters

Processes in the debris like pyrite oxidation and carbonate dissolution are expected to be determining factors for a range of parameters in the leaching experiments, and are most probably directly responsible for leachate pH. The lowest measured pH value in the duration of the experiment was 6.5 (Figure 1 a), and pH was about 7.7 at the end of all

cycles. This reflects that calcite was still available for acid neutralization at the end of the last cycle. In the first cycle, pH increased from 4.97 in the artificial rainwater to about 8 at 1 h. Then, a sudden drop to 7.4 at 24 h was observed, before pH increased again to 7.8-7.9. This behaviour was also seen by Wærsted et al. (in prep.), and might be caused by precipitation of Fe (oxy)hydroxides from pyrite oxidation, removing OH^- from solution. Similar curves at somewhat lower pH values were seen for later cycles. The pH in the DRY treatment seemed to be a bit lower than pH in the WET treatment, especially at the beginning of the cycles. In the last cycle the pH values in the two treatments was quite similar.

E_h values measured in the leachate varied from 360 to 490 mV, with no marked differences between the two treatments. Together with the measured pH values, this places the experiment conditions within the stability range of Fe^{III} and $S^{VI}O^{-II}_4{}^{2-}$, and oxidation of pyrite ($Fe^{II}S^{-I}_2$) was, thus, expected (Appelo & Postma, 2010; Grundl et al., 2011).

Conductivity reflects the total amount of ions in the leachate, and, thus, gives an indication about the total leaching from the debris to the aqueous phase for each treatment. The increase in conductivity was faster in DRY than in WET for cycles 2-6 (Figure 1 b), indicating that the drying period caused oxidation of the debris which lead to a higher release rate of elements. However, due to the longer contact period in the WET treatment, the difference between the two treatments were evened out and in total the DRY treatment was just 2 % higher than the WET treatment ($p = 0.03$).

Alkalinity is a measure of the buffer capacity of aqueous solutions, and will, in this case, mainly reflect dissolved carbonates from the calcite. Alkalinity gradually decreased from cycle to cycle in the WET treatment, while for the DRY treatment, the alkalinity in cycle 2 was less than half of that in cycle 1, and leachates in following cycles all reached about the same levels (~0.5 mmol L^{-1}) (Figure 1 c). Similar trends were seen for pH. Summing the measured alkalinity at the end of each cycle gives a total of 29 % less buffer capacity in the DRY leachates compared to the WET ($p = 2e\text{-}8$). While the longer contact time in the WET treatment gave more time for dissolution of calcite, the changes in calcite and TIC content of the debris were about the same for both treatments, thus, the difference in measured alkalinity was likely caused by greater sulphide oxidation in the DRY treatment. When comparing TIC concentrations in the starting material with the debris

after leaching, it was found that 19 mmol of carbonates were missing in the WET treatment and 18 mmol in the DRY treatment. At the measured pH, aqueous carbonates will mainly be present as HCO_3^-. Assuming that the measured alkalinity represents only carbonates, the carbonates in the leachates at the end of each cycle added up to 9.0 mmol in the WET treatment and 6.4 mmol in the DRY. Thus, a substantial amount of the buffer capacity of the debris has simply been removed by changing the leachant, and has not contributed to acid neutralization. This loss of buffer capacity was greater in the WET treatment than in the DRY treatment, likely because of greater acid production and carbonate consumption in the DRY treatment.

Sulphate concentrations increased more rapidly in the DRY compared to the WET treatment in cycles 2-6 (Figure 1 d). In line with the alkalinity results, this suggests that oxidation of sulphides happened to a larger extent in the DRY samples. This was also expected from the greater oxygen access in the drying period. In cycles 2-6, sulphate was about twice as high in the DRY treatment compared to the WET at the same time points. The sum of leached sulphate in the whole experiment was 14 % higher in DRY compared to WET ($p = 5e\text{-}6$).

Leachate concentrations of Cl^-, NO_3^- and F^- (Figures S1-S3) were negligible compared to SO_4^{2-}. Cl^- did not change much from the concentration of the synthetic rainwater (Table 1). Concentrations of NO_3^- decreased in each cycle from the concentration of the synthetic rainwater (1.31 mg L^{-1}), possibly indicating biological activity in the samples as NO_3^- is an important nutrient. The reduction was greatest in the first cycles, and in the last cycles there was about 0.5 mg L^{-1} left at the end of the cycles. Concentrations of F^- increased from <DL (0.04 mg L^{-1}) in the synthetic rainwater to about 0.3 mg L^{-1} in the first cycle, then lower concentrations were observed for each cycle and about 0.05 mg L^{-1} in the last cycle. The F^- might originate from the muscovite.

Overall, the measurements of pH, conductivity, alkalinity and sulphate in the leachate all support the initial expectations of greater oxidation rate of sulphides in the DRY treatment compared to the WET, but differences between the treatments seemed to be greatest in cycle 2 and then get smaller for each cycle.

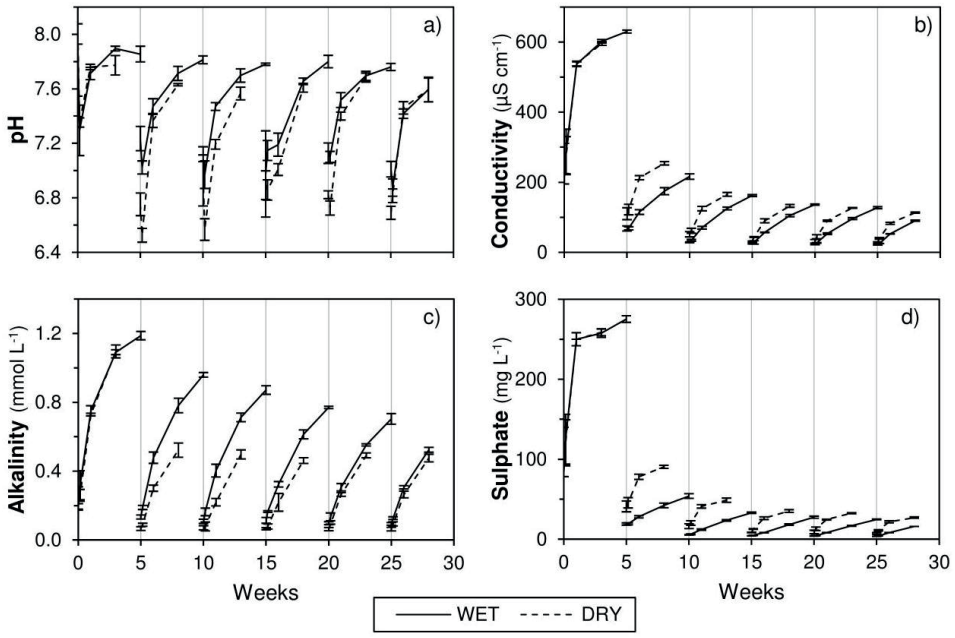

Figure 1: Changes in water quality parameters with time in the cyclic leaching experiment. Each vertical line represents the start of a new cycle. Full (WET) and dashed (DRY) lines are connecting average concentrations of samples. The error bars represent one standard deviation of replicate samples. For all sampling points, n=4.

3.3 Leaching of elements over time

All elements leached most rapidly in the first part of the first cycle, likely an artefact resulting from crushing of the rock as hypothesized by Yu et al. (2014). Only for Ba similar leaching rates were observed in later cycles. For most elements, there were statistically significant differences between treatments (see Table 5), even where actual differences were very small and not of any practical or environmental implications. Most elements leached more in the DRY treatment despite shorter contact time with the leachant, thus supporting the expectation of greater oxidation in the DRY treatment due to direct contact with air. The higher release rate of an element in the DRY treatment indicates that this element is released from a rock phase directly or indirectly affected by the drying period, e.g., by increased oxidation. The only elements that leached considerably slower in DRY compared to WET were U and Sb. The greatest leaching relative to debris content over the course of the experiments was observed for alkaline earth metals Sr and Ca (21-26 %), and transition metals Mn and Mo (8.6-18 %) (Table 5). Na, Mg, Co, Ni, Zn, Cd, Sb, S and U leached a few percent of the debris content and the remaining elements < 1 %.

Results for selected elements are presented in more detail in the following sections.

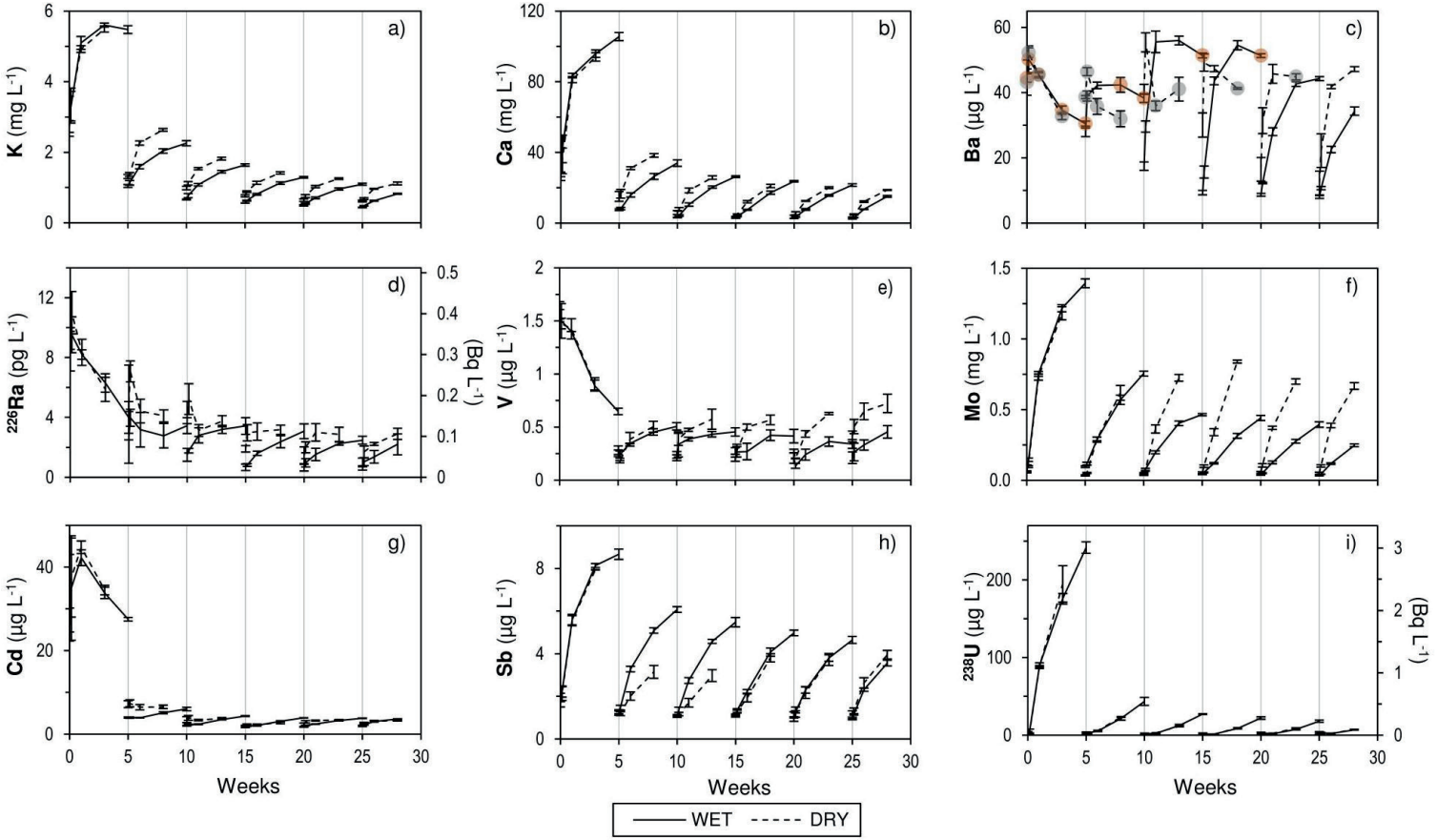

Figure 2: Dissolved (0.45 µm) concentrations of selected elements as a function of time in the cyclic leaching experiment. Each vertical line represents the start of a new cycle. Full (WET) and dashed (DRY) lines are connecting average concentrations of samples. The error bars represent one standard deviation of replicate samples. For all sampling points, n=4. In figure c), grey (DRY) and orange (WET) circles mark the sampling points were K_{SP} for $BaSO_4$ is exceeded.

3.3.1 Alkali metals

The alkaline metals Li, Na and K were all released rapidly within the first week of the first cycle, after which the release rate decreased. In the first cycle, K reached about 5.5 mg L^{-1}, and then leached to lower and lower concentrations in the following cycles (Figure 2 a). Leaching in cycles 2-6 was quicker in DRY than in WET, and in the end 9 % more leached in the DRY treatment compared to the WET treatment ($p = 6\times10^{-7}$). Leaching behaviour of Li (Figure S4) was very similar to K. Li concentrations reached almost 24 µg L^{-1} in the first cycle, and in later cycles, 2-5 µg L^{-1} in the DRY treatment and 0.7-3.5 µg L^{-1} in the WET treatment. Overall, 24 % more Li leached in the DRY treatment compared to the WET ($p = 10^{-6}$). Thus, Li and K seem to originate from rock phases that are affected by the increased oxidation in the drying period. All K in the debris can be accounted for by muscovite, which is not expected to weather before pH drops considerably. However, as only ~0.3 % of K was released in the experiment, it could also be originating from an amorphous phase or a phase that was not sufficiently abundant for detection by XRD.

In the first cycle, Na (Figure S5) concentrations in both treatments reached about the same concentrations as K. In the second cycle there was some release of Na (0.8-0.9 mg L^{-1}), while in later cycles the concentrations barely exceeded the concentration of the synthetic rainwater used as leachant (0.32 mg L^{-1}). Over the course of the experiment, 3 % more Na leached in the DRY than in the WET phase ($p = 0.01$).

3.3.2 Alkaline earth metals

The lighter alkaline earth metals Mg, Ca and Sr all exhibited similar leaching behaviour – though at different concentrations levels – exemplified by Ca in Figure 2 b. Leaching was quickest in the first cycle, but continued in the following cycles. Leaching was quicker in the DRY treatment in cycles 2-6, but the longer contact time in the WET treatment made the total % leached in both treatments quite similar for all three elements. Ca leached to the highest concentrations of the three, with about 100 mg L^{-1} in the first cycle and 19-38 mg L^{-1} at the end of the following cycles. Mg reached just above 12 mg L^{-1} in the first cycle and about 1-3 mg L^{-1} in the remaining cycles, while for Sr these numbers were about 2 mg L^{-1} and 0.2 – 0.7 mg L^{-1}, respectively. Mg leached only about 2 % of the total debris content while the other two more than 20 %. This could indicate that the fraction of Mg that leached is associated with the same minerals as Ca and Sr, e.g. as replacement

for Ca in calcite, which can also be the source of the Sr (Appelo & Postma, 2010; Gabitov et al., 2013), while the main fraction of Mg is bound in a different phase.

Due to the high sulphate concentrations from the pyrite oxidation and dissolution of sulphate minerals, leaching of the heavier alkaline earth metals Ba and ^{226}Ra was expected to be limited by the solubility of $BaSO_4$ and co-precipitation of ^{226}Ra. The peak concentrations of Ba were quite similar in all cycles and both treatments, but the peak appeared at different time points, generally later in the WET compared to the DRY treatment, and later in later cycles (Figure 2 c), as expected from the observed sulphate concentrations. The points where the solubility product for $BaSO_4$ (K_{SP} = 1.08 × 10^{-10}, 25 °C) (*CRC Handbook of Chemistry and Physics*, 1993) is exceeded are marked with grey (DRY) and orange (WET) circles in Figure 2 c. K_{SP} values can be slightly exceeded without precipitation because the conditions in the leachate are different from standard conditions; due to all the other ions in solution, the activity coefficient of Ba^{2+} and SO_4^{2-} can be below 1. Precipitation of $BaSO_4$ was predicted at all sampling points in the first cycle. For the DRY treatment, this was also the case for all of cycle 2 and the last part of cycles 3-5. In the WET treatment, $BaSO_4$ precipitation is expected in the last part of cycles 2 and 3, as well as in 2 out of 4 replicates at 5 weeks in cycle 4. In cycle 6, neither treatments reached K_{SP}.

Leaching behaviour for ^{226}Ra (Figure 2 d) was similar to what was observed for Ba, except that ^{226}Ra did not reach the same concentrations in later cycles as measured in cycle 1. Furthermore, the total leached mass of ^{226}Ra was 22 % higher in the DRY treatment compared to WET ($p = 0.01$), while Ba leached 4 % less in DRY ($p = 0.01$). Almost half of the difference between the total ^{226}Ra leaching in the two treatments can be ascribed to the steep decrease in concentrations in the first cycle, caused by increasing sulphate concentrations and precipitation of $BaSO_4$, resulting in lower concentrations at the end of the first cycle of the WET treatment compared to the DRY treatment. At the same time, a higher leaching rate of ^{226}Ra in the DRY treatment in later cycles was observed, which is likely an actual effect from the drying. The greater leaching of ^{226}Ra in the DRY treatment is opposite of what is expected from the sulphate concentrations. However, this indicates that ^{226}Ra is present in a phase that is sensitive to oxidation effects. Differences in observed behaviour for ^{226}Ra and Ba could be caused by different source

phases in the alum shale or that they in fact are different elements. Both, leached Ba and ^{226}Ra, amounted for less than 1 % of the total debris content.

3.3.3 Transition metals and group 12

While concentrations of Fe in solution were below DL (1 µg L^{-1}) for most of the time, Fe was likely important for processes both in the debris and in the solution. As pyrite is oxidized, Fe^{2+} will be released to solution and oxidized to Fe^{3+}, which has a low solubility at circumneutral pH and precipitates as iron (oxy)hydroxides (Chandra & Gerson, 2010; Singer & Stumm, 1970). Fe (oxy)hydroxides are important scavenging agents, and can reduce leachate concentrations of a number of elements (Braunschweig et al., 2013).

Only about 0.001 % of V was released in both treatments, and aqueous concentrations were below 2 µg L^{-1} (Figure 2 e). In total, 38 % more leached in the DRY treatment compared to the WET ($p = 0.00002$), making it one of the elements with the greatest difference between treatments. Aqueous concentrations of V were clearly highest in the first cycle, but for the DRY treatment the leaching seemed to speed up from cycle 2 to 6, indicating that V was present in a phase sensitive to the drying period. V can occur as a contaminant in pyrite (Mindat.org, 2019). Solubility of V can be limited by scavenging by Fe (oxy)hydroxides, thus, pyrite oxidation can both increase and decrease V concentrations.

For Mo, there was a clear difference between the two treatments (Figure 2 f). While leaching slowed from cycle 2 to 6 in the WET treatment, it stayed the same in the DRY treatment. In total 28 % more leached in that treatment ($p = 3\times10^{-6}$). Thus, Mo is likely also released from a phase that is sensitive to the drying period.

Leaching curves for Mn (Figure S8) were very similar to those for the lighter alkaline earth metals (Mg, Ca and Sr, see Figure 2 b), likely because it is often present as a bivalently charged ion and is a common impurity in calcite (Appelo & Postma, 2010; Rayner-Canham & Overton, 2006). The concentrations reached about 1.5 mg L^{-1} in the first cycle, and 0.15 – 0.4 mg L^{-1} in the rest of the cycles. As seen for Mg, Ca and Sr, Mn was released quicker in the DRY than in the WET treatment in cycles 2-6, but the overall difference between the treatments was rather small with 4 % greater release in the DRY treatment ($p = 0.01$).

Cd concentrations peaked after 1 week in the first cycle at close to 45 μg L^{-1} in both treatments (Figure 2 g) after which the concentrations decreased. In the following cycles, the Cd concentrations reached about 3-7 μg L^{-1}, with only small differences between the two treatments and slightly lower concentrations for each cycle. Very similar leaching behaviour was observed for Co, Ni and Zn (Figures S9-S11), though at much higher concentrations of Ni and Zn, and lower of Co. Ni peaked at almost 800 μg L^{-1} in the first cycle, and in the following cycles the highest measured concentration decreased from ~110 μg L^{-1} in cycle 2 to ~40 μg L^{-1} in cycle 6. Zn peaked at about 500 μg L^{-1} in the first cycle and reached 40-140 μg L^{-1} in the following cycles, while for Co these numbers were about 26 μg L^{-1} and 2-5 μg L^{-1}, respectively. Of these four elements, Cd exhibited the greatest difference between the treatments with totally 10 % greater leaching in the DRY treatment. While this difference was significant ($p = 0.002$), it seemed to be unrelated to the drying period of the rock, as most of it was caused by the shorter first cycle for the DRY treatment, and, thus, less reduction in concentrations. Similar statements can be made about the differences for Co, Ni and Zn displayed in Table 5.

3.3.4 Group 15

Concentrations of As were very low, with maximum concentrations below 0.6 μg L^{-1} in the first cycle and lower concentrations in the following cycles (Figure S12). While leaching was quicker in the DRY treatment compared to the WET treatment for the last three cycles, indicating that the drying period had an effect on the release of As, the total mass leached in the two treatments was the same. When leaching black shale, Yu et al. (2014) observed low leaching of As as long as pH was above 3, and up to 1000 μg L^{-1} As in the leachate at lower pH values. Thus, we could likely have expected increased leaching of As if the system had reached low pH values.

The total mass of Sb that leached in the duration of the experiments was 24 % lower in DRY compared to WET ($p = 6\times10^{-6}$). In cycle 2 and 3, concentrations in WET increased faster than in DRY, possibly because of limited scavenging by Fe (oxy)hydroxides due to less pyrite oxidation. In the later cycles, the leaching rate was the same in the two treatments, but the longer contact time caused higher leaching in WET compared to DRY (Figure 2 h).

3.3.5 Uranium

The total leached mass of U was 29 % lower in the DRY compared to the WET treatment ($p = 0.0001$). This difference seemed to be caused only by the different contact time between debris and leachant in the two treatments, as the leaching curves followed each other in all cycles (Figure 2 i). Thus, leaching of U seemed to not at all be affected by the drying periods.

3.3.6 Fractionation

From the measured dissolved (<0.45 μm) and low molecular mass (LMM, <10 kDa) fractions, the colloidal fraction (= dissolved – LMM) can be calculated. Colloids in the leachates can for example be finely crushed alum shale particles, newly formed precipitation products or results from flocculation and scavenging by Fe. Of the elements measured in the leachates, most were present as 95-100 % LMM species. S, K, Ca, As, Sr, Mo, Cd and Ba seemed to have a minor colloidal fraction, sometimes up to 10 % of the dissolved element concentration. The LMM fraction of ^{226}Ra was only measured in a few time points (end of cycles 3-6 for WET and 4-6 for DRY), but indicated that ^{226}Ra as expected mainly was present as LMM species. U, on the other hand, had up to 90 % colloidal fraction at the beginning of the cycles, though < 10 % in the end of the cycles (Figure 3). This cyclic variation can mainly be ascribed to lower dissolved concentrations of ^{238}U in the leachate in the beginning of the cycles, but there was also a decreasing trend in colloidal concentrations in each cycle with 1-3 μg L^{-1} in the beginning of a cycle and about 0.5 μg L^{-1} later in the cycle – except in cycle 1, where calculated colloidal concentrations were up to 18 μg L^{-1}.

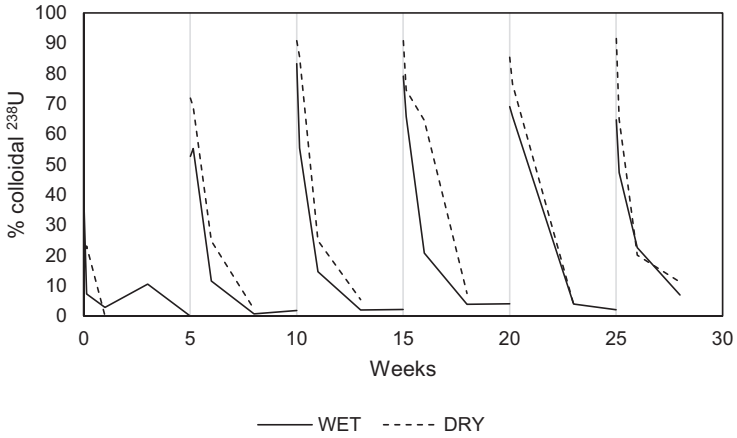

Figure 3: Percentage colloidal fraction of ^{238}U with time in the cyclic leaching experiment.

3.4 Implications for storage of acid-producing rock

The highest release rate of the measured elements occurred in the first cycle, while in later cycles the release rate was slower. As already mentioned, this can be an artefact caused by crushing of the rock that creates very reactive fresh surfaces. These findings suggest that if rock masses are stored in water, there will be an initial release of a range of elements in high concentrations. Then, slower release rates can be expected – at least until the buffer capacity is exhausted and ARD develops.

No significant change in the pyrite content of the debris was observed in either treatment, even though the water quality parameters quite clearly indicated pyrite oxidation, and the prevailing conditions (i.e., measured pH and E_h values) also favoured oxidation of pyrite. However, the leaching of S only accounted for 4.4 and 5.0 % of the total S in the debris in the WET and DRY treatment, respectively, and a part of this is likely accounted for by dissolution of sulphate minerals. Thus, only a small fraction of the pyrite may have been oxidized, explaining the lack of significant change in measured mineral content. Leaching experiments with other Scandinavian alum shales have resulted in pH levels down to 2-3 (e.g. Falk et al., 2006; Jeng, 1991; Yu et al., 2014). In the long term, a pH drop is also expected for the alum shale from Gran in the conditions tested in this experiment, as pyrite content was basically unchanged while the buffer capacity was > 50 % depleted. The original AP to NP ratio of 0.18 also illustrates this. Based on the observed release of S and measured TIC in the debris after treatments, new estimates for NP:AP are 0.08 and

0.09 for the debris from the WET and DRY treatment, respectively. The slightly lower estimate for WET reflects that while the pyrite oxidation (approximated by the S release) seemed to be slower in this treatment, the reduction in buffer capacity was about the same, due to the exchange of water. Thus, when the buffer capacity eventually is depleted, more pyrite is expected to be left in the WET treatment, giving a higher resulting potential for acid production.

As mentioned, rock with NP:AP > 3 is considered neutralizing (Pabst et al., 2016). However, depending on local practice and regulations, a smaller uncertainty zone can be used, and some places rocks with NP:AP > 1.2 are considered safe (Dold, 2017). For calculating the NP, the measured carbonates were all assumed to be calcite – which fits well to the XRD results in this case – and each mole of calcite were expected to neutralize two moles of protons (Lawrence & Wang, 1996; Pabst et al., 2016). However, because the pK_{a1} for carbonic acid is 6.3, the pH will be below 6.3 when all carbonates are spent for neutralization – which is often lower than the optimal pH in a disposal site (Dold, 2017). Thus, Dold (2017) argues that when calculating NP, only one mole of protons should be assumed neutralized per mole of calcite. Using this assumption, estimated NP to AP ratio of the alum shale starting material used in this experiment is 0.092. This rock debris is considered clearly acid-producing in either case, but if dealing with rock masses close to being considered safe (and especially if 1.2 is used as the "safe" ratio for NP:AP), this difference in calculations can be crucial. It should be noted that another consequence of protonating HCO_3^- at low pH is outgassing of the greenhouse gas CO_2 from the disposal site.

If there is any exchange of water in a disposal site, dissolved carbonates can be transported out and buffer capacity is lost, as was seen when exchanging the water in both treatments. This means that a large fraction of the assumed buffer capacity of calcite can be lost without contributing to neutralization of acid. Thus, these results clearly show that if a disposal site is not completely sealed, the effective NP of the rock masses can be lower than expected, supporting Dold's (2017) arguments for using one mole of H^+ per mole of calcite for NP:AP calculations. The issues with washing out of buffer capacity should also be kept in mind if a storage solution with addition of neutralizing material is chosen: if the site is not properly sealed the added buffer capacity can be washed out.

Fe and Al, major components of the debris, leached in very low concentrations. As mentioned, Fe released in the pyrite oxidation will by the pH and redox conditions of the experiment precipitate as Fe (oxy)hydroxides (Appelo & Postma, 2010; Chandra & Gerson, 2010; Grundl et al., 2011). If pH is reduced, Fe^{3+} becomes soluble and the scavenging effect of the Fe (oxy)hydroxides ceases. Furthermore, elements previously removed from solution can be released again causing a plume of contaminants, and the presence of Fe^{3+} in solution will accelerate the pyrite oxidation (Chandra & Gerson, 2010; Singer & Stumm, 1970). Muscovite, which likely contains all of the Al in the sample, is expected to be stable under the observed conditions, but weathering of this mineral and concomitant great release of Al is expected at lower pH values (Appelo & Postma, 2010; Hindar, 2010). Thus when a pH drop happens, considerably greater leaching of Al and Fe, together with a range of trace elements, is expected, with potentially detrimental effects on the local environment (Hindar, 2010; Rosseland et al., 1990). $BaSO_4$, on the other hand, has a low solubility also at lower pH values and Ba and ^{226}Ra are not expected to be released in case of a pH drop.

The results demonstrate that the alum shale from Gran is somewhat resistant towards a pH drop, and even with drying periods and exchange of water the buffer capacity was not depleted after 28 weeks. This was also observed in previous leaching results with alum shale from this area (Fjermestad et al., 2017; Hjulstad, 2015; Wærsted et al., in prep.), and makes the establishment of a storage site easier as there is some time to establish desired conditions before a pH drop. On the other hand, the results clearly show that a drop in pH can be expected if oxygen is available and especially if water is exchanged, and rock debris of this type should be properly stored and precautions for avoiding oxidation should be made.

4 Conclusions

The effect of water exchange and drying periods on the leaching of alum shale was investigated. Most measured elements leached the greatest amount in the first cycle – the first contact with water – giving neutral rock drainage. Thus, when storing alum shale debris in water, an initial high release of contaminants can be expected, then leaching rates are expected to decrease for most elements until an eventual pH drop that is likely to increase leaching and solubility for a range of elements. Some elements showed

588 continued leaching in cycle after cycle, especially Ba, ^{226}Ra, Sb, V and Mo, though Ba was
589 the only element that reached similar concentrations in later cycles as in the first.

590 Higher concentrations of SO_4^2, conductivity and lower alkalinity indicated a greater
591 extent of oxidation of sulphides in debris that was allowed to dry in air between leaching
592 cycles (DRY) compared to the debris kept submerged in water at all times (WET).
593 However, the differences were rather small, and for some elements the quicker leaching
594 in DRY was compensated by the longer contact time with water in WET, and the resulting
595 total leached concentrations were the same. Increased leaching of several investigated
596 elements, most clearly for Li, V, Mo, SO_4 and ^{226}Ra, was observed after periods when the
597 rock debris was exposed directly to air and allowed to dry. Sb and U leached more in the
598 WET treatment compared to the DRY. For U, the only factor of importance for the leaching
599 seemed to be the contact time between debris and leachant.

600 The results from these experiments clearly demonstrate the challenges of storing alum
601 shale or other acid-producing rock in water that is not completely stagnant. Exchange of
602 water not only causes oxygenated water to enter and contaminated water to leach out,
603 but can also increase leaching of elements with limited by solubility (like Ba and ^{226}Ra)
604 and wash out important buffer capacity in the form of dissolved carbonates. Washing out
605 of the inherent buffer capacity of the stored rock masses can increase risk of ARD and
606 reduce time before onset of ARD. Thus, exchange of the water in a storage site decreases
607 the buffer capacity of the debris (depletes the carbonates) – with or without oxygen
608 coming in. Ultimately, wash-out of buffer capacity could potentially transform net
609 neutralizing rocks (considered safe and not disposed of under special storage conditions)
610 into net acid-producing rocks. The potential for wash-out of buffer capacity under
611 different conditions and for different rock types should therefore be further investigated.

612 While the treatment with drying periods resulted in greater leaching in the duration of
613 the experiment, the treatment with exchange of water without drying seemed to result in
614 slightly lower NP:AP values at the end of the experiment, and, thus, in debris with an even
615 greater potential for ARD. Despite the slight differences, neither of the tested treatments
616 are recommended for storage of alum shale or other acid-producing rock: if such rock is
617 stored in water, exchange of water and intrusion of air should be kept at an absolute
618 minimum.

Supporting information:

Leaching graphs for Cl^-, NO_3^-, F^-, Li, Na, Mg, Sr, Mn, Co, Zn, Ni and As. XRD results and X-ray diffractograms for alum shale analyses.

Acknowledgements

This study has been funded by the Norwegian Public Road Administration through the NORWAT (Nordic Road Water) programme and by the Norwegian Research Council through its Centre of Excellence (CoE) funding scheme (Project 223268/F50).

5 References

Aas, W., Platt, S., Solberg, S., & Yttri, K. E. (2015). *Monitoring of long-range transported air pollutants in Norway, annual report 2014* (M-367).

Alloway, B. J. (2013). *Heavy Metals in Soils: Trace Metals and Metalloids in Soils and their Bioavailability* (B. J. Alloway & J. T. Trevors Eds., 3rd ed.): Springer.

Appelo, C. A. J., & Postma, D. (2010). *Geochemistry, groundwater and pollution* (2nd ed.): CRC press.

Braunschweig, J., Bosch, J., & Meckenstock, R. U. (2013). Iron oxide nanoparticles in geomicrobiology: from biogeochemistry to bioremediation. *New Biotechnology, 30*(6), 793-802. doi:https://doi.org/10.1016/j.nbt.2013.03.008

Chandra, A. P., & Gerson, A. R. (2010). The mechanisms of pyrite oxidation and leaching: A fundamental perspective. *Surface Science Reports, 65*(9), 293-315. doi:http://dx.doi.org/10.1016/j.surfrep.2010.08.003

CRC Handbook of Chemistry and Physics. (1993). (D. R. Lide Ed., 74th ed.). U.S.A.: CRC.

Dold, B. (2017). Acid rock drainage prediction: A critical review. *Journal of Geochemical Exploration, 172*, 120-132. doi:https://doi.org/10.1016/j.gexplo.2016.09.014

Falk, H., Lavergren, U., & Bergbäck, B. (2006). Metal mobility in alum shale from Öland, Sweden. *Journal of Geochemical Exploration, 90*(3), 157-165. doi:http://dx.doi.org/10.1016/j.gexplo.2005.10.001

Fjermestad, H., Gundersen, E., Hagelia, P., Moen, A. B., & Torp, M. (2018). *National Road 4, utilization of black shale - Final report and experiences gathered* (333). Retrieved from www.vegvesen.no/

Fjermestad, H., Hagelia, P., & Thomassen, T. (2017). *Large-scale leaching experiment with black shale from National Road 4, Hadeland* (665). Retrieved from www.vegvesen.no

Gabitov, R. I., Gagnon, A. C., Guan, Y., Eiler, J. M., & Adkins, J. F. (2013). Accurate Mg/Ca, Sr/Ca, and Ba/Ca ratio measurements in carbonates by SIMS and NanoSIMS and an assessment of heterogeneity in common calcium carbonate standards. *Chemical Geology, 356*, 94-108. doi:https://doi.org/10.1016/j.chemgeo.2013.07.019

Grundl, T. J., Haderlein, S., Nurmi, J. T., & Tratnyek, P. G. (2011). Introduction to Aquatic Redox Chemistry. In *Aquatic Redox Chemistry* (Vol. 1071, pp. 1-14): American Chemical Society.

Hindar, A. (2010). *Highway E18 Grimstad-Kristiansand; effects and quantification of acid runoff from deposits of sulphide-bearing rock*. Retrieved from http://brage.bibsys.no

Hjulstad, M. (2015). *Leaching, Uptake and Effects in Brown Trout (Salmo trutta) of Radionuclides and Metals from Black Shales and Sulphur Bearing Gneiss* (MSc), Norwegian University of Life Sciences, Ås, Norway.

Jeng, A. S. (1991). Weathering of Some Norwegian Alum Shales. I. Laboratory simulations to study acid generation and the release of sulfate and metal cations (calcium, magnesium,

663 and potassium). *Acta Agriculturae Scandinavica, 41*(1), 13-35.
664 doi:10.1080/00015129109438580
665 Jeng, A. S. (1992). Weathering of Some Norwegian Alum Shales, II. Laboratory Simulations to
666 Study the Influence of Aging, Acidification and Liming on Heavy Metal Release. *Acta*
667 *Agriculturae Scandinavica, Section B — Soil & Plant Science, 42*(2), 76-87.
668 doi:10.1080/09064719209410203
669 Lavergren, U., Åström, M. E., Falk, H., & Bergbäck, B. (2009). Metal dispersion in groundwater in
670 an area with natural and processed black shale – Nationwide perspective and comparison
671 with acid sulfate soils. *Applied Geochemistry, 24*(3), 359-369.
672 doi:https://doi.org/10.1016/j.apgeochem.2008.11.022
673 Lawrence, R. W., & Scheske, M. (1997). A method to calculate the neutralization potential of
674 mining wastes. *Environmental Geology, 32*(2), 100-106. doi:10.1007/s002540050198
675 Lawrence, R. W., & Wang, Y. (1996). *Determination of Neutralization Potential for Acid Rock*
676 *Drainage Prediction* (MEND Project 1.16.3). Retrieved from http://mend-
677 nedem.org/mend-report/determination-of-neutralization-potential-for-acid-rock-
678 drainage-prediction/
679 Miller, J. N., & Miller, J. C. (2005). *Statistics and Chemometrics for Analytical Chemistry*. Great
680 Britain: Pearson Education Limited.
681 Mindat.org. (2019). Pyrite. Retrieved from https://www.mindat.org/min-3314.html on
682 22.06.2019
683 Owen, A. W., Bruton, D. L., Bockelie, J. F., & Bockelie, T. G. (1990). *The Ordovician successions of the*
684 *Oslo Region, Norway*. D. Roberts (Eds.), Geological survey of Norway (NGU): Retrieved
685 from http://paleoarchive.com/
686 Pabst, T., Sørmo, E., & Endre, E. (2016). Geochemical characterisation of Norwegian Cambro-
687 Ordovician black mudrocks for building and construction use. *Bulletin of Engineering*
688 *Geology and the Environment, 76*(4), 1577–1592. doi:https://doi.org/10.1007/s10064-
689 016-0941-z
690 Pipkin, B., Trent, D. D., Hazlett, R., & Bierman, P. (2008). *Geology and the environment* (P. Adams
691 Ed., 5th ed.). USA: Thomson Brooks/Cole.
692 Pollution Control Act (Forurensningsforskriften), FOR-2004-06-01-931 (2004).
693 Pratt, A. R., Nesbitt, H. W., & Mycroft, J. R. (1996). The increased reactivity of pyrrhotite and
694 magnetite phases in sulphide mine tailings. *Journal of Geochemical Exploration, 56*(1), 1-
695 11. doi:https://doi.org/10.1016/0375-6742(96)00008-8
696 Rayner-Canham, G., & Overton, T. (2006). *Descriptive inorganic chemistry* (J. Fiorillo Ed., 4th ed.).
697 Houndmills, England: W. H. Freeman and Company.
698 Rosseland, B. O., Eldhuset, T. D., & Staurnes, M. (1990). Environmental effects of aluminium.
699 *Environmental Geochemistry and Health, 12*(1-2), 17-27. doi:10.1007/bf01734045
700 Singer, P. C., & Stumm, W. (1970). Acidic Mine Drainage: The Rate-Determining Step. *Science,*
701 *167*(3921), 1121-1123. doi:10.2307/1728684
702 Stegnar, P., Shishkov, I., Burkitbayev, M., Tolongutov, B., Yunusov, M., Radyuk, R., & Salbu, B.
703 (2013). Assessment of the radiological impact of gamma and radon dose rates at former
704 U mining sites in Central Asia. *Journal of Environmental Radioactivity, 123*, 3-13.
705 doi:10.1016/j.jenvrad.2012.12.005
706 Forskrift om strålevern og bruk av stråling (strålevernforskriften), FOR-2016-12-16-1659
707 (2016).
708 Sørmo, E., Breedveld, G., & Pabst, T. (2015). *Deponering av syredannende bergarter. Grunnlag for*
709 *veileder.* (M-385).
710 vanLoon, G. W., & Duffy, S. J. (2011). *Environmental Chemistry - a global perspective* (3rd ed.). New
711 York: Oxford University Press.
712 Wærsted, F. M., Jensen, K. A., Reinoso-Maset, E., & Skipperud, L. (2018). High Throughput, Direct
713 Determination of 226Ra in Water and Digested Geological Samples. *Analytical Chemistry,*
714 *90*(20), 12246-12252. doi:10.1021/acs.analchem.8b03494

715 Wærsted, F. M., Reinoso-Maset, E., Salbu, B., & Skipperud, L. (in prep.). *Rainwater leaching of alum*
716 *shale debris under atmospheric and low-oxygen conditions*. Faculty of Environmental
717 Science and Natural Resource Management. Norwegian University of Life Sciences.
718 Yu, C., Lavergren, U., Peltola, P., Drake, H., Bergbäck, B., & Åström, M. E. (2014). Retention and
719 transport of arsenic, uranium and nickel in a black shale setting revealed by a long-term
720 humidity cell test and sequential chemical extractions. *Chemical Geology, 363*, 134-144.
721 doi:http://dx.doi.org/10.1016/j.chemgeo.2013.11.003

722

Paper III: Supporting information

Supporting information to

The effect of water exchange on the leaching of alum shale

F. M. Wærsted*[1], P. J. Riss[2] and L. Skipperud[1]

[1]Centre for Environmental Radioactivity (CERAD), Faculty of Environmental Sciences and Natural Resource Management, Norwegian University of Life Sciences, P.O. Box 5003, N-1432 Ås, Norway

[2]Department of Chemistry, Faculty for Mathematics and Natural Sciences, University of Oslo, Sem Sælands vei 26, N-0371 Oslo, Norway

*Corresponding author email: frwa@nmbu.no

Table of Contents

1.1 Leaching graphs

Leaching curves that are discussed but not presented in the article follows here.

1.1.1 Anions

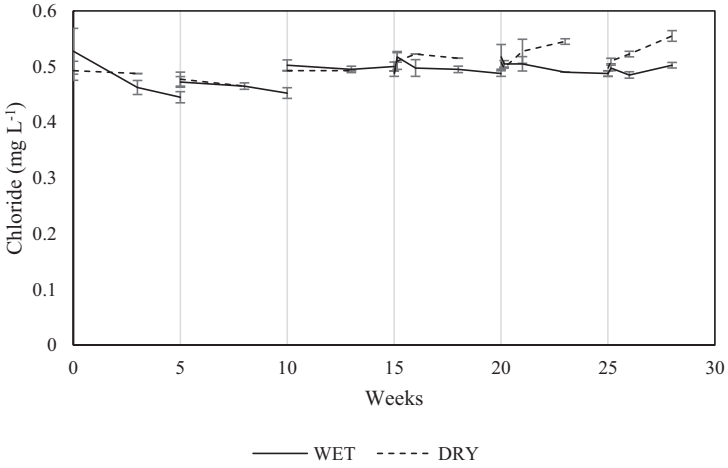

Figure S 1: Leaching of chloride over time in the cyclic leaching experiment. Results from samples filtered through 0.45 µm membrane filters. Each vertical line represents the start of a new cycle. Full (WET) and dashed (DRY) lines are connecting average concentrations of samples. The error bars represent one standard deviation of replicate samples. For all sampling points, n=4.

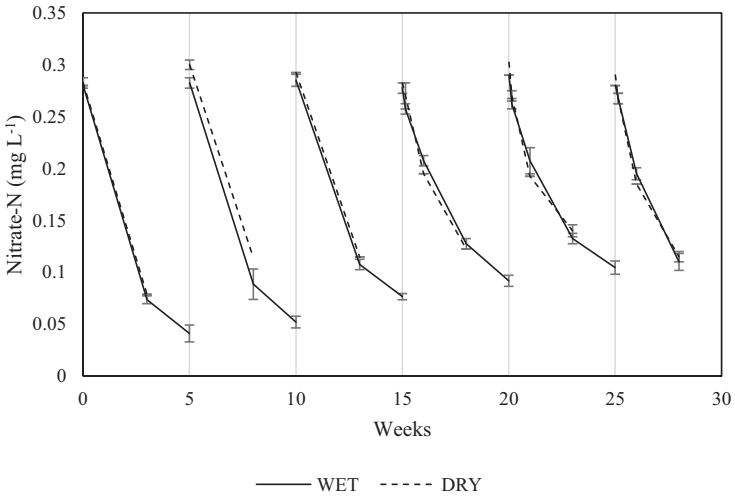

Figure S 2: Leaching of nitrate-N over time in the cyclic leaching experiment. Results from samples filtered through 0.45 µm membrane filters. Each vertical line represents the start of a new cycle. Full (WET) and dashed (DRY) lines are connecting average concentrations of samples. The error bars represent one standard deviation of replicate samples. For all sampling points, n=4.

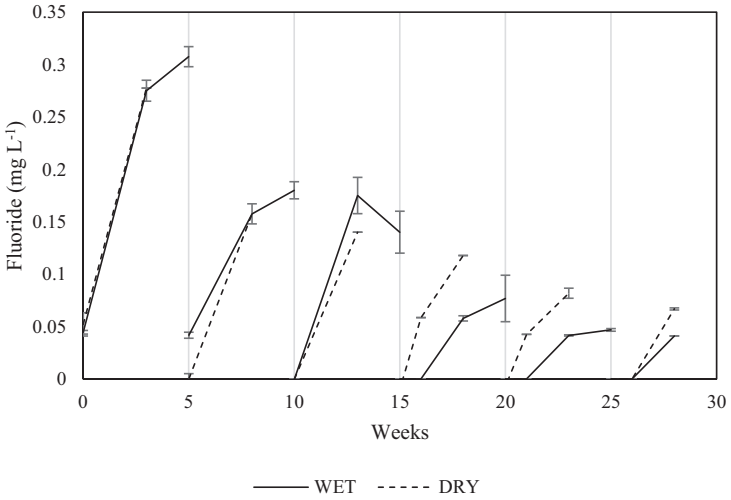

Figure S 3: Leaching of fluoride over time in the cyclic leaching experiment. Results from samples filtered through 0.45 µm membrane filters. Each vertical line represents the start of a new cycle. Full (WET) and dashed (DRY) lines are connecting average concentrations of samples. The error bars represent one standard deviation of replicate samples. For all sampling points, n=4.

1.1.2 Alkali metals

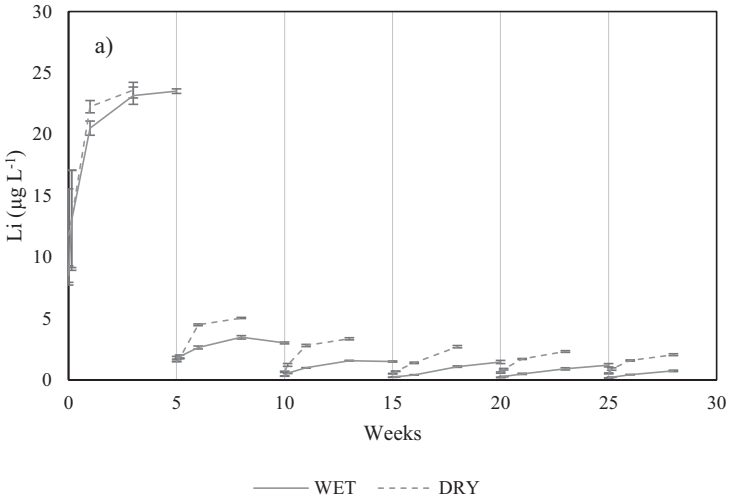

Figure S 4: Leaching of lithium over time in the cyclic leaching experiment. Results from samples filtered through 0.45 µm membrane filters. Each vertical line represents the start of a new cycle. Full (WET) and dashed (DRY) lines are connecting average concentrations of samples. The error bars represent one standard deviation of replicate samples. For all sampling points, n=4.

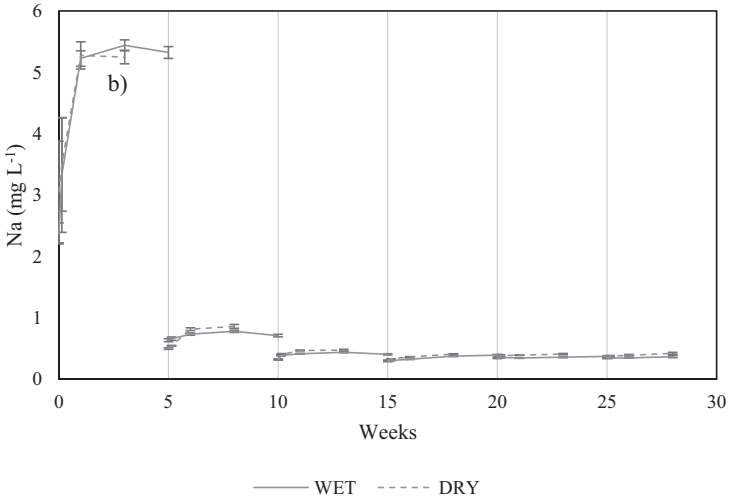

Figure S 5: Leaching of sodium over time in the cyclic leaching experiment. Results from samples filtered through 0.45 µm membrane filters. Each vertical line represents the start of a new cycle. Full (WET) and dashed (DRY) lines are connecting average concentrations of samples. The error bars represent one standard deviation of replicate samples. For all sampling points, n=4.

1.1.3 Alkaline earth metals

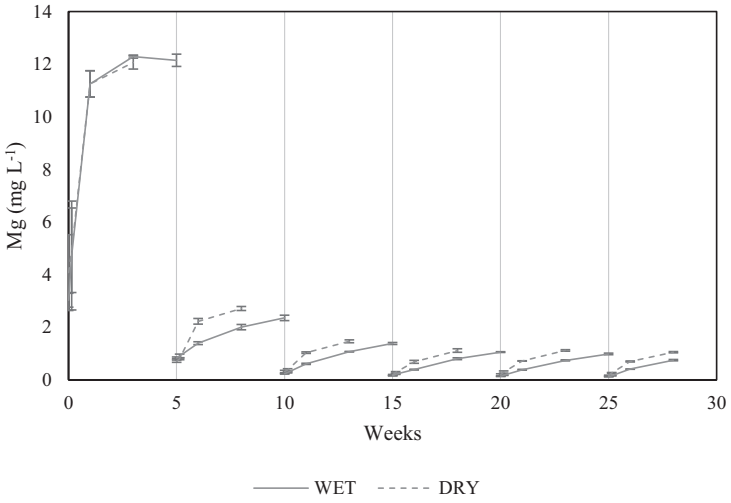

Figure S 6: Leaching of magnesium over time in the cyclic leaching experiment. Results from samples filtered through 0.45 µm membrane filters. Each vertical line represents the start of a new cycle. Full (WET) and dashed (DRY) lines are connecting average concentrations of samples. The error bars represent one standard deviation of replicate samples. For all sampling points, n=4.

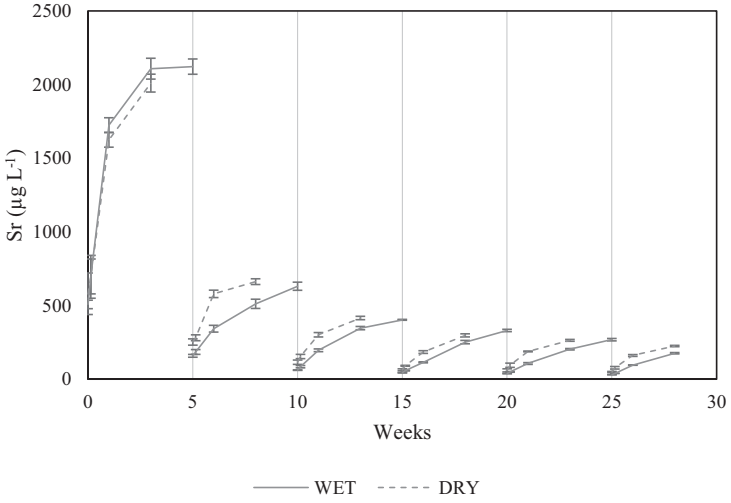

Figure S 7: Leaching of strontium over time in the cyclic leaching experiment. Results from samples filtered through 0.45 µm membrane filters. Each vertical line represents the start of a new cycle. Full (WET) and dashed (DRY) lines are connecting average concentrations of samples. The error bars represent one standard deviation of replicate samples. For all sampling points, n=4.

1.1.4 Transition metals and group 12 elements

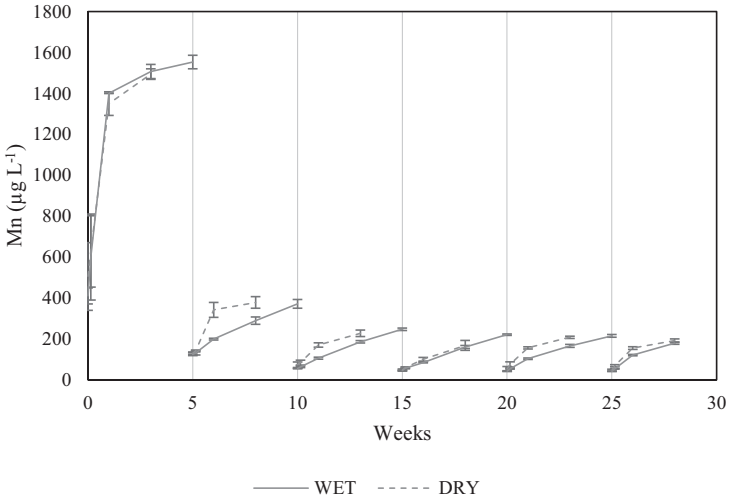

Figure S 8: Leaching of manganese over time in the cyclic leaching experiment. Results from samples filtered through 0.45 µm membrane filters. Each vertical line represents the start of a new cycle. Full (WET) and dashed (DRY) lines are connecting average concentrations of samples. The error bars represent one standard deviation of replicate samples. For all sampling points, n=4.

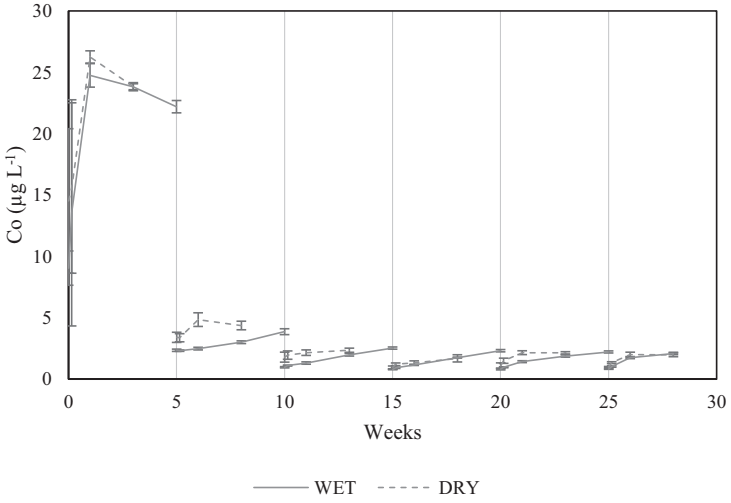

Figure S 9: Leaching of cobalt over time in the cyclic leaching experiment. Results from samples filtered through 0.45 µm membrane filters. Each vertical line represents the start of a new cycle. Full (WET) and dashed (DRY) lines are connecting average concentrations of samples. The error bars represent one standard deviation of replicate samples. For all sampling points, n=4.

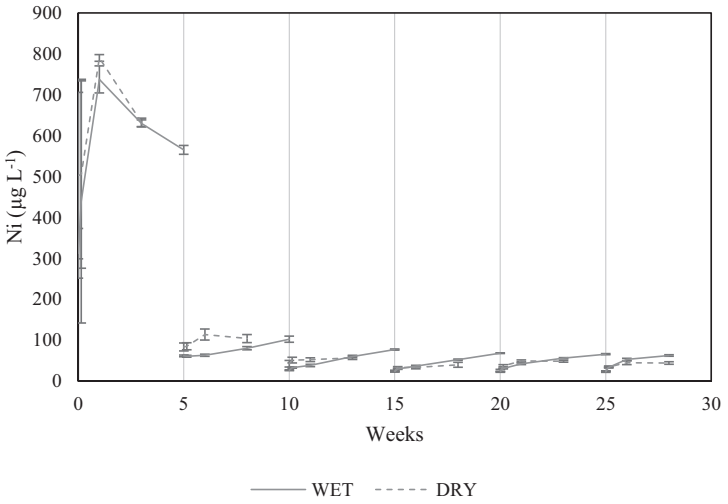

Figure S 10: Leaching of nickel over time in the cyclic leaching experiment. Results from samples filtered through 0.45 µm membrane filters. Each vertical line represents the start of a new cycle. Full (WET) and dashed (DRY) lines are connecting average concentrations of samples. The error bars represent one standard deviation of replicate samples. For all sampling points, n=4.

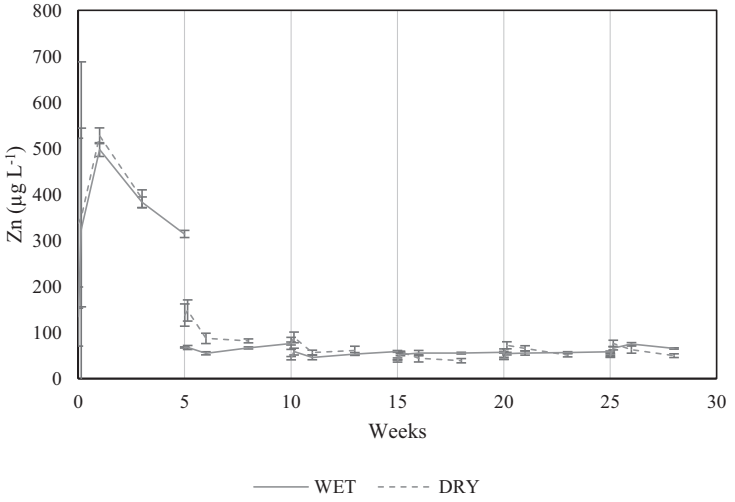

Figure S 11: Leaching of zinc over time in the cyclic leaching experiment. Results from samples filtered through 0.45 µm membrane filters. Each vertical line represents the start of a new cycle. Full (WET) and dashed (DRY) lines are connecting average concentrations of samples. The error bars represent one standard deviation of replicate samples. For all sampling points, n=4.

1.1.5 Group 15

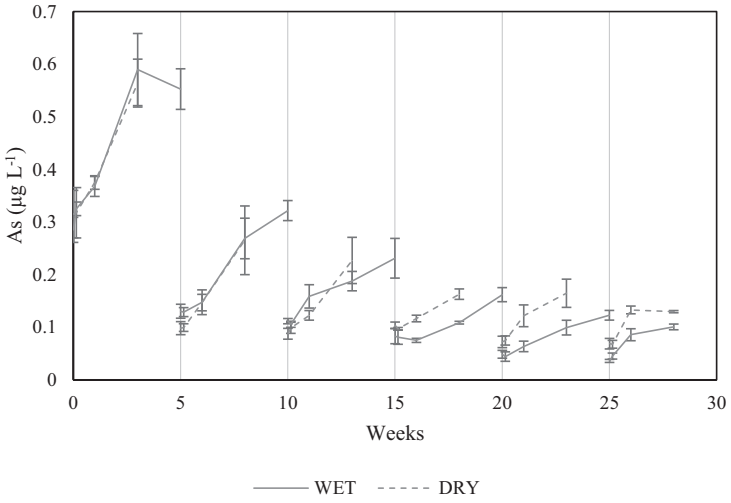

Figure S 12: Leaching of arsenic over time in the cyclic leaching experiment. Results from samples filtered through 0.45 µm membrane filters. Each vertical line represents the start of a new cycle. Full (WET) and dashed (DRY) lines are connecting average concentrations of samples. The error bars represent one standard deviation of replicate samples. For all sampling points, n=4.

1.2 XRD graphs

Results below show the XRD spectrum (blue line) and the fitted line for quantification (red line). Results are in % of crystalline material, and thus higher than the results in the article that are in % of weight.

The results for takovite were excluded from the article, as the concentration was very low, the mineral composition did not fit with the measured elemental composition of the debris and the mineral was not expected to be found in this area (Mindat.org, 2019).

1.2.1 Starting material

R-Values

```
Rexp : 9.52    Rwp : 16.98    Rp  : 12.99  GOF : 1.78
Rexp`: 23.25   Rwp`: 41.48    Rp` : 42.01  DW  : 0.71
```

Quantitative Analysis - Rietveld

```
   Phase 1  : "Muscovite 2M1"              60.9(10) %
   Phase 2  : Quartz                       30.0(8) %
   Phase 3  : Takovite                     0.5(4) %
   Phase 4  : Pyrite                       6.2(3) %
   Phase 5  : Calcite                      2.4(4) %
```

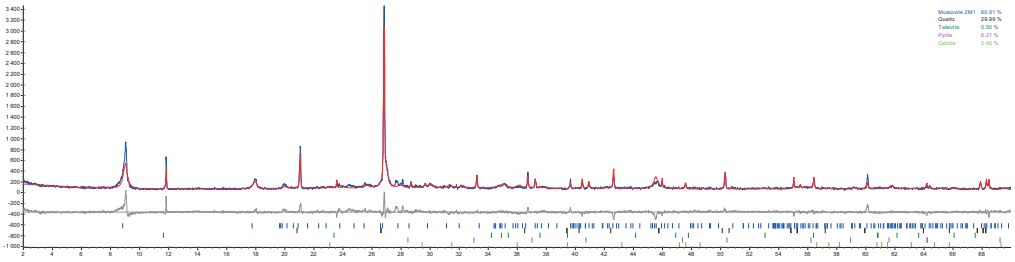

Figure S 13: XRD spectrum from analysis of the alum shale starting material used for the cyclic leaching experiment.

1.2.2 WET replicate 1

R-Values

```
Rexp : 14.15    Rwp : 17.71     Rp  : 13.68  GOF : 1.25
Rexp`: 36.52    Rwp`: 45.73     Rp` : 43.28  DW  : 1.29
```

Quantitative Analysis - Rietveld

```
   Phase 1  : "Muscovite 2M1"                 55.3(10) %
   Phase 2  : Quartz                          37.4(10) %
   Phase 3  : Pyrite                          6.5(4) %
   Phase 4  : Calcite                         0.7(3) %
```

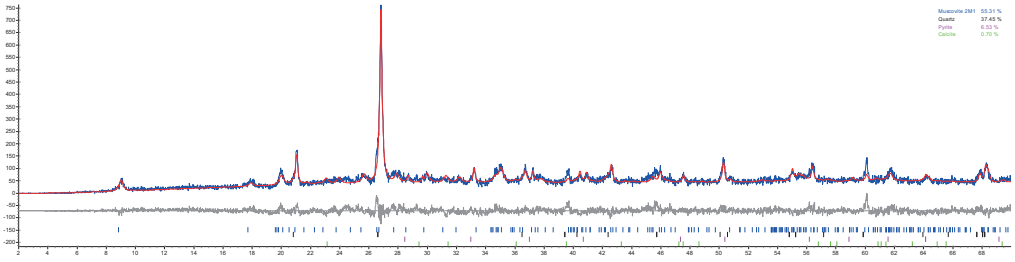

Figure S 14: XRD spectrum from analysis of alum shale from one sample after WET treatment.

1.2.3 WET replicate 2

R-Values

```
Rexp : 9.01     Rwp : 16.80     Rp  : 12.75  GOF : 1.86
Rexp`: 22.79    Rwp`: 42.47     Rp` : 43.16  DW  : 0.64
```

Quantitative Analysis - Rietveld

```
   Phase 1  : "Muscovite 2M1"                 63.7(9) %
   Phase 2  : Quartz                          29.8(8) %
   Phase 3  : Pyrite                          5.9(3) %
   Phase 4  : Calcite                         0.6(4) %
```

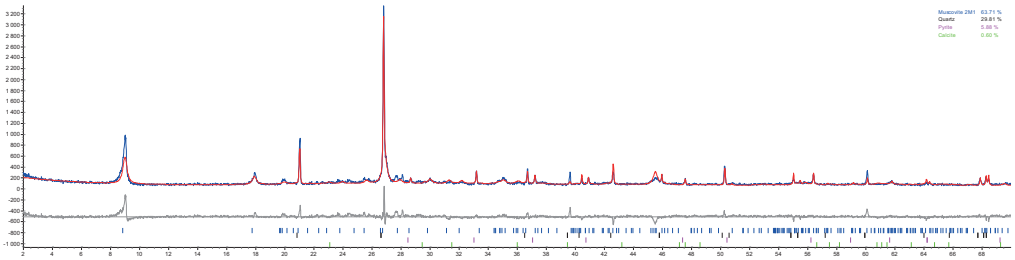

Figure S 15: XRD spectrum from analysis of alum shale from one sample after WET treatment.

1.2.4 WET replicate 3

R-Values

```
Rexp : 9.33     Rwp : 16.45     Rp  : 12.64  GOF : 1.76
Rexp`: 23.79    Rwp`: 41.92     Rp` : 43.16  DW  : 0.70
```

Quantitative Analysis - Rietveld

Phase 1	: "Muscovite 2M1"	62.3(9) %
Phase 2	: Quartz	30.5(8) %
Phase 3	: Pyrite	6.0(3) %
Phase 4	: Calcite	1.3(4) %

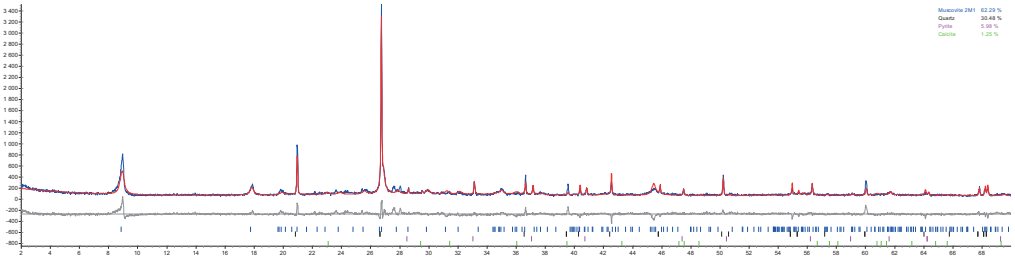

Figure S 16: XRD spectrum from analysis of alum shale from one sample after WET treatment.

1.2.5 WET replicate 4

R-Values

```
Rexp : 9.08     Rwp : 16.71     Rp  : 12.83  GOF : 1.84
Rexp`: 23.26    Rwp`: 42.81     Rp` : 44.48  DW  : 0.64
```

Quantitative Analysis - Rietveld

```
   Phase 1  : "Muscovite 2M1"                63.7(9) %
   Phase 2  : Quartz                          30.0(8) %
   Phase 3  : Pyrite                          5.9(3) %
   Phase 4  : Calcite                         0.4(3) %
```

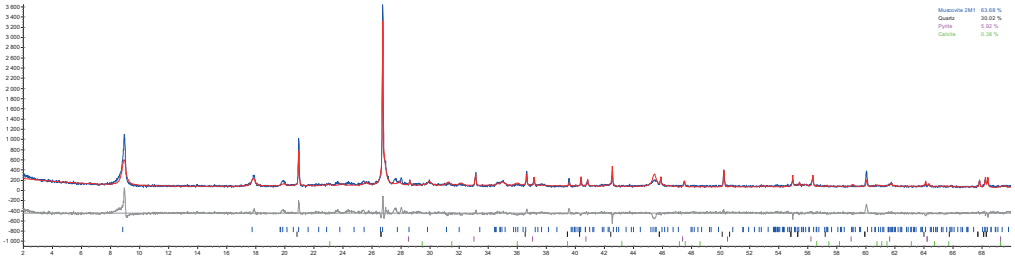

Figure S 17: XRD spectrum from analysis of alum shale from one sample after WET treatment.

1.2.6 DRY replicate 1

R-Values

```
Rexp : 9.27    Rwp : 16.88    Rp  : 13.09  GOF : 1.82
Rexp`: 23.32   Rwp`: 42.47    Rp` : 43.96  DW  : 0.66
```

Quantitative Analysis - Rietveld

```
   Phase 1  : "Muscovite 2M1"                62.6(9) %
   Phase 2  : Quartz                          30.1(8) %
   Phase 3  : Pyrite                          5.7(3) %
   Phase 4  : Calcite                         1.5(4) %
```

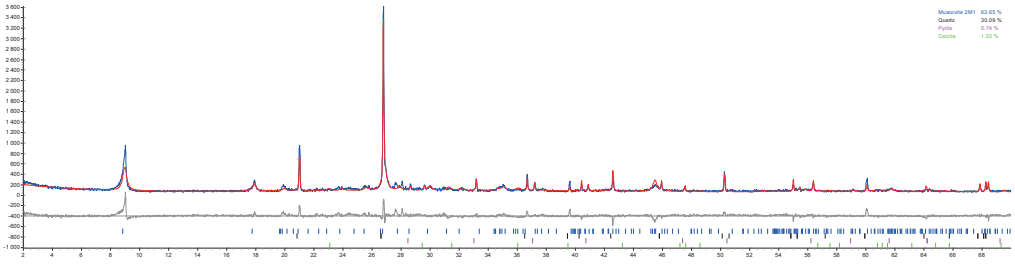

Figure S 18: XRD spectrum from analysis of alum shale from one sample after DRY treatment.

1.2.7 DRY replicate 2

R-Values

```
Rexp : 8.80    Rwp : 17.11    Rp  : 13.07  GOF : 1.94
Rexp`: 22.46   Rwp`: 43.66    Rp` : 45.16  DW  : 0.58
```

Quantitative Analysis - Rietveld

Phase 1	: "Muscovite 2M1"	64.1(9) %
Phase 2	: Quartz	29.8(8) %
Phase 3	: Pyrite	5.7(3) %
Phase 4	: Calcite	0.4(3) %

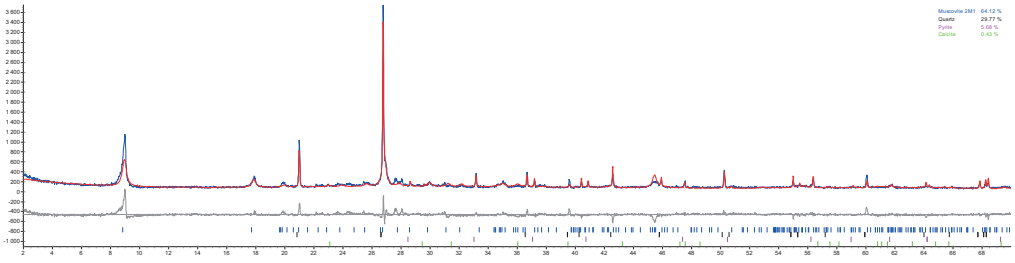

Figure S 19: XRD spectrum from analysis of alum shale from one sample after DRY treatment.

1.2.8 DRY replicate 3

R-Values

Rexp : 9.82	Rwp : 16.66	Rp : 12.94	GOF : 1.70
Rexp`: 24.94	Rwp`: 42.33	Rp` : 43.86	DW : 0.79

Quantitative Analysis - Rietveld

Phase 1	: "Muscovite 2M1"	62.1(9) %
Phase 2	: Quartz	31.2(8) %
Phase 3	: Pyrite	6.2(3) %
Phase 4	: Calcite	0.5(4) %

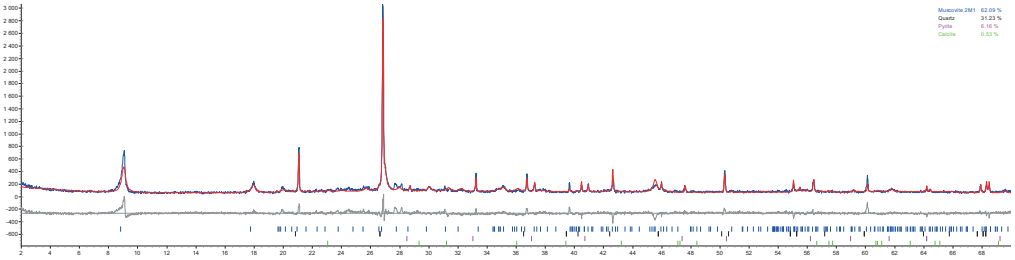

Figure S 20: XRD spectrum from analysis of alum shale from one sample after DRY treatment.

1.2.9 DRY replicate 4

R-Values

Rexp : 9.45	Rwp : 17.07	Rp : 13.15	GOF : 1.81
Rexp`: 23.62	Rwp`: 42.64	Rp` : 43.83	DW : 0.71

Quantitative Analysis - Rietveld

Phase 1	: "Muscovite 2M1"	62.6(9) %
Phase 2	: Quartz	30.5(8) %
Phase 3	: Pyrite	5.9(3) %

```
Phase 4   : Calcite                          0.9(4) %
```

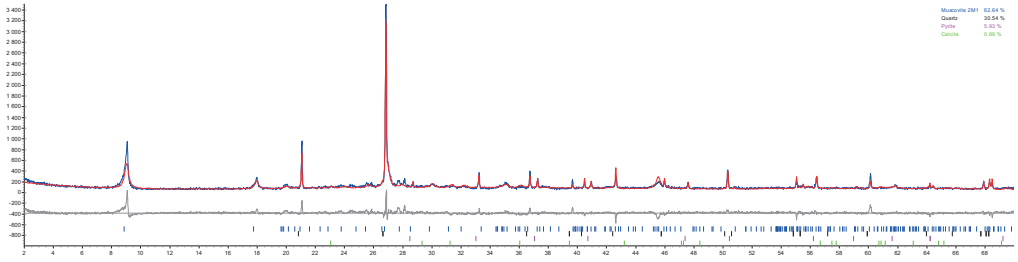

Figure S 21: XRD spectrum from analysis of alum shale from one sample after DRY treatment.

1.3 References

Mindat.org. (2019). Takovite. Retrieved from https://www.mindat.org/min-3874.html on 27.06.2019

ISBN: 978-82-575-1632-1
ISSN: 1894-6402

Norwegian University
of Life Sciences

Postboks 5003
NO-1432 Ås, Norway
+47 67 23 00 00
www.nmbu.no